

**TUNABLE-Q WAVELET TRANSFORM BASED
FILTER BANKS FOR NON-STATIONARY
SIGNALS ANALYSIS AND CLASSIFICATION**

Ph.D. Thesis

By

ANURAG NISHAD



**DISCIPLINE OF ELECTRICAL ENGINEERING
INDIAN INSTITUTE OF TECHNOLOGY
INDORE**

TUNABLE-Q WAVELET TRANSFORM BASED FILTER BANKS FOR NON-STATIONARY SIGNALS ANALYSIS AND CLASSIFICATION

A THESIS

*Submitted in partial fulfillment of the
requirements for the award of the degree*

of

DOCTOR OF PHILOSOPHY

by

ANURAG NISHAD



**DISCIPLINE OF ELECTRICAL ENGINEERING
INDIAN INSTITUTE OF TECHNOLOGY
INDORE**

December 2018



INDIAN INSTITUTE OF TECHNOLOGY INDORE

CANDIDATE'S DECLARATION

I hereby certify that the work which is being presented in the thesis entitled “**TUNABLE-Q WAVELET TRANSFORM BASED FILTER BANKS FOR NON-STATIONARY SIGNALS ANALYSIS AND CLASSIFICATION**” in the partial fulfillment of the requirements for the award of the degree of **DOCTOR OF PHILOSOPHY** and submitted in the **DISCIPLINE OF ELECTRICAL ENGINEERING, Indian Institute of Technology Indore**, is an authentic record of my own work carried out during the time period from December 2014 to December 2018 under the supervision of Prof. Ram Bilas Pachori, Indian Institute of Technology Indore, Indore, India.

The matter presented in this thesis has not been submitted by me for the award of any other degree of this or any other institute.

Signature of the student with date
(ANURAG NISHAD)

This is to certify that the above statement made by the candidate is correct to the best of my knowledge.

Signature of Thesis Supervisor with date
(PROF. RAM BILAS PACHORI)

ANURAG NISHAD has successfully given his Ph.D. Oral Examination held on

Signature of Chairperson (OEB)
Date:

Signature External Examiner
Date:

Signature of Thesis Supervisor
Date:

Signature of PSPC Member:1
Date:

Signature of PSPC Member:2
Date:

Signature of Convener, DPGC
Date:

Signature of Head of Discipline
Date:

ACKNOWLEDGEMENTS

I am immensely grateful to my supervisor Prof. Ram Bilas Pachori for his sustained inspiration, guidance, and support throughout my research work. It was my pleasure to work under the supervision of such an esteemed professor.

I would like to express my sincere gratitude to Prof. U. R. Acharya, Ngee Ann Polytechnic, Singapore, for providing valuable suggestions for my research work. I am also grateful towards my PSPC committee members Dr. Amod C. Umarikar and Prof. Anand Parey for their interesting discussions and suggestions during my research.

I would like to thank my friends Rajeev Sharma, Abhay Upadhyay, Mohit Kumar, Abhijit Bhattacharyya, Shishir Maheshwari, Rishi Raj Sharma, Vipin Gupta, Ashwani Kumar Tiwari, and Rajat Katiyar, who helped me in various ways during my thesis work.

Also I wish to thank Curtis Condon, Ken White, and Al Feng of the Beckman Institute of the University of Illinois for the bat data and for permission to use it in this thesis.

Above all, I am indebted to my parents, my wife, and my sister for their unconditional love and support. I cannot express my gratitude to my parents in words, without their blessings and inspiration, I would not have been able to accomplish the most significant milestones in my life.

Last but not the least, I thank God Almighty to enlighten my mind for carrying out this research work.

ANURAG NISHAD

Dedicated
to
My Family

ABSTRACT

The non-stationary signals are the one which consist of time-varying parameters. These signals are generated through complex process in nature and they can be found in many areas such as speech signal processing and synthesis, mechanical engineering, biomedical engineering, etc. These signals contain hidden and meaningful information regarding the characteristic of source from which it has generated. However, extraction of these information is not simple through visual inspection.

To extract hidden information from non-stationary signals, the advanced signal processing techniques are required. The analysis can be done through time-frequency (T-F) representation or through decomposition technique. In this thesis, we have proposed a decomposition technique which is based on filter-bank (FB) developed from tunable- Q wavelet transform (TQWT). It is termed as TQWT based FB (TQWT-FB). The TQWT-FB consists of constant and narrow bandwidth (BW) sub-bands to decompose the signal. Hence, constant resolution in frequency-domain is achieved. The TQWT is chosen as it provides the flexibility to tune Q -factor of wavelet, due to which, different mother wavelets are generated for the analysing different oscillatory behaviour in the non-stationary signal. Also, wavelets as basis functions are used to represent the signal which are localized in time-domain and frequency-domain. The application of proposed TQWT-FB is then shown in following areas:

The proposed TQWT-FB is used to reduce the cross-term from Wigner-Ville distribution (WVD). The proposed TQWT-FB decomposes the multi-component non-stationary signal into several sub-band signals. The obtained sub-band signal is further segmented in time-domain by time-domain segmentation (TDS) section if more than one components are present in a sub-band signal at different time intervals. Then, the WVD of each segmented component is computed and added to obtain a WVD with reduced cross-terms. The proposed method is tested on different multi-component non-stationary signals under different noisy environments. The efficacy of proposed method is compared with other methods in terms of normalized

Renyi entropy. The lowest value of Renyi entropy obtained for proposed method as compared to other methods suggests that the proposed method provides better localization of signal in the WVD.

Another application of TQWT-FB is shown to estimate the instantaneous fundamental frequency (IFF) of speech signals. The proposed method uses a TQWT-FB which has common or nearly uniform BW for all sub-bands. The TQWT-FB is used to decompose the speech signal. The fundamental frequency component (FFC) of speech signal may be present in many sub-bands at different time intervals. The time interval at where FFC is present, in a sub-band, is identified using TDS section. In the similar way, the harmonic of FFC can also be present in different sub-bands at different time-durations. The proposed method extracts FFC from different sub-bands and constructs a FFC for entire speech signal. Then, Hilbert transform is applied on constructed FFC to obtain IFF of speech signal. In order to show the efficacy of proposed method, its performance has been compared with performance of other existing methods in terms of gross error (GE) in percentage in different noisy conditions. Through simulations, it is observed that the performance of proposed method is better than other compared methods.

The developed TQWT-FB is used for developing computer aided system for the diagnosis of disease from physiological signals. This is useful as visual inspection of physiological signals by experts in order to detect disease is time-consuming and error prone. The developed TQWT-FB is applied in the screening of sleep apnea. The sleep apnea is a disease in which there is the absence of airflow during respiration for at least 10 s. This disease can lead to many types of cardiovascular diseases. An automated system is developed to detect the sleep apnea with few channels. The single-lead electrocardiogram (ECG) signal is used to detect apneic and non-apneic events. The segments of ECG signal are decomposed by TQWT-FB. Then centered correntropies (CCEs) are computed from the various sub-band signals. The obtained features are ranked and then fed to the various classifiers to select the optimum performing classifier. In this work, we have obtained the highest

classification accuracy(ACC), specificity (SPE), and sensitivity (SEN) of 92.78%, 93.91%, and 90.95% respectively using random forest (RF) classifier.

The proposed TQWT-FB is applied for the diagnosis of epilepsy. The epilepsy is a neurological disorder and the seizure events frequently appear in epileptic patients. This disorder can be analysed through electroencephalogram (EEG) signals. A novel approach for automated identification of seizure EEG signals has been proposed. The TQWT-FB decomposes the EEG signal into number of sub-band signals. The features are computed by applying cross-information potential (CIP) on sub-band signals and then ranked. The features are then fed to RF classifier. In this work, we have obtained classification ACC of 99%. Among the epileptic patients, a large number of patients suffer from focal epilepsy. The detection of focal EEG signal helps surgeon to identify part of brain effect from focal epilepsy and the identified regions of brain are useful for surgery for the patients who are suffering from focal epilepsy. The proposed method is also applied in classification of focal and non-focal EEG signals. After decomposing EEG signals by proposed TQWT-FB, mixture correntropy (MCE) based features are obtained from sub-band signals. The least squares support vector machine (LS-SVM) classifier along with radial basis function (RBF) kernel is used for the classification of these extracted features. The feature ranking methods are also used to reduce the features space. The achieved maximum classification accuracy in this proposed methodology is 90.01%.

The application of proposed TQWT-FB is shown in the area of rehabilitation also. To perform basic hand movements, a hand amputee person needs an exoskeleton prosthetic hand (EPH). The EPH can be controlled through EEG or electromyogram (EMG) signals. The EMG signals are preferred as they are acquired from surface of forearm and termed as surface EMG (sEMG). It is very challenging to design the control section for EPH. It should be able to classify different hand movements accurately based on the acquired sEMG signals. Also the sEMG signals must be acquired from minimum number of electrodes to make EPH cost-effective. A novel technique to classify the basic hand movements is proposed. The TQWT-

FB is used for decomposition of cross-covariance of sEMG (csEMG) signals. Then, Kraskov entropy (KRE) features are extracted and ranked. The proposed method is tested on the data obtained from five subjects and achieved the average classification ACC of 98.55% using k -nearest neighbour (k -NN) classifier.

Contents

ABSTRACT	i
LIST OF FIGURES	xi
LIST OF TABLES	xviii
LIST OF ABBREVIATIONS	xxi
1 Introduction	1
1.1 Non-stationary signals analysis techniques	2
1.2 Classification of physiological signals	6
1.3 Overview of Tunable- Q wavelet transform	7
1.4 Motivation	12
1.5 Objectives	15
1.6 Contributions	15
1.7 Organization of the thesis	18
2 Tunable-Q wavelet transform based filter-bank	22
2.1 Introduction	22
2.2 Design of TQWT-FB	22
2.3 Summary	28
3 Reduction of cross-terms in WVD using TQWT-FB	30
3.1 Introduction	30
3.2 Overview of the WVD	33

3.3	Proposed methodology for cross-terms reduction in WVD	35
3.3.1	Signal decomposition by TQWT-FB	36
3.3.2	TDS section	37
3.3.3	The WVD computation	40
3.4	Performance evaluation	41
3.5	Simulation results	42
3.6	Discussion	55
3.7	Summary	58
4	Estimation of IFF of speech signals using TQWT-FB	61
4.1	Introduction	61
4.2	Proposed methodology for IFF estimation of speech signals	63
4.2.1	Speech signal decomposition by TQWT-FB	63
4.2.2	TDS section	65
4.2.3	SFFC extraction unit	65
4.2.4	Computation of IFF using the Hilbert transform	67
4.3	Performance evaluation	67
4.4	Simulation results	67
4.5	Discussion	71
4.6	Summary	73
5	Screening of sleep apnea from ECG signals using TQWT-FB	76
5.1	Introduction	76
5.2	Database	80
5.3	Proposed method	82
5.3.1	Preprocessing unit	83
5.3.2	TQWT-FB design	83
5.3.3	Computation of features and ranking	85
5.3.4	Classification	88
5.4	Performance measures	90

5.5	Simulation results	91
5.6	Discussion	93
5.7	Summary	97
6	Classification of epileptic EEG signals using TQWT-FB	99
6.1	Introduction	99
6.1.1	Background	99
6.1.2	Literature review	100
6.1.3	Overview of proposed method	104
6.2	Database	105
6.3	Proposed method	105
6.3.1	TQWT-FB design	107
6.3.2	Feature computation	107
6.3.3	Classification	110
6.4	Performance measure	110
6.5	Simulation results	111
6.6	Discussion	113
6.7	Summary	119
7	Focal EEG signal detection based on TQWT-FB	122
7.1	Introduction	122
7.2	Database	125
7.3	Proposed method	125
7.3.1	TQWT-FB design	125
7.3.2	Feature extraction	127
7.3.3	Feature ranking	128
7.3.4	Classification	128
7.4	Results and discussion	131
7.5	Summary	134

8 Automated classification of hand movements using TQWT-FB with surface EMG signals	138
8.1 Introduction	138
8.2 Database	141
8.3 Proposed method	143
8.3.1 Cross-covariance of sEMG signals	143
8.3.2 Design of TQWT-FB	144
8.3.3 Features computation and ranking	144
8.3.4 Classification	147
8.4 Performance measure	149
8.5 Simulation results	149
8.6 Discussion	160
8.7 Summary	164
9 Conclusion and future work	166
9.1 Conclusion	166
9.2 Future work	168
LIST OF PUBLICATIONS	201

List of Figures

1.1	The effect of Q -factor for TQWT based decomposition at redundancy rate $R=9$ and levels of decomposition $D=10$: (a) Wavelet corresponding to $Q=1$, (b) Wavelet corresponding to $Q=3$, (c) Frequency response of sub-bands corresponding to wavelet for $Q=1$, and (d) Frequency response of sub-bands corresponding to wavelet for $Q=3$	9
1.2	Block diagram of a TCFB.	9
1.3	Block diagram to show the implementation of TQWT using TCFB. .	10
2.1	TQWT array for design of TQWT-FB based on method I.	23
2.2	TQWT-FB designed from method I	25
2.3	TQWT array for design of TQWT-FB based on method II.	26
2.4	TQWT-FB designed from method II	27
3.1	Block diagram of the proposed method for cross-term reduction in WVD	36
3.2	Frequency response of TQWT-FB	37
3.3	Different stages of TDS section: (a) A sub-band signal from i^{th} sub-band (b) Computed $FC_i[n]$ (c) the normalized $dFC_i[n]$ and TH value (shown in red) (d) variable $F_i[n]$ (e) first segmented component, and (f) second segmented component	39

3.4 Plot of the signals used in simulation study: (a) Multi-component signal with two linear FM chirp ($s_1[n]$), (b) Multi-component signal with a linear FM chirp and a non-linear FM chirp ($s_2[n]$), (c) Bat echo signal ($s_3[n]$), (d) Multi-component signal with two time-limited and band-limited pulses ($s_4[n]$). 44

3.5 The T-F representation based on WVD of the signals used in simulation study: (a) Multi-component signal with two linear FM chirp ($s_1[n]$), (b) Multi-component signal with a linear FM chirp and a non-linear FM chirp ($s_2[n]$), (c) Bat echo signal ($s_3[n]$), (d) Multi-component signal with two time-limited and band-limited pulses ($s_4[n]$). 45

3.6 T-F representation based on the WVD of $s_1[n]$ at different SNRs: Proposed method; (a) Clean, (b) SNR = 20 dB, (c) SNR = 10 dB, (d) SNR = 0 dB, Fourier-Bessel series expansion based method; (e) Clean, (f) SNR = 20 dB, (g) SNR = 10 dB, (h) SNR = 0 dB, FB based method; (i) Clean, (j) SNR = 20 dB, (k) SNR = 10 dB, (l) SNR = 0 dB. 47

3.7 T-F representation based on the WVD of $s_2[n]$ at different SNRs: Proposed method; (a) Clean, (b) SNR = 20 dB, (c) SNR = 10 dB, (d) SNR = 0 dB, Fourier-Bessel series expansion based method; (e) Clean, (f) SNR = 20 dB, (g) SNR = 10 dB, (h) SNR = 0 dB, FB based method; (i) Clean, (j) SNR = 20 dB, (k) SNR = 10 dB, (l) SNR = 0 dB. 48

3.8 T-F representation based on the WVD of $s_3[n]$ at different SNRs: Proposed method; (a) Clean, (b) SNR = 20 dB, (c) SNR = 10 dB, (d) SNR = 0 dB, Time-order based method; (e) Clean, (f) SNR = 20 dB, (g) SNR = 10 dB, (h) SNR = 0 dB, FB based method; (i) Clean, (j) SNR = 20 dB, (k) SNR = 10 dB, (l) SNR = 0 dB. 49

3.9	T-F representation based on the WVD of $s_4[n]$ at different SNRs: Proposed method; (a) Clean, (b) SNR = 20 dB, (c) SNR = 10 dB, (d) SNR = 0 dB, Fourier-Bessel series expansion based method; (e) Clean, (f) SNR = 20 dB, (g) SNR = 10 dB, (h) SNR = 0 dB, FB based method; (i) Clean, (j) SNR = 20 dB, (k) SNR = 10 dB, (l) SNR = 0 dB.	50
3.10	WVD based T-F representation of clean signal ($s_1[n]$) using proposed method with different values of TH: (a) TH = 0.001, (b) TH = 0.01, (c) TH = 0.05, (d) TH = 0.07, (e) TH = 0.1, (f) TH = 0.2, (g) TH = 0.35, (h) TH = 0.4, (i) TH = 0.5.	51
3.11	WVD based T-F representation of clean signal ($s_2[n]$) using proposed method with different values of TH: (a) TH = 0.001, (b) TH = 0.01, (c) TH = 0.05, (d) TH = 0.07, (e) TH = 0.1, (f) TH = 0.2, (g) TH = 0.35, (h) TH = 0.4, (i) TH = 0.5.	52
3.12	WVD based T-F representation of clean signal ($s_3[n]$) using proposed method with different values of TH: (a) TH = 0.001, (b) TH = 0.01, (c) TH = 0.05, (d) TH = 0.07, (e) TH = 0.1, (f) TH = 0.2, (g) TH = 0.35, (h) TH = 0.4, (i) TH = 0.5.	53
3.13	WVD based T-F representation of clean signal ($s_4[n]$) using proposed method with different values of TH: (a) TH = 0.001, (b) TH = 0.01, (c) TH = 0.05, (d) TH = 0.07, (e) TH = 0.1, (f) TH = 0.2, (g) TH = 0.35, (h) TH = 0.4, (i) TH = 0.5.	54
4.1	Block diagram of the proposed method for determining IFF from speech signals	64
4.2	TQWT-FB designed for determination of IFF from speech signals . .	64
4.3	Obtained mean DA (%) for different value of F_{TH} in different cases .	69

4.4	(a) Speech signal in case 1 (b) obtained SFFC from proposed method, obtained IFF (red) by (c) Proposed method, (d) MBSC method, (e) AC based method, and (f) CC based method. Reference IFF (blue and dashed) is shown in (c) to (f).	70
4.5	(a) Speech signal in case 2 (b) obtained SFFC from proposed method, obtained IFF (red) by (c) Proposed method, (d) MBSC method, (e) AC based method, and (f) CC based method. Reference IFF (blue and dashed) is shown in (c) to (f).	70
4.6	(a) Speech signal in case 3 (b) obtained SFFC from proposed method, obtained IFF (red) by (c) Proposed method, (d) MBSC based method, (e) AC based method, and (f) CC based method. Reference IFF (blue and dashed) is shown in (c) to (f).	71
5.1	The segment of (a) non-apneic ECG signal and (b) apneic ECG signal.	81
5.2	Block diagram of proposed method for automated detection of apneic segments of ECG signal.	82
5.3	Designed TQWT-FBs: (a) FB 1 and (b) FB 2.	84
5.4	The box plot of CCE computed for FB 1 from sub-band signals from (a) sub-band 1 and sub-band 2, (b) sub-band 2 and sub-band 3, (c) sub-band 3 and sub-band 4, (d) sub-band 4 and sub-band 5, (e) sub-band 5 and sub-band 6, (f) sub-band 6 and sub-band 7.	86
5.5	The box plot of CCE computed for FB 1 from sub-band signals from (a) sub-band 1 and sub-band 7, (b) sub-band 2 and sub-band 6, (c) sub-band 3 and sub-band 5.	87
5.6	The box plot of CCE computed for FB 2 from sub-band signals from (a) sub-band 1 and sub-band 2, (b) sub-band 2 and sub-band 3, (c) sub-band 3 and sub-band 4, (d) sub-band 4 and sub-band 5, (e) sub-band 5 and sub-band 6, (f) sub-band 6 and sub-band 7, (g) sub-band 7 and sub-band 8, (h) sub-band 8 and sub-band 9.	87

5.7	The box plot of CCE computed for FB 2 from sub-band signals from (a) sub-band 1 and sub-band 9, (b) sub-band 2 and sub-band 8, (c) sub-band 3 and sub-band 7, (d) sub-band 4 and sub-band 6.	88
5.8	Obtained ACC (%) by different classifiers when FB 1 is considered in proposed method	91
5.9	Obtained ACC (%) by different classifiers when FB 2 is considered in proposed method	92
6.1	The EEG signal from (a) F class, (b) N class, (c) S class, (d) O class, and (e) Z class	106
6.2	Block diagram for the detection of epileptic EEG signals.	106
6.3	TQWT-FB used in proposed method for the classification of seizure, seizure-free, and normal EEG signals.	107
6.4	The box plot of CIP computed from sub-band signals from (a) sub-band 3 and sub-band 4, (b) sub-band 3 and sub-band 5, (c) sub-band 3 and sub-band 6, and (c) sub-band 3 and sub-band 7.	109
6.5	Statistical analysis (mean and SD) of features computed in (Tzallas et al, 2007).	113
6.6	Statistical analysis (mean and SD) of (a) real part of features and (b) imaginary part of features computed in (Peker et al, 2016).	114
6.7	Statistical analysis (mean and SD) of computed (a) W features, (b) X features, (c) Y features, and (d) Z features, in (Tiwari et al, 2017).	114
6.8	Statistical analysis (mean and SD) of features computed in (Bhattacharyya et al, 2017b).	115
6.9	Statistical analysis (mean and SD) of features computed in our proposed method.	115
7.1	Plot of "x" and "y" pair of focal EEG signals	126
7.2	Plot of "x" and "y" pair of non-focal EEG signals	126
7.3	Block diagram for the detection of focal EEG signals.	127

7.4	Variation of ACC with respect to number of features for different feature ranking methods obtained with FB 1.	132
7.5	Variation of ACC with respect to number of features for different feature ranking methods obtained with FB 2.	132
8.1	Basic hand movements. (a) cylindrical (CY), (b) hook (HO), (c) lateral (LA), (d) palmar (PA), (e) spherical (SP), and (f) tip (TI) . .	141
8.2	The sEMG signal corresponding to (a) CY acquired from electrode 1, (b) CY acquired from electrode 2, (c) HO acquired from electrode 1, (d) HO acquired from electrode 2, (e) LA acquired from electrode 1, (f) LA acquired from electrode 2, (g) PA acquired from electrode 1, (h) PA acquired from electrode 2, (i) SP acquired from electrode 1, (j) SP acquired from electrode 2, (k) TI acquired from electrode 1, and (l) TI acquired from electrode 2.	142
8.3	Block diagram of proposed method for basic hand movements classification.	143
8.4	Assigned Q -factor values for different TQWT blocks.	144
8.5	Assigned D values for different TQWT blocks.	145
8.6	The designed TQWT-FB used in our proposed method.	145
8.7	Statistical analysis (mean and SD) of features for S1 data.	153
8.8	Statistical analysis (mean and SD) of features for S2 data.	154
8.9	Statistical analysis (mean and SD) of features for S3 data.	154
8.10	Statistical analysis (mean and SD) of features: (a) F1 to F40, (b) F41 to F80, and (c) F81 to 121, for S4 data.	155
8.11	Statistical analysis (mean and SD) of features: (a) F1 to F40 and (b) F41 to F79, for S5 data.	156
8.12	Illustration of web-based application of the proposed model using IOT.	164

List of Tables

3.1	Chosen Q -factor values and sub-bands in the design of TQWT-FB . . .	37
3.2	Normalized Rényi entropy measure for different methods for cross-terms reduction in the WVD based T-F representation	51
4.1	Chosen values of Q -factor and D in the design of TQWT-FB	65
4.2	Percentage GEs for different methods for estimation of IFF of speech signals	70
5.1	The chosen value of TQWT parameters for FB 1.	84
5.2	The chosen value of TQWT parameters for FB 2.	85
5.3	Statistical analysis of features obtained by computing CCE with kernel size equal to 0.5.	94
5.4	Comparison of proposed method with other existing techniques using the same database.	95
6.1	Chosen values Q -factor and D in the design of TQWT-FB	108
6.2	Obtained ACC for different segment length	111
6.3	Sub-bands used to compute ranked features	112
6.4	Summary of automated detection of seizure, seizure-free, and normal EEG signals using the same database.	113
7.1	Classification performance measure parameters based on the maximum ACC obtained with 50 focal and 50 non-focal EEG signals on selected values from the range of RBF kernel and MCE parameters. .	131

7.2	Classification performance measure parameters based on the maximum ACC obtained with 3750 focal and 3750 non-focal EEG signals on selected parameters of MCE.	131
7.3	Classification performance measure parameters based on the maximum ACC obtained with feature ranking methods for 3750 focal and 3750 non-focal EEG signals.	133
7.4	Comparison of the classification performance parameters for the proposed methodology with the existing methodologies.	134
7.5	Comparison of the methodology of compared method and proposed method for focal EEG signal detection.	135
8.1	ACC(%) obtained for Case-A to Case-F with change in k_f	151
8.2	ACC(%) obtained for Case-G with change in k_r and k_f	151
8.3	ACC(%) obtained for Case-H with change in k_r and k_f	152
8.4	ACC(%) obtained for Case-I with change in k_r and k_f	152
8.5	Results of highest ACC obtained for each subject for different values of k_c and NORF.	153
8.6	The p -values of all features extracted from S1 data.	157
8.7	The p -values of all features extracted from S2 data.	157
8.8	The p -values of all features extracted from S3 data.	157
8.9	The p -values of all features extracted from S4 data.	158
8.10	The p -values of all features extracted from S5 data.	158
8.11	Confusion matrix obtained for the proposed method using S1 data.	159
8.12	Confusion matrix obtained for the proposed method using S2 data.	159
8.13	Confusion matrix obtained for the proposed method using S3 data.	159
8.14	Confusion matrix obtained for the proposed method using S4 data.	159
8.15	Confusion matrix obtained for the proposed method using S5 data.	160
8.16	Comparison of proposed method based on ACC(%) with other existing methods using the basic hand movements database (Sapsanis et al, 2013b).	160

List of Abbreviations

AC:	Autocorrelation
ACC:	Accuracy
AM:	Amplitude modulation
ARM:	Arithmetic mean
AWGN:	Additive white Gaussian noise
BW :	Bandwidth
CC:	Cross-correlation
CCE:	Centered correntropy
CIP:	Cross-information potential
csEMG:	Cross-covariance of surface electromyogram
CY:	Cylindrical
D :	Levels of decomposition
DA:	Detection accuracy
DTCWT:	Dual tree complex wavelet transform
ECG:	Electrocardiogram
EEG:	Electroencephalogram
EGG:	Electroglottograph
EMD:	Empirical mode decomposition
EMG:	Electromyogram
EPH:	Exoskeleton prosthetic hand
EVD:	Eigenvalue decomposition
EVDHM-HT:	Eigenvalue decomposition of Hankel matrix and Hilbert transform
FB:	Filter-bank

f_c :	Centre frequency
FFC:	Fundamental frequency component
FM:	Frequency modulation
FN:	False negative
FP:	False positive
F_s :	sampling rate
FT:	Fourier transform
GE:	Gross error
HC:	High pass channel
HHT:	Hilbert-Huang transform
HMM:	Hidden Markov model
HO:	Hook
HPF:	High pass filter
IEVDHM-HT:	Improved eigenvalue decomposition of Hankel matrix and Hilbert transform
IF:	Instantaneous frequency
IFF:	Instantaneous fundamental frequency
IMF:	Intrinsic mode function
IOT:	Internet of things
IP:	Information potential
k -NN:	k -nearest neighbour
KRE:	Kraskov entropy
LA:	Lateral
LC:	Low pass channel
LFR:	Low frequency region
LLCFS:	Local learning-based clustering feature selection
LPF:	Low pass filter
LS-SVM:	Least squares support vector machine
M:	Number of tunable- Q wavelet transform blocks
MAXV:	Maximum value

MBSC: Multi-band summary correlogram
MCC: Matthews correlation coefficient
MCE: Mixture correntropy
MCFS: Multi-cluster feature selection
MD: Median
MINV: Minimum value
MLP: Multilayer perceptron
NORF: Number of ranked features
NPV : Negative predictive value
 p : Probability
PA: Palmar
PPV: Positive predictive value
 Q : Quality
R: Redundancy factor
RBF: Radial basis function
RF: Random forest
SD: Standard deviation
sEMG: Surface electromyogram
SEN: Sensitivity
SFFC: Scaled fundamental frequency extraction
SMO: Sequential minimal optimization
SNR: Signal to noise ratio
SP: Spherical
SPE: Specificity
 S_pO_2 : Saturation of peripheral oxygen
STFT: Short time Fourier transform
SVM: Support vector machine
T-F: Time-frequency
TBN: Tunable- Q wavelet transform block number
TCFB: Two-channel filter-bank

TDS:	Time-domain segmentation
TH:	Threshold
TI:	Tip
TN:	True negative
TP:	True positive
TQWT:	Tunable- Q wavelet transform
TQWT-FB:	Tunable- Q wavelet transform based filter-bank
WEKA:	Waikato environment for knowledge analysis
WT:	Wavelet transform
WVD:	Wigner-Ville distribution

Chapter 1

Introduction

The non-stationary signals consist of time-varying statistical parameters. The parameters are time-varying because they are generated through time-varying system. They can be observed in many fields such as radar, communication, mechanical engineering, etc. Some commonly known non-stationary signals such as speech signals and physiological signals can be found in our day to day life. The speech signal produces when human speaks and it consists of several components such as fundamental frequency component (FFC), harmonics of FFC, etc (Oshaughnessy, 2000). Similarly physiological signals are obtained from the human body and they differ in frequency content, oscillatory behaviour, etc (Reilly and Lee, 2010).

Hence, there can be several hidden and meaningful information present in the non-stationary signals. The hidden information can be the number of components present in the signal, instantaneous frequency (IF) of components, energy of components, etc.

Though the extraction of hidden information from non-stationary signals is a difficult task, the processing of signal can be faster and easy through its sparse representation where few coefficients provides the hidden information (Mallat, 2009). To extract information from non-stationary signals, there are many methods proposed in literature. Some methods are time-frequency (T-F) based where the amplitude or energy of the signal is represented in two dimensional T-F plane. However, the res-

olution and distortion appear on T-F plane depends on the applied method. Other methods are based on decomposition of non-stationary signals. The decomposition methods decompose non-stationary signals into less complex signals from where it is easy to analyse them and extract meaningful information.

1.1 Non-stationary signals analysis techniques

The analysis of non-stationary signal can be achieved from T-F based methods when model of signal is not available (Sejdi et al, 2009). The major aim of T-F representation of non-stationary signal is to provide energy concentration of the signal in frequency-domain with respect to each instant of time (Cohen, 1995). Ideally, T-F representation of non-stationary signal must provide information of frequency components at any instant of time (Grochenig, 2001; Stankovic, 1994). The efficacy of the method to generate T-F representation, depends on the T-F resolution.

Depending upon the approach for the analysis of non-stationary signals, the T-F representation can be classified in two classes (Sejdi et al, 2009). In the first class, there is a finite energy basis function which is localized in time-domain and frequency-domain. The representation of signal in T-F domain is obtained by modulating, scaling, and translating these basis functions. In this class, a signal $s(t)$ is mathematically expressed in T-F representation as follows (Sejdi et al, 2009):

$$TF_s(t, \omega) = \int_{-\infty}^{\infty} s(\tau) \xi_{t, \omega}^*(\tau) d\tau \quad (1.1)$$

Here, $\xi_{t, \omega}$ is the basis function and $*$ indicates the complex conjugate. The short time Fourier transform (STFT) (Grochenig, 2001), wavelet transform (WT) (Daubechies, 1992; Mallat, 1999) and matching pursuit (Mallat, 1999; Mallat and Zhang, 1993), etc are some T-F representations of this class.

The STFT method computes Fourier transform (FT) of the windowed version

of signal (Grochenig, 2001). The entire signal is segmented by a fixed length window and hence the resolution of STFT depends on the length of the window. When the magnitude of the STFT is squared, then it generates a spectrogram (Boashash, 2003). The resolution in STFT and spectrogram is limited by the length of the window. To overcome limitation in STFT and spectrogram, the WT is proposed in which resolution in time-domain and frequency-domain can be varied and hence multi-resolution analysis can be achieved (Rioul and Vetterli, 1991). A non-stationary signal may have low and high frequency components. Thus good frequency-domain resolution can be achieved at low frequencies and good time-domain resolution can achieve at high frequencies through multi-resolution analysis (Rioul and Vetterli, 1991). Here, the basis functions known as wavelets are used to represent the signal. The wavelets are well localized in time-domain and frequency-domain and has zero mean. In discrete WT, the wavelets are scaled by factor of two to represent the signal. Whereas in continuous WT, the wavelets can be scaled by any real scale factor.

Most of the WT do not provide much flexibility to tune the quality (Q)-factor of wavelet except continuous WT (Selesnick, 2011c). The tunable- Q WT (TQWT) is proposed in (Selesnick, 2011c), where Q -factor can be tuned to generate different mother wavelets according to oscillatory nature of the signal. Apparently, the oscillatory nature can be quantified by Q -factor (Selesnick, 2011a). Similar to TQWT, the flexible analytic WT is proposed in (Bayram, 2013). Here, the Q -factor, the dilation factor, and the factor of redundancy can be easily tuned for analysis of signal.

Other than STFT and WT, the matching pursuit algorithm is another method of class one for signal representation in T-F plane. It represents the signal in the form of linear expansion of waveforms. These waveforms are chosen from the library such as Gabor functions in a way that they match best with the signals T-F structure (Mallat and Zhang, 1993).

The second class of T-F representation is the Cohens class of T-F distribution as

proposed in (Cohen, 1966). This class of T-F representation is quadratic in nature as it involves computation of instantaneous autocorrelation (AC) of the signal $s(t)$ to represent T-F distribution. The mathematical representation of such kind of T-F representation is given as follows (Sejdi et al, 2009):

$$TFD_s(t, \omega) = \frac{1}{4\pi^2} \int_{-\infty}^{\infty} \int_{-\infty}^{\infty} \int_{-\infty}^{\infty} s(v + \frac{1}{2}\tau) s^*(v - \frac{1}{2}\tau) \psi(\theta, \tau) e^{-j\theta t - j\tau\omega + j\theta v} dv d\tau d\theta \quad (1.2)$$

Here, $\psi(\theta, \tau)$ is the kernel function in two dimension. The change in kernel function generates different types of T-F distributions in Cohens class. The Wigner-Ville distribution (WVD) (Boashash, 2003), Born-Jordan (Cohen, 1995), Choi-Williams distribution (Choi and Williams, 1989), etc. are some T-F distributions in Cohens class. The WVD has best resolution in T-F representation of signal.

The analysis of non-stationary signal is also accomplished with several decomposition techniques in literature. The empirical mode decomposition (EMD) decomposes the signal in to number of intrinsic mode functions (IMFs) through sifting process (Huang et al, 1998). It is an iterative process and there is no mathematical model of EMD. Also there is the problem of mode mixing in EMD in which intermittency is present in some region of signal (Huang et al, 1999; Oweis and Abdulhay, 2011). To overcome this problem, the authors in (Wu and Huang, 2009), proposed ensemble EMD. In this method, a white noise of fixed variance is added to the signal, and then IMFs are extracted as the average of some trailed ensembles. Another extension of EMD is the multivariate EMD as proposed in (Rehman and Mandic, 2010). It is developed for the multivariate signals. Then a decomposition technique termed as variational mode decomposition is proposed in (Dragomiretskiy and Zosso, 2014). It decomposes a real signal into finite set of components. The generated components satisfy the definition of new IMFs as explained in (Daubechies et al, 2011). This method is iterative in nature and generated components are localized around their centre frequency (f_c).

The other popular decomposition technique to analyse non-stationary signal is Hilbert-Huang transform (HHT) (Huang et al, 1998). In this method, first the IMFs are obtained by applying EMD on the signal. Then, the Hilbert spectrum of obtained IMFs is obtained. The Hilbert spectrum is obtained by converting the IMF into an analytic signal, and then computing its instantaneous amplitude and instantaneous phase.

The method proposed in (Jain and Pachori, 2015) decomposes multi-component non-stationary signals into amplitude modulated (AM) and frequency modulated (FM) mono-components. The methodology involve the eigenvalue decomposition (EVD) of square Hankel matrix in iterative way. The extracted AM-FM components are narrow band in nature. Based on this decomposition technique, a T-F representation is developed in (Sharma and Pachori, 2018b) and termed as improved EVD of Hankel matrix and Hilbert transform (IEVDHM-HT). This method proves to better than EVD of Hankel matrix and Hilbert transform (EVDHM-HT) (Sharma and Pachori, 2017b) in terms of T-F resolution.

Recently, the decomposition of non-stationary signals through FT based method is suggested in (Singh et al, 2017). Here, authors proposed a novel Fourier decomposition method which decomposes the signal into Fourier intrinsic band functions which are band limited. The analysis of non-stationary signals through decomposition is also accomplished by filtering in literature. The Gabors filtering as suggested in (Mertins, 1999), is used to estimate amplitude envelope and IF of AM-FM signal. However, the filtering technique induces modulation in phase and amplitude. To overcome this problem, the Fourier-Bessel coefficients are applied for signal extraction in (Pachori and Sircar, 2010). This methodology requires the identification of Fourier-Bessel coefficients manually.

1.2 Classification of physiological signals

The analysis of non-stationary signals can give many meaningful information also known as features regarding signal characteristics. The characteristics of the non-stationary signal depend on the source from which it is originated. Therefore, the extracted features can be useful in classifying the non-stationary signals.

The physiological signals are also non-stationary signals. These signals are obtained from human body (Broek and Spitters, 2013). Due to the electrochemical variations in the neurons, muscle, and gland cells, these signals are transmitted from their source to the skin of body (Broek and Spitters, 2013). The common physiological signals in electrical signal form are electroencephalogram (EEG), electrocardiogram (ECG), and electromyography (EMG). The EEG signals are obtained from the human brain and it carries the electrical activity of the brain. Similarly, the ECG signals contains the electrical activity of heart and EMG signals carry the electrical activity of muscles.

The disease in the human results in the change in the characteristics of these physiological signals. The visual inspection of these signals in order to detect disease for diagnosis is time consuming job and also not reliable. On the other hand, advanced signal processing techniques can be used to develop a computer-aided automated system for diagnosis of disease. The advanced signal processing technique can obtain features from physiological signals either by T-F analysis or through decomposition technique. The T-F representation can provide features like energy concentration, amplitude levels in T-F bands, wavelets, etc (Sejdi et al, 2009). The decomposition technique decompose complex physiological signals in to less complex signals from where feature extraction is simple. From decomposed signals, features like energy of decomposed signals, oscillatory nature of decomposed signals, etc, can be used for classification.

While developing a computer-aided system, the extraction of features for classification is not enough. Some extracted features may be not significant and they even

might degrade the classifiers performance. Therefore, it is necessary to rank the features according to their significance level. This step also reduces the complexity of the system as classifier can classify signals more accurately with less number of significant features.

The last stage of computer-aided system is the classification stage. It is an important stage as decision regarding the class of the signal is made here. The diagnosis is then made according to the decision made by classifiers. In literature, the classifiers are support vector machine (SVM), least squared SVM (LS-SVM), tree based classifiers, neural network, etc, are used (Acharya et al, 2011c; Pachori and Patidar, 2014; Sharma and Pachori, 2015; Sharma et al, 2017b).

1.3 Overview of Tunable- Q wavelet transform

Since the work in this thesis involve filter-banks (FBs) developed from TQWT, the overview of TQWT is presented in this section.

The TQWT decomposes a signal into the number of sub-band signals. It has three governing parameters termed as TQWT parameters. They are level of decomposition (D), Q -factor, and redundancy factor (R) (Selesnick, 2011c). The role of these parameters while applying TQWT on a signal is as follows:

1. Level of decomposition (D): To implement TQWT, there is D number of two-channel FBs (TCFBs) required (Selesnick, 2011c). When TQWT is applied on a signal, each TCFB except one produces one sub-band. One TCFB produces two sub-bands. Therefore, the signal is decomposed into $D + 1$ sub-bands.
2. Q -factor: Depending upon the nature of signal, the Q -factor in TQWT can be modified. For high and low oscillatory signals, it is recommended to set the value of Q -factor high and low respectively (Selesnick, 2011c). By changing the Q -factor, the amount of oscillations in wavelet changes which results in the creation of different mother wavelets. The Q – factor = $\frac{f_c(i)}{BW(i)}$, where $f_c(i)$ is the f_c and

$BW(i)$ is the bandwidth (BW) of i^{th} sub-band. Here $1 \leq i \leq D+1$. Therefore, change in value of Q -factor affects the value of $f_c(i)$ and $BW(i)$ (Selesnick, 2011c).

3. Redundancy factor (R): The parameter R governs the localization of wavelet in the time-domain (Selesnick, 2011c). In the frequency domain, it controls the overlapping among the sub-bands (Patidar et al, 2015b). It is mathematically defined as $R = \frac{Y}{1-X}$ (Selesnick, 2011c). Here X and Y are the scale factors of TCFB's low pass filter (LPF) and TCFB's high pass filter (HPF), respectively. They are explained in next few paragraphs.

The effect of parameter Q -factor at two values 1 and 3 on wavelet (first sub-band) and frequency responses of the sub-bands for $D = 10$ corresponding to $R = 9$ is shown in Fig. 1.1. The sub-band D i.e. sub-band 10 and sub-band 1 are mentioned in Fig. 1.1(c) and (d).

As mentioned earlier, the TQWT is implemented using TCFBs. The Fig. 1.2 shows a TCFB or analysis FB. The TCFB in Fig. 1.2 has a low pass channel (LC) and high pass channel (HC). The LC consists of a LPF followed by a scale factor (X). Similarly, HC contains a high pass filter HPF whose output is given as input to a scale factor (Y). The frequency response of LPF and HPF depends on the frequency response of Daubechies filter with two vanishing moments (Selesnick, 2011c).

The input signal is given to both LC and HC simultaneously. Thus a TCFB has one input and two outputs (Selesnick, 2011c).

TQWT is implemented by connecting the D number of TCFBs in an iterative way as shown in Fig. 1.3. The connection is such that the output from LC of first TCFB is given as input to second TCFB. Similarly, output from second TCFB's LC is given as input to third TCFB and so on (Selesnick, 2011c). When TQWT is applied on a signal, the signal is given as input to first TCFB. The HC of each TCFB produces a sub-band. Therefore, D sub-bands will be obtained by HC of all TCFB. Also the output from LC of D^{th} TCFB is considered as a sub-band. The sub-band signals from sub-bands can be obtained by applying inverse TQWT (Selesnick,

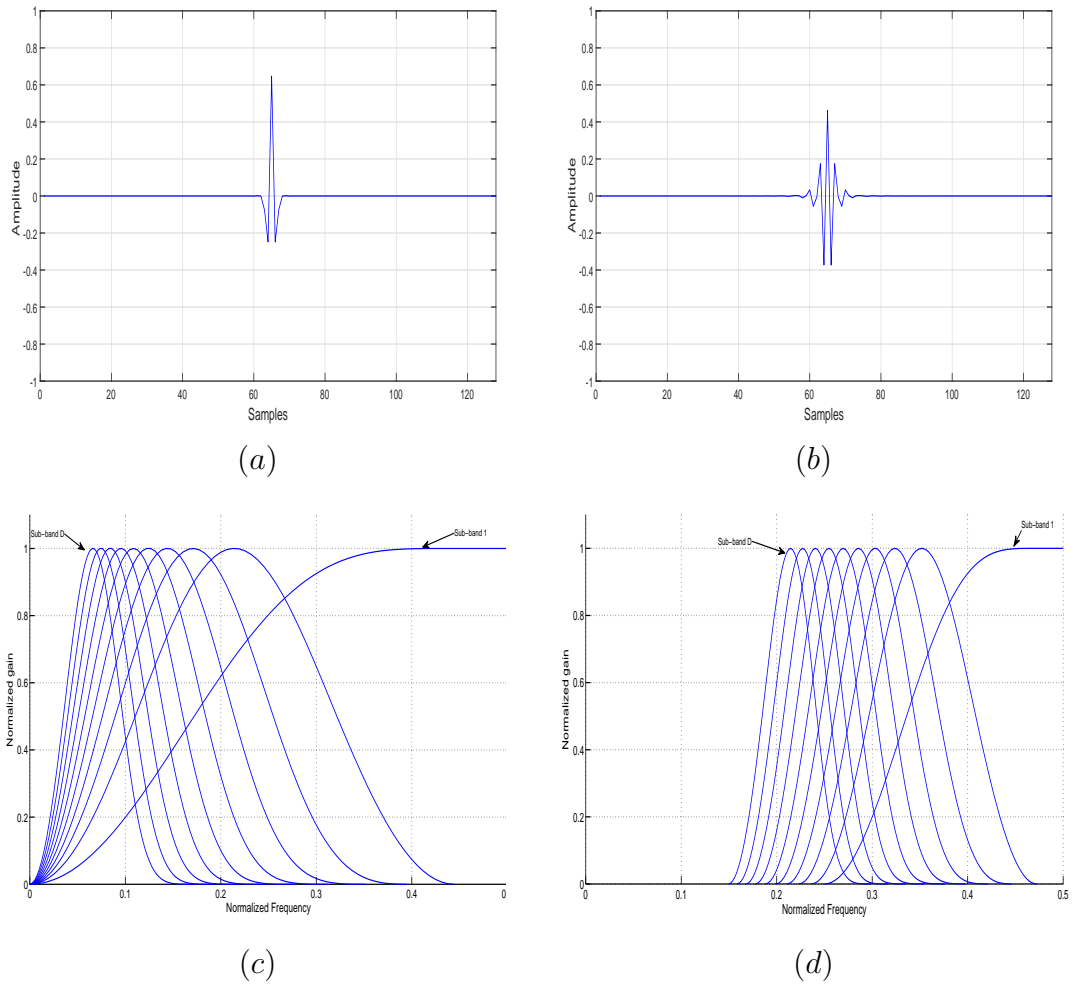


Figure 1.1: The effect of Q -factor for TQWT based decomposition at redundancy rate $R=9$ and levels of decomposition $D=10$: (a) Wavelet corresponding to $Q=1$, (b) Wavelet corresponding to $Q=3$, (c) Frequency response of sub-bands corresponding to wavelet for $Q=1$, and (d) Frequency response of sub-bands corresponding to wavelet for $Q=3$.

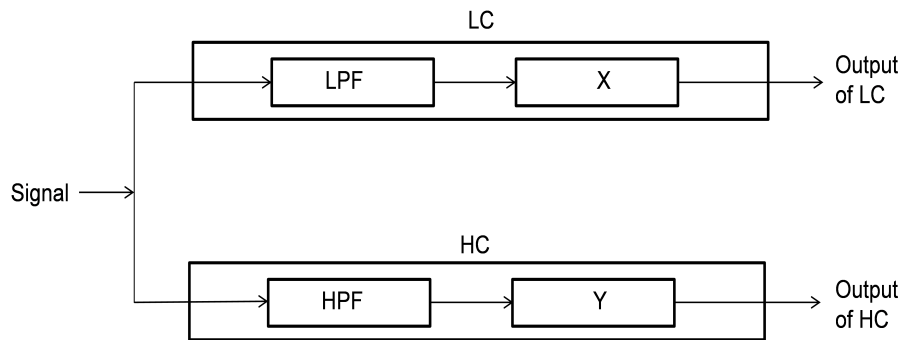


Figure 1.2: Block diagram of a TCFB.

2011b,c). In frequency response of TQWT, there will be $D + 1$ number of sub-bands.

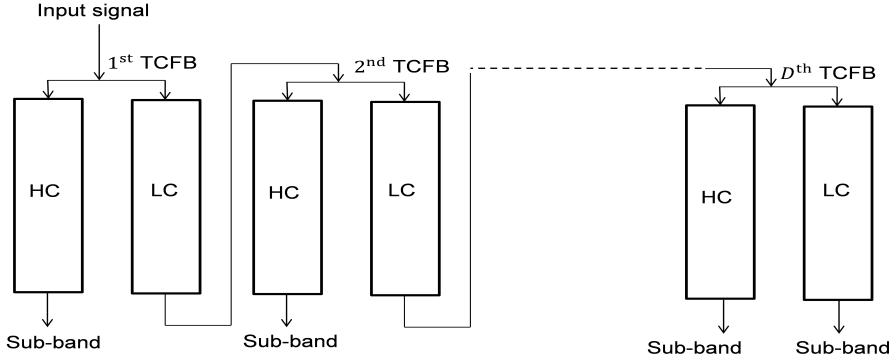


Figure 1.3: Block diagram to show the implementation of TQWT using TCFB.

The highest f_c sub-band as shown in Fig. 1.1 (c) and (d) is sub-band 1 and it is obtained from HC of first TCFB in iterative connection of TCFBs as shown in Fig. 1.3. Similarly the lowest f_c sub-band is sub-band $D + 1$ obtained from LC of D^{th} TCFB. It should be noted that the sub-bands shown in Fig. 1.1(c) and (d) are sub-bands obtained from HC only. Therefore frequency response is zero till 0.15 normalized frequency in Fig. 1.1(d) because there exist sub-band $D + 1$ obtained from LC. The sub-band D shown in Fig. 1.1 (c) and (d) is obtained by HC of D^{th} TCFB.

The scale factors X and Y in TCFB control the $f_c(i)$ and $BW(i)$ of i^{th} sub-band and the value of X and Y depends on the governing parameters Q -factor and R . Their relations are given below (Selesnick, 2011c):

$$f_c(i) = X^i \left(\frac{2 - Y}{4X} \right) F_s \quad (1.3)$$

$$BW(i) = \frac{YX^{i-1}\pi}{2} \quad (1.4)$$

$$X = 1 - \frac{Y}{R} \quad (1.5)$$

$$Y = \frac{2}{Q + 1} \quad (1.6)$$

Here, F_s is the sampling rate. The value of X and Y are related as, $0 < X < 1$, $0 < Y \leq 1$, and $X + Y > 1$ (Selesnick, 2011c). This condition is imposed so that the impulse response of LPF and HPF shall remain localized in time-domain (Selesnick, 2011c). Therefore, before applying TQWT on input signal, the choice of governing parameters should be such that it satisfies the conditions on scale parameters.

The TQWT provide perfect reconstruction of the signal. For perfect reconstruction, the following condition must be true (Selesnick, 2011c):

$$|T_0(\omega)|^2 + |T_1(\omega)|^2 = 1, 0 \leq \omega \leq \pi \quad (1.7)$$

Here, $T_0(\omega)$ and $T_1(\omega)$ are transfer function of LPF and HPF in TCFB, respectively. They are mathematically expressed as follows (Selesnick, 2011c):

$$T_0(\omega) = \begin{cases} 1, & |\omega| \leq (1 - Y)\pi \\ \Theta\left(\frac{\omega + (Y-1)\pi}{X+Y-1}\right), & (1 - Y)\pi < |\omega| < X\pi \\ 0, & X\pi \leq |\omega| \leq \pi \end{cases} \quad (1.8)$$

$$T_1(\omega) = \begin{cases} 0, & |\omega| \leq (1 - Y)\pi \\ \Theta\left(\frac{X\pi - \omega}{X+Y-1}\right), & (1 - Y)\pi < |\omega| < X\pi \\ 1, & X\pi \leq |\omega| \leq \pi \end{cases} \quad (1.9)$$

Here, $\Theta(\omega)$ is the Daubechies filter frequency response with two vanishing moments, which is expressed as follows (Selesnick, 2011c):

$$\Theta(\omega) = \frac{[1 + \cos(\omega)][2 - \cos(\omega)]^{\frac{1}{2}}}{2}, |\omega| \leq \pi \quad (1.10)$$

From (1.8), (1.9), and (1.10), it can be noted that the transfer functions of FBs to implement TQWT are defined directly in frequency-domain and they are not rational (Selesnick, 2011c). In case of rational transfer function, the condition for perfect reconstruction as specified in (1.7) must be true (Selesnick, 2011c).

The scale factors X and Y can be non-rational. In discrete time case, they are implemented based on the length of the signal before scaling and length of the signal after scaling (Selesnick, 2011c). According to (Selesnick, 2011c), $N_0 \approx XN$ and $N_1 \approx YN$, where N is the signal length before scaling, N_0 is the signal length after scaling when scaled by X , and N_1 is the signal length after scaling when scaled by Y . It may be possible that XN and YN are not integers, hence they are rounded off to nearest even integer as follows (Selesnick, 2011c):

$$N_0 = 2\text{round}\left(\frac{X}{2}N\right) \quad (1.11)$$

$$N_1 = 2\text{round}\left(\frac{Y}{2}N\right) \quad (1.12)$$

Then the scale parameters for LPF and HPF in TCFB are N_0/N and N_1/N respectively (Selesnick, 2011c).

The TQWT has been used in the analysis and classification of many non-stationary signals. It has been used in the detection of epilepsy (Bhattacharyya et al, 2017b; Sharma and Pachori, 2017a), focal EEG signals (Bhattacharyya et al, 2017a; Sharma et al, 2017a), coronary artery disease (Patidar et al, 2015a), heart sounds (Patidar and Pachori, 2014), and neuromuscular disease (Joshi et al, 2017).

1.4 Motivation

The analysis of non-stationary signals require advanced signal processing techniques as they are complicated signals. The T-F representation of non-stationary signals presents the spectral and temporal information simultaneously. Several T-F representation methods are proposed in literature. However, the resolution in T-F representation depends on the applied method. The WVD shows the infinite resolution in T-F representation due to absence of averaging over any finite time duration (Boashash, 2003). However, since it is a quadratic distribution, it shows the

cross-terms when the WVD is computed for a multi-component and non-linear FM signals (Boashash, 2003). The cross-terms mislead as auto-terms in the WVD of the signal. The cross-terms can be reduced if the non-stationary signal is decomposed and the WVD of decomposed components are added. This brings motivation to develop a method to reduce cross-terms in the WVD.

The speech signals are also non-stationary signals. The accurate estimation of instantaneous fundamental frequency (IFF) of speech signal is required in many applications such as speech compression (Taori et al, 1995), speaker recognition (Shriberg et al, 2005), text to speech synthesis (Moulines and Charpentier, 1990), etc. The speech signals are multi-component non-stationary signals. They consist of FFC and may be its harmonics in the low frequency region (LFR) of voiced speech signals (Jain and Pachori, 2013). Therefore, it arises a motivation to estimate IFF by separating the FFC from its harmonics in LFR. If speech signal is decomposed in LFR to extract components belonging to FFC, then IFF can be estimated at each sample instant.

In medical science, the physiological signals are important for diagnosis of many diseases. The change in the characteristics of physiological signals depends on the disease of the patient. The visual inspection of these signals by experts to identify disease is laborious and error prone. Therefore, there is need to develop the automated systems for detection and classification of disease through these signals. As these signals are non-stationary, it is difficult to extract hidden inform from them directly. On the other hand, if these signals are decomposed into simpler components, then features can be extracted from decomposed components for detection and classification.

In case of screening of sleep apnea, the ECG signals vary in oscillatory behaviour at some time-intervals for healthy subject and sleep apnea patient (Hassan, 2016). It motivates us to develop a decomposition technique which decomposes ECG signal into different oscillatory signals and then extract features for screening. Another common disease from which many people in world are affected is epilepsy. Epilepsy

is a neurological disorder. The EEG signals can be used to detect this disease. The EEG signals obtained during seizure and seizure-free events, and from normal subjects, differ in characteristics (Andrzejak et al, 2001). However, it is hard to classify them visually. Therefore, it gives motivation to prepare an algorithm in which EEG signals can be decomposed into narrow BW sub-bands, and from the energy level of sub-bands, these signals can be classified. Also among the epileptic patients, more than 60% are affected by focal epilepsy (Gloor and Fariello, 1988; Pati and Alexopoulos, 2010). The area of brain, from where the recorded EEG signal shows first change in ictal EEG signal is termed as focal EEG signal (Andrzejak et al, 2012). Otherwise, remaining brain portions which are not involved in seizure onset provides non-focal EEG signals (Andrzejak et al, 2012). Therefore, a methodology can also be designed in order to classify focal and non-focal EEG signals in order to identify focal epileptic zones.

Other than diagnosis, the advanced signal processing technique can also be applied for rehabilitation. For a hand amputee person, the EMG signals can be acquired from the forearm and can be used to classify different hand movements. However, there are many hand movements and it is a challenging task to identify the changes in surface EMG (sEMG) signals. As there are many hand movements, the sEMG signals can be decomposed into many very narrow BW sub-bands. In this way, many features can be extracted from sub-bands to classify the hand movements.

All the above mentioned problems and their motivations require a decomposition technique. Therefore a FB is developed using TQWT for the decomposition of non-stationary signals. The TQWT is chosen because it gives freedom to vary Q -factor of the wavelet according to the oscillatory nature of signal. The low and high values of Q -factor is suitable to analyse low and high oscillatory signals (Selesnick, 2011c). However, the oscillatory nature of non-stationary signals are different and varies over time. Hence, if only TQWT is used for analysis, then there is need of identifying optimum value of Q -factor which would be suitable to analyse many non-stationary signals. A TQWT based FB (TQWT-FB) consists of many sub-bands whose BW

are narrow and nearly same. These sub-bands are generated by different values of Q -factor. Hence, the entire frequency range of the signal is decomposed into constant BW sub-bands and the obtained sub-band signals from sub-bands differ in oscillatory behaviour.

1.5 Objectives

The objectives of this dissertation are as follows:

- Objective 1: To develop a methodology for reducing the cross-terms in the WVD from TQWT-FB.
- Objective 2: To develop a methodology for estimating IFF of speech signals based on TQWT-FB.
- Objective 3: To develop an automated system for screening of sleep apnea from ECG signals using TQWT-FB.
- Objective 4: To develop an automated system for classification of epileptic seizure EEG signals by applying TQWT-FB.
- Objective 5: To develop a system for automated identification of focal EEG signals based on TQWT-FB.
- Objective 6: To develop an automated system for classification of hand movements from sEMG signals by employing TQWT-FB.

1.6 Contributions

The contributions of this thesis are summarized as follows:

- The WVD of non-stationary signal has the best resolution in time-domain and frequency-domain (Boashash, 2003). However, cross-terms exist in the WVD

if signal is multi-component or non-linearly modulated. A new methodology is proposed to reduce the cross-terms in the WVD using TQWT-FB. The non-stationary signal is decomposed into several narrow and nearly constant BW sub-band signals by TQWT-FB. Then components existing in same sub-band signal but at different time interval are separated by time-domain segmentation (TDS) section. Finally the WVD of segmented components are computed and added to obtain the cross-terms free WVD. The efficacy of proposed method is shown by computing normalized Renyi entropy measure (Sang and Williams, 1995).

- The IFF of speech signal varies with time and proposed methodology estimates IFF at each instant of time. The speech signals are decomposed into narrow BW sub-band signals by TQWT-FB in LFR. Then TDS section separates components lying at different time duration. Then scaled FFC (SFCC) extraction unit chooses those segmented component which is obtained by lowest f_c sub-band at each sample instant. Then SFCC unit performs weighted addition of chosen components in order to reduce the effect of harmonic component. This generates FFC with scaled amplitude. In the final stage, the Hilbert transform is used to compute the IFF of speech signal. The gross error (GE) is computed in order to show efficacy of proposed method.
- An automated system is proposed for the screening of sleep apnea using ECG signals. The proposed methodology deals with two-class classification problem. The methodology identifies the apneic and non-apneic events in each minute of ECG signal. The ECG segment of one minute duration is decomposed by TQWT-FB. Then centered correntropies (CCEs) (Rao et al, 2011) are computed as features from adjacent sub-band signals. The statistical analysis of features is performed using Kruskal-Wallis test (McKight and Najab, 2010). Then features are ranked using student's t-test (Acharya et al, 2015a,b; Box, 1987). After feature ranking, they are fed into classifier. Three classifiers namely multilayer perceptron (MLP) (Lippmann, 1987; Madyastha and

Aazhang, 1994), bagging (Breiman, 1996), and random forest (RF) (Breiman, 2001) are tested. The classifiers are implemented using Waikato environment for knowledge analysis (WEKA) toolbox. Through simulation, it is observed that the RF classifier classifies apneic and non-apneic ECG segments with more accuracy (ACC) than ACC obtained by other classifiers.

- The EEG signals are used for detection of epilepsy. At the time of epilepsy, frequent seizure events occur in epileptic patient. A methodology is designed for the classification of seizure, seizure-free, and normal EEG signals. Hence it deals with three-class classification problem. A TQWT-FB decomposes the EEG signals into sub-band signals. Then, some sub-bands signals are selected from total sub-band signals generated by TQWT-FB for feature computation. The features are obtained by computing cross information potential (CIP) (Xu et al, 2008) from every possible pair from the selected sub-band signals. After computing features, they are ranked using RELIEFF algorithm (Kononenko et al, 1997; Robnik-Sikonja and Kononenko, 2003). The ranking of features shows their significance. In the first step, best rank feature is fed to classifier. Then in next step, best two significant features are fed to classifier and so on. In this way, with fewer features, the classifier shows best ACC and complexity of system reduces.
- A methodology is proposed for the detection of focal and non-focal EEG signals as many patients suffers from focal epilepsy (Gloor and Fariello, 1988; Pati and Alexopoulos, 2010). The EEG signals of focal and non-focal classes are decomposed by proposed TQWT-FB. Then from sub-band signals, mixture correntropy (MCE) features are extracted. These extracted features are ranked and classified by LS-SVM classifier which classifies focal and non-focal EEG signals with good ACC.
- A hand amputee person can perform desired hand movement task through an exoskeleton prosthetic hand (EPH). The controller in the EPH must classify

hand movements accurately according to the sEMG signals obtained from the forearm. The proposed methodology classifies six basic hand movements. The cross-covariance of sEMG signals obtained from two electrodes are computed and termed as cross-covariance of sEMG (csEMG) signal. Then TQWT-FB decomposes the csEMG signal into narrow *BW* sub-band signals. In the next stage, the Kraskov entropy (KRE) (Kraskov et al, 2004; Veselkov et al, 2010) as feature is computed from each sub-band signal. The obtained features are then ranked. Three ranking methods namely local learning-based clustering feature selection (LLCFS) (Zeng and Cheung, 2011), multi-cluster feature selection (MCFS) (Cai et al, 2010), and RELIEFF algorithm (Kononenko et al, 1997; Robnik-Sikonja and Kononenko, 2003) are tested. After ranking of features, the classifier classifies six hand movements. In this stage, three classifiers are tested. They are C4.5 classifier (Ruggieri, 2002), sequential minimal optimization (SMO) classifier (Platt, 1998), and k -nearest neighbour (k -NN) classifier (Aha et al, 1991). Through simulation, it is observed that the RELIEFF ranking method and k -NN classifier in proposed model classify hand movements with high ACC. The proposed method can also be implemented as web based application in internet of things (IOT) technology. For each hand movement, the sEMG signals can be collected in cloud and train the proposed model. In this way, proposed model can be improved and EPH can perform hand movement more accurately.

1.7 Organization of the thesis

The rest of the thesis is organized as follows:

- In the chapter 2, The proposed FB termed as TQWT-FB is explained.
- The cross-terms exist in WVD due to it's quadratic nature. Therefore, a methodology based on TQWT-FB is proposed in chapter 3 to reduce the

cross-terms in WVD. The efficacy of proposed method in terms of normalized Rényi entropy is shown and compared with other methods in this chapter.

- A methodology based on TQWT-FB for the estimation of IFF of speech signals is presented in chapter 4. The proposed TQWT-FB decomposes the speech signals and then FFC is extracted for estimation of IFF. The performance of proposed method is evaluated in terms of GE in percentage and compared with other methods.
- In chapter 5, a methodology is proposed for screening of sleep-apnea from segments of ECG signals. The chapter includes segmentation of ECG signal, then its decomposition by designed TQWT-FB, then computation and ranking of CCE features, and finally classification of apneic and non-apneic ECG segments to screen the sleep apnea. The comparison of proposed method in terms of ACC with other existing methods, is also shown in this chapter.
- The chapter 6 addresses classification of seizure, seizure-free, and normal EEG signals. The EEG signals from each class is decomposed by a designed TQWT-FB. Then CIP features are computed from decomposed sub-band signals. Then the RF classifier is used to classify EEG signals. The performance of proposed method and its comparison with other existing methods are presented in this chapter.
- The classification of focal and non-focal EEG signals using TQWT-FB is shown in the chapter 7. This chapter presents the decomposition of EEG signals by TQWT-FB, features extraction using MCE, and application of LS-SVM classifier for classification. The obtained results are compared and shown in this chapter.
- This chapter 8 shows the application of designed TQWT-FB in rehabilitation. This chapter presents a methodology for design of controller in EPH which would perform desired hand movements of a hand amputee person by

extracting sEMG signals. The classification of sEMG signals by TQWT-FB, computation of KRE features and its ranking, and finally classification of hand movements are presented in this chapter.

- The entire work of this thesis along with research work for future is concluded in chapter 9.

Chapter 2

Tunable- Q wavelet transform based filter-bank

2.1 Introduction

To analyse non-stationary signals which vary in oscillatory behaviour by TQWT, there is need of optimal value of Q -factor. This is because, we can use only one value of Q -factor in TQWT and the mother wavelet generated by chosen Q -factor may not be suitable to analyse all signals which vary in their oscillatory behaviour. On the other hand, the sub-bands in TQWT-FB are generated corresponding to different value of Q -factors. Therefore, many other wavelets are available to analyse signals with varying oscillations. Therefore, TQWT-FB is more suitable in such cases. The detail description and design of TQWT-FB is presented in Section 2.2 and finally this chapter is summarized in Section 2.3.

2.2 Design of TQWT-FB

The TQWT-FB consists of nearly constant BW sub-bands who differ in their f_c . Therefore, TQWT-FB decomposes the input signal into number of constant BW

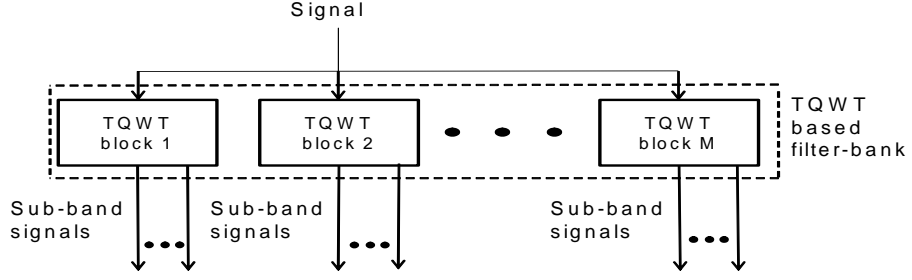


Figure 2.1: TQWT array for design of TQWT-FB based on method I.

sub-band signals. The motivation for the choice of TQWT to implement FB arises due to its ability to analyse oscillatory signals as its Q -factor can be tuned to desired value (Selesnick, 2011c). In this work, the TQWT-FB is designed in two ways. They are describe as follows:

1. Method I: From Fig. 1.1 (c) and (d), it can be observed that the low f_c sub-bands in the frequency response of TQWT are narrow in BW and also the increase in Q -factor value increases the f_c of narrow BW sub-bands. Hence, unlike frequency response of TQWT, we can achieve frequency response which consists of narrow and nearly constant BW sub-bands over the span of entire frequency range of the signal with varying Q -factor. The steps to design TQWT-FB in this method are as follows:
 - (a) Construct an array of TQWT blocks as shown in Fig. 2.1 and assign a constant value of R and D to each TQWT block. Here M is the number of TQWT blocks in array.
 - (b) Assign different values of Q -factor to TQWT blocks. Lets say $Q(j)$ is the Q -factor assigned to j^{th} TQWT block. Here, $1 \leq j \leq M$.
 - (c) Assign low value of Q -factor for first TQWT block, i.e. $j = 1$. Then from frequency response of TQWT obtained by $Q(1)$, R , and D , choose few narrow BW sub-bands randomly and assign their band number to first TQWT block. The band number varies from 1 to $D + 1$. For example,

sub-band D has band number D .

- (d) Repeat step (c) with higher value of Q -factor and j , until $j = M$.

When TQWT parameters are assigned to each TQWT block, the design of TQWT-FB is complete. Since the value of Q -factor is different in each TQWT block, the value of scale factors X and Y are different in every TQWT block as they depend on TQWT parameters (Selesnick, 2011c). The process of decomposing input signal into sub-band signals by TQWT-FB is explained as follows:

- (a) The input signal is given simultaneously to each TQWT block.
- (b) Each TQWT block applies TQWT with assigned value of Q -factor, R , and D .
- (c) The sub-band number of chosen sub-band is already stored in TQWT block. Lets say the store sub-band numbers are D , $D - 1$, and $D - 2$ in j^{th} TQWT block. Then this TQWT block, after applying TQWT, sets the wavelet coefficients of all sub-bands to zero except the wavelet coefficients of sub-band with band number D .
- (d) Apply inverse TQWT to obtain a sub-band signal.
- (e) Repeat steps (c) and (d) with next chosen sub-band number. In this example, the next sub-band number will be $D - 1$, and then $D - 2$.

In this method, each TQWT block may produce one or more than one sub-band signals. If it produces more than one sub-band signals, then their BW are not same but nearly same since they are generated by a particular value of Q -factor. Therefore, the BW of sub-bands in designed TQWT-FB are nearly same. An example of designed TQWT-FB from this method is shown in Fig. 2.2.

2. Method II: In this method, the f_c and BW of each sub-band in TQWT-FB is already chosen and accordingly the value of TQWT parameters are assigned to TQWT blocks. The BW of sub-bands in TQWT-FB are very close to each

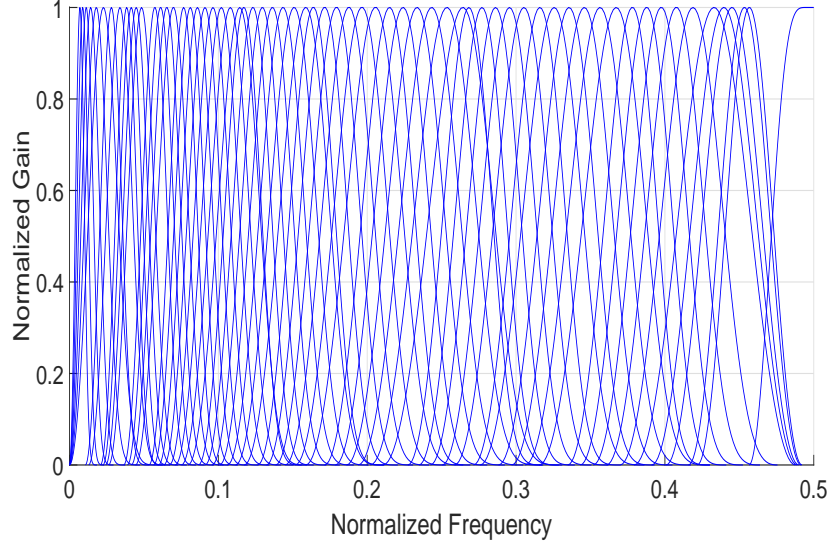


Figure 2.2: TQWT-FB designed from method I

other in this method. The procedure to design TQWT-FB in this method is as follows:

- (a) Decide the constant BW for each sub-band in TQWT-FB.
- (b) The sub-bands in TQWT-FB must be uniformly distributed over entire frequency range of signal. Accordingly, decide the f_c for each sub-band in TQWT-FB.
- (c) From (1.3), (1.4), (1.5), and (1.6), express f_c and BW in terms of Q -factor and R .
- (d) In this design, we focus on the BW of D^{th} sub-band only, which is shown in Fig. 1.1(c) and (d). Hence, in (1.3) and (1.4), put $i = D$.
- (e) In (1.3) and (1.4), we have three variables Q -factor, R , and D to obtain desired f_c and BW for each sub-band.
- (f) There can be more than one combination of TQWT parameters to obtain desired f_c and BW . However, the chosen value of TQWT parameters must be such that the conditions on scale factors X and Y as mentioned in previous section do not get violated.

From above mentioned steps, we assign TQWT parameters to each TQWT

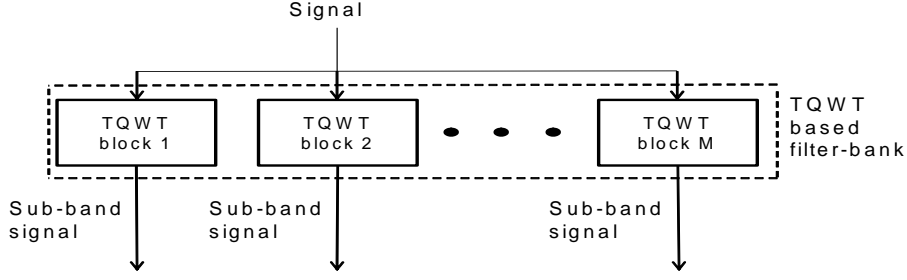


Figure 2.3: TQWT array for design of TQWT-FB based on method II.

block as shown in Fig. 2.3. Here also, the value of X and Y in every TQWT block is different due to different assigned value of TQWT parameters. After assigning TQWT parameters, the working of TQWT-FB is as follows:

- (a) The input signal is given to each TQWT block simultaneously.
- (b) Each TQWT block applies TQWT on input signal according to assigned value of Q -factor, R , and D . Then each TQWT block made the wavelet coefficients of all sub-bands except D^{th} sub-band, equal to zero.
- (c) Then each TQWT block applies inverse TQWT to obtain a sub-band signal.

In this method, each TQWT block produces one sub-band signal only. Therefore, the number of sub-bands in TQWT-FB is equal to the number of TQWT blocks in this method. A sample TQWT-FB designed from this method is shown in Fig. 2.4.

The proposed TQWT-FB is capable of decomposing a signal into several constant BW sub-band signals. The sub-bands in TQWT-FB are generated corresponding to different Q -factor values. Hence, there are several mother wavelets are available for the analysis of the non-stationary signal which may contain several oscillatory components. Also unlike basis functions of FT, these mother wavelets are well localized in time and space for analysing the signal.

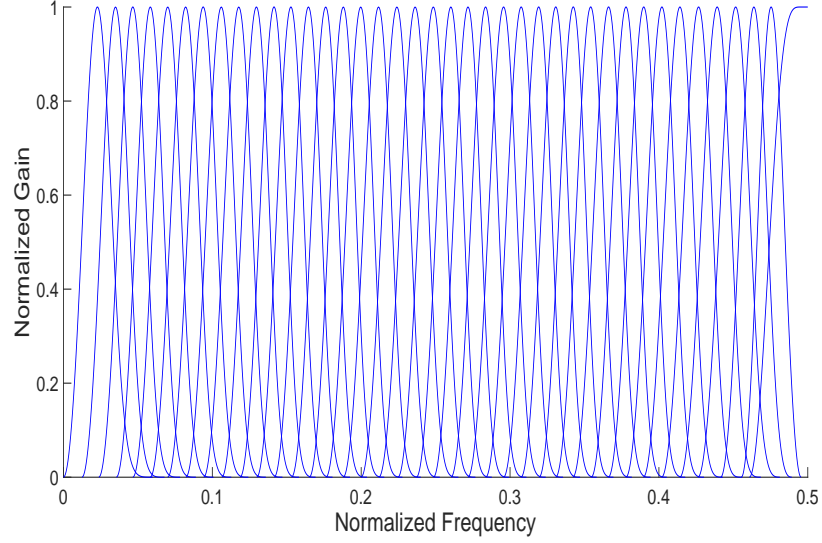


Figure 2.4: TQWT-FB designed from method II

The BW of sub-bands in TQWT-FB can be decided depending upon the application and signal properties. For example, if TQWT-FB is applied to decompose a multi-component signal into its mono-components, then the BW should be narrow enough so that no two components of signal lie in same sub-band. Also if TQWT-FB is applied to decompose naturally generated non-stationary signal like physiological signals, it is better to choose narrow BW of sub-bands. This is because these signals have many oscillatory components, and by choosing narrow BW sub-bands to design TQWT-FB, more number of Q -factors are available to analyse different oscillatory components.

A FB satisfies perfect reconstruction criteria if overlapping among sub-bands is such that the magnitude of FB is one over entire frequency range. The proposed TQWT-FB usually don't satisfy this criteria. The magnitude of TQWT-FB rises from 0 at frequencies close to 0. Also overlapping among sub-bands may increase the magnitude over one. However, the purpose of TQWT-FB in this thesis is to only decompose the non-stationary signals. Therefore reconstruction of signal perfectly is not required.

2.3 Summary

The methodologies are proposed for the design of TQWT-FB from TQWT. Unlike TQWT, there is no need to find optimum value of Q -factor in TQWT-FB for analysis of a signal. The TQWT-FB is suitable to analyse many non-stationary signals which differ in oscillatory behaviour. The sub-bands in TQWT-FB are produced by different value of Q -factors which indicates that different mother wavelets are present to analyse different oscillatory signals.

Chapter 3

Reduction of cross-terms in WVD using TQWT-FB

3.1 Introduction

The T-F representation based methods are suitable to analyse non-stationary signals as they provide temporal and spectral information of signal simultaneously. Among several T-F representations proposed in the literature, the WVD of signal produce best resolution. In ideal case, the WVD has very high resolution in time-domain and frequency-domain due to absence of averaging over any finite time duration (Boashash, 2003).

It should be noted that in nature the WVD is quadratic and generates cross-terms for the multi-component non-stationary signals. The cross-terms in the WVD consist of outer-interference-terms and inner-interference-terms (Boashash, 2003). The outer-interference-terms result if there are more than one mono-component, and inner-interference-terms result due to nonlinear FM components (Boashash, 2003). The presence of cross-terms is a serious limitation of the WVD based method for T-F representation of non-stationary signals and sometimes these cross-terms can have significant magnitude in T-F plane which may mislead analysis interpretation (Kadambe and Boudreaux-Bartels, 1992a).

In the literature, many methods have been proposed for the reduction of cross-terms. By using appropriate kernel functions, distributions with reduced interference terms were suggested which can suppress cross-terms and also preserve the mathematical properties of the WVD (Boashash, 2003). One such distribution using exponential kernel is known as the Choi-Williams distribution or exponential distribution (Choi and Williams, 1989). This distribution contains many mathematical properties of the WVD. It has been shown that, kernels can be designed for reducing the interference from the WVD (Baraniuk and Jones, 1993). However, the fixed kernel based methods work only for a particular class of signals and does not provide cross-terms free T-F representation for non-stationary signals in general (Hlawatsch et al, 1995). Significant distortions can take place in kernel based methods for cross-terms reduction in WVD (Sattar and Salomonsson, 1999). Signal dependent kernel for reduction of cross-terms in WVD is proposed in (Baraniuk and Jones, 1993). A comparison of signal dependent T-F representation with fixed kernel T-F representations like as WVD, Choi-Williams distribution, etc has been studied (Thomas et al, 2012a,b). In (Pikula and Benes, 2014), a method is presented where the multiple pseudo WVDs are used to reduce interference in the WVD. Similarly, an auto term window method is presented in (Liu, 2013) to reduce the cross-terms in the WVD by appropriate selection of parameters like window function and threshold (TH) value. The auto term window presented in (Liu et al, 2013) is used to suppress cross-terms in the WVD where it enhances the energy of auto-terms also.

New T-F distribution based on the polynomial WVD and L class of the WVD has been developed specially for polynomial phase signals (Wang and Jiang, 2010). An IF estimation algorithm in noisy environment has been suggested based on the local singular value decomposition and the WVD (Xianglong and Jinghuai, 2009). It has been studied only for mono-component nonlinear FM signals. In (Lerga and Sucic, 2009), a method has been proposed where IF of mono-component nonlinear FM signal is estimated using pseudo WVD along with adaptive window. A method based on shift invariant wavelet packet decomposition is developed for cross-terms

reduction in WVD (Cohen et al, 1999). IF estimation has been studied for non-linear FM signals in the presence of noise using polynomial WVD in (Barkat, 2001). Statistical modeling and denoising methods were proposed to remove noise component and to estimate IF in the WVD and smoothed pseudo WVD (Amirmazlaghani and Amindavar, 2013). Use of two-dimensional signal processing techniques to reduce interference in WVD has been proposed in which fractional FT are used to isolate components, which are identified using image processing technique (Khan et al, 2011). Use of morphological operators to remove cross-terms in the WVD has been proposed in (Gomez et al, 2011). In this method, the T-F image generated by thresholding spectrogram is used as the marker for performing λ -reconstruction. Only those components in the WVD of signal are retained which are also present in spectrogram. IF estimation for multi-component signals based on image processing techniques in T-F domain is proposed in (Rankine et al, 2007). Cross-terms reduction in the discrete WVD by applying non-linear filtering is suggested in (Arce and Hasan, 2000).

It has been shown that if the signal has a single component without non-linear FM then the WVD will not have cross-terms (Boashash, 2003). Interference terms can be removed if the signal under analysis is decomposed into mono-component signals without non-linear FM. The uses of FB and signal decomposition have been suggested before applying the WVD (Narasimhan et al, 2008; Sattar and Salomonsson, 1999). A band-pass FB is used to separate the signal in frequency-domain and the WVD is computed for each sub-band signal in (Sattar and Salomonsson, 1999). Cross-terms can also result, if signal has components separable in time-domain. To avoid such type of cross-terms, the pseudo WVD has been used in (Gaunard and Strifors, 1996). The band-pass filters also have inherently poor time-domain resolution. The Fourier-Bessel series expansion is used to separate the signal into components before computing the WVD (Pachori and Sircar, 2007). This method proved effective for signals when components are separable in frequency-domain. When mono-component signals are well separated in T-F domain then time-order represen-

tation based on the short-time Fourier-Bessel series expansion has been proposed to separate the mono-component signals before computing the WVD in order to reduce cross-terms (Pachori and Sircar, 2008b). Similarly in (Pachori and Sircar, 2006), the Fourier-Bessel transform has been used to separate the mono-component signals from the multi-component non-stationary signals before computing the WVD. The methods proposed in (Pachori and Sircar, 2006, 2007, 2008b) require the identification of range of Fourier-Bessel coefficients corresponding to each mono-component signals in order to separate the mono-component signals. In this work, we propose a method to reduce cross-terms by segmenting signal both in frequency-domain and time-domain. In the proposed method, the TQWT-FB provides a frame work for sub-band filtering of signals. The TQWT-FB is used to decompose the signal in frequency-domain. Then an energy distribution based algorithm is used to separate components of signal in time-domain in order to avoid windowing and achieve high concentrated energy distributions in obtained WVD based T-F representation by proposed method. The proposed method for cross-terms reduction in the WVD shows better performance even in the presence of noise.

The remaining part of this work is organised as follows: A brief overview of the WVD is presented in Section 3.2. The proposed method for cross-term reduction is presented in Section 3.3. The Rényi entropy which has been used for performance evaluation of the proposed method is discussed in Section 3.4. Simulation results and discussion are presented in Section 3.5 and 3.6, respectively. Finally, the summary of this work is presented in Section 3.7.

3.2 Overview of the WVD

The WVD can be considered FT of the instantaneous AC function. Its mathematical expression in time-domain is as follows (Boashash, 2003; Claasen and Mecklen-

brauker, 1980; Kadambe and Boudreaux-Bartels, 1992a):

$$\text{WVD}_s(t, \omega) = \int_{-\infty}^{+\infty} s\left(t + \frac{\tau}{2}\right) s^*\left(t - \frac{\tau}{2}\right) e^{-j\omega\tau} d\tau \quad (3.1)$$

where $s^*(t)$ represents the complex conjugate of signal $s(t)$.

It can be seen from (3.1) that, the WVD is quadratic in nature since there is multiplication of a signal with its conjugate version with some delay. Therefore, it deteriorates from the presence of cross-terms, if the signal under analysis is either multi-component signal or non-linear FM mono-component signal. The WVD has cross-terms for every set of two of mono-component signals (Kadambe and Boudreaux-Bartels, 1992a). For example, if a signal $s(t)$ consists of Z mono-component signals $s_1(t), s_2(t), \dots, s_Z(t)$ such as: $s(t) = \sum_{i=1}^Z s_i(t)$, then the WVD for signal $s(t)$ can be given as follows (Kadambe and Boudreaux-Bartels, 1992a):

$$\text{WVD}_s(t, \omega) = \underbrace{\sum_{i=1}^Z \text{WVD}_{s_i}(t, \omega)}_{\text{Part 1}} + 2 \underbrace{\sum_{k=1}^{Z-1} \sum_{l=k+1}^Z \Re[\text{WVD}_{s_k s_l}(t, \omega)]}_{\text{Part 2}} \quad (3.2)$$

where \Re represents the real part. In (3.2), Part 1 represents the WVDs of the mono-component signals, and Part 2 represents the WVDs due to cross component signals (Kadambe and Boudreaux-Bartels, 1992a). In this case, the number of cross-components will be $\binom{Z}{2}$ (Kadambe and Boudreaux-Bartels, 1992a). So there will be $\binom{Z}{2}$ additional components other than mono-components in the WVD based representation of the signal. Due to these cross-terms, the WVD may mislead these cross-terms as auto-terms. Theoretically, the WVD provides the best energy concentration, and has many desirable mathematical properties (Boashash, 2003). In spite of its obvious advantages, the presence of cross-terms limits its use for the analysis of multi-component non-stationary signals. There are two types of cross-terms in the distribution (Boashash, 2003). The outer-interference-terms lie in between the WVDs of two mono-component signals, whereas inner-interference-terms occur due to the different points which present in the same WVD of a mono-component

signal. If the signal is segmented in such a way that the components do not produce cross-terms in the WVD, then it is possible to get a T-F representation of the original signal by summing up the T-F distribution of the components. In this work, we propose the partitioning signal using TQWT-FB and energy based algorithm to obtain the WVD with reduced cross-terms. The method is discussed in detail in Section 3.3.

3.3 Proposed methodology for cross-terms reduction in WVD

It should be noted that there will be no cross-terms in the WVD if the signal under analysis consists of a single linear FM mono-component signal. If a multi-component signal is decomposed into number of such signals, then it will be possible to have a cross-terms free T-F representation by summing up the WVD of the individual components. The problem lies in decomposition of a multi-component, non-linear FM signals into such linear FM mono-component signals. In this work, we propose the use of TQWT-FB in frequency-domain followed by an energy based algorithm in time-domain for decomposing a multi-component signal into such mono-component signals which are well separated in T-F-domain. The TQWT-FB provides a method of sub-band decomposition using wavelets tuned to that band thereby achieving better frequency localization. Energy based segmentation in time-domain avoids use of constant windowing resulting in time-domain decomposition of the signal into its actual components. This energy based time-domain decomposition also results in better energy concentration in T-F plane as shown in the simulation results section. The three stages of proposed method are shown in Fig. 3.1, which are frequency-domain decomposition of the signal based on TQWT-FB, TDS of the signal, and the WVD computation of signal. In the sub-section 3.3.1, signal decomposition in frequency-domain based on TQWT-FB is explained. The sub-section 3.3.2 explains

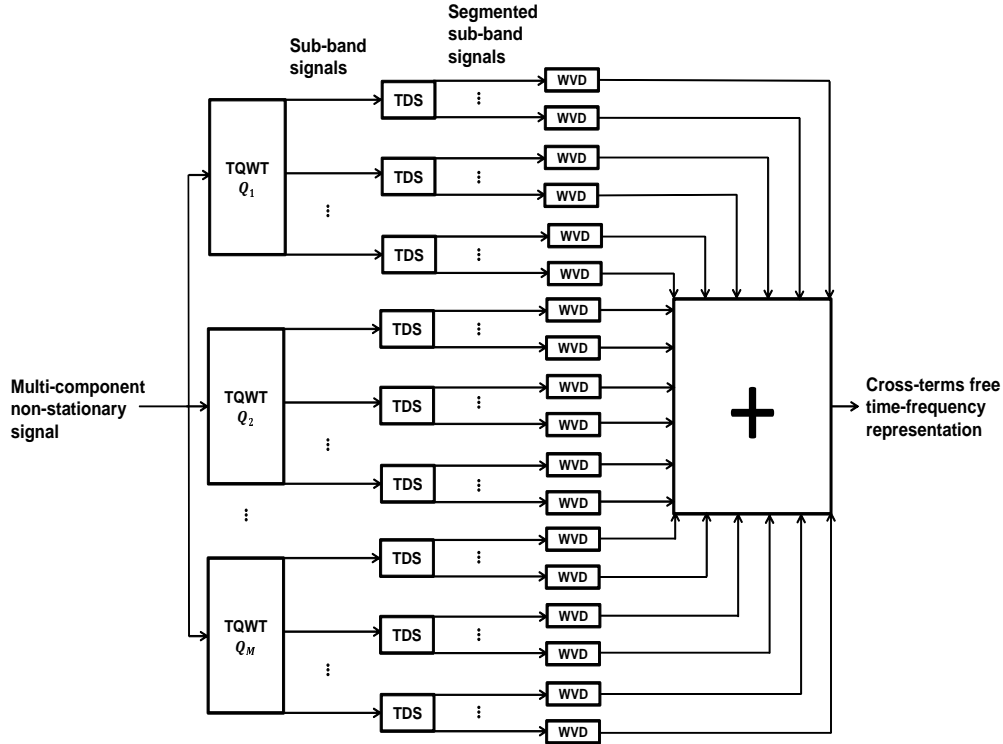


Figure 3.1: Block diagram of the proposed method for cross-term reduction in WVD

the TDS algorithm and the cross-terms free WVD computation is explained in subsection 3.3.3.

3.3.1 Signal decomposition by TQWT-FB

The TQWT-FB is used to decompose a multi-component non-stationary signal in frequency-domain. The TQWT-FB has been designed using method I presented in Section 2.2. The frequency response of designed TQWT-FB is shown in Fig. 3.2.

The $M = 16$ is used in designed TQWT-FB. The $R = 9$ and $D = 30$ is assigned to each TQWT block. The value of Q -factor assigned to each block with its TQWT block number (TBN), and sub-bands chosen for TQWT-FB design are mentioned in Table 3.1. The assigned TQWT parameters i.e. Q -factor, R , and D decides the BW of chosen sub-bands. Hence the basis for the choice of TQWT parameters is such that any sub-band should not cover more than one component at any instant of time. Otherwise the proposed method will not be able to discriminate multi-

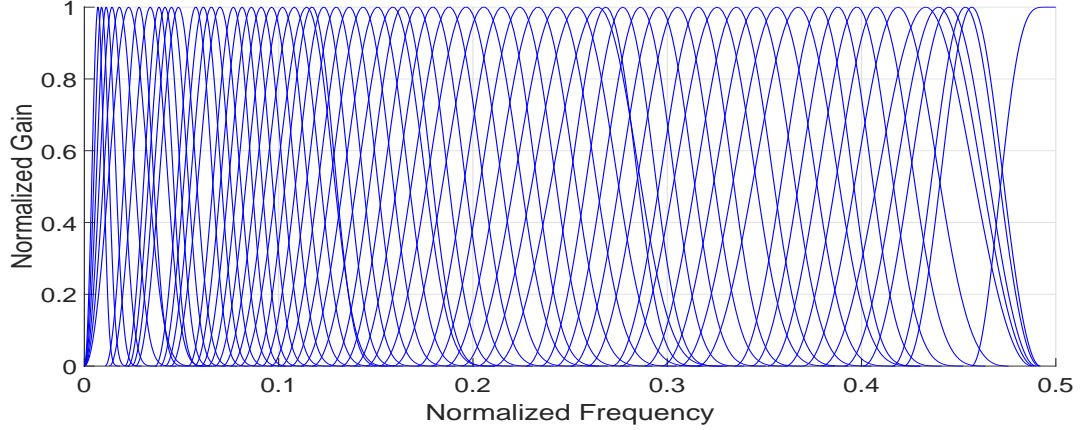


Figure 3.2: Frequency response of TQWT-FB

Table 3.1: Chosen Q -factor values and sub-bands in the design of TQWT-FB

TBN	Q -factor	Chosen sub-bands	TBN	Q -factor	Chosen sub-bands
1	1	29, 27, 25, 23, 21, and 19	9	6	15, 14, 13, 12, 11, and 9
2	1.5	25 and 23	10	6.5	11, 9, 8, 7, and 6
3	2	28, 27, 26, and 25	11	8	7, 6, 5, 4, 3, and 2
4	2.5	28, 27, 26, and 25	12	9	2
5	3	28, 27, 26, 25, 24, 23, 22, and 21	13	10	2
6	3.5	24, 23, 22, 21, 20, 19, and 18	14	12	2
7	4	20, 19, 18, 17, 16, and 15	15	13	2
8	4.5	16, 15, 14, 13, 12, and 11	16	22	1

components and then cross-terms will exist. Also, all the chosen sub-bands from TQWT blocks should cover normalized frequency range 0 to 0.5.

The number of sub-bands in designed TQWT-FB are 65. Therefore, the signal is decomposed into 65 sub-band signals and then each sub-band signal is given as input to TDS section as shown in Fig. 3.1.

3.3.2 TDS section

Signal components present in the same sub-band signal but in different time intervals result cross-terms in the WVD based T-F representation. Therefore, after signal decomposition by TQWT-FB, segmentation of the signal in time-domain is performed by TDS section in order to obtain the mono-component signals which are disjoint in time-domain. Automatic detection of the mono-component signals which are disjoint in time-domain may be a difficult task in the presence of higher noise (low signal to noise ratio (SNR)). In this work, we have used energy based method

to identify the presence of time-domain separated components in a sub-band signal. The presence of component is determined by following steps implemented in TDS section:

Step 1: In order to find the presence of components in i^{th} sub-band signal $SBS_i[n]$, its cumulative energy $C_i[n]$ is computed as follows:

$$C_i[n] = \sum_{k=0}^{n-1} SBS_i^2[k] \quad (3.3)$$

where n is the sample instant.

Step 2: In TDS algorithm, it is required that the $C_i[n]$ should be increasing function during the components interval. If there is zero crossing during a components interval, then there will be no increment in the value of $C_i[n]$ at sample instant where zero crossing occurs. Therefore, the $C_i[n]$ is further smoothed by moving average filter in order to reduce this effect.

Step 3: The expression of filtered version of $C_i[n]$ denoted by $FC_i[n]$ is given as follows (Jain and Pachori, 2013):

$$FC_i[n] = \frac{1}{2LL + 1} \sum_{p=-LL}^{LL} C_i[n + p] \quad (3.4)$$

Here, LL is the length of the filter.

Step 4: After computing $FC_i[n]$, its approximated derivative $dFC_i[n]$ is computed as follows:

$$dFC_i[n] = FC_i[n] - FC_i[n - 1] \quad (3.5)$$

Step 5: Then, $dFC_i[n]$ is normalized in the range $[0, 1]$ by dividing it from maximum value of $dFC_i[n]$.

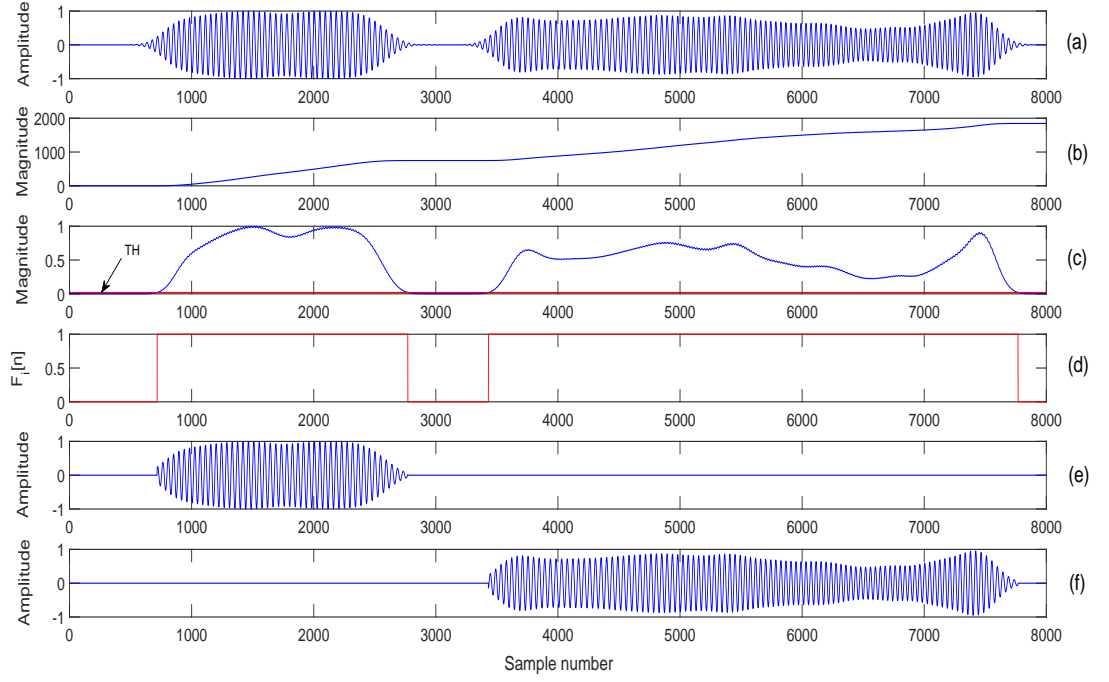


Figure 3.3: Different stages of TDS section: (a) A sub-band signal from i^{th} sub-band (b) Computed $FC_i[n]$ (c) the normalized $dFC_i[n]$ and TH value (shown in red) (d) variable $F_i[n]$ (e) first segmented component, and (f) second segmented component

Step 6: Then the normalized $dFC_i[n]$ ($ndFC_i[n]$) has been compared with the chosen TH. The normalization is by dividing $dFC_i[n]$ by its maximum value. Then a variable $F_i[n]$ for detection of duration of component is defined as follows:

$$F_i[n] = \begin{cases} 1, & ndFC_i[n] > \text{TH} \\ 0, & ndFC_i[n] \leq \text{TH} \end{cases} \quad (3.6)$$

The value of $F_i[n] = 1$ at a sample indicates the presence of component in the sub-band signal. The absence of component is determined by value $F_i[n] = 0$ at a sample.

As an example, various stages of TDS section are shown in Fig. 3.3. The Fig. 3.3(a) shows a sub-band signal. It is obtained from a speech signal (identity number 30203) of CMU-Arctic database (Kominek and Black, 2004a,b). Let say it

is generated from i^{th} sub-band. The location of time-domain separated components can be identified by observing the value of function $FC_i[n]$. The value of $FC_i[n]$ would be increasing for the interval where component exists and constant for the interval where components are absent as shown in Fig. 3.3(b). As the value of $F_i[n]$ depends on the derivative of function $FC_i[n]$. Hence, its value will be equal to 1 for the samples for which $FC_i[n]$ is increasing. This indicates the presence of component as shown in Fig. 3.3(d). The constant value of $FC_i[n]$ will result 0 value of $F_i[n]$ which indicates absence of component. The sequences of 1's and 0's have been used for identifying the beginning and ending locations of the components in the same sub-band signal in order to separate them in time-domain. The Fig. 3.3(e) and (f) show segmented first and second component respectively. Since, there are two components separated in time-domain in sub-band signal as shown in Fig. 3.3, there are two outputs generated by TDS section.

Based on the energy of the component of a signal and value of TH, the proposed TDS method can detect the component. The TDS method can detect transient signals of significant energy.

3.3.3 The WVD computation

In the last step of the proposed method, the WVD has been computed for each time-domain segmented component. The output of TDS section may have multiple time-domain segmented components corresponding to the same sub-band signal. Therefore, the WVD is computed for each analytic time-domain segmented components obtained using the Hilbert transform. The analytic signal representation of these time-domain segmented components has only positive frequencies and helps in overcoming the aliasing problem in WVD (Boashash, 2003). The summation of all WVDs corresponding to segmented components in all sub-bands provides cross-terms free WVD of the multi-component non-stationary signals. It should be noted that the proposed method of T-F representation is based on the decomposition

in frequency-domain and segmentation in time-domain. The proposed structure is helpful in obtaining good resolution of different components in T-F domain by performing weighted addition of WVDs of different segmented components from TDS section.

3.4 Performance evaluation

To evaluate the performance of proposed T-F distribution, the performance evaluation parameter must examine the concentration or time-bandwidth product, moments on T-F plane, etc. The Rényi entropy as computed in (Flandrin et al, 1994; Williams et al, 1991) measures the complexity and information content of the signal in T-F plane which includes time-bandwidth product and moments on T-F plane (Flandrin et al, 1994). Due to these reasons, we choose normalized Rényi entropy measure proposed in (Sang and Williams, 1995) to quantitatively judge the performance of suggested T-F representation based on WVD.

The normalized Rényi entropy measure is computed using Rényi entropy (Flandrin et al, 1994; Williams et al, 1991). The mathematical expression of Rényi entropy is given as follows (Sang and Williams, 1995):

$$R_\gamma = \frac{1}{1-\gamma} \log_2 \left[\sum_{l=-L}^L \sum_{k=-K}^K [C_s(l, k)]^\gamma \right] \quad (3.7)$$

where $C_s(l, k)$ in (3.7) is a Cohen's class T-F distribution (Sang and Williams, 1995) which spans from $-L$ to L in time-domain and $-K$ to K in frequency-domain. Here, the γ is the order of information and chosen as 3 (Flandrin and Borgnat, 2010) for performance evaluation. In order to compare different T-F distributions, the normalization of Rényi entropy is important (Stankovic, 2001). The normalized Rényi entropy measure for T-F distribution can be given as follows (Stankovic, 2001):

$$R_{\gamma\text{norm}} = \frac{1}{1-\gamma} \log_2 \left[\frac{\sum_{l=-L}^L \sum_{k=-K}^K [C_s(l, k)]^\gamma}{\sum_{l=-L}^L \sum_{k=-K}^K [C_s(l, k)]} \right], \gamma \geq 2 \quad (3.8)$$

In (3.8), the normalization of $C_s(l, k)^\gamma$ with respect to its energy $C_s(l, k)$ is shown in order to make it energy unbiased (Stankovic, 2001). After normalization, its logarithm to the base 2 is computed and then it is multiplied by weight $\frac{1}{1-\gamma}$.

The low value of normalized Rényi entropy measure depicts the better T-F distribution (Sang and Williams, 1995). The normalized Rényi entropy measure has been computed for Fourier-Bessel series expansion based method (Pachori and Sircar, 2007) or time-order based method (Pachori and Sircar, 2008b), FB based method (Sattar and Salomonsson, 1999), and the proposed method. In the proposed method, the values of normalized Rényi entropy measure are low as compared to the value of normalized Rényi entropy measure computed for other compared methods which has been shown in simulation result section.

3.5 Simulation results

The proposed method for cross-terms reduction in WVD has been studied for four test multi-component non-stationary signals and the same is compared with the WVD based T-F representation obtained using Fourier-Bessel series expansion based method (Pachori and Sircar, 2007) or time-order based method (Pachori and Sircar, 2008b), and FB based method (Sattar and Salomonsson, 1999). The brief description of these signals namely $s_1[n]$, $s_2[n]$, $s_3[n]$, and $s_4[n]$ is as follows:

Signal 1: $s_1[n]$: The signal $s_1[n]$ is a two-component linear FM non-stationary signal whose components are well separated in T-F domain and frequency-domain. The mathematical expression for the signal $s_1[n]$ can be given

as follows (Choi and Williams, 1989; Pachori and Sircar, 2007):

$$s_1[n] = \frac{1}{100} \cos \left[\left(\frac{\pi n}{2000} + 1 \right) \frac{3n}{5} \right] + \frac{1}{100} \cos \left[\left(\frac{3\pi n}{100} + 188 \right) \frac{n}{100} \right] \quad (3.9)$$

Signal 2: $s_2[n]$: The signal $s_2[n]$ is a two-component non-stationary signal. The components of signal $s_2[n]$ are well-separated in T-F domain and frequency-domain. One component is linear FM whereas other component is non-linear FM chirp. The mathematical expression for the signal $s_2[n]$ can be given in discrete time-domain as follows (Stankovic, 2001):

$$s_2[n] = \frac{1}{50} \cos \left[\left(\frac{3\pi n}{500} + 471 \right) \frac{n}{500} + 30 \cos \left(\frac{\pi n}{256} \right) \right] + \frac{1}{100} \cos \left[\left(\frac{\pi n}{1000} + 22 \right) \frac{n}{10} \right] \quad (3.10)$$

Signal 3: $s_3[n]$: The signal $s_3[n]$ is a multi-component bat echo signal whose components are well-separated in T-F domain only. This is a natural signal emitted by a large brown bat (*Eptesicus fuscus*) and signal is publicly available at (Baraniuk, 2009). The duration of the signal is 2.5 ms with sampling period $7\mu\text{sec}$.

Signal 4: $s_4[n]$: The signal $s_4[n]$ is a multi-component non-stationary signal which has well-separated components in frequency and T-F domain. Signal $s_4[n]$ can be mathematically expressed as follows (Choi and Williams, 1989):

$$s_4[n] = \frac{w[n]}{10} \left(\cos \left[\frac{90\pi n}{256} \right] + \cos \left[\frac{115\pi n}{256} \right] \right) \quad (3.11)$$

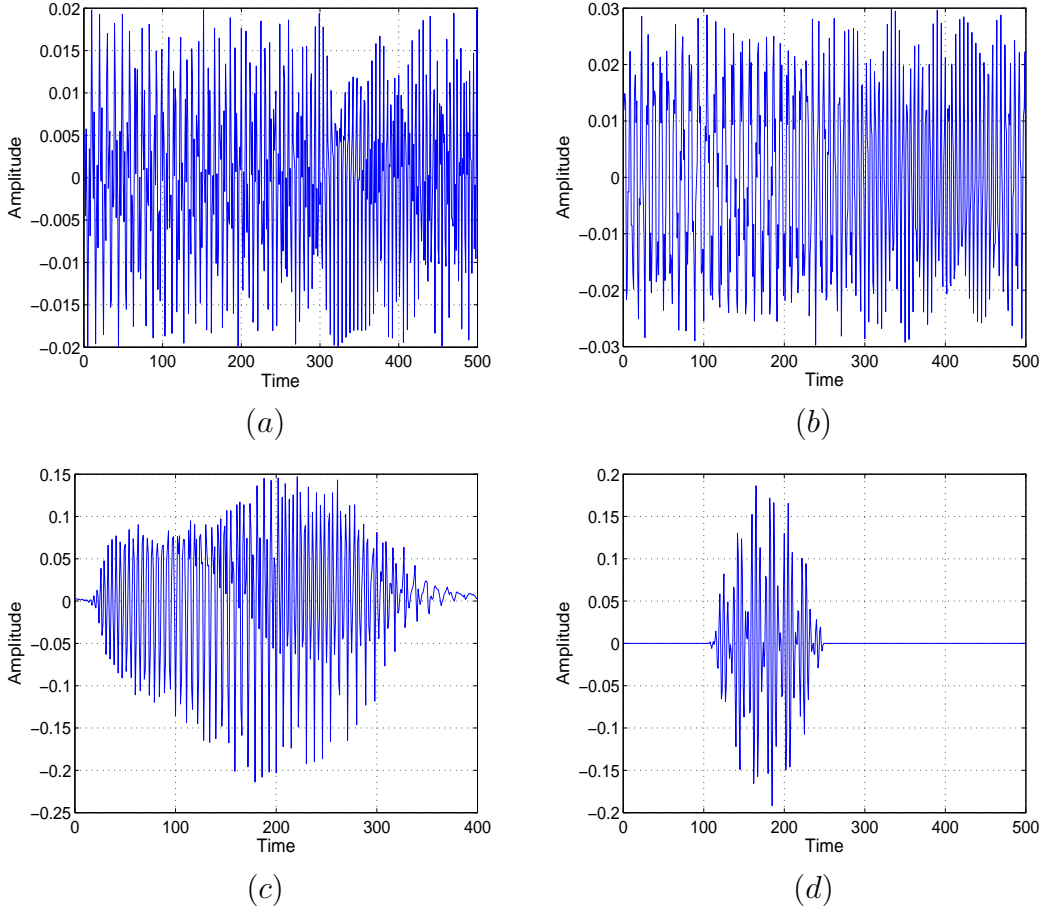


Figure 3.4: Plot of the signals used in simulation study: (a) Multi-component signal with two linear FM chirp ($s_1[n]$), (b) Multi-component signal with a linear FM chirp and a non-linear FM chirp ($s_2[n]$), (c) Bat echo signal ($s_3[n]$), (d) Multi-component signal with two time-limited and band-limited pulses ($s_4[n]$).

where, $w[n]$ is given by:

$$w[n] = \begin{cases} 0, & n < 108 \\ 1 - \left[\frac{(n-178)^2}{5000} \right], & 108 \leq n \leq 248 \\ 0, & n > 248 \end{cases}$$

The time-domain plots of the four signals $s_1[n]$, $s_2[n]$, $s_3[n]$, and $s_4[n]$ used in simulation are shown in Fig. 3.4 (a)-3.4 (d), respectively. The T-F representation based on WVD of these signals are shown in Fig. 3.5:

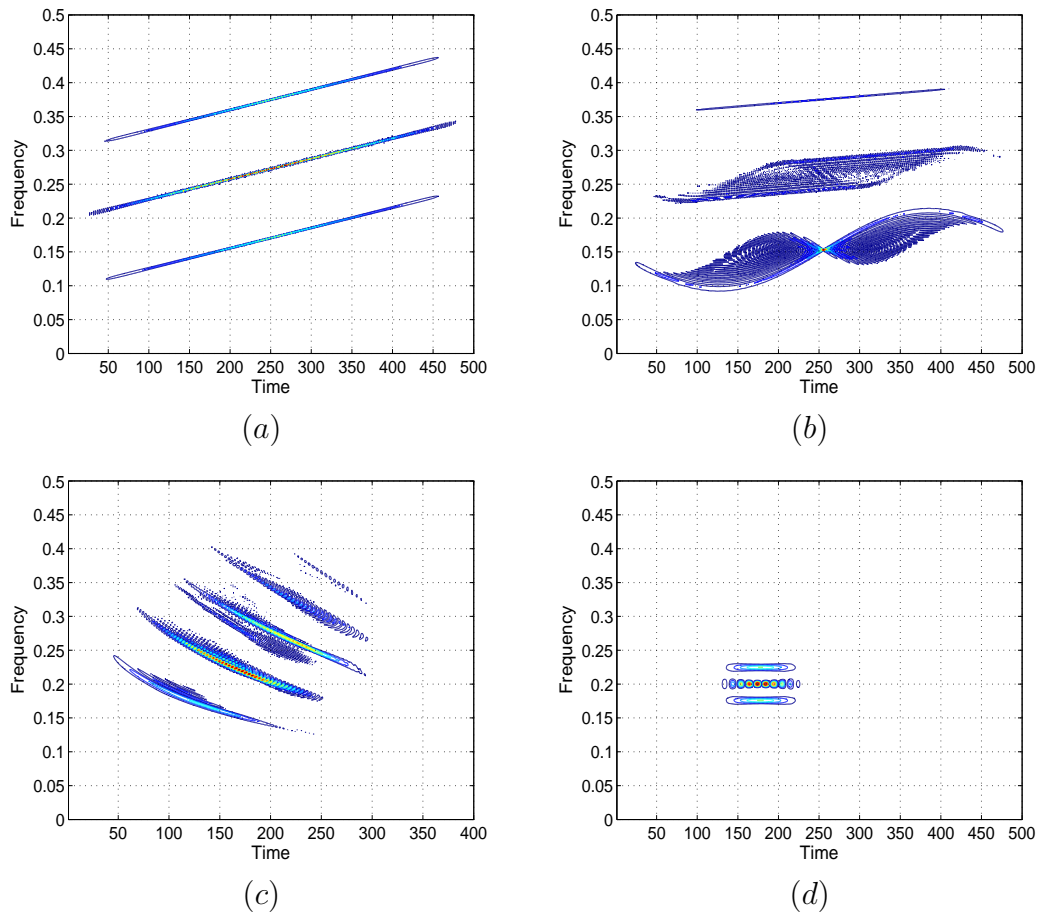


Figure 3.5: The T-F representation based on WVD of the signals used in simulation study: (a) Multi-component signal with two linear FM chirp ($s_1[n]$), (b) Multi-component signal with a linear FM chirp and a non-linear FM chirp ($s_2[n]$), (c) Bat echo signal ($s_3[n]$), (d) Multi-component signal with two time-limited and band-limited pulses ($s_4[n]$).

The proposed method's performance is compared with the Fourier-Bessel series expansion based method (Pachori and Sircar, 2007) for signals $s_1[n]$, $s_2[n]$, and $s_4[n]$ as these signals are well disjoint in frequency-domain. For signal $s_3[n]$, the proposed method is compared with time-order based method (Pachori and Sircar, 2008b). The Fourier-Bessel series expansion based method is not suitable signals like $s_3[n]$ whose components are overlapped in frequency-domain. The performance of the suggested method is also compared with the FB based method (Sattar and Salomonsson, 1999) for all four test signals. The signal decomposition obtained by discrete cosine transform-harmonic wavelet transform (DCTHWT), has many advantages over the sub-band decomposition by perfect reconstruction filter-bank (PRFB) proposed in (Sattar and Salomonsson, 1999) like less computational complexity, frequency resolution improvement, and good signal detection (Narasimhan et al, 2008). Due to these reasons, we have implemented sub-band decomposition using DCTHWT in the filter-bank based method for all four signals namely $s_1[n]$, $s_2[n]$, $s_3[n]$, and $s_4[n]$.

The WVD based T-F representation obtained by applying proposed method and other compared methods on representative signals $s_1[n]$, $s_2[n]$, $s_3[n]$, and $s_4[n]$ under different noise environments are shown in Figs. 3.6-3.9.

The noise used for simulation study is additive white Gaussian noise (AWGN). The WVD of representative signals by proposed method as shown in Figs. 3.6-3.9 are obtained at optimum value TH in TDS section. The optimum value of TH is determined empirically for each signal. The effect of TH on WVD obtained by proposed method in clean case is shown in Fig. 3.10 to Fig. 3.13.

The performance evaluation of proposed method for WVD based T-F representation has been measured in terms of normalized Rényi entropy measure. The normalized Rényi entropy measures for WVD based T-F representation obtained from proposed method, Fourier-Bessel series expansion based method (Pachori and Sircar, 2007) or time-order based method (Pachori and Sircar, 2008b), and FB based method (Sattar and Salomonsson, 1999) are computed and shown in Table 3.2.

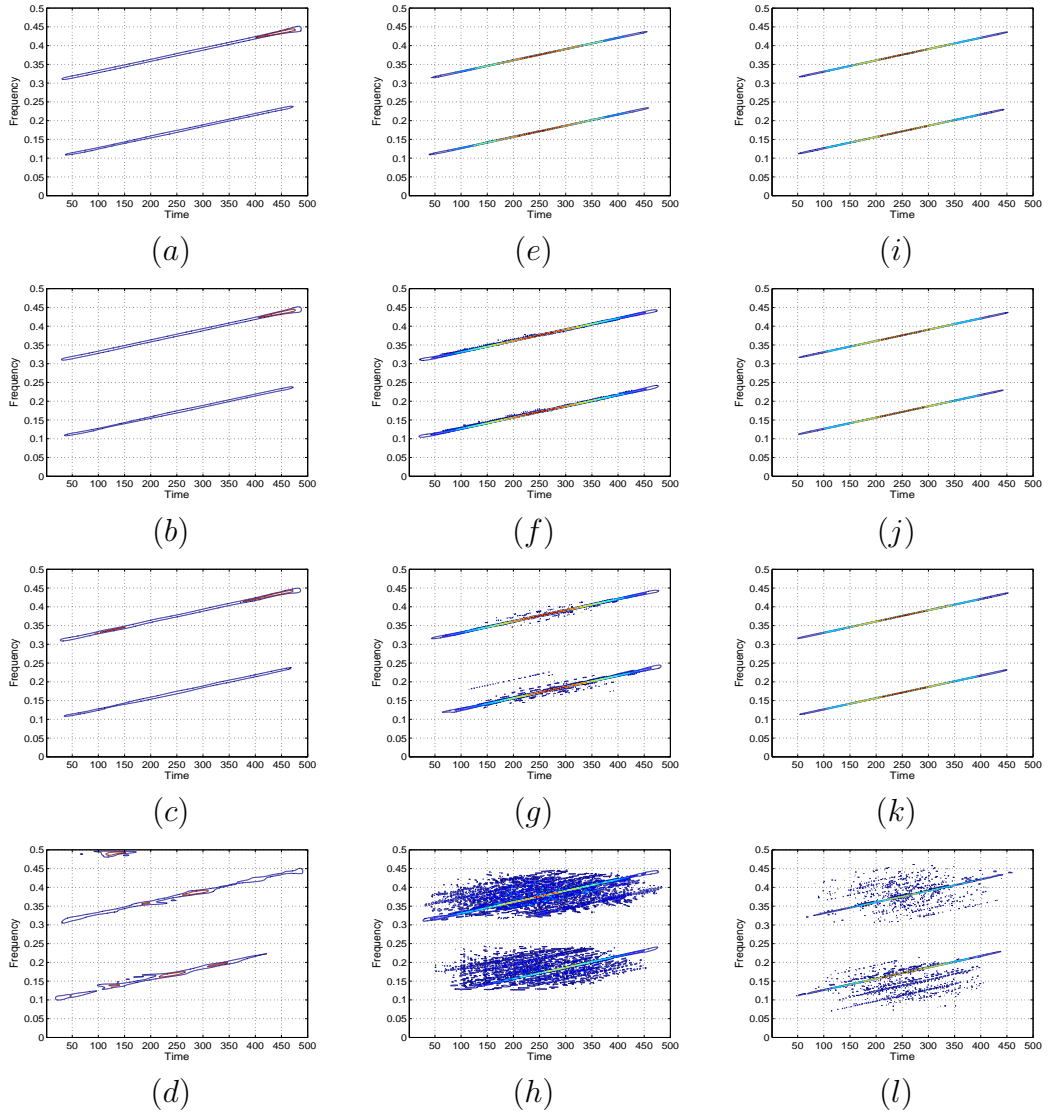


Figure 3.6: T-F representation based on the WVD of $s_1[n]$ at different SNRs: Proposed method; (a) Clean, (b) SNR = 20 dB, (c) SNR = 10 dB, (d) SNR = 0 dB, Fourier-Bessel series expansion based method; (e) Clean, (f) SNR = 20 dB, (g) SNR = 10 dB, (h) SNR = 0 dB, FB based method; (i) Clean, (j) SNR = 20 dB, (k) SNR = 10 dB, (l) SNR = 0 dB.

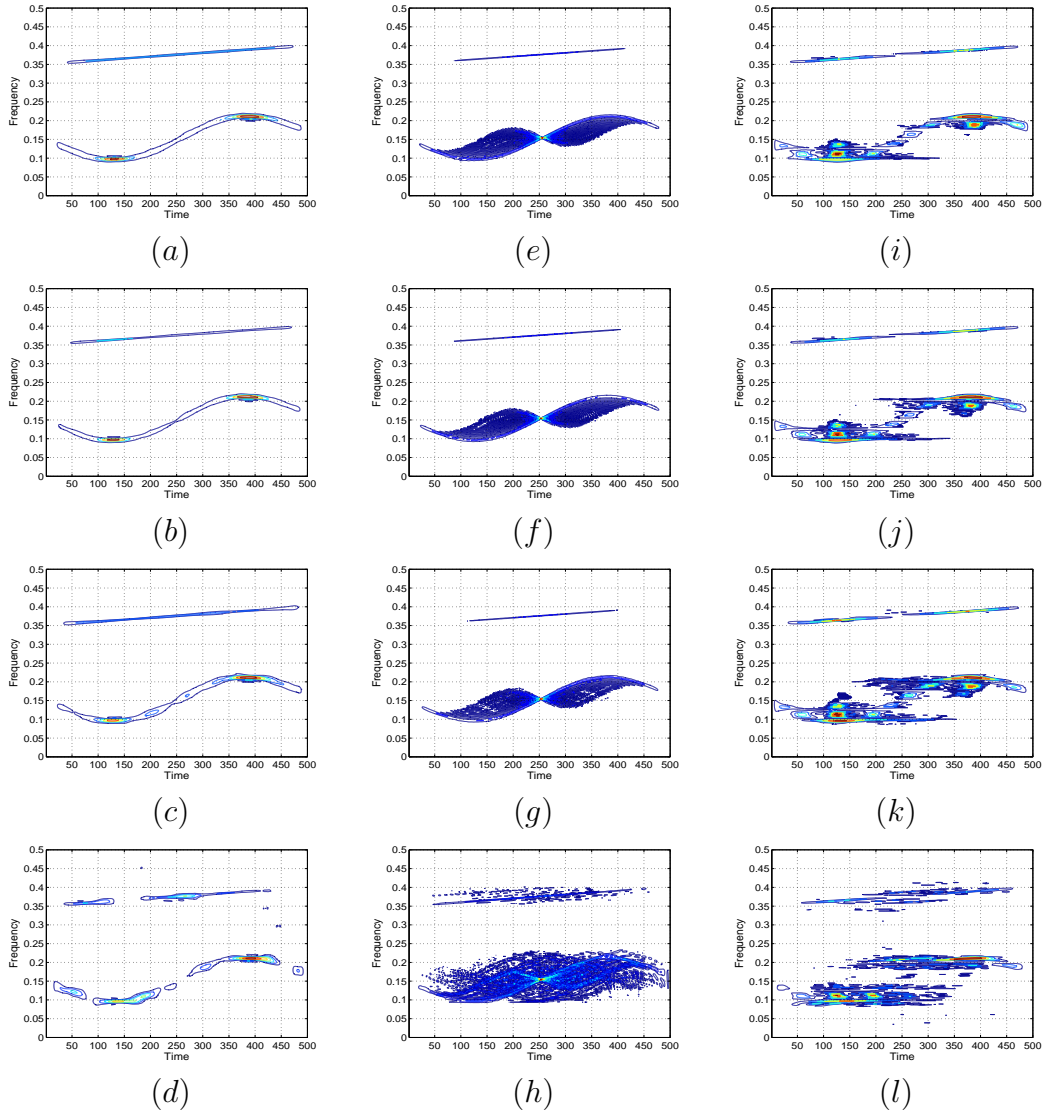


Figure 3.7: T-F representation based on the WVD of $s_2[n]$ at different SNRs: Proposed method; (a) Clean, (b) SNR = 20 dB, (c) SNR = 10 dB, (d) SNR = 0 dB, Fourier-Bessel series expansion based method; (e) Clean, (f) SNR = 20 dB, (g) SNR = 10 dB, (h) SNR = 0 dB, FB based method; (i) Clean, (j) SNR = 20 dB, (k) SNR = 10 dB, (l) SNR = 0 dB.

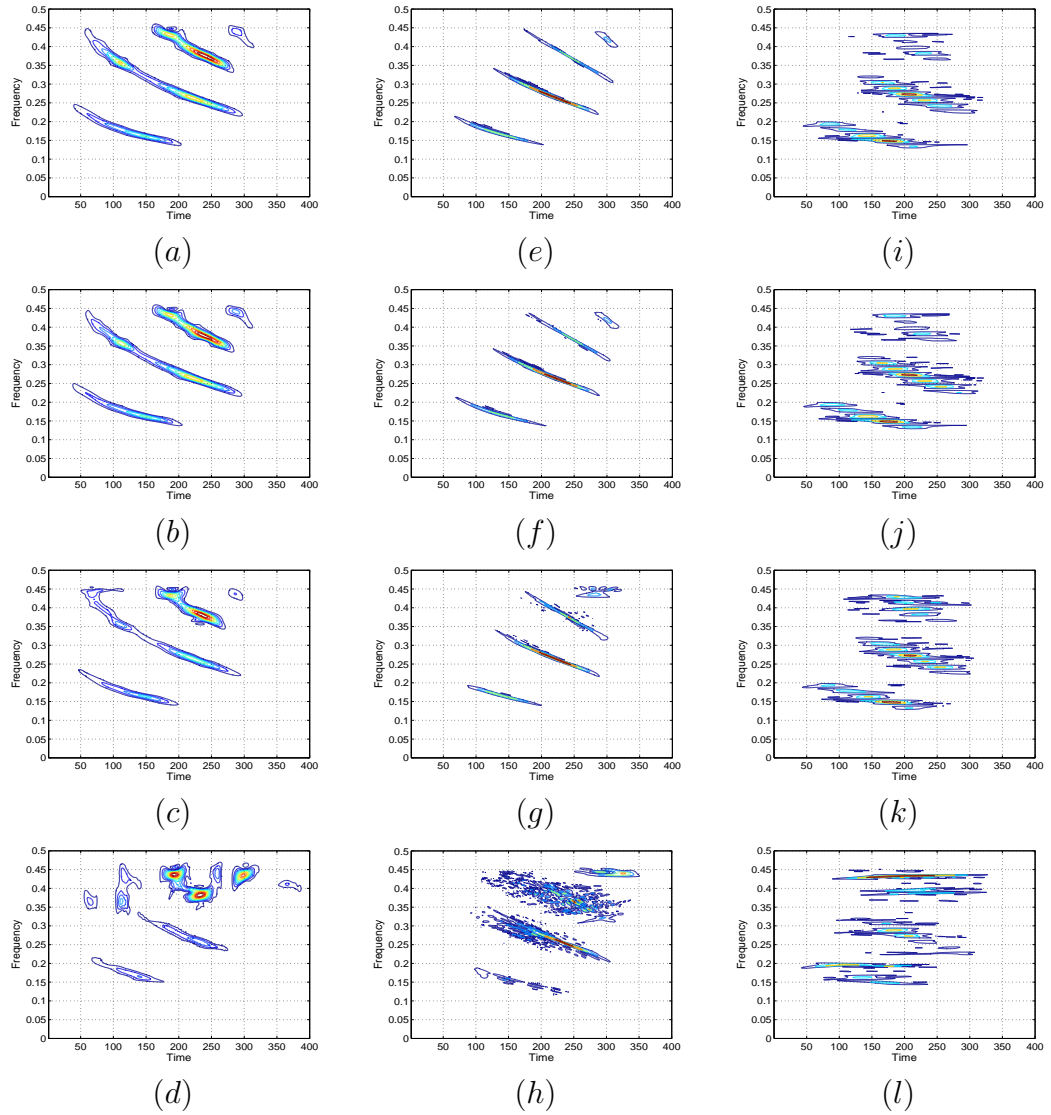


Figure 3.8: T-F representation based on the WVD of $s_3[n]$ at different SNRs: Proposed method; (a) Clean, (b) SNR = 20 dB, (c) SNR = 10 dB, (d) SNR = 0 dB, Time-order based method; (e) Clean, (f) SNR = 20 dB, (g) SNR = 10 dB, (h) SNR = 0 dB, FB based method; (i) Clean, (j) SNR = 20 dB, (k) SNR = 10 dB, (l) SNR = 0 dB.

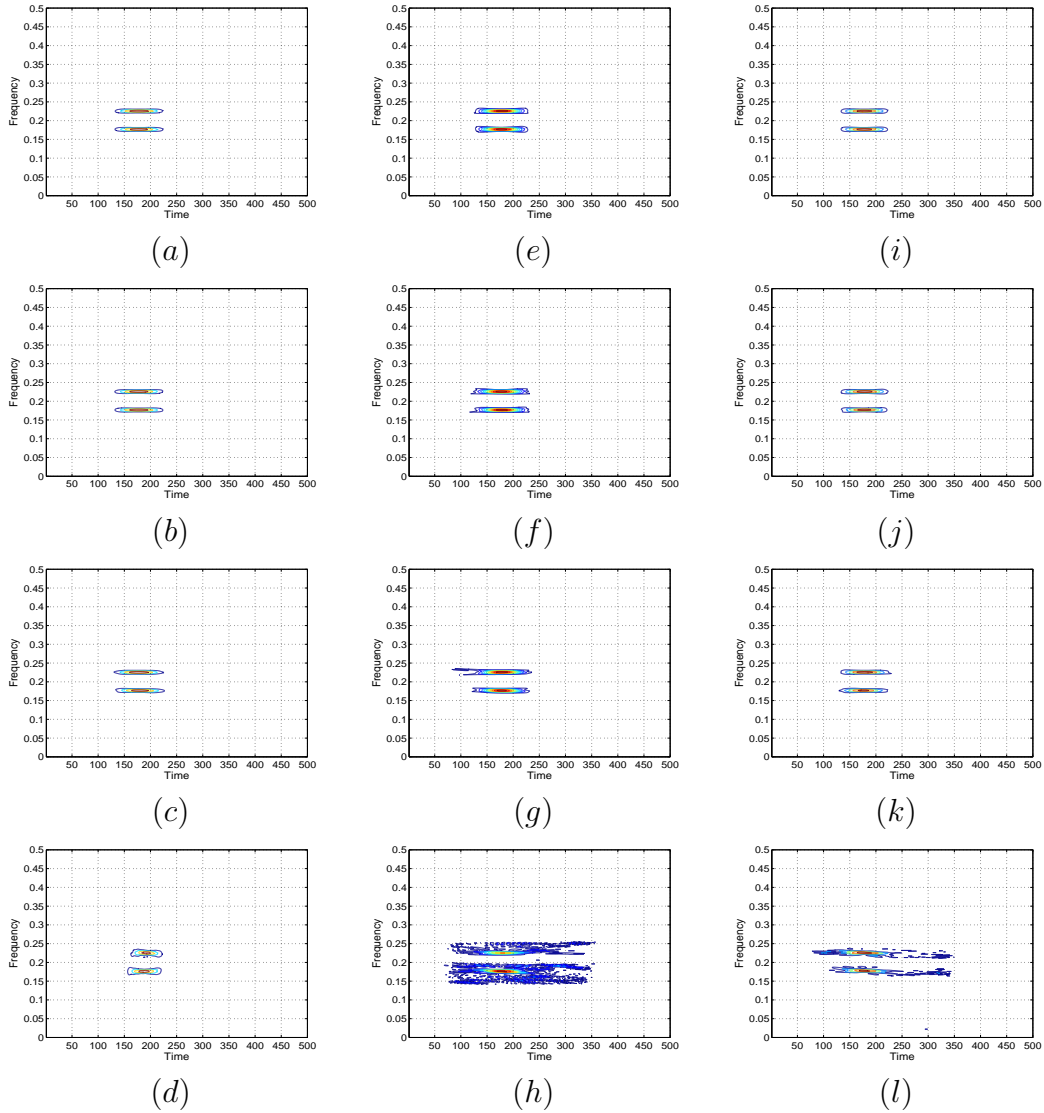


Figure 3.9: T-F representation based on the WVD of $s_4[n]$ at different SNRs: Proposed method; (a) Clean, (b) SNR = 20 dB, (c) SNR = 10 dB, (d) SNR = 0 dB, Fourier-Bessel series expansion based method; (e) Clean, (f) SNR = 20 dB, (g) SNR = 10 dB, (h) SNR = 0 dB, FB based method; (i) Clean, (j) SNR = 20 dB, (k) SNR = 10 dB, (l) SNR = 0 dB.

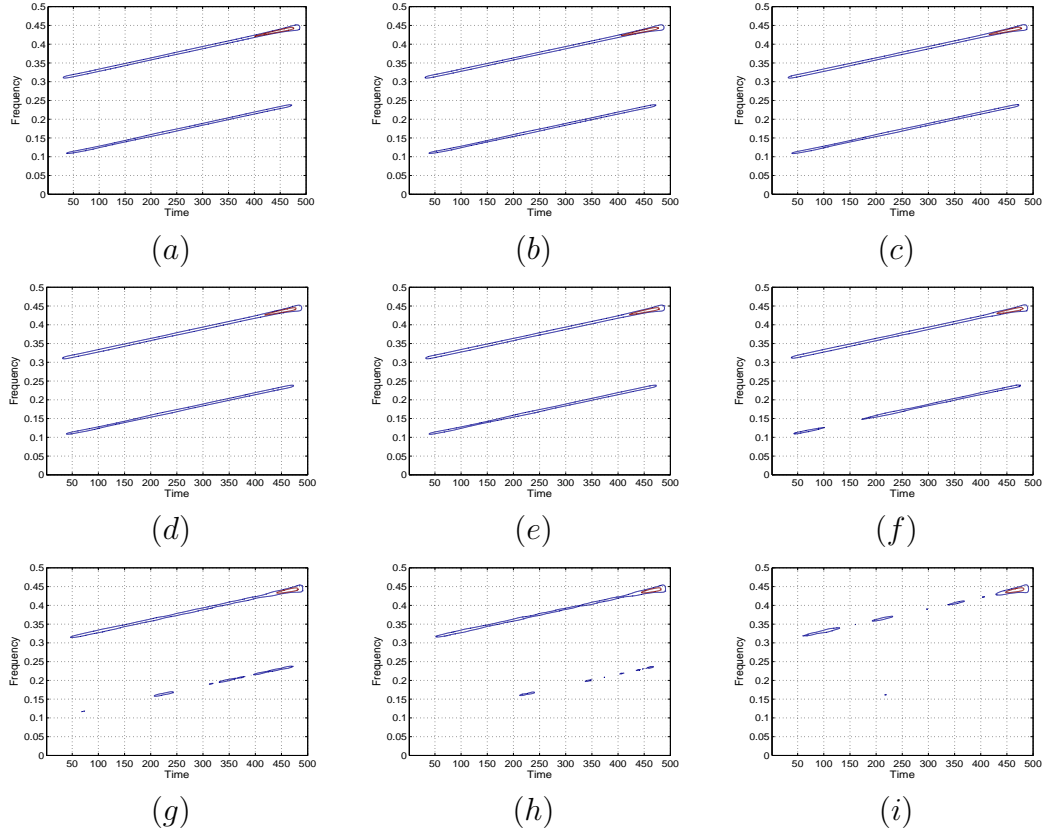


Figure 3.10: WVD based T-F representation of clean signal ($s_1[n]$) using proposed method with different values of TH: (a) TH = 0.001, (b) TH = 0.01, (c) TH = 0.05, (d) TH = 0.07, (e) TH = 0.1, (f) TH = 0.2, (g) TH = 0.35, (h) TH = 0.4, (i) TH = 0.5.

Table 3.2: Normalized Rényi entropy measure for different methods for cross-terms reduction in the WVD based T-F representation

Signal	SNR	Fourier-Bessel series		Proposed method
		expansion based method (Pachori and Sircar, 2007) /Time-order based method (Pachori and Sircar, 2008b)	based method (Sattar and Salomonsson, 1999)	
$s_1[n]$	0 dB	2.4920	2.7328	1.8900
	10 dB	2.2246	2.1815	1.6043
	20 dB	1.9694	1.8898	1.3688
	clean	1.9248	1.8049	1.3513
$s_2[n]$	0 dB	3.300	2.2689	1.9288
	10 dB	3.0900	1.9141	1.7759
	20 dB	3.0282	1.8348	1.6895
	clean	2.9962	1.8216	1.6891
$s_3[n]$	0 dB	1.9333	1.9604	1.6790
	10 dB	1.9223	1.9552	1.3343
	20 dB	1.7463	1.9293	1.3039
	clean	1.7290	1.9242	1.2922
$s_4[n]$	0 dB	1.8700	2.1091	1.3800
	10 dB	1.0714	1.2431	1.0652
	20 dB	0.9342	0.9602	0.8921
	clean	0.9341	0.8749	0.8638

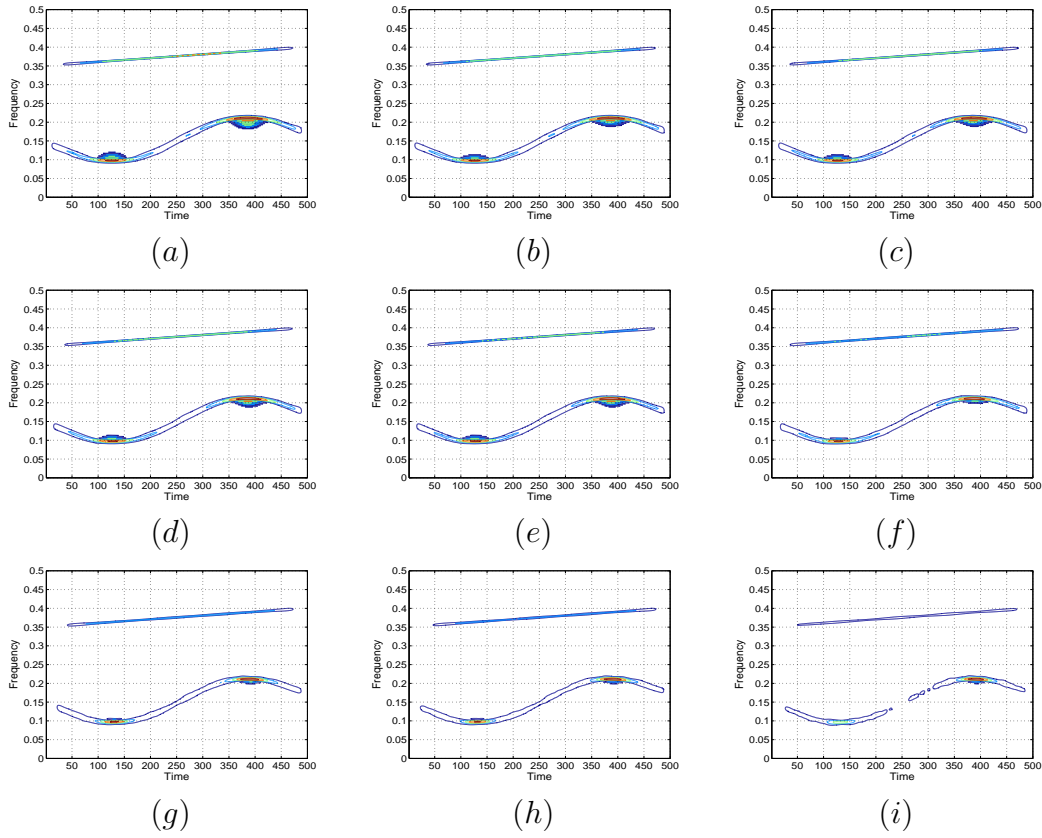


Figure 3.11: WVD based T-F representation of clean signal ($s_2[n]$) using proposed method with different values of TH: (a) TH = 0.001, (b) TH = 0.01, (c) TH = 0.05, (d) TH = 0.07, (e) TH = 0.1, (f) TH = 0.2, (g) TH = 0.35, (h) TH = 0.4, (i) TH = 0.5.

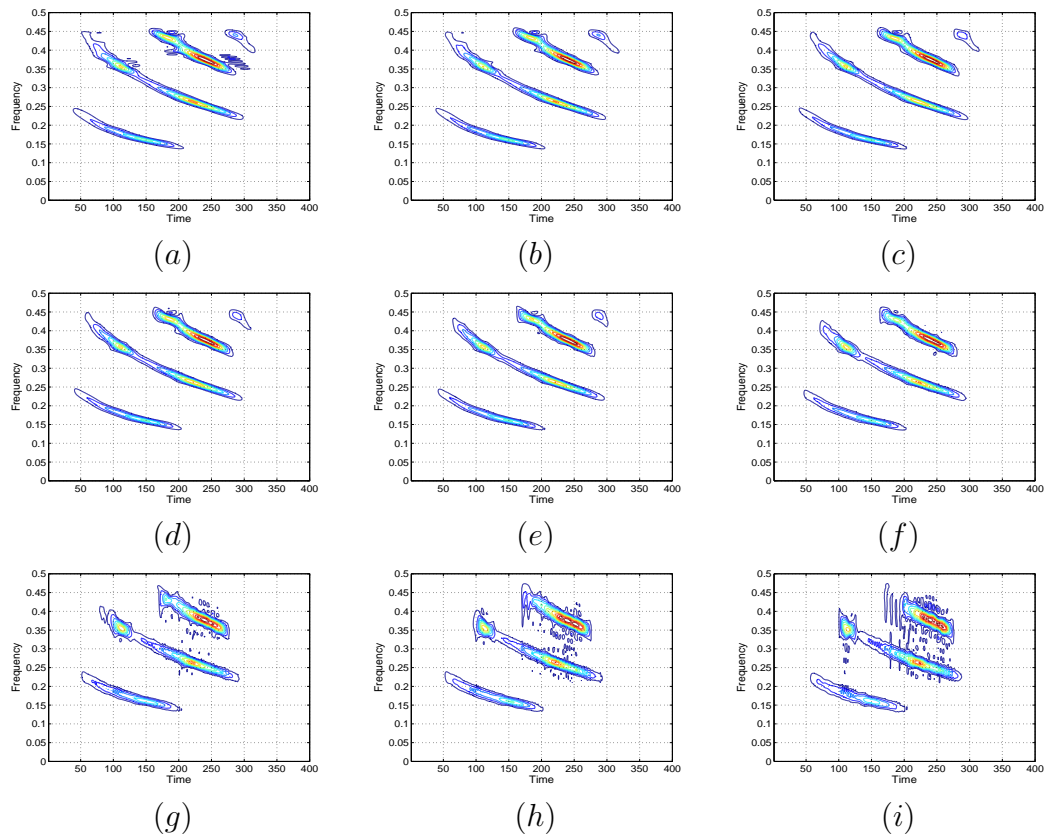


Figure 3.12: WVD based T-F representation of clean signal ($s_3[n]$) using proposed method with different values of TH: (a) TH = 0.001, (b) TH = 0.01, (c) TH = 0.05, (d) TH = 0.07, (e) TH = 0.1, (f) TH = 0.2, (g) TH = 0.35, (h) TH = 0.4, (i) TH = 0.5.

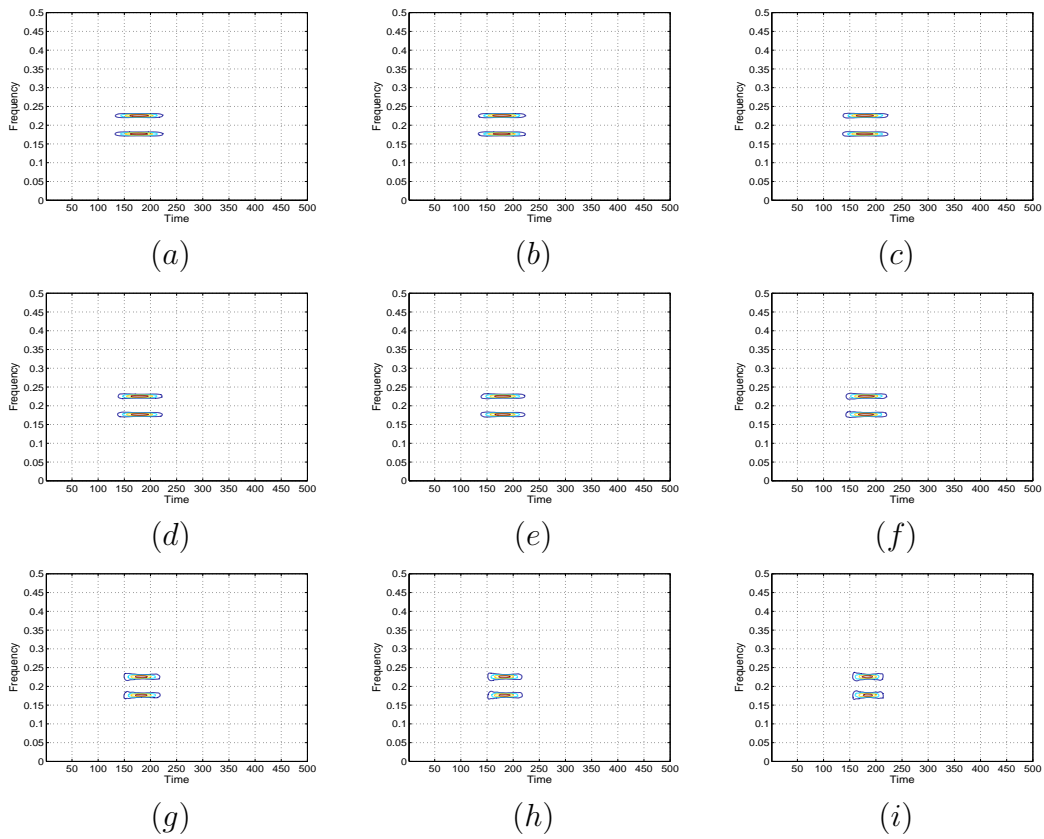


Figure 3.13: WVD based T-F representation of clean signal ($s_4[n]$) using proposed method with different values of TH: (a) TH = 0.001, (b) TH = 0.01, (c) TH = 0.05, (d) TH = 0.07, (e) TH = 0.1, (f) TH = 0.2, (g) TH = 0.35, (h) TH = 0.4, (i) TH = 0.5.

The methods mentioned in Table 3.2 are run on the same machine (Intel Pentium CPU B940 @ 2.00 GHz). When these methods are run for signal $s_1[n]$ under clean case, then the computation time by proposed method, Fourier-Bessel series expansion based method (Pachori and Sircar, 2007), and FB based method (Sattar and Salomonsson, 1999) is 8.19 seconds, 1.5 seconds, and 1.8 seconds, respectively. Similarly for clean signal $s_2[n]$, the computational time is 6.95 seconds, 1.79 seconds, and 1.52 seconds for proposed method, Fourier-Bessel series expansion based method (Pachori and Sircar, 2007), and FB based method (Sattar and Salomonsson, 1999), respectively. For signal $s_3[n]$ in clean case, the computational time by proposed method, time-order based method (Pachori and Sircar, 2008b), and FB based method (Sattar and Salomonsson, 1999) is 9.26 seconds, 1.72 seconds, and 1.66 seconds, respectively. For last signal $s_4[n]$ in clean case, the time consumed by proposed method, Fourier-Bessel series expansion based method (Pachori and Sircar, 2007), and FB based method (Sattar and Salomonsson, 1999) is 6.02 seconds, 1.27 seconds, and 1.08 seconds, respectively.

3.6 Discussion

A methodology is proposed in this work for the reduction of cross-terms in WVD which arises due to presence of multi-components and non-linear FM components present in the signal. The proposed method applies TQWT-FB for signal decomposition and then TDS section segments the components in time-domain. Then in last stage, the WVD of segmented components are computed and added to achieve a WVD based T-F representation with reduced cross-terms.

In Fig. 3.6, T-F representations obtained by applying the suggested method, Fourier-Bessel series expansion based method, and FB based method on signal $s_1[n]$ are depicted for clean signal, and signal corrupted by AWGN with different noise levels such as 0 dB, 10 dB, and 20 dB SNRs. In Fig. 3.6, first column shows the WVD based T-F representation for the proposed method. Similarly, second and

third column of Fig. 3.6 shows the WVD based T-F representation obtained from Fourier-Bessel series expansion based method and FB based method, respectively. It can be noticed that in case of clean signal, signal corrupted with AWGN at 20 dB and 10 dB SNRs all studied methods are able to identify two linear FM chirps signals in WVD based T-F representation. However, in case of signal corrupted with 0 dB SNR, the proposed method is better able to distinguish two linear FM chirps as compare to Fourier-Bessel series expansion based method and FB based method in T-F plane. In Fig. 3.7, the T-F representations of signal $s_2[n]$ obtained from the proposed method, Fourier-Bessel series expansion based method, and FB based method have been shown. It can be observed from the T-F representations that the effect of inner interference terms in non-linear FM chirp is clearly visible in T-F representations obtained from Fourier-Bessel series expansion based method and FB based method. However, this effect is significantly reduced using proposed method. It can be observed that in case of clean signal, signal corrupted with AWGN at 10 dB and 20 dB SNRs, all methods are able to identify two separate linear FM and non-linear FM chirp in T-F plane. In case of signal corrupted with 0 dB SNR, the two chirps are better visible in T-F representation obtained using proposed methodology. The T-F representations of signal $s_3[n]$ obtained from proposed method, time-order representation based method and FB based method are shown in Figs. 3.8 (a)-3.8 (l). The T-F representation of proposed method and time-order method are able to classify different components of signal $s_3[n]$ even at signal corrupted at 0 dB and 10 dB SNR. In FB based method, the components are less well separated. The T-F representations based on proposed method, Fourier-Bessel series expansion based method and FB based method for last representative signal $s_4[n]$ are shown in Figs. 3.9 (a)-3.9 (l). It can be observed that at 10 dB SNR, the proposed method and FB based method is able to classify the two frequency-domain separated components of signal $s_4[n]$ whereas at 0 dB SNR, only proposed method can classify the two components of signal $s_4[n]$.

The suitable value of TH for each representative signals $s_1[n]$, $s_2[n]$, $s_3[n]$, and

$s_4[n]$ has been selected empirically. The effect of TH value on WVD based T-F representation by proposed method has been shown in Figs. 3.10-3.13. The TH values chosen for analysing its effect on WVD based T-F representation by proposed method are as follows: TH = 0.001, TH = 0.01, TH = 0.05, TH = 0.07, TH = 0.1, TH = 0.2, TH = 0.35, TH = 0.4, and TH = 0.5. In Fig. 3.10, the effect of different TH values on WVD based T-F representation of clean signal $s_1[n]$ is shown. As signal $s_1[n]$ consists of two well separated linear FM chirps, they are clearly visible in T-F representation at all TH values. However, when TH value is chosen as 0.2 or above, these linear FM chirps started missing T-F information in T-F representation based on WVD by proposed method. Similarly for clean signal $s_2[n]$, the non-linear FM chirp and linear FM are well separated at all TH values but the inner interference term in non-linear FM vanishes at TH 0.35 and above. This is shown in Fig. 3.11. It can be observed from Fig. 3.11 (i), that for TH = 0.5, non-linear FM chirp started losing information in WVD based T-F representation from proposed method. For clean signal $s_3[n]$ (bat signal), at high TH values, components started disperse in T-F representation. This effect can be seen in Fig. 3.12. Similarly in Fig. 3.13, it can be observed that the components of signal $s_4[n]$ are dispersing in T-F plane as TH increases. The value of TH as 0.001 and 0 has been found to be giving stable results for clean signals $s_1[n]$ and $s_4[n]$ respectively whereas for clean signal $s_2[n]$, TH equals to 0.35 is found suitable. For clean signal $s_3[n]$, TH equals to 0.05 is found suitable.

For signals affected by noise, the same TH value used for clean signal may not reduce the effect of noise in WVD based T-F representation. Therefore, TH values are varied in order to achieve cross-terms free T-F representation from proposed method. The suitable TH for signal $s_1[n]$ corrupted with 0 dB SNR is found to be 0.05, whereas when signal $s_1[n]$ is corrupted with 10 dB SNR and 20 dB SNR, the TH values 0.001 is found suitable. For signal $s_2[n]$, TH value 0.35 is found optimum under all noise cases studied. This may be because 0.35 value of TH is high enough to remove both outer-interference terms and inner-interference-terms. Similarly for

signal $s_3[n]$, the signal corrupted with 20 dB SNR and 10 dB SNR, TH equals to 0.05 is found optimum, whereas when signal is corrupted with 0 dB SNR, TH value as 0.2 is found optimum. For signal $s_4[n]$, when signal corrupted with 0 dB SNR, TH value equal to 0.5 is found suitable whereas when signal is corrupted with 10 dB SNR and 20 dB SNR, TH value 0.001 is found suitable. The performance of the suggested method has been assessed at these specified TH values for different noise environments.

The computation of normalized Rényi entropy measure is done for test signals as clean, signals corrupted by AWGN at 0 dB, 10 dB, and 20 dB SNRs. In the simulation, the normalized Rényi entropy measure is computed 100 times at each SNR value. As the characteristic of noise changes for each iteration, the average of all results will give the robust value of normalized Rényi entropy measure. It can be observed from Table 3.2 that the normalized Rényi entropy measures of proposed method for T-F distribution are low as compared to other compared methods. The computational time by proposed method is higher than other compared methods. However, the aim of this work is to reduce cross-terms from WVD irrespective of computational time.

3.7 Summary

This work presents a novel technique for reduction of cross-terms from WVD using TQWT-FB. The cross-terms are reduced by decomposing the multi-component non-stationary signal into constant and narrow BW sub-band signal by TQWT-FB. These components in a sub-band signal are further segmented by TDS section. Finally the computed WVD of segmented components are added to achieve the WVD with reduced cross-terms. The proposed method is tested on four test signals when these signals are effected by AWGN at 0dB SNR, 10 dB SNR, 20 dB SNR, and infinite SNR. The Rényi entropies obtained by proposed method in all noisy cases is less than the Rényi entropies obtained by Fourier-Bessel series expansion based

method, time-order based method, and FB based method. This shows that the WVD based T-F representation obtained by proposed method has better resolution in T-F domain as compared to resolution obtained by other methods.

Chapter 4

Estimation of IFF of speech signals using TQWT-FB

4.1 Introduction

The IFF of the speech signal is the result of vibration of vocal folds in the human neck. The rate of vocal folds vibration is defined as IFF of speech signal (Oshaughnessy, 2000). Hence, IFF of the speech signal is generated only in voiced regions of speech signal where vocal chords vibrate and generate a quasi-periodic type of signal (Deller et al, 2011; Upadhyay and Pachori, 2015b). The IFF, which is a function of time, can depend on gender, age, health, emotion, accent, and language of a speaker (Jain and Pachori, 2014; Kadambe and Boudreaux-Bartels, 1992b). The accurate estimation of fundamental frequency is required for many applications like as speech compression (Taori et al, 1995), speaker recognition (Shriberg et al, 2005), text to speech synthesis (Moulines and Charpentier, 1990), etc.

The developed techniques in literature can be classified into three main categories (Jain and Pachori, 2014). These categories include block based methods, instantaneous methods, and event based methods (Hess, 1983; Veprek and Scordilis, 2002). The block based methods segment the voiced speech signal before estimating the fundamental frequency. The duration of each segment is short so that

the speech signal can be assumed stationary within block duration and the fundamental frequency is estimated corresponding to each block. Therefore, these methods do not compute fundamental frequency at each sample instant. Some examples of block based methods are average magnitude difference function based method (Ross et al, 1974), AC function based method (Rabiner, 1977), and cepstrum based method (Noll, 1964).

Unlike block based methods, the instantaneous methods compute fundamental frequency at each sample instant of voiced regions of speech signals (Jain and Pachori, 2014). Some well-known techniques in the instantaneous methods category are the HHT based method (Huang and Pan, 2006), ensemble EMD based method (Schlotthauer et al, 2009), and empirical WT based method (Li et al, 2014). However, the performance of these methods degrades when the speech signal is corrupted by noise (Jain and Pachori, 2014). The third category for fundamental frequency estimation is based on the characteristic event of glottal cycles (Ghosh et al, 2007; Jain and Pachori, 2014; Seshadri and Yegnanarayana, 2011; Yegnanarayana and Murty, 2009). The glottal closure instants are the instants where the excitation in vocal tract system is maximum. In (Rathore and Pachori, 2013), the glottal closure instants are determined in LFR which is defined from 50 Hz to 500 Hz (Jain and Pachori, 2013). The fundamental frequency is determined by the inverse of time duration between two successive glottal closure instants.

The proposed method decomposes the speech signal in LFR using a TQWT-FB. Then signals are reconstructed from each sub-band in time-domain and called as sub-band signal. The FFC and its harmonics may be present in different sub-band signals at different time intervals. These intervals in sub-band signal are identified using TDS section. The TDS section segments the sub-band signal in time-domain. Each segmented sub-band signal belongs to either FFC or its harmonic. We termed a segmented sub-band signal as a component. There can be many components obtained from many TDS sections used in the proposed method. Among all these components, the proposed method chose few of them to generate FFC. Then, IFF

is computed by applying Hilbert transform on FFC.

The chapter is organized as follows: The proposed method for estimation of IFF is presented in Section 4.2. Then the performance evaluation parameter is discussed in Section 4.3. The Section 4.4 and 4.5 presents the simulation results and discussion respectively. Finally, Section 4.6 summarizes this work.

4.2 Proposed methodology for IFF estimation of speech signals

The proposed method has several stages which are shown in block diagram in Fig. 4.1. Stage 1 is TQWT-FB which is used to decompose input speech signal in LFR and stage 2 is the set of TDS sections to segment sub-band signals. Then stage 3 is scaled (SFFC) extraction unit which is used for extracting FFC. Finally, stage 4 performs the IFF computation based on the Hilbert transform. These stages are explained in sub-sections below.

4.2.1 Speech signal decomposition by TQWT-FB

A TQWT-FB is designed to decompose the input speech signal, which contains nearly constant BW sub-bands. As the FFC lies in LFR, the designed TQWT-FB has the non-zero response in LFR as shown in Fig. 4.2.

The TQWT-FB is designed using method II as discussed in Section 2.2. The parameter $M = 25$ is chosen for the design of TQWT-FB. This indicates that there are 25 sub-bands in the frequency response of TQWT-FB and the BW of each sub-band is nearly 50 Hz as shown in Fig. 4.2. The BW of each sub-band in TQWT-FB is kept low so that the chances of FFC and its harmonic components lying in the same sub-band are less. However, choosing very narrow BW sub-bands for the design of TQWT-FB will affect the time-domain localization of sub-band signals.

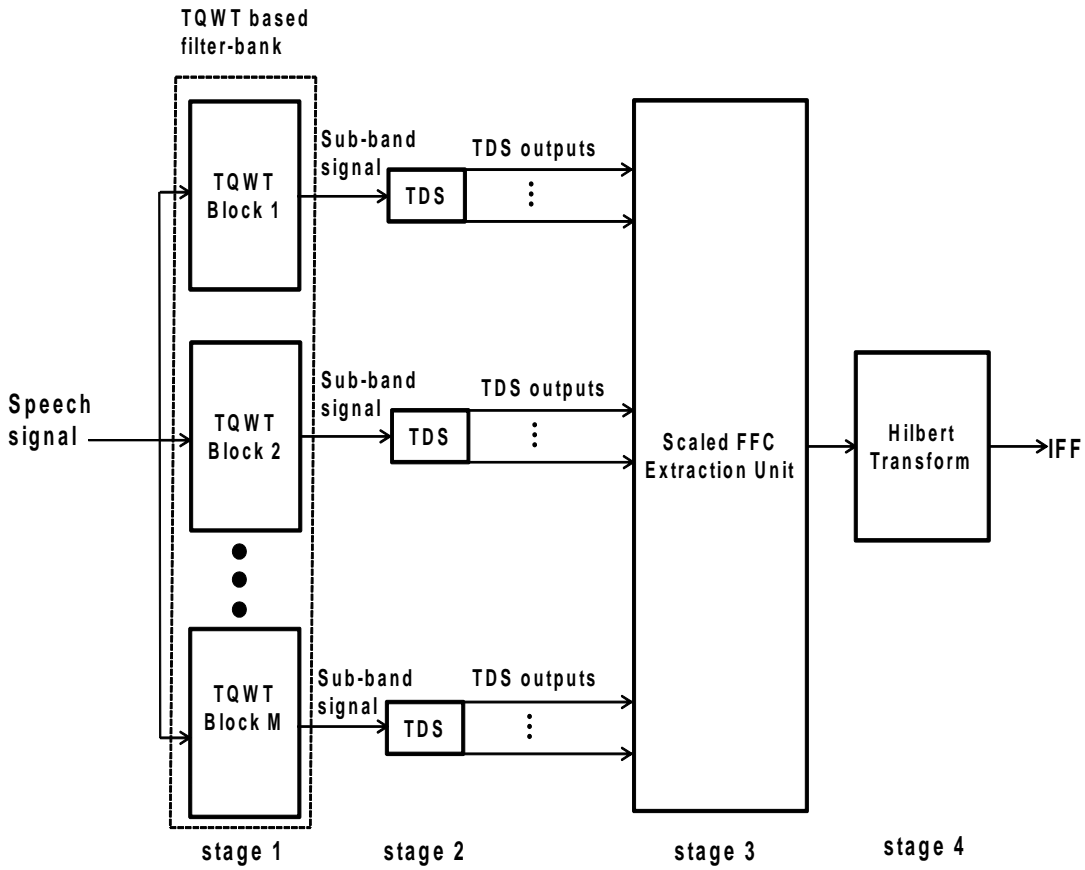


Figure 4.1: Block diagram of the proposed method for determining IFF from speech signals

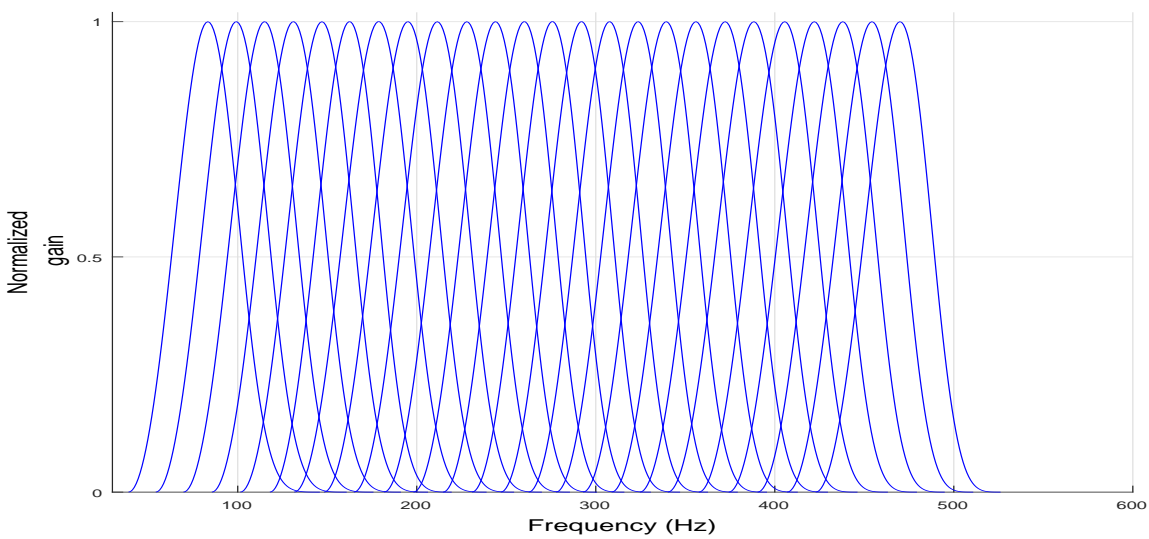


Figure 4.2: TQWT-FB designed for determination of IFF from speech signals

Table 4.1: Chosen values of Q -factor and D in the design of TQWT-FB

TBN	Q -factor	D	TBN	Q -factor	D
1	1.73	40	14	5.93	76
2	2.017	43	15	6.24	78
3	2.313	46	16	6.47	79
4	2.62	49	17	6.7	80
5	2.935	52	18	6.94	81
6	3.323	56	19	7.18	82
7	3.45	56	20	7.42	83
8	3.79	59	21	7.77	85
9	4.14	62	22	8.12	87
10	4.5	65	23	8.47	89
11	4.865	68	24	8.83	91
12	5.24	71	25	9.19	93
13	5.62	74			

The parameter $R = 9$ is assigned to each TQWT block in designing of TQWT-FB. The assigned values of Q -factor and D to each TQWT block are mentioned in Table 4.1.

4.2.2 TDS section

The TDS section segments the components lying at different time interval in a sub-band signal using algorithm mentioned in sub-section 3.3.2. The value of TH in TDS section is chosen low because there may be some low energy FFC present in the speech signal. The chosen values of TH under different circumstances are mentioned in simulation and results section.

4.2.3 SFFC extraction unit

The components from outputs of TDS sections are given input to SFFC extraction unit. Each component can be represented by a band number b_n and component number c_n . Let the sub-band signal shown in Fig. 3.3(a) is the output of l^{th} TQWT block, where $1 \leq l \leq 25$, then b_n of components shown in Fig. 3.3(e) and (f)

is equal to l . Since the component in Fig. 3.3(e) exist before component in Fig. 3.3(f) in time-domain, therefore $c_n = 1$ for component in Fig. 3.3(e) and $c_n = 2$ for component in Fig. 3.3(f). There is possibility that two components having different b_n value, exist in same time duration. Since the frequency of FFC is lower than that of its harmonic component, the SFFC extraction unit will select that component which has lower b_n value. It may be possible that this section could not find any component at particular sample instant. Then that sample instant is assumed to be part of a non-voiced region and no component is selected in that region. However, it is not necessary that selected components belong to FFC only. It may be possible that the time-duration of harmonic component is slightly more than time-duration of FFC by few samples. For these few samples, this unit will select harmonic component. When a harmonic component is selected, then by simple addition of components will not produce FFC. Therefore, this section performs weighted addition of selected components which gives more weight to components which belong to FFC. The weight assigned to a component is the number of times that component is selected by SFFC extraction unit.

Suppose a component Cp_1 , exists from sample instants n_1 to n_2 , and another component Cp_2 exists from sample instants n_0 to n_2 , where $n_0 < n_1$. Let b_{n1} is the band number of Cp_1 and b_{n2} is the band number of Cp_2 , and $b_{n1} < b_{n2}$. Then from sample instant n_0 to $n_1 - 1$, this unit will select Cp_2 , $n_1 - n_0$ times. Similarly Cp_1 will be selected $n_2 - n_1 + 1$ times from sample instant n_1 to n_2 because $b_{n1} < b_{n2}$. Hence weight of Cp_1 will be $n_2 - n_1 + 1$ and weight of Cp_2 will be $n_1 - n_0$. Usually the difference $n_1 - n_0$ is very low in speech signal, hence if Cp_2 is harmonic of Cp_1 , then weight of Cp_2 will be very less.

The components are added after assigning weights to them to obtain FFC with scaled amplitude which we termed as SFFC. The SFFC may have samples of small amplitude in non-voiced regions as well. These low amplitude samples exist because value of TH is chosen low in TDS section in order to retain FFC with low energy. Therefore, to eliminate such samples, the envelope of normalized SFFC is computed.

The normalization is done by dividing SFFC by the maximum value of SFFC. The envelope is compared with a TH termed as F_{TH} to eliminate those samples which occur in non-voiced regions. The value of F_{TH} is determined empirically as mentioned in simulation results section.

4.2.4 Computation of IFF using the Hilbert transform

From SFFC, an analytic signal can be obtained whose real and imaginary part would be SFFC and Hilbert transform of SFFC respectively. The IFF is computed using the derivative of the phase angle of analytic signal and smoothing operation (Upadhyay and Pachori, 2015a; Upadhyay et al, 2017).

4.3 Performance evaluation

In order to determine the efficacy of the proposed method, a performance evaluation parameter known as percentage GE is used. The percentage GE is the percentage of voiced frames of 10 milliseconds duration, whose estimated IFF differs from reference IFF by more than 20 percent (Yegnanarayana and Murty, 2009). A better method is one which has lower percentage GE.

4.4 Simulation results

The proposed method for estimation of IFF from speech signal has been studied on CMU-Arctic database (Kominek and Black, 2004a,b). The CMU-Arctic database has 1150 sentences which are phonetically balanced sentences. The duration of these sentences are about 3 seconds and their F_s is 32 kHz (Jain and Pachori, 2013). These sentences are spoken by five-male and two-female speakers and simultaneous electroglottograph (EGG) recorded signals are also available for two-male and one-

female speakers. In the simulation study, the speech signal has been downsampled by a factor of 4 before the study of the proposed method. The proposed method has been analysed on two-male and two-female speech signals. The identity number of these speech signals are "10004", "10290", "30114", and "30203". These chosen speech signals for simulation are available together with their EGG signals in CMU-Arctic database. Similar to speech signals, the EGG signals are also downsampled by a factor of 4. The reference IFF is generated manually by finding locations of glottal closure instant from difference EGG signal in voiced regions. The difference EGG signal is obtained by applying difference operation on EGG signal after downsampling. The reference IFF is obtained by computing inverse of the time duration between successive glottal closure instants and then moving average based smoothing operation is performed with the window length of 200 samples.

The performance of the proposed method is compared with three other methods. They are multi-band summary correlogram (MBSC) method (Tan and Alwan, 2013), AC based method (Boersma, 1993), and cross-correlation (CC) based method (Goldberg and Riek, 2000). The MBSC method is implemented using MATLAB toolbox available at <http://www.seas.ucla.edu/spapl/shareware.html>. Whereas AC and CC based methods are implemented using Praat software available from (Boersma and Weenink, 2013).

The proposed method and compared methods are examined under three cases. Case 1 is when the speech signal is not corrupted by any noise. Case 2 and case 3 are when the speech signal is corrupted by AWGN at 5 dB SNR and 0 dB SNR, respectively. In the proposed method, if the value of TH is kept high, then low energy FFC may not be detected by TDS section. Therefore TH is kept low. However, in noisy conditions, the TH is slightly increased. The TH = 0.01, TH = 0.03, and TH = 0.05 is chosen in case 1, case 2, and case 3 respectively. Since TH is low, there may be some samples present in non-voiced region. Therefore the value of F_{TH} is determined empirically to eliminate such samples. For each speech signal under test, the detection ACC (DA) in percentage is determined for different value

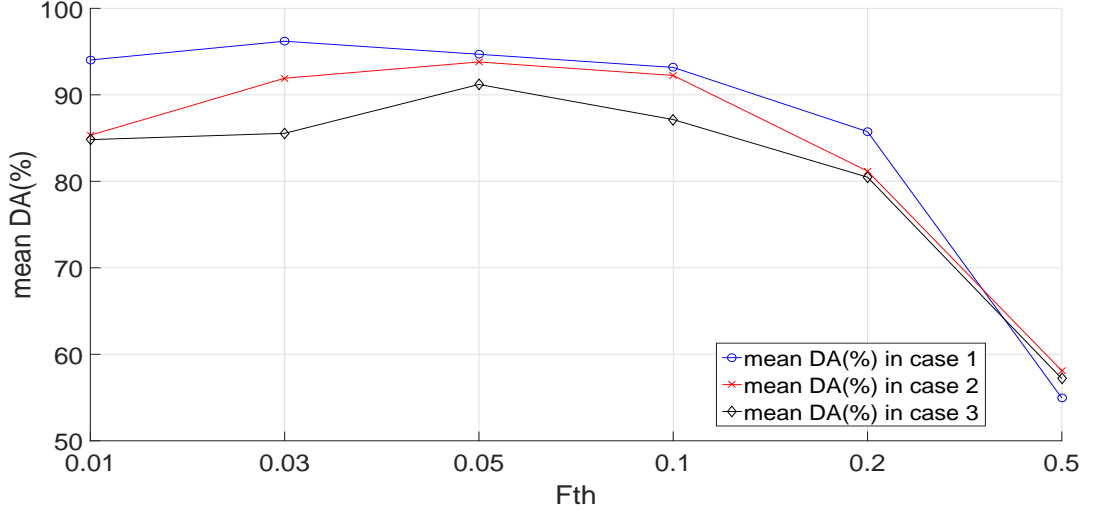


Figure 4.3: Obtained mean DA (%) for different value of F_{TH} in different cases

of F_{TH} under different cases. The DA is the number of samples detected correctly out of total number of samples (Upadhyay and Pachori, 2015b). For each case and for each value of F_{TH} , the mean of DAs obtained for each test signal, is computed. The mean value of DA(%) for different values of F_{TH} in different cases are shown in Fig. 4.3. The $F_{TH} = 0.03$ in case 1 and $F_{TH} = 0.05$ in case 2 and 3 is chosen since at these values, the mean DA(%) is highest.

The Fig. 4.4(a) shows the waveform of a speech signal in case 2 and Fig. 4.4(b) shows the obtained SFFC from proposed method. The obtained IFF from proposed method along with the reference IFF has been shown in Fig. 4.4(c). Similarly, the obtained IFF from MBSC method, AC based method, and CC based method are shown in Fig. 4.4(d), (e), and (f) respectively. From Fig. 4.4(c), (d), (e), and (f), it can be observed that the estimated IFF from the proposed method is more close to reference IFF as compared to IFF obtained from most of the other compared methods. In a similar way, Fig. 4.5 and Fig. 4.6 show obtained IFF from proposed and other compared methods for case 2 and case 3 respectively. The computed percentage GEs for proposed method and other compared methods in different cases are shown in Table 4.2.

The percentage GEs shown in Table 4.2, is the mean of the GEs(%) obtained by four test signals by a particular method. The variance of percentage GEs in case1 by proposed method, MBSC method (Tan and Alwan, 2013), Praat's AC based

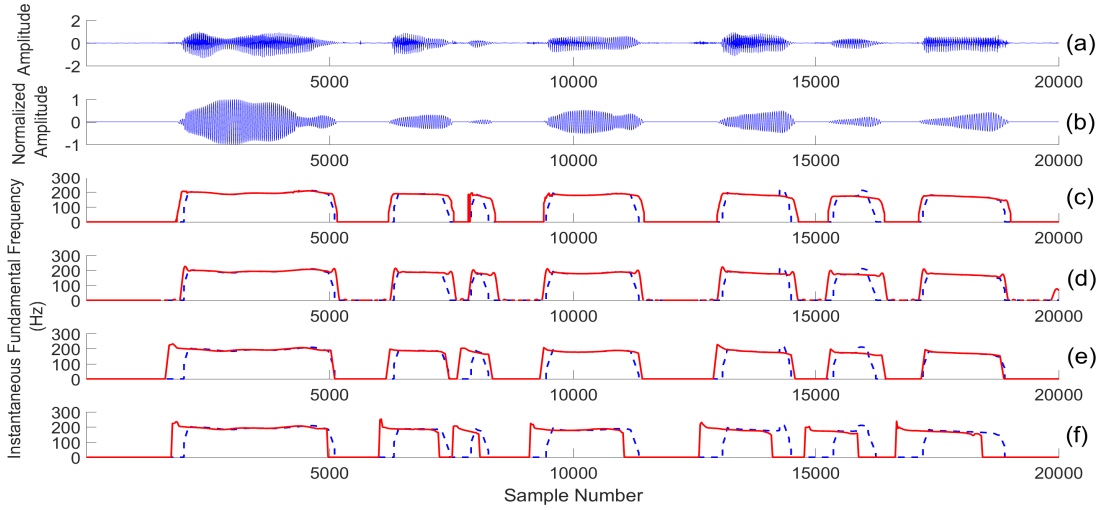


Figure 4.4: (a) Speech signal in case 1 (b) obtained SFFC from proposed method, obtained IFF (red) by (c) Proposed method, (d) MBSC method, (e) AC based method, and (f) CC based method. Reference IFF (blue and dashed) is shown in (c) to (f).

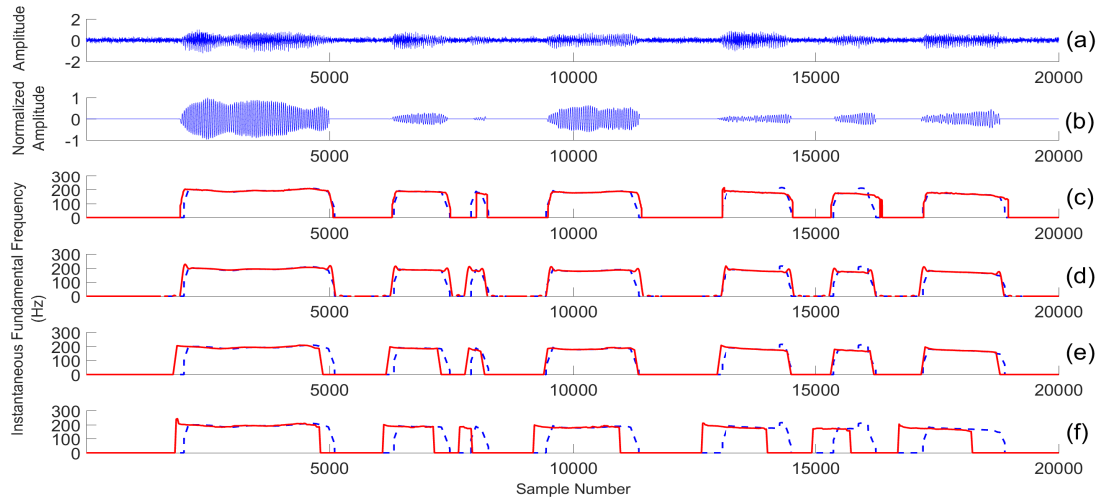


Figure 4.5: (a) Speech signal in case 2 (b) obtained SFFC from proposed method, obtained IFF (red) by (c) Proposed method, (d) MBSC method, (e) AC based method, and (f) CC based method. Reference IFF (blue and dashed) is shown in (c) to (f).

Table 4.2: Percentage GEs for different methods for estimation of IFF of speech signals

Case	Proposed method	MBSC method (Tan and Alwan, 2013)	Praat's AC based method (Boersma, 1993)	Praat's CC based method (Goldberg and Riek, 2000)
Case 1	1.35	2.17	4.12	13.87
Case 2	7.34	7.82	14.17	24.92
Case 3	12.42	16.45	29.43	45.10

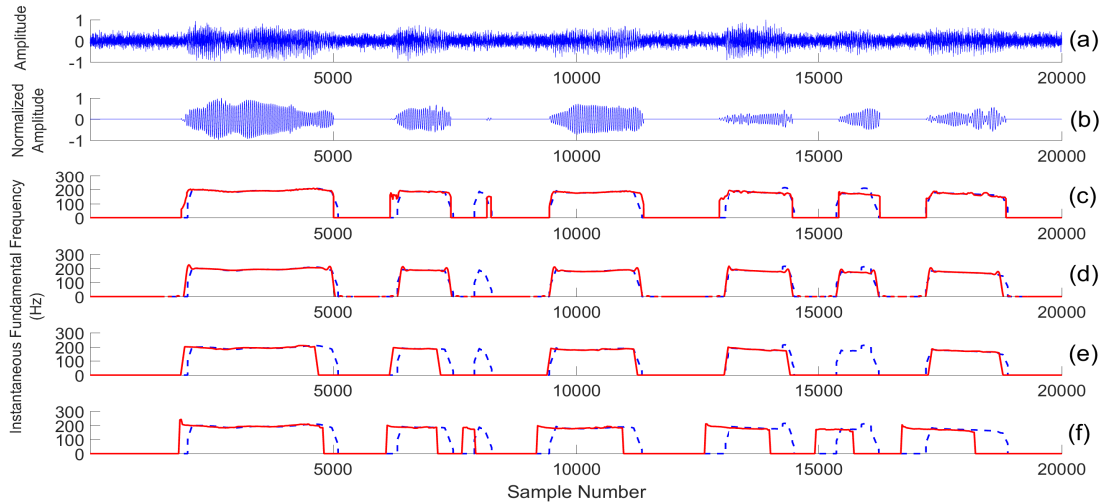


Figure 4.6: (a) Speech signal in case 3 (b) obtained SFFC from proposed method, obtained IFF (red) by (c) Proposed method, (d) MBSC based method, (e) AC based method, and (f) CC based method. Reference IFF (blue and dashed) is shown in (c) to (f).

method (Boersma, 1993), and Praat’s CC based method (Goldberg and Riek, 2000) is 1.57, 6.99, 23.82, and 17.92, respectively. Similarly, the variance of percentage GEs in case2 is 60.83, 50.8, 165.23, and 115.83 for proposed method, MBSC method (Tan and Alwan, 2013), Praat’s AC based method (Boersma, 1993), and Praat’s CC based method (Goldberg and Riek, 2000), respectively. At the last, for case 3, the variance of percentage GEs by proposed method, MBSC method (Tan and Alwan, 2013), Praat’s AC based method (Boersma, 1993), and Praat’s CC based method (Goldberg and Riek, 2000) is 85.69, 153.1, 168.36, and 13.43, respectively.

4.5 Discussion

The proposed method is designed for the estimation of the IFF of speech signals. The TQWT-FB in proposed model decomposes the speech signal in LFR and then TDS section segments the sub-band signals in time-domain. The components obtained from TDS section are then fed to SFFC extraction unit where FFC with scaled amplitude is obtained. The amplitude is scaled due to weighted addition of components in SFFC extraction unit. The Hilbert transform in the last stage of

proposed method is used to compute the IFF of speech signal.

The efficacy of proposed method is compared with MBSC method (Tan and Alwan, 2013), AC based method (Boersma, 1993), and CC based method (Goldberg and Riek, 2000). The MBSC method catches many harmonics in the sub-bands by apply four finite impulse response filters. Then the envelope of the signal is used to estimate IFF in all sub-bands. In AC based method, When a signal is windowed, it is difficult to determine the peak which corresponds to the fundamental period in AC function. Hence, a mechanism is implemented in Praats AC based method in which error due to windowing a signal is minimized. The ratio of AC of windowed voiced speech signal to the AC of window function is computed in order to reduce the artifacts generated by windowing. In this method, due to limitation of F_s , a sinc interpolation is used close to local maxima which correspond to fundamental frequency of speech signal. The CC based method eliminates the rolling off effect which occurs at higher lag values in AC. Here the CC function operates on two different windows of data (Goldberg and Riek, 2000).

The visual representation of estimated IFF by proposed method and compared method in different noisy conditions can be found in Fig. 4.4, Fig. 4.5, and Fig. 4.6. The Fig. 4.4 shows the estimated IFF by different methods in case 1. The Fig. 4.4(a) shows the speech signal and Fig. 4.4(b) shows the extracted SFFC with normalized amplitude. The components in voiced regions are clearly visible in Fig. 4.4(b). It can be observed from Fig. 4.4(c) and Fig. 4.4(d) that IFFs estimated by proposed method and MBSC method are very close to reference IFF. On the other hand, the AC and CC based methods are not able to track IFF within voiced region.

Similarly in Fig. 4.5(a), the speech signal corrupted with noise in case 2, can be seen. The extracted SFFC can be seen in Fig. 4.5(b) where components in voiced region are visible. From Fig. 4.5(c), (d), (e), and (f), it can conclude that the IFFs estimated by proposed method and MBSC method are near to reference IFF whereas IFFs obtained by AC and CC methods are not able to estimate IFF in some part of voiced region.

The speech signal for case 3 in which the signal is corrupted by AWGN at 0 dB SNR can be seen in Fig. 4.6(a). It can be observed that the strength of the noise increased in this case and it is difficult to find voiced and non-voiced regions from Fig. 4.6(a). The SFFC obtained by proposed method is shown in Fig. 4.6(b). Here, it can be observed that one component in voiced region of SFFC is significantly attenuated by TDS section because of its low energy. It can be observed from Fig. 4.6(c) that the IFF estimated by proposed method is close to reference IFF for most of the voiced region. However, the MBSC method is not able to compute IFF for one voiced region. The estimated IFF by AC and CC based methods is zero for some part or entire voiced region.

The estimated IFF by proposed method and MBSC method is close to the reference IFF in all cases. On the other hand AC and CC based methods are not able to track IFF accurately. The GE (%) obtained by proposed method is lowest than compared methods in all cases which can be noted from Table 4.2. The variance of computed GE (%) from four speech signals is high in many cases, since only four signals are used to test the proposed method and compared methods.

4.6 Summary

The method proposed in this chapter estimates the IFF of the speech signals by applying TQWT-FB. The speech signal is decomposed by TQWT-FB in LFR and then components from sub-band signal are segmented by TDS section. Then the SFFC is extracted from segmented components and finally Hilbert transform is applied on SFFC to obtain the IFF. The proposed methodology is tested on two male and two female speech signals obtained from CMU-Arctic database under clean and different noisy conditions. The noise cases are when speech signal is corrupted by AWGN at 0 dB SNR and 5 dB SNR. The performance of proposed method is evaluated in terms of GE(%) and compared with MBSC method, AC based method, and CC based method. In clean and all noise conditions, the computed GE(%) for

proposed method is lower than other methods. This indicates that the estimated IFF by proposed method is closer to reference IFF as compared to other methods.

Chapter 5

Screening of sleep apnea from ECG signals using TQWT-FB

5.1 Introduction

The sleep apnea and hypopnea are the common respiratory disorders which occur during the sleep (Xie and Minn, 2012). There is a complete absence of airflow during apnea and partial blockage of airflow for the minimum of 10 seconds during hypopnea (American Academy of Sleep Medicine Task Force, 1999). These events can occur several times during the sleep. The sleep apnea can be categorized into three classes namely obstructive, central, and mixed (Mendez et al, 2009). In obstructive sleep apnea, the breathing of subject stops due to blockage of the upper airways due to which air does not enter into the lungs (Varon et al, 2015). During central sleep apnea, the muscles of the subject, which control the breathing, do not receive signals from brain properly (Javaheri and Dempsey, 2013). The mixed sleep apnea is the combination of obstructive sleep apnea and central sleep apnea. The symptoms of sleep apnea are the sleepiness during daytime, irritation, depression, tiredness, lack of concentration, and low learning capacity (White, 2006). These symptoms may create social problems and traffic accidents. A person having undiagnosed obstructive sleep apnea may get cardiovascular diseases such as congestive heart failure,

stroke, hypertension, etc (Young et al, 1997).

Currently, polysomnography is used to diagnose sleep apnea (Nguyen et al, 2014). In this technique, the patient has to sleep in a special laboratory for one or two nights. There are many electrodes and sensors attached to patient's body which may degrade the subject's quality of sleep (Arqub, 2017; Arqub and Abo-Hammour, 2014; Li et al, 2016; Peker, 2016). During the sleep time, physicians monitor cardiorespiratory signals (Nguyen et al, 2014). Physicians need to identify the events of apnea by observing the signals visually. The physicians may need to screen the voluminous data which may lead to human errors and thus, not reliable. Moreover, polysomnography technique is expensive since many channels are required to detect the sleep apnea. Hence, it is required to develop novel methods using a single channel which will reduce the cost of the device (Hassan and Haque, 2017) and use advanced signal processing techniques for reliable detection of sleep apnea (Penzel et al, 2002). There are number of methods proposed in the literature using single channeled signal instead of polysomnography method. A review of various methods used to diagnose obstructive sleep apnea is presented in (Faust et al, 2016).

The screening of sleep apnea from ECG signal using EMD is shown in (Hassan, 2015b) and (Hassan, 2015a). The EMD in (Hassan, 2015b) and (Hassan, 2015a) is used to decompose the segments of ECG signals to detect apneic events. The authors used EMD to decompose the segmented ECG signals and then extracted statistical features like mean, skewness, variance, and kurtosis. In (Hassan, 2015b), extreme learning machine is used for classification of apneic and non-apneic segments of ECG signal. In (Hassan, 2015a), performance of nine different classifiers are studied in classification problem of apneic and non-apneic events. The authors in (Acharya et al, 2011a) used non-linear parameters like approximate entropy, fractal dimension, correlation dimension, largest Lyapunov exponent, and Hurst exponent as features to detect sleep apnea from ECG signals. They used artificial neural network classifier to categorize ECG signal in either apnoea, hypopnoea, or normal group.

The work proposed in (Chen et al, 2015a) used an automatic ECG signal segmen-

tation scheme, in which segments of unequal length are obtained for classification. A local median filter is employed to minimize the unexpected RR intervals and SVM is used to screen apneic segments of ECG signal. In (Mendez et al, 2009), authors used the ECG characteristics like QRS complex area and RR interval to screen the obstructive sleep apnea. The power spectral densities of RR interval and area of QRS complex are evaluated by bivariate time-varying autoregressive model for each beat. Then, neural networks and k -NN were used to classify apneic and non-apneic segments of ECG signal.

In (Khandoker et al, 2009), the features are obtained by wavelet decomposition of heart rate variability and ECG-derived respiration signals. The classification is performed using SVM to detect apnea. The use of heart rate variability and ECG-derived respiration signals for the detection of sleep apnea is also proposed in (Tripathy, 2018). In (Nguyen et al, 2014), the recurrence quantification analysis statistics of heart rate variability data are used to measure the heart rate complexity. The recurrence quantification analysis statistics are used as features as they can identify non-linear dynamics of the complex cardiorespiratory system during sleep apnea. In (Kesper et al, 2012), authors have developed modules to evaluate sleep-disorder breathing from ECG signals. These mutually dependent modules are cyclical variations of the heart rate analysis, QRS detection, ECG-derived respiration curves calculations, and sleep pattern estimation.

In (Hassan and Haque, 2016), authors proposed low power automatic identification of sleep apnea using spectral and statistical features. They used single-lead ECG signals to detect sleep apnea. The author in (Hassan, 2016) used TQWT to decompose segments of ECG signal. The features obtained by normal inverse Gaussian parameters are estimated from each sub-band. Similarly, in (Hassan and Haque, 2017), the authors have classified apneic and non-apneic segments of ECG signal using TQWT method. They have extracted statistical features.

In (Xie and Minn, 2012), the authors proposed the detection of sleep apnea from ECG and saturation of peripheral oxygen (SpO_2) signals. They have performed

the study using only ECG signals, only SpO₂ signals, and combining both signals. They have extracted ECG and SpO₂ features and run the simulation on ten different classifiers. The discriminative hidden Markov model (HMM) is used to detect apnea in (Song et al, 2016). The authors of (Kumar and Kanhangad, 2018) propose novel phase descriptors for obstructive sleep apnea detection using ECG signals. They have considered phase descriptor obtained from phase responses of Gabor filter as feature vector.

In literature, authors have used signals other than ECG for the screening of sleep apnea. For example in (Azarbarzin and Moussavi, 2013), many features like zero crossing rate, peak frequency, etc, are extracted from signals of snoring sound and detected apneic events using linear discrimination analysis. The EMD has been used to decompose pulse oximetry signals to classify obstructive sleep apnea (Schlotthauer et al, 2014).

In this work, we are screening the apneic event for each minute of ECG signal. We have proposed a methodology to classify apneic and non-apneic segments of ECG signal. These segments are of one minute duration. These ECG segments are non-stationary in nature. Also the apneic segment of ECG signal is more oscillatory than the non-apneic segment of ECG signal at some time interval (Hassan, 2016). Therefore, it motivates us to develop a technique which decomposes ECG segment into the number of sub-band signals having different oscillatory nature and then try to classify apneic and non-apneic segments of ECG signal by capturing similarity between decomposed sub-band signals. Therefore, we have employed TQWT-FB rather than TQWT, to decompose the segments of ECG signal into sub-band signals. Since several mother wavelets are available to analyse various oscillatory signals.

After decomposition of a segment of ECG signal from TQWT-FB, the sub-band signals are used to compute features from which apneic and non-apneic segments can be classified with good ACC. The features are computed by applying CCE on sub-band signals. The correntropy measures the similarity between sub-band signals (Reddy and Rao, 2017). The novelty of proposed method can be listed as

follows:

1. This is the first work to apply TQWT-FB for screening of sleep apnea.
2. To the best of our knowledge, the CCE is used to compute features in TQWT-FB frame work for the first time in apneic and non-apneic ECG segments classification problem.

The rest of the chapter is constructed as follows. A brief description of the database is given Section 5.2. Then Section 5.3 describes the proposed methodology followed by performance evaluation parameters in Section 5.4. Then the simulation results are shown in Section 5.5 and discussed in Section 5.6. Finally, this chapter is summarized in Section 5.7.

5.2 Database

In this work, the apnea-ECG database (Penzel et al, 2000) has been used. It is a public database available at Physionet (Goldberger et al, 2000). The database was used in Computers in Cardiology challenge in the year 2000 (Penzel et al, 2002). The database consists of 70 recordings, of which 35 of them are training data and rest of them are testing data. The ECG signals recorded from 35 subjects of training data are categorized into three groups namely group A, B, and C. The subjects of group A, also known as the group of apnea have minimum 100 minutes of apneic events (Penzel et al, 2000). Group B or borderline apnea group has 10 to 96 minutes of apneic events and control group or group C has less than 5 minutes of apneic events (Penzel et al, 2000). The age of subjects varies from 27 to 63 years and the average age of subjects belonging to group A, B, and C is 50 years, 46 years, and 33 years respectively. The recording duration of each signal is between 7 to 10 hours. The F_s is 100 Hz and signal resolution is 12 bits.

There were two types of study conducted in Computers in Cardiology challenge 2000. The first one is to discriminate patients with apnea and without apnea based

on the training and testing data given in the database. The second study is to detect the apneic event for each minute of ECG recording. The database provides the annotations to indicate the presence of apneic or non-apneic event for each minute of ECG signal. These annotations are given for 35 ECG signals of training data (Penzel et al, 2002). In this work, we did the study of classification of the apneic and non-apneic events for each minute of ECG signals from 35 ECG signals. There are 6514 ECG segments of apneic class and 10531 ECG segments of non-apneic class. In literature, lot of work has been done in classification of apneic and non-apneic segments of ECG signals of this database (Hassan, 2015a; Hassan and Haque, 2017; Nguyen et al, 2014). The apneic and non-apneic segments of ECG signal are shown in Fig. 5.1 and explained in following sub-sections.

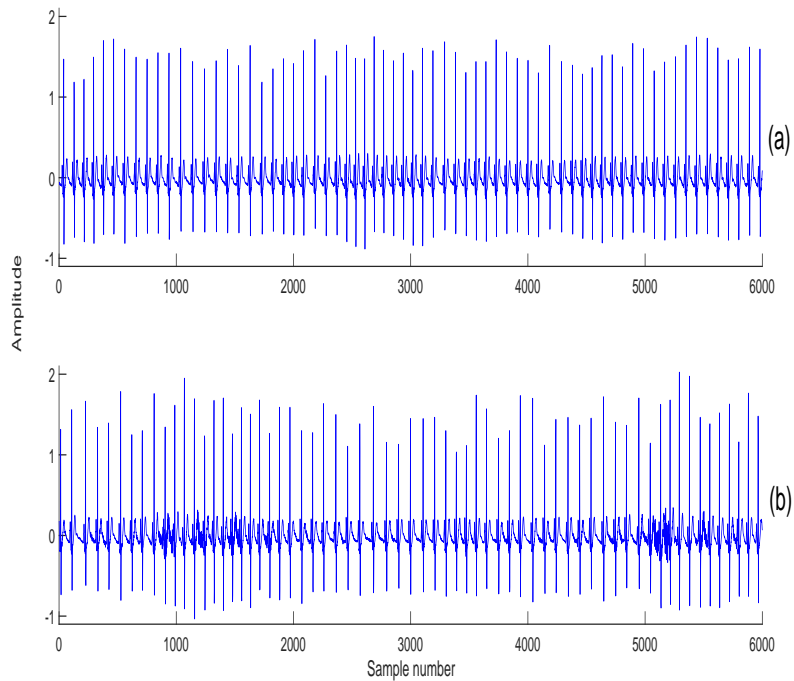


Figure 5.1: The segment of (a) non-apneic ECG signal and (b) apneic ECG signal.

5.3 Proposed method

The method proposed in this work performs the classification of apneic and non-apneic segments of ECG signal. The proposed method divides the ECG signal into segmented signals of one-minute duration in the first stage. Then, TQWT-FB is used to decompose the segment of ECG signal in the second stage. The decomposed signals are band-limited signals and called as sub-band signals. Then in next stage, features are computed from sub-band signals and ranked. Then in the final stage, a classifier is used for the classification. These stages are shown in Fig. 5.2 and explained in following sub-sections.

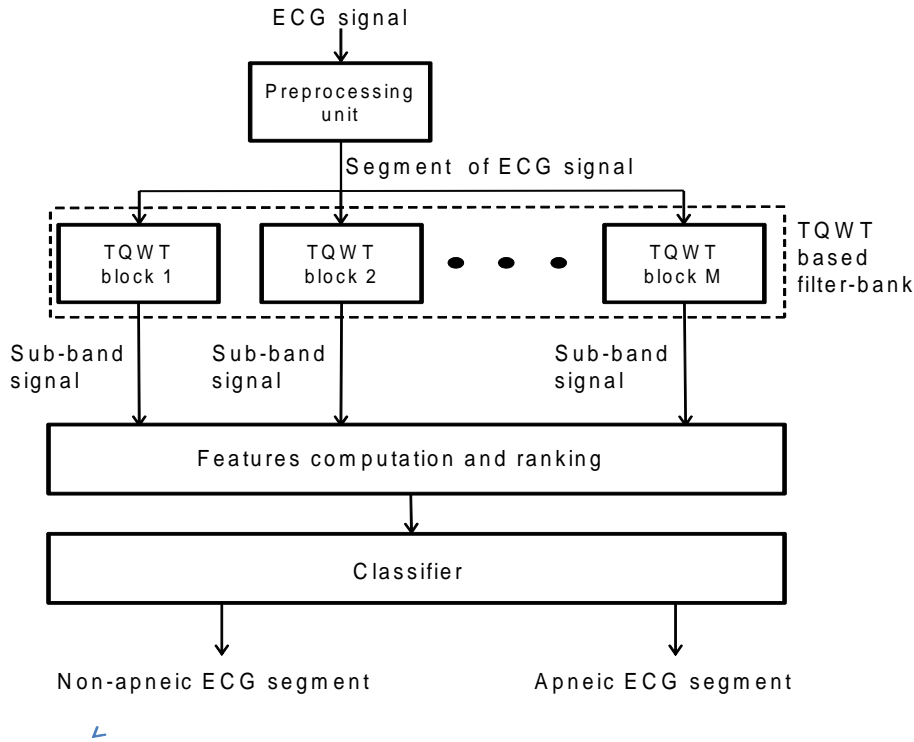


Figure 5.2: Block diagram of proposed method for automated detection of apneic segments of ECG signal.

5.3.1 Preprocessing unit

In this section, ECG signals are segmented. From the database, we have the annotation for each minute of ECG signal. In this work, we are classifying the apneic and non-apneic segments of ECG signals of one-minute duration. Therefore, ECG signals from the database are segmented into one-minute duration.

5.3.2 TQWT-FB design

The TQWT-FB used to address classification problem in this work, is designed using Method II as described in Section 2.2. Depending upon the designing of TQWT-FB, the ECG segment can be decomposed into any number of sub-bands. If M is low, then ECG segments will be decomposed into few sub-bands of large BW . On the other hand, if M is large, the TQWT-FB will decompose ECG segments into more number of sub-bands of low BW . This also increases the computational complexity of the system. In this work, we tested the effect of BW of sub-bands on the performance of our method on two types of TQWT-FBs. The two FBs namely FB 1 and FB 2 are shown in Fig. 5.3. The BW of sub-bands in FB 1 is wider than the FB 2. The $BW = 0.05$ (normalized frequency) for FB 1 and $BW = 0.03$ (normalized frequency) for FB 2 is chosen. The $M = 27$ and $M = 45$ are chosen for FB 1 and FB 2 respectively. The Fig. 5.3 also shows that the sub-band 1 has lowest f_c and f_c of subsequent sub-bands are gradually increasing. The sub-band M has highest f_c .

The assigned values for Q -factor, R , and D in different TQWT blocks for both FBs are mentioned in Table 5.1 and Table 5.2.

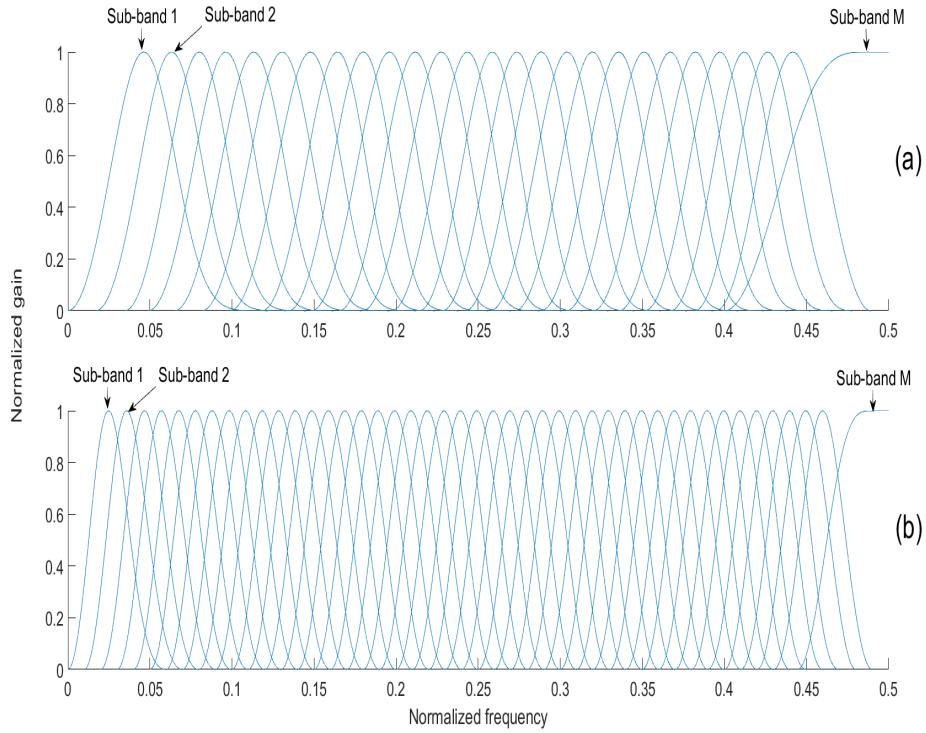


Figure 5.3: Designed TQWT-FBs: (a) FB 1 and (b) FB 2.

Table 5.1: The chosen value of TQWT parameters for FB 1.

TBN	Q -factor	R	D	TBN	Q -factor	R	D
1	1	9	13	15	5.5	9	13
2	1.29	9	14	16	5.7	9	12
3	1.62	9	15	17	5.95	9	11
4	1.87	9	15	18	6.2	9	10
5	2.14	9	15	19	6.5	9	9
6	2.43	9	15	20	6.8	9	8
7	2.74	9	15	21	7.17	9	7
8	3.25	9	16	22	7.55	9	6
9	3.6	9	16	23	7.97	9	5
10	3.76	9	15	24	8.46	9	4
11	4.15	9	15	25	8.95	9	3
12	4.33	9	14	26	9.34	9	2
13	4.8	9	14	27	9	9	1
14	5.3	9	14				

Table 5.2: The chosen value of TQWT parameters for FB 2.

TBN	<i>Q</i> -factor	<i>R</i>	<i>D</i>	TBN	<i>Q</i> -factor	<i>R</i>	<i>D</i>	TBN	<i>Q</i> -factor	<i>R</i>	<i>D</i>
1	1	3.35	7	16	6	3.1	10	31	11	3.12	7
2	1.33	3.06	7	17	6.33	3.12	10	32	11.33	3.31	7
3	1.66	3.25	8	18	6.66	3.15	10	33	11.66	3.53	7
4	2	3.06	8	19	7	3.19	10	34	12	3.17	6
5	2.33	3.29	9	20	7.33	3.23	10	35	12.33	3.43	6
6	2.66	3.16	9	21	7.66	3.29	10	36	12.66	3.02	5
7	3	3.06	9	22	8	3.35	10	37	13	3.34	5
8	3.33	3.32	10	23	8.33	3.06	9	38	13.33	3.77	5
9	3.66	3.24	10	24	8.66	3.14	9	39	13.66	3.26	4
10	4	3.19	10	25	9	3.23	9	40	14	3.86	4
11	4.33	3.15	10	26	9.33	3.33	9	41	14.33	3.19	3
12	4.66	3.12	10	27	9.66	3.03	8	42	14.66	4.19	3
13	5	3.1	10	28	10	3.15	8	43	15	3.12	2
14	5.33	3.09	10	29	10.33	3.29	8	44	15.33	6.12	2
15	5.66	3.09	10	30	10.66	3.45	8	45	17	6	1

5.3.3 Computation of features and ranking

As apneic and non-apneic ECG segments differ in their oscillatory nature in some interval of time (Hassan, 2016), and since these ECG segments are decomposed into different oscillatory sub-band signals by TQWT-FB, these oscillatory sub-band signals corresponding to apneic and non-apneic ECG segments must differ in some sense. The correntropy examine the similarity among various sub-band signals (Reddy and Rao, 2017). Therefore, the features are computed using CCE. The CCE is the difference of correntropy and mean correntropy (Patidar et al, 2017) and the correntropy computes the correlation in non-linear domain (Santamaria et al, 2006). The CCE for two random variables U and V is defined as (Rao et al, 2011):

$$\begin{aligned}
\text{CCE}(U, V) &= E_{U,V}[K(U - V)] - E_U E_V[K(U - V)] \\
&= \int \int K(u - v) \{dF_{U,V}(u, v) - dF_U(u)dF_V(v)\}
\end{aligned} \tag{5.1}$$

The E is expectation operator, $F_{U,V}(u, v)$ is joint probability density function of U and V , $F_U(u)$ is marginal probability distribution function of U , and $F_V(v)$ is marginal probability distribution function of V . The $K(\cdot)$ is a shift invariant kernel

function (Rao et al, 2011).

To compute CCE, two sub-band signals are required. However, there is question on the choice of sub-band signals for computation of CCE. The Fig. 5.5 and Fig. 5.7 show the box plots, when CCE is computed from sub-band signals belonging to non-adjacent sub-bands of FB 1 and FB 2 respectively. Similarly, box plots in Fig. 5.4 and Fig. 5.6 are shown, when adjacent sub-bands of FB1 and FB2 respectively, are involved in computation of CCE. It can be observed from Fig. 5.4 and Fig. 5.6, that the features computed from sub-band signal belonging to adjacent sub-bands show some variation in mean and interquartile range in the box plot of apneic and non-apneic classes. Whereas this phenomenon can be observed only in Fig. 5.5(c) and Fig. 5.7(d).

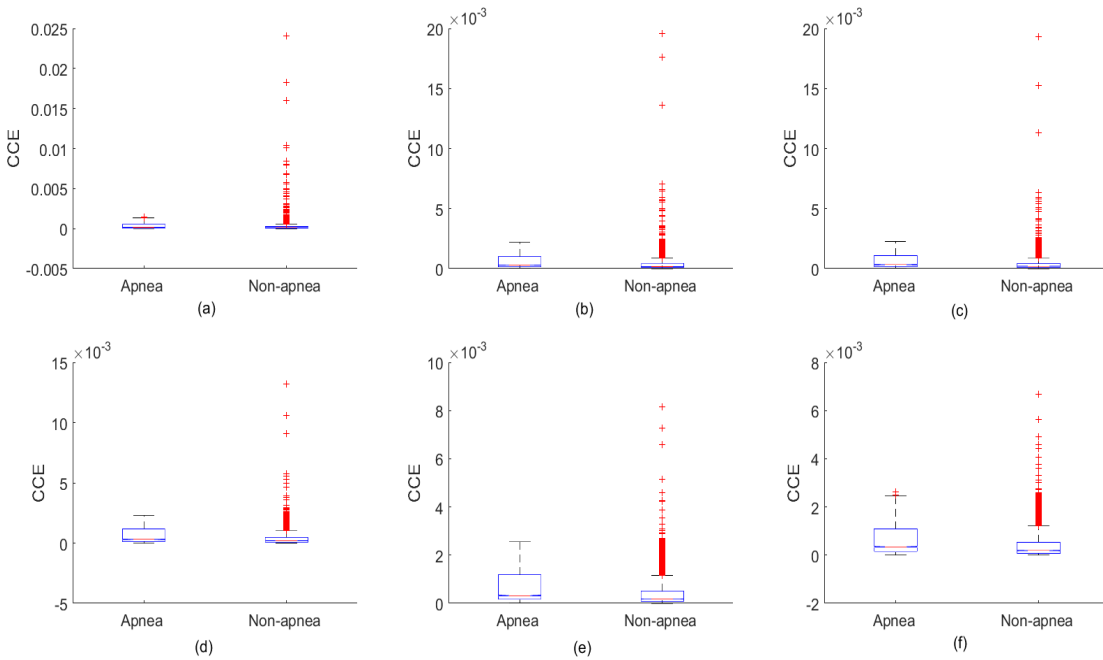


Figure 5.4: The box plot of CCE computed for FB 1 from sub-band signals from (a) sub-band 1 and sub-band 2, (b) sub-band 2 and sub-band 3, (c) sub-band 3 and sub-band 4, (d) sub-band 4 and sub-band 5, (e) sub-band 5 and sub-band 6, (f) sub-band 6 and sub-band 7.

Due to this reason, the CCE is computed from sub-band signals obtained from adjacent sub-bands only. In total $M - 1$ features are computed. The CCE is computed by using ITL toolbox available at <http://www.sohanseth.com/Home/codes>. The features obtained are ranked in order to obtain most effective features. This

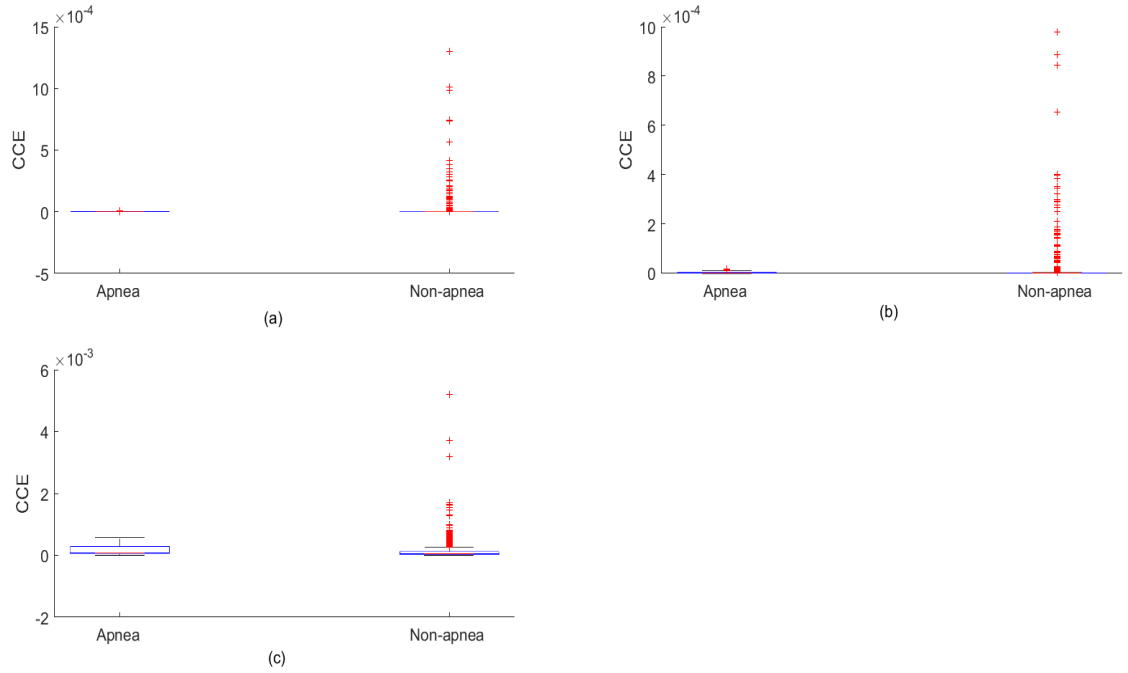


Figure 5.5: The box plot of CCE computed for FB 1 from sub-band signals from (a) sub-band 1 and sub-band 7, (b) sub-band 2 and sub-band 6, (c) sub-band 3 and sub-band 5.

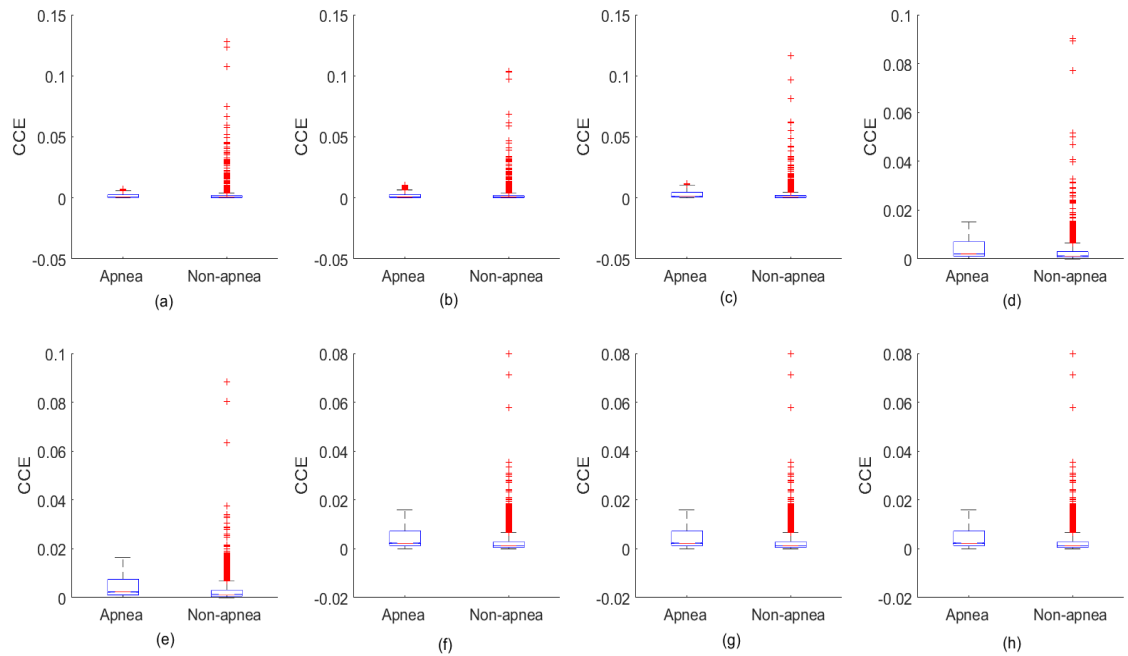


Figure 5.6: The box plot of CCE computed for FB 2 from sub-band signals from (a) sub-band 1 and sub-band 2, (b) sub-band 2 and sub-band 3, (c) sub-band 3 and sub-band 4, (d) sub-band 4 and sub-band 5, (e) sub-band 5 and sub-band 6, (f) sub-band 6 and sub-band 7, (g) sub-band 7 and sub-band 8, (h) sub-band 8 and sub-band 9.

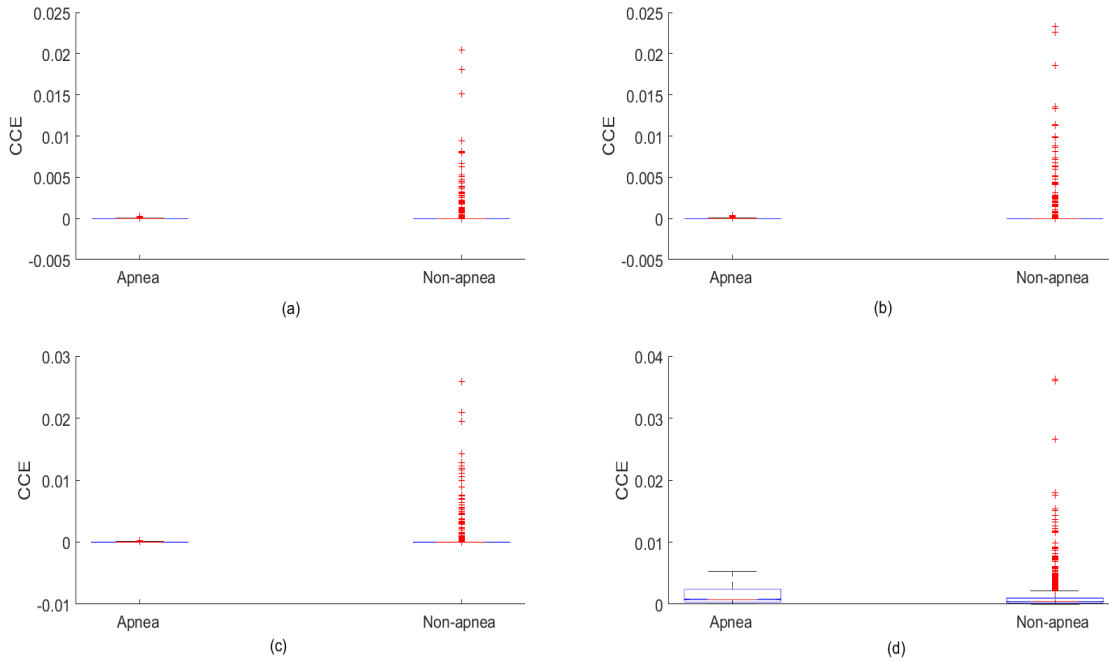


Figure 5.7: The box plot of CCE computed for FB 2 from sub-band signals from (a) sub-band 1 and sub-band 9, (b) sub-band 2 and sub-band 8, (c) sub-band 3 and sub-band 7, (d) sub-band 4 and sub-band 6.

process is basically used to select higher ranked features and the features with lower rank can be omitted. Therefore, a highest classification ACC can be obtained with the less number of features using feature ranking test. The ranking is performed using Students t-test algorithm (Acharya et al, 2015a,b; Box, 1987). The features are ranked according to t-values obtained by t-test. A feature having higher t-value will have a better rank.

The application of CCE in the analysis of physiological signal can be found in (Patidar et al, 2017). The CCE is used to classify normal and alcoholic EEG signals. Similarly, in (Reddy and Rao, 2017), the CCE is used for the classification of epileptic EEG signals.

5.3.4 Classification

In this work, we have tested three types of classifiers belonging to different family of classifiers. The extracted features are given as input to these classifiers and

then variation in performance parameters is observed. These classifiers are briefly described below:

1. Multilayer perceptron (MLP): This classifier is neural network based (Lippmann, 1987; Madyastha and Aazhang, 1994). It is a feed-forward network which consists of HL number of hidden layers between input and output layer. Here $1 \leq HL$. A node on a layer is attached to each node of another layer with some weight. These weights are optimized using back-propagation algorithm (Lippmann, 1987) which uses gradient search technique to decrease the cost function.
2. Bagging classifier: It is an ensemble kind of classifier. The bootstrap aggregating or bagging classifier was introduced in (Breiman, 1996). If there are I instances, then the algorithm obtains the training data of size I from original instances. The size of training data is same as the original instances but they are not the same. There may be few instances in original instances which may not present in training data and there may be few instances from the original instances which are repeated in the training data. Then a weak classifier is generated by the learning system. These steps are repeated for T trials. In each trial, a weak classifier is generated and then finally a strong classifier is obtained by aggregating the weak classifiers. In (Afkhami et al, 2016), bagging classifier has been used in the classification of cardiac arrhythmias from ECG signals. It is also used in (Hajinoroozi et al, 2015), for the classification of cognitive states of the driver.
3. Random forest (RF) classifier: It is one of the tree based classifier. It depends on classification results from many classification trees (Breiman, 2001). The trees are produced by random tree technique (Fraivan et al, 2012). Then each tree is assigned with a random vector before the classification. These assigned random vectors are independent of each other but they have the same distribution. Thus the classification performed by a tree depends on the training data and assigned

random vector. At the time of performing classification, the class is decided by a margin function. The margin function depends on tree classifier (Breiman, 2001). A high value of margin function shows classification with good ACC. The RF classifier is used in (Fraiwan et al, 2012) for the classification of sleep stages from EEG signals and in (Acharya et al, 2011b), to detect glaucoma.

The WEKA software (Hall et al, 2009) is used to perform classification in this work. All the classifiers mentioned in the sub-section are available in WEKA.

5.4 Performance measures

The performance measures parameters namely ACC, specificity (SPE), and sensitivity (SEN) are used to evaluate the classifiers. The ACC is the percentage of apneic ECG segments and non-apneic ECG segments identified correctly from the total ECG segments. The SPE is the percentage of non-apneic ECG segments identified as non-apneic ECG segments and SEN is the percentage of apneic ECG segments classified as apneic ECG segments. These parameters can be expressed in terms of four variables namely true positive (TP), true negative (TN), false positive (FP), and false negative (FN). Here, TP, TN, FP, and FN are total number of accurately identified true positive samples, true negative samples, false positive samples and false negative samples, respectively. The expressions for the performance parameters are shown as follows (Azar and El-Said, 2014):

$$\text{ACC} = \frac{\text{TP} + \text{TN}}{\text{TP} + \text{TN} + \text{FP} + \text{FN}} \times 100(\%) \quad (5.2)$$

$$\text{SEN} = \frac{\text{TP}}{\text{TP} + \text{FN}} \times 100(\%) \quad (5.3)$$

$$\text{SPE} = \frac{\text{TN}}{\text{TN} + \text{FP}} \times 100(\%) \quad (5.4)$$

5.5 Simulation results

In the experiment, first, we considered only the best ranked feature for classification. Then in next step, we considered top two ranked features for classification. Then top three ranked features are selected and so on. The variation in ACCs with respect to the selected number of ranked features (NORF), for different classifiers with FB 1 and FB 2 are shown in Fig. 5.8 and Fig. 5.9 respectively. The performance is evaluated using ten-fold cross-validation strategy (Kohavi, 1995). In this strategy, the entire sample is randomly divided into 10 mutually exclusive sub-samples. One sub-sample is considered as test data and remaining 9 sub-samples are used for training the classifier. This process is repeated for 10 times and each sub-sample is used as test data exactly once. The performance parameters obtained by the classifier in each process are averaged to obtain the final result.

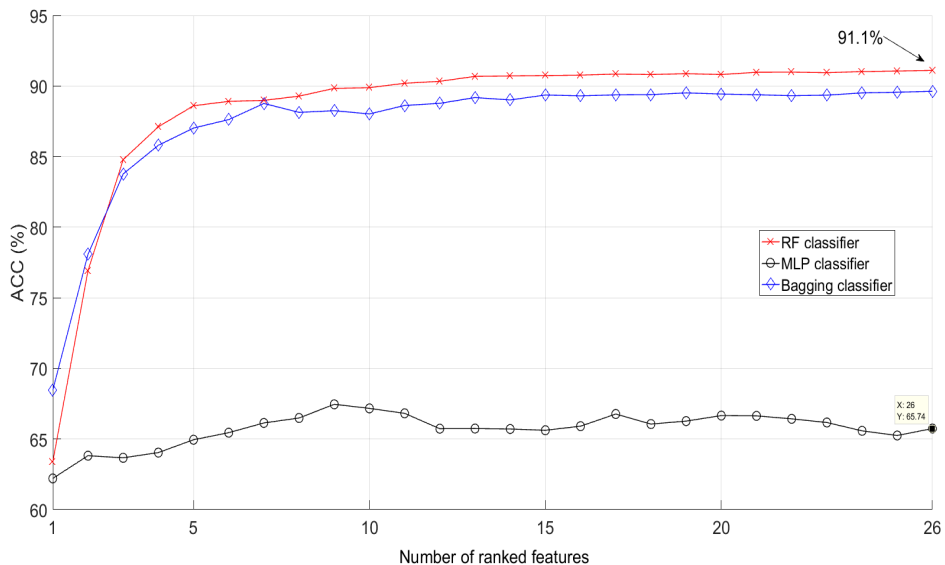


Figure 5.8: Obtained ACC (%) by different classifiers when FB 1 is considered in proposed method

It can be observed from Fig. 5.8 and Fig. 5.9, that the maximum ACC obtained by RF classifier is more than the other classifiers. The maximum ACC achieved by RF classifier is shown in both figures Fig. 5.8 and Fig. 5.9. The ACC obtained by bagging classifier is very close to the ACC obtained by RF classifier for most of the

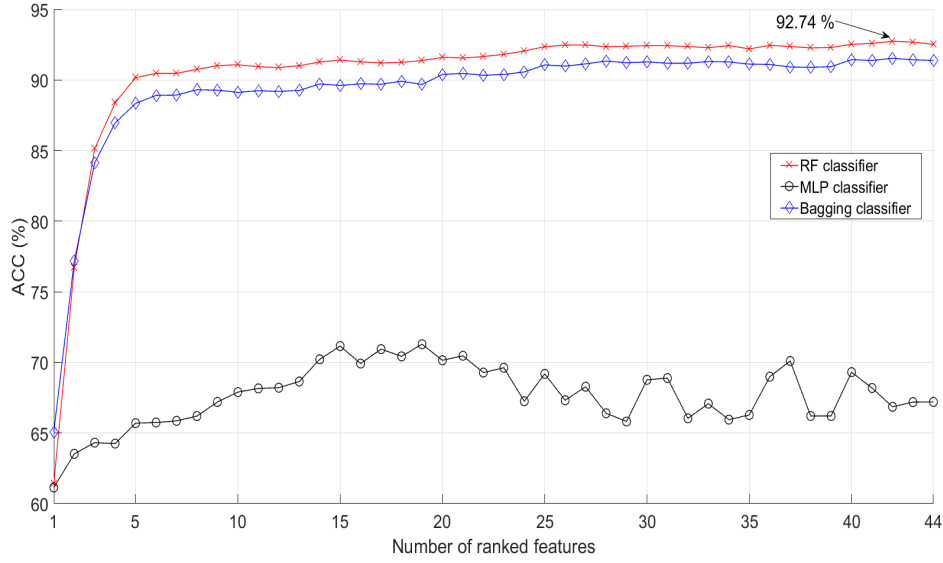


Figure 5.9: Obtained ACC (%) by different classifiers when FB 2 is considered in proposed method

times and the performance of MLP is poor in both cases. Also, the ACC obtained by each classifier increases when the *BW* of sub-band reduces. Since the *BW* of sub-bands for FB 2 is lower than the FB 1, the ACC shown in Fig. 5.9 is higher than the ACC shown in Fig. 5.8. The highest ACC of 92.74% is obtained with RF classifier for FB 2 experiment when 42 ranked features are selected for classification.

In this simulation, the kernel size used to compute CCE is equal to one for selection of best FB and classifier. The size of kernel provides the resolution where correntropy measures similarities in high dimensional kernel feature space (Huijse et al, 2012). To study the effect of kernel size, we performed simulation study for different kernel sizes. From Fig. 5.8 and Fig. 5.9, it can be concluded that use of FB 2 and RF classifier gives the best result. Therefore, we chose FB 2 and RF classifier in proposed method and varied the kernel size to compute CCE. The different kernel sizes chosen are 0.5, 1, 2, and 10. The maximum ACC achieved by proposed method for kernel size 0.5, 1, 2, and 10 is 92.78%, 92.74%, 92.64%, and 92.57% respectively. It can be observed that the variation in obtained ACC by change in kernel size is small. However, the maximum obtained ACC is equal to 92.78%. It is achieved when kernel size is equal to 0.5 to compute features and

NORF = 28 for classification. The obtained SPE is 93.91% and SEN is 90.95%. The statistical analysis of features for this case is presented in Table 5.3. It shows the mean and standard deviation (SD) of each feature for each class. The Table 5.3 also specifies probability (p)-value obtained from Kruskal-Wallis statistical test (McKight and Najab, 2010) corresponding to each feature. In the Table 5.3, (a,b) represents the feature computed from sub-band signals of sub-band a and sub-band b .

The performance of the proposed method is compared with other existing methods in terms of ACC(%), SPE(%), and SEN(%) is shown in Table 5.4. Also, the length of ECG segment used by different methods is mentioned in Table 5.4. Based on the length of ECG segment, and annotation of apneic and non-apneic events given in database, the number of ECG segments in each class used by different methods can be determined.

5.6 Discussion

In this work, TQWT-FB is used to decompose segment of ECG signal. The TQWT-FB has M number of sub-bands and the BW of each sub-band is nearly same. Each sub-band produces a sub-band signal. The features are computed by applying CCE on sub-band signals generated from adjacent sub-bands of TQWT-FB. The features are then ranked using Student's t-test. Then several experiments are performed in which the different NORF are fed to the different classifiers. The best result was given by RF classifier. Also, the effect of change in kernel size to compute features is also observed. These changes affect the ACC, SEN, and SPE obtained by the classifier.

In this work, two types of TQWT-FBs namely FB 1 and FB 2 are examined. The BW of sub-bands of FB 1 is higher than BW of sub-bands of FB 2 as shown in Fig. 5.3. From this figure, it can be observed that more than one sub-band of FB 2, are required to cover the frequency range spanned by one sub-band of FB 1 and the proposed method takes into account the similarity between these sub-bands of

Table 5.3: Statistical analysis of features obtained by computing CCE with kernel size equal to 0.5.

(a,b)	Feature rank	Mean \pm SD of apneic class	Mean \pm SD of non-apneic class	p -value
(1,2)	6	$6.2 \times 10^{-3} \pm 5.9 \times 10^{-3}$	$5.6 \times 10^{-3} \pm 7.7 \times 10^{-3}$	5.06×10^{-15}
(2,3)	4	$7.9 \times 10^{-3} \pm 8.8 \times 10^{-3}$	$6.6 \times 10^{-3} \pm 9.3 \times 10^{-3}$	3.55×10^{-19}
(3,4)	5	$9.9 \times 10^{-3} \pm 10.2 \times 10^{-3}$	$7.4 \times 10^{-3} \pm 9.9 \times 10^{-3}$	1.38×10^{-39}
(4,5)	7	$14.5 \times 10^{-3} \pm 13.4 \times 10^{-3}$	$10.3 \times 10^{-3} \pm 12.1 \times 10^{-3}$	3.68×10^{-96}
(5,6)	9	$15.2 \times 10^{-3} \pm 14.1 \times 10^{-3}$	$11.0 \times 10^{-3} \pm 13.0 \times 10^{-3}$	7.83×10^{-94}
(6,7)	10	$15.3 \times 10^{-3} \pm 14.2 \times 10^{-3}$	$10.9 \times 10^{-3} \pm 13.2 \times 10^{-3}$	8.88×10^{-109}
(7,8)	8	$14.2 \times 10^{-3} \pm 13.3 \times 10^{-3}$	$10.2 \times 10^{-3} \pm 12.2 \times 10^{-3}$	9.63×10^{-92}
(8,9)	11	$13.6 \times 10^{-3} \pm 12.9 \times 10^{-3}$	$9.8 \times 10^{-3} \pm 11.9 \times 10^{-3}$	4.81×10^{-84}
(9,10)	12	$14.0 \times 10^{-3} \pm 13.2 \times 10^{-3}$	$10.1 \times 10^{-3} \pm 12.4 \times 10^{-3}$	7.90×10^{-103}
(10,11)	14	$14.2 \times 10^{-3} \pm 13.4 \times 10^{-3}$	$10.4 \times 10^{-3} \pm 12.5 \times 10^{-3}$	5.48×10^{-100}
(11,12)	13	$13.9 \times 10^{-3} \pm 13.2 \times 10^{-3}$	$10.3 \times 10^{-3} \pm 12.3 \times 10^{-3}$	2.93×10^{-89}
(12,13)	15	$13.0 \times 10^{-3} \pm 12.2 \times 10^{-3}$	$9.7 \times 10^{-3} \pm 11.5 \times 10^{-3}$	6.04×10^{-86}
(13,14)	21	$11.9 \times 10^{-3} \pm 11.2 \times 10^{-3}$	$8.8 \times 10^{-3} \pm 10.6 \times 10^{-3}$	5.20×10^{-90}
(14,15)	20	$10.7 \times 10^{-3} \pm 10.1 \times 10^{-3}$	$7.9 \times 10^{-3} \pm 9.6 \times 10^{-3}$	2.03×10^{-96}
(15,16)	16	$9.4 \times 10^{-3} \pm 9.0 \times 10^{-3}$	$6.9 \times 10^{-3} \pm 8.6 \times 10^{-3}$	1.08×10^{-104}
(16,17)	19	$8.0 \times 10^{-3} \pm 7.7 \times 10^{-3}$	$5.9 \times 10^{-3} \pm 7.5 \times 10^{-3}$	1.06×10^{-109}
(17,18)	22	$6.7 \times 10^{-3} \pm 6.5 \times 10^{-3}$	$5.0 \times 10^{-3} \pm 6.4 \times 10^{-3}$	5.42×10^{-121}
(18,19)	18	$5.6 \times 10^{-3} \pm 5.3 \times 10^{-3}$	$4.2 \times 10^{-3} \pm 5.3 \times 10^{-3}$	6.11×10^{-140}
(19,20)	17	$4.5 \times 10^{-3} \pm 4.3 \times 10^{-3}$	$3.4 \times 10^{-3} \pm 4.4 \times 10^{-3}$	4.24×10^{-159}
(20,21)	3	$3.6 \times 10^{-3} \pm 3.3 \times 10^{-3}$	$2.7 \times 10^{-3} \pm 3.6 \times 10^{-3}$	2.31×10^{-182}
(21,22)	23	$2.8 \times 10^{-3} \pm 2.5 \times 10^{-3}$	$2.1 \times 10^{-3} \pm 3.0 \times 10^{-3}$	2.34×10^{-195}
(22,23)	24	$2.4 \times 10^{-3} \pm 2.1 \times 10^{-3}$	$1.8 \times 10^{-3} \pm 2.6 \times 10^{-3}$	9.88×10^{-203}
(23,24)	25	$2.0 \times 10^{-3} \pm 1.7 \times 10^{-3}$	$1.5 \times 10^{-3} \pm 2.5 \times 10^{-3}$	5.28×10^{-210}
(24,25)	26	$1.50 \times 10^{-3} \pm 1.2 \times 10^{-3}$	$1.1 \times 10^{-3} \pm 2.2 \times 10^{-3}$	2.16×10^{-218}
(25,26)	27	$1.20 \times 10^{-3} \pm 0.89 \times 10^{-3}$	$0.87 \times 10^{-3} \pm 2.0 \times 10^{-3}$	1.24×10^{-242}
(26,27)	2	$0.99 \times 10^{-3} \pm 0.76 \times 10^{-3}$	$0.75 \times 10^{-3} \pm 2.0 \times 10^{-3}$	2.46×10^{-278}
(27,28)	28	$0.84 \times 10^{-3} \pm 0.65 \times 10^{-3}$	$0.64 \times 10^{-3} \pm 1.9 \times 10^{-3}$	1.24×10^{-299}
(28,29)	1	$0.63 \times 10^{-3} \pm 0.51 \times 10^{-3}$	$0.50 \times 10^{-3} \pm 2.0 \times 10^{-3}$	9.86×10^{-283}
(29,30)	44	$0.47 \times 10^{-3} \pm 0.40 \times 10^{-3}$	$0.41 \times 10^{-3} \pm 2.0 \times 10^{-3}$	1.94×10^{-232}
(30,31)	42	$0.42 \times 10^{-3} \pm 0.38 \times 10^{-3}$	$0.38 \times 10^{-3} \pm 2.0 \times 10^{-3}$	6.87×10^{-185}
(31,32)	43	$0.38 \times 10^{-3} \pm 0.36 \times 10^{-3}$	$0.36 \times 10^{-3} \pm 2.0 \times 10^{-3}$	1.06×10^{-157}
(32,33)	41	$0.29 \times 10^{-3} \pm 0.28 \times 10^{-3}$	$0.30 \times 10^{-3} \pm 1.9 \times 10^{-3}$	1.17×10^{-139}
(33,34)	40	$0.26 \times 10^{-3} \pm 0.25 \times 10^{-3}$	$0.29 \times 10^{-3} \pm 2.1 \times 10^{-3}$	7.04×10^{-116}
(34,35)	39	$0.23 \times 10^{-3} \pm 0.23 \times 10^{-3}$	$0.29 \times 10^{-3} \pm 2.4 \times 10^{-3}$	6.26×10^{-88}
(35,36)	38	$0.22 \times 10^{-3} \pm 0.23 \times 10^{-3}$	$0.29 \times 10^{-3} \pm 2.5 \times 10^{-3}$	1.00×10^{-61}
(36,37)	37	$0.20 \times 10^{-3} \pm 0.22 \times 10^{-3}$	$0.29 \times 10^{-3} \pm 2.8 \times 10^{-3}$	2.49×10^{-43}
(37,38)	36	$0.15 \times 10^{-3} \pm 0.17 \times 10^{-3}$	$0.24 \times 10^{-3} \pm 2.5 \times 10^{-3}$	2.59×10^{-33}
(38,39)	29	$0.13 \times 10^{-3} \pm 0.15 \times 10^{-3}$	$0.23 \times 10^{-3} \pm 2.6 \times 10^{-3}$	2.25×10^{-27}
(39,40)	35	$0.12 \times 10^{-3} \pm 0.14 \times 10^{-3}$	$0.23 \times 10^{-3} \pm 2.9 \times 10^{-3}$	1.96×10^{-23}
(40,41)	34	$0.11 \times 10^{-3} \pm 0.13 \times 10^{-3}$	$0.22 \times 10^{-3} \pm 2.8 \times 10^{-3}$	1.00×10^{-14}
(41,42)	30	$0.09 \times 10^{-3} \pm 0.12 \times 10^{-3}$	$0.23 \times 10^{-3} \pm 3.2 \times 10^{-3}$	2.44×10^{-8}
(42,43)	33	$0.14 \times 10^{-3} \pm 0.08 \times 10^{-3}$	$0.21 \times 10^{-3} \pm 2.8 \times 10^{-3}$	1.45×10^{-4}
(43,44)	31	$0.06 \times 10^{-3} \pm 0.10 \times 10^{-3}$	$0.20 \times 10^{-3} \pm 3.2 \times 10^{-3}$	1.89×10^{-1}
(44,45)	32	$0.03 \times 10^{-3} \pm 0.04 \times 10^{-3}$	$0.13 \times 10^{-3} \pm 2.3 \times 10^{-3}$	2.40×10^{-1}

Table 5.4: Comparison of proposed method with other existing techniques using the same database.

Authors	Length of ECG segment	ACC(%)	SPE(%)	SEN (%)
(Nguyen et al, 2014)	Sliding window of 500 RR intervals with window step of 1 minute	85.26	83.47	86.37
(Hassan, 2015a)	-	83.77	82.79	85.2
(Hassan and Haque, 2016)	1 minute	85.97	86.93	84.14
(Varon et al, 2015)	1 minute	84.74	84.69	84.71
(Chen et al, 2015b)	1 minute	82.07	80.24	83.23
(Hassan, 2016)	1 minute	87.33	90.72	81.99
(Song et al, 2016)	1 minute	86.2	88.4	82.6
(Hassan and Haque, 2017)	1 minute	88.88	91.49	87.58
(Tripathy, 2018)	1 minute	76.37	74.64	78.02
(Janbakhshi and Shamsollahi, 2018)	1 minute	90.9	91.8	89.6
Proposed work	1 minute	92.78	93.91	90.95

FB 2 for classification problem. In the proposed method, the features are obtained by computing CCE between sub-band signals and CCE depends on the correntropy which computes the similarity of two sub-band signals (Reddy and Rao, 2017). The results from Fig. 5.8 and Fig. 5.9 clearly indicate the rise in the values of ACC when BW of sub-bands is reduced. Therefore, the benefit of the proposed method is that it can classify apneic and non-apneic ECG segments more accurately by decomposing ECG segment into narrow sub-bands, and then computing CCE to find similarity among them. When BW is reduced, the TQWT-FB has more number of sub-bands to cover the entire range of frequencies of the signal. The segmented ECG signal is decomposed into more number of sub-band signals and therefore the limitation of proposed method is that the complexity of the system increases as BW is reduced. Also we observed that there is not much change in obtained performance measure parameters if features are computed with different kernel size. The maximum ACC is achieved when kernel size is 0.5.

The maximum ACC is achieved when RF classifier is used in proposed model. Also the RF classifier is suitable for handling big data in less time and yields high performance (Genuera et al, 2017). As there are 6514 segments of ECG signal be-

longing to apneic class and 10531 segments of ECG signals of non-apneic class. Hence the data used in this work is big and RF classifier is suitable in this application.

The Table 5.3 presents the statistical analysis in terms of mean, SD, and p -value of CCE computed from sub-band signals. The Table 5.3 show that most of the features computed by CCE, have p – value < 0.05 indicating statistical significance.

The proposed method outperformed other existing methods in terms of performance measure parameters, which is shown in Table 5.4. In (Nguyen et al, 2014), recurrence quantification analysis statics are used as features and then SVM and neural network are employed for the classification. They achieved ACC of 85.26%. The author in (Hassan, 2015a) tested neural network, k -NN, adaptive boosting, RF, bagging, naive bayes, discriminant analysis, restricted boltzmann machine, and extreme learning machine for classification. The best ACC is achieved by extreme learning machine classifier. They obtained ACC of 83.77%. In (Hassan and Haque, 2016), the authors used bagging classifier and obtained ACC = 85.97% by using statistical and spectral features. The authors in (Varon et al, 2015) used four features to detect the sleep apnea from ECG signals. The four features are serial correlation coefficients, SD of RR interval, principal components of QRS complexes and orthogonal subspace projections between heart rate and respiration. The authors used LS-SVM for classification. They achieved ACC in this method is 84.74%. The apnea detection algorithm proposed in (Chen et al, 2015b) extracted the features from segmented RR intervals. Then kernel density classifier is used to detect apneic event using these features where they achieved ACC of 82.07%. In (Hassan, 2016), the authors used adaptive boosting for classification to obtain ACC = 87.33%. The authors in (Song et al, 2016) considered the momentary dependence within the segmented ECG signals. The discriminative HMM is used to capture the momentary dependence. They obtained ACC = 86.2%. In (Tripathy, 2018), The author extracted features from intrinsic band functions of heart rate variability and ECG-derived respiration signals. The extracted features are (energy and fuzzy entropy) are fed to the kernel extreme learning machine classifier for classification. In (Hassan

and Haque, 2017), segmented ECG signal is decomposed by TQWT and then statistical features like variance, skewness, and kurtosis are computed from sub-band signals and finally used random under sampling boosting classifier. In (Janbakhshi and Shamsollahi, 2018), the ECG-derived respiration based features are used in the screening of sleep apnea using ECG signals. The classification has been performed using artificial neural network. The authors achieved $ACC = 90.9\%$ in this work. In proposed method, the similarity among uniform BW sub-band signals is considered by computing CCE as features. Then by using RF classifier, we obtained $ACC = 92.78\%$.

5.7 Summary

In this chapter, a novel system for the classification of apneic and non-apneic segments of ECG signal is proposed. The segmented (one-minute duration) ECG signals are decomposed by TQWT-FB. In this work, we tested our system with two types of FBs (FB 1 and FB 2) with different BW of their sub-bands. The decomposed signals are then used to compute the features. The CCE features are obtained from sub-band signals generated from adjacent sub-bands. We have achieved an ACC of 92.78% for FB 2 with RF classifier. Our proposed method performed better than the existing methods.

Chapter 6

Classification of epileptic EEG signals using TQWT-FB

6.1 Introduction

In this chapter, we have presented our introduction in three sub-sections: (i) background, (ii) literature review, and (iii) overview of proposed method. In the background, detailed information on epilepsy disease is explained. Various automated detection systems developed for the detection of epilepsy using EEG signal is described in literature review sub-section. Then overview of proposed method is presented in third sub-section.

6.1.1 Background

Almost sixty million people throughout the world are affected with epilepsy disorder and most of them belong to the developing countries (Witte et al, 2003). The epilepsy is the neurological disorder occurs inside human brain. During epilepsy, seizure events occur frequently. To analyse the neurological activity of brain, the EEG signals are commonly used. The EEG signals are the electrical activity of brain and it was first observed by Caton in 1875 (Caton, 1875). Later, in 1929, Hans

Berger experimentally showed the presence of EEG signals by placing galvanometer connected electrodes on the head (Berger, 1929). Since then, EEG signals are used in many research areas including the diagnosis of epilepsy (Peker et al, 2016). However, it is difficult and time-consuming for neurologists to detect the epileptic seizure visually. Therefore, many automated techniques using advanced signal processing algorithms have been proposed to detect epileptic seizures (Bajaj and Pachori, 2012; Bhattacharyya et al, 2017b; Sharma and Pachori, 2015). These techniques classify and detect epileptic seizure based on the extracted features from the EEG signals.

6.1.2 Literature review

In literature, there are many studies presented for the diagnosis of epilepsy through EEG signals. These studies perform detection and classification of EEG signals. Generally, the classification problems which are dealt in literature are classification of seizure and seizure-free EEG signals, classification of seizure and non-seizure EEG signals, classification of seizure and normal EEG signals, and classification of seizure, seizure-free, and normal EEG signals. The seizure EEG signals are recorded during seizure activities and seizure-free EEG signals are recorded when seizure activities are absent from the patient suffering from epilepsy (Andrzejak et al, 2001). The normal EEG signals are recorded from healthy subjects and non-seizure EEG signals include both normal and seizure-free EEG signals (Andrzejak et al, 2001). These classifications can be performed by extracting features from EEG signals. The features can be extracted in frequency-domain, time-domain, T-F domain, or by non-linear signal analysis methods.

Due to non-stationary nature of EEG signals (Boashash et al, 2003), the features in T-F domain can be extracted. In (Sharma and Pachori, 2018b), the authors proposed IEVDHM-HT based T-F representation to analyse the non-stationary signals. The proposed T-F representation in (Sharma and Pachori, 2018b), has been used to classify seizure-free and seizure EEG signals. If the signals length is large, then

size of Hankel matrix used in T-F representation would be more. This increases the complexity of the system. In (Samiee et al, 2015), the features used to classify seizure and non-seizure EEG signals are extracted from rational discrete STFT and then MLP classifier is used as classifier. The T-F based methods along with artificial neural network were used to classify epileptic seizure from EEG signals (Tzallas et al, 2009, 2007). Different T-F distributions are considered in (Samiee et al, 2015; Tzallas et al, 2009, 2007). The choice of T-F distribution may affect the performance analysis of non-stationary signal like EEG. Since, these distributions differ in terms of their T-F localization and complexity. Therefore T-F distribution with good localization and less complexity should be chosen to analyze the EEG signals in T-F domain. There are different kinds of T-F distributions are considered in (Samiee et al, 2015; Tzallas et al, 2009, 2007). Different T-F distributions differ in terms of localization and complexity. The features based on time and frequency domain are used to detect epileptic seizure EEG signals as shown in (Polat and Gunes, 2007; Srinivasan et al, 2005). However, in these methods, the non-stationary nature of EEG signals is not considered.

In non-linear signal analysis methods, classification of seizure EEG signals have been performed using nonlinear parameters as features. The correlation dimension (Lehnertz and Elger, 1995), fractal dimension (Accardo et al, 1997; Patidar et al, 2015a), Lyapunov exponent (Guler et al, 2005; Ubeyli, 2010), Higher order spectra (Acharya et al, 2011d), continuous WT (Acharya et al, 2013b), recurrence quantification analysis (Acharya et al, 2011c), Hurst exponent (Acharya et al, 2009), approximate entropy (Liang et al, 2010), sample entropy and phase entropy (Acharya et al, 2012) are the various nonlinear features used for the seizure detection with EEG signals. However, there is need to find the suitable non-linear parameter which can provide significant information for accurate classification, since they are applied directly on the EEG signals.

Since the nature of EEG signal is non-stationary (Boashash et al, 2003), there are many studies presented in which features are extracted after the decomposed EEG

signals. The EMD has been used to decompose EEG signals (Sharma and Pachori, 2015) into set of IMFs. Then features based on phase space representation of IMFs are obtained for classification of seizure-free and seizure EEG signals. Similarly in (Pachori and Patidar, 2014), 95% confidence area of ellipse has been computed from second order difference plot of IMFs and used as feature to classify seizure and seizure-free EEG signals. Similarly in (Pachori et al, 2015), classification of normal and seizure EEG signals is shown. The Fourier-Bessel series expansion has been used to compute the mean frequency of IMFs (Pachori, 2008). The mean frequency is used as feature to classify seizure-free and seizure EEG signals. Also in (Oweis and Abdulhay, 2011), the weighted mean frequency of IMFs are introduced to find epileptic seizure EEG signals. From the plots of analytic IMFs, area used to classify seizure and normal EEG signals (Pachori and Bajaj, 2011). In (Bajaj and Pachori, 2012), the non-seizure and seizure EEG signals are classified by feature set obtained by FM and AM bandwidths of IMFs. These methods make use of EMD for signal decomposition. However, the EMD suffers from mode-mixing problem which is the presence of intermittency at some part of the signal (Huang et al, 1999; Oweis and Abdulhay, 2011). Due to this mode-mixing, it is hard to predict whether different time-scale oscillations occur in a single mode or oscillation of constant time scale given to different modes (Oweis and Abdulhay, 2011).

Apart from EMD, the wavelet transform has been used for signal decomposition in various methods. In (Subasi and Gursoy, 2010), the EEG signal is decomposed into number of sub-bands by applying discrete WT and then statistical features are computed from sub-bands. Then, SVM after data dimension reduction, has been applied for classification of normal and seizure EEG signals. Similar classification problem is addressed in (Lee et al, 2014), where features have been computed from Euclidean distance, which are computed from wavelet coefficients. In (Orhan et al, 2011), the discrete WT is used to decompose EEG signal into sub-bands. Then clustering of wavelet coefficients using k -means algorithm is accomplished for each sub-bandss. Using distribution of wavelet coefficients, the probability distributions

were computed and fed as input to MLP neural network. The discrete WT is unable to differentiate input signal changes and the phase information of signal is absent (Peker et al, 2016). To overcome these limitations, the authors in (Peker et al, 2016), extracted features from EEG signals using dual tree complex wavelet transform (DTCWT). Then, complex valued neural networks is used for diagnosis of epilepsy. Also in (Chen, 2014), DTCWT and Fourier features have been used to detect seizure by using nearest neighbor classifier. Other wavelet transform and multi-wavelet transform based techniques for classification and detection of epileptic seizure can be found in (Adeli et al, 2003, 2007; Ghosh-Dastidar et al, 2007; Guo et al, 2010; Khan and Gotman, 2003; Ocak, 2009; Subasi, 2007). In (Patidar and Panigrahi, 2017), the EEG signals are decomposed into sub-bands by applying TQWT and features were obtained by applying Kraskov entropy. The authors used LS-SVM classifier to classify seizure and seizure-free EEG signals. The application of TQWT to decompose EEG signals can also be found in (Hassan et al, 2016), where authors classify normal, seizure-free, and seizure EEG signals by using bagging classifier. Similarly in (Sharma and Pachori, 2017a), authors applied TQWT to decompose EEG signals and computed fractal dimension as feature to address various kinds of classification problems. In (Bhattacharyya et al, 2017b), EEG signals are decomposed by TQWT and then k -NN based entropies were estimated in order to classify epileptic EEG signals. These methods which used TQWT to decompose the EEG signals need to find optimum value of Q -factor before decomposition. This is because a Q -factor defines a mother wavelet which is not suitable to analyse signals of different oscillatory nature (Selesnick, 2011c). In (Bhati et al, 2017b) and (Bhati et al, 2017a), optimal wavelet filter-banks are designed to classify seizure-free and seizure EEG signals.

6.1.3 Overview of proposed method

In this work, we address the classification of seizure, seizure-free, and normal EEG signals. The EEG signals are non-stationary in nature and hence it would be better if they are decomposed into less complex signals. The seizure, seizure-free, and normal EEG signals has different characteristics (Andrzejak et al, 2001). Therefore, it gives us motivation to classify EEG signals by decomposing them into set of sub-band signals. Then by selecting optimum number of sub-band signals and capturing similarity among these sub-bands would result in good ACC. Therefore, we employed a TQWT-FB to decompose EEG signals. The TQWT-FB contains nearly constant BW sub-bands which are obtained from different Q -factor values. These different Q -factor values generate various mother wavelets, which are suitable to analyse different EEG signals which vary in oscillatory nature since they are non-stationary (Boashash et al, 2003). If different EEG signals of different oscillatory nature are decomposed by TQWT, then only single value of Q -factor can be used. Then, there is need to determine optimum value of Q -factor for decomposing different EEG signals. Since, only one value of Q -factor can be used by TQWT and single Q -factor value is not suitable to analyse both low and high oscillatory signals (Selesnick, 2011c).

After decomposition of EEG signals by TQWT-FB, the cross information potential (CIP) is applied on sub-band signals to compute features. The CIP captures the similarity between two random variables (Xu et al, 2008). The application of TQWT-FB and CIP for the detection of epilepsy are the novelties of this work.

The rest of the chapter is organized as follows: A brief overview of dataset used in this study is presented in Section 6.2. Section 6.3 describes the proposed methodology which includes description of design of TQWT-FB, method to compute features, and classifier used in this work. The simulation results are presented in Section 6.5. The Section 6.6 presents the discussion and finally Section 6.7 concludes the chapter.

6.2 Database

The dataset used in this study is obtained from University of Bonn, Germany (An-drzejak et al, 2001). It is publicly available online database which contains EEG signals recorded from healthy and epileptic subjects. The duration and F_s of each signal is 23.6 seconds and 173.67 Hz, respectively. The signals are categorized into five classes, namely Z, O, N, F, and S. Each class contains 100 EEG signals. The EEG signals of classes Z and O are the recorded from five healthy subjects using surface recording and standard 10-20 electrode placement system. The EEG signals from classes Z and O belong to normal EEG signals with eye open and closed respectively.

The class N and class F EEG signals are seizure-free signals since these signals are recorded in seizure-free interval. Class F EEG signals are recorded from epileptogenic zone and class N EEG signals are recorded from hippocampal portion of brain which is opposite to the hemisphere. Signals in class S carry seizure activities. In the study, class N and class F EEG signals are termed as seizure-free class and class S EEG signals are termed as seizure class. The EEG signal from each class is shown in Fig. 6.1

6.3 Proposed method

The proposed method for classification of normal, seizure-free, and seizure EEG signals consists of three stages. The block diagram of proposed method is shown in Fig. 6.2. First stage in block diagram is decomposition of EEG signals by TQWT-FB. The second stage is feature computation from decomposed signals and final stage is classification of EEG signals using a classifier. These stages are described below.

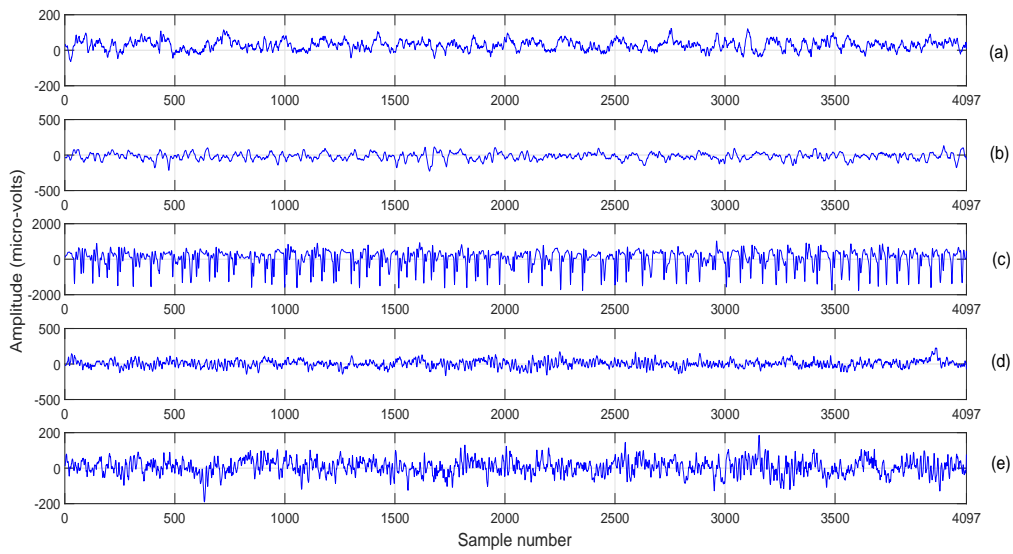


Figure 6.1: The EEG signal from (a) F class, (b) N class, (c) S class, (d) O class, and (e) Z class .

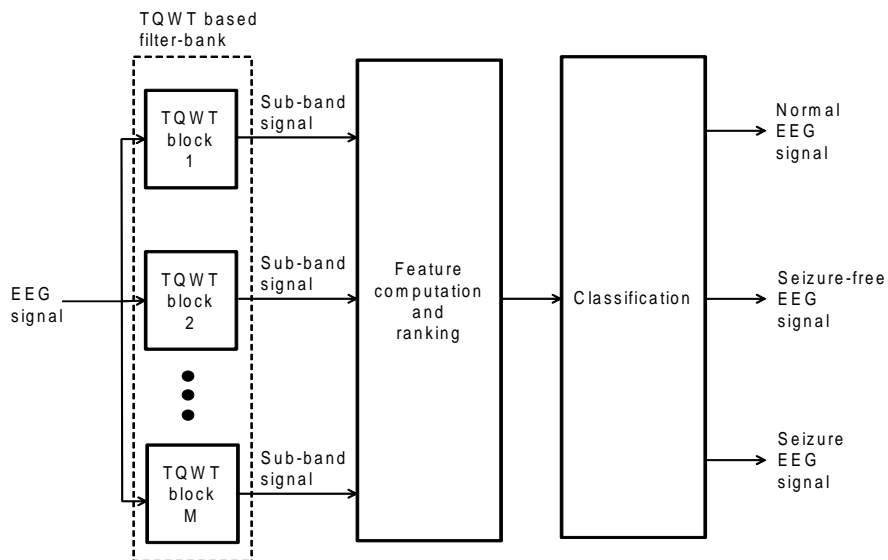


Figure 6.2: Block diagram for the detection of epileptic EEG signals.

6.3.1 TQWT-FB design

The TQWT-FB is implemented using method II as described in Section 2.2. The designed TQWT-FB which is used in this work is shown in Fig. 6.3.

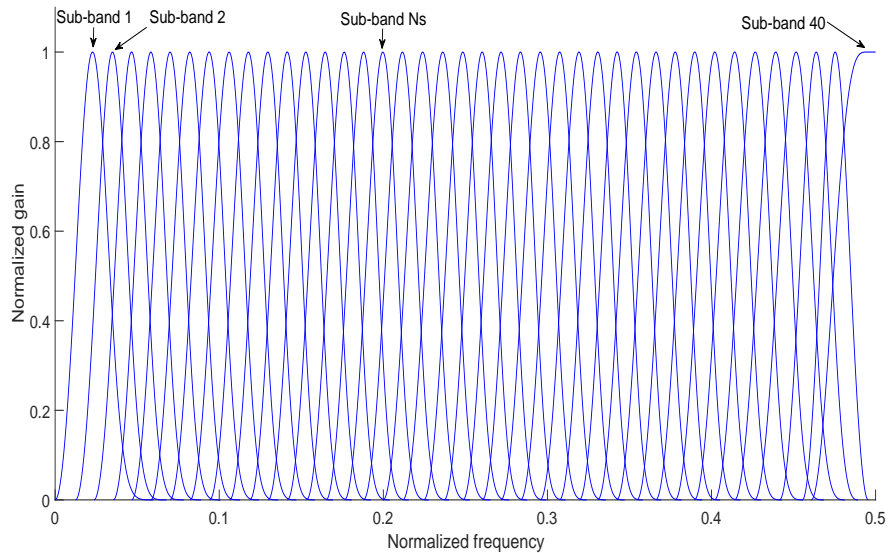


Figure 6.3: TQWT-FB used in proposed method for the classification of seizure, seizure-free, and normal EEG signals.

There are total 40 sub-bands and the BW of each sub-band in frequency response of TQWT-FB is nearly 0.025 (normalized frequency). The chosen values of Q -factor and D in each TQWT block are mentioned in the Table 6.1. The $R = 9$ is assigned to each TQWT block.

6.3.2 Feature computation

After decomposition of EEG signal by TQWT-FB, the CIP (Xu et al, 2008) is used to obtain features. The information potential (IP) estimates the Renyi's quadratic entropy. If it is applied on a sub-band signal then it can be expressed as (Xu and Erdogmuns, 2010):

Table 6.1: Chosen values Q -factor and D in the design of TQWT-FB

TBN	Q -factor	D	TBN	Q -factor	D
1	1	19	21	10.37	29
2	1.45	22	22	10.8	28
3	1.87	24	23	11.28	27
4	2.33	26	24	11.4	25
5	2.72	27	25	11.93	24
6	3.14	28	26	12.5	23
7	3.58	29	27	13.1	22
8	4.06	30	28	13.8	21
9	4.56	31	29	13.94	19
10	5.1	32	30	14.1	17
11	5.68	33	31	14.98	16
12	6.1	33	32	15.17	14
13	6.56	33	33	15.4	12
14	7.04	33	34	15.6	10
15	7.56	33	35	15.9	8
16	7.87	32	36	16.2	6
17	8.2	31	37	16.5	4
18	8.56	30	38	19.5	3
19	8.93	29	39	23.7	2
20	9.63	29	40	24.5	1

$$\text{IP}(\text{SBS}_i) = \frac{1}{T_s^2} \sum_{ia=1}^{T_s} \sum_{ib=1}^{T_s} R(\text{SBS}_{ia} - \text{SBS}_{ib}) \quad (6.1)$$

where, T_s is the total number of samples in sub-band signal SBS_i and $R(\text{SBS}_{ia} - \text{SBS}_{ib})$ is the kernel function. The a^{th} and b^{th} sample of sub-band signal SBS_i is represented by SBS_{ia} and SBS_{ib} , respectively. The CIP measures the similarity between two probability density functions (Xu et al, 2008) and can be expressed as follows:

$$\text{CIP}(\text{SBS}_i, \text{SBS}_j) = \frac{1}{T_s^2} \sum_{ia=1}^{T_s} \sum_{jb=1}^{T_s} R(\text{SBS}_{ia} - \text{SBS}_{jb}) \quad (6.2)$$

where SBS_{ia} is the a^{th} sample of sub-band signal SBS_i and SBS_{jb} is the b^{th} sample of sub-band signal SBS_j . In order to chose sub-band signals for feature computation, we run a test in which box plots are obtain when CIP is computed from different sub-band signals. As shown in Fig. 6.4, the box plots corresponding to different

class, shows variation in mean and interquartile range when CIP is computed from sub-band signals originated from adjacent and non-adjacent sub-bands. Therefore, both adjacent and non-adjacent sub-bands of TQWT-FB are considered in feature computation.

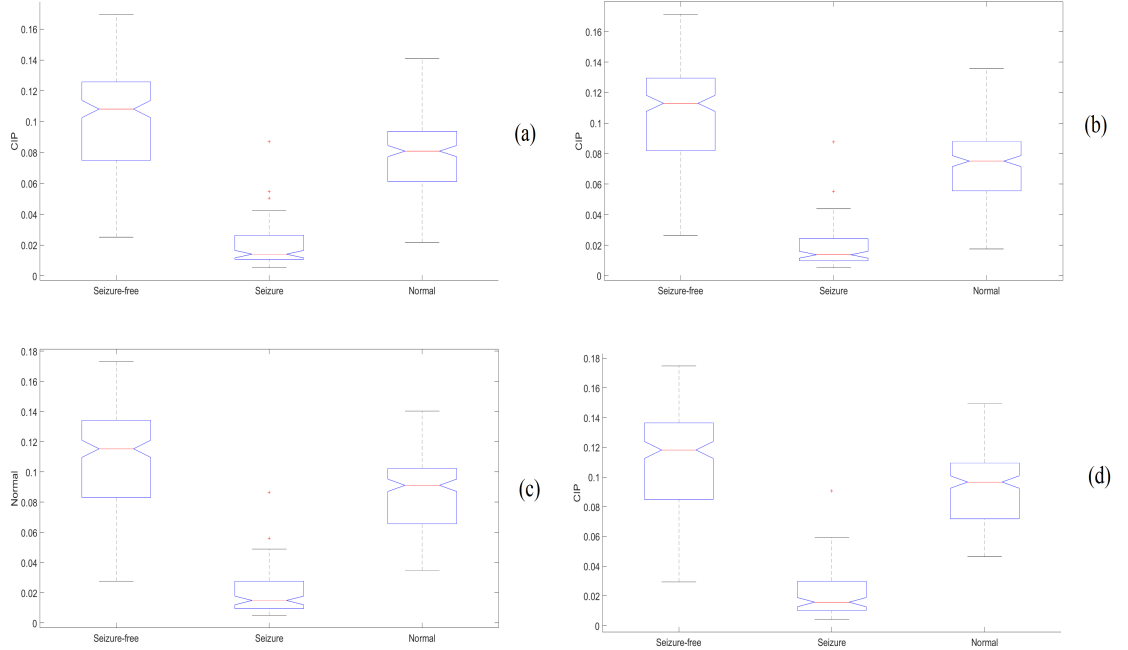


Figure 6.4: The box plot of CIP computed from sub-band signals from (a) sub-band 3 and sub-band 4, (b) sub-band 3 and sub-band 5, (c) sub-band 3 and sub-band 6, and (c) sub-band 3 and sub-band 7.

The sub-band signals from sub-band 1 to sub-band N_s are chosen for computation of features, where $2 \leq N_s \leq 40$. The sub-band 1 as shown in Fig. 6.3 is the lowest f_c sub-band among the sub-bands present in TQWT-FB. Then f_c of subsequent sub-bands increases gradually. The CIP is computed between i^{th} sub-band signal SBS_i and j^{th} sub-band signal SBS_j , where $1 \leq i \leq N_s$, $1 \leq j \leq N_s$, and $i \neq j$. Therefore, there will be $\frac{N_s(N_s-1)}{2}$ number of CIPs are computed. In this work, the CIP is computed using ITL toolbox which can be downloaded from <http://www.sohanseth.com/Home/codes>. The incomplete Cholesky decomposition is used by ITL toolbox to compute CIP. The kernel size is set equal to two in classification problem. The analysis of physiological signal using CIP can be found in (Kumar et al, 2017) in which diagnosis of coronary artery disease using ECG signals is shown.

It is not necessary that all extracted features would be significant in classification. Therefore, after having $\frac{N_s(N_s-1)}{2}$ number of features from N_s sub-band signals, they are ranked. The ranking of features is performed using RELIEFF algorithm (Kononenko et al, 1997; Robnik-Sikonja and Kononenko, 2003). The RELIEFF algorithm estimates quality features according to their ability to discriminate instances which are close to each other (Kononenko et al, 1997; Robnik-Sikonja and Kononenko, 2003). The algorithm randomly selects an instance. Then, it searches k -NNs which belongs to same class and k -NNs which belongs to other class (Kononenko et al, 1997; Robnik-Sikonja and Kononenko, 2003). The significance of feature is determined by its quality estimation variable W which depends on the value of the instance and searched k -NNs belonging to same class and different class (Kononenko et al, 1997; Robnik-Sikonja and Kononenko, 2003). In the proposed method, number of neighbour k in k -NN is set to one in RELIEFF algorithm.

After ranking the features, the highest ranked feature is used for classification. Then, next best two features are considered during classification and so on. In this way, the NORF given as input to the classifier is different in each step. Accordingly, the obtained ACC varies with the change in NORF.

6.3.3 Classification

The classifier used for classification is RF. The brief overview of RF classifier has been presented in Section 5.3.4. The classification is performed using ten fold cross-validation approach (Kohavi, 1995).

6.4 Performance measure

The performance measures, as defined in Section 5.4 are used to evaluate the efficacy of proposed method.

Table 6.2: Obtained ACC for different segment length

Segment length	ACC (%)	N_s	NORF
4097	99	12	35
2000	98.8	31	400
1000	98.2	39	715
500	98	39	741

6.5 Simulation results

As shown in Fig. 6.3, there are 40 sub-bands in TQWT-FB. If sub-band signals generated from all 40 sub-bands are considered in feature computation, then the complexity of the system would be very high. Therefore, we run the series of simulation in which features are computed from sub-band signals originated from sub-band 1 to sub-band N_s and in each simulation, the value of N_s is different. In first simulation run, the $N_s = 2$ is chosen since sub-band signals from at least two sub-bands are required to compute CIP. Then in subsequent simulations, the value of N_s is incremented by one. The maximum value of N_s is the number of sub-bands in TQWT-FB. Then the features are ranked after feature computation and fed to the classifier. The best value of N_s or best set of N_s sub-band is one for which the classifier achieves maximum ACC. When N_s sub-bands are selected for classification, then there will be $\frac{N_s(N_s-1)}{2}$ number of features available because CIP is computed from every possible pair of sub-band signals obtained from N_s selected sub-bands. When the value of N_s is varied, then number of sub-band signals used in feature computation also changes. During the simulation, the proposed method is tested for different length of EEG segments. The segment length, which is considered during simulation are 500 samples, 1000 samples, 2000 samples and entire length (4097 samples) of EEG signal. The obtained ACC for different segment length of EEG signal is shown in Table 6.2. The Table 6.2 shows the maximum obtained ACC when sub-band signals from minimum N_s sub-bands are used in feature computation and minimum NORF are used.

Table 6.3: Sub-bands used to compute ranked features

Cm	(a,b)	Cm	(a,b)	Cm	(a,b)	Cm	(a,b)
C1	(3,12)	C10	(2,3)	C19	(9,11)	C28	(3,4)
C2	(3,11)	C11	(1,6)	C20	(4,12)	C29	(4,11)
C3	(3,10)	C12	(3,6)	C21	(2,11)	C30	(4,10)
C4	(3,9)	C13	(5,9)	C22	(1,8)	C31	(2,10)
C5	(1,7)	C14	(3,7)	C23	(4,9)	C32	(11,12)
C6	(1,11)	C15	(2,12)	C24	(1,5)	C33	(8,9)
C7	(1,12)	C16	(9,10)	C25	(5,12)	C34	(2,8)
C8	(3,8)	C17	(9,12)	C26	(2,9)	C35	(5,6)
C9	(1,10)	C18	(1,9)	C27	(5,11)		

From Table 6.2, it can be noted that maximum obtained ACC = 99% for segment length of 4097 samples. This ACC is obtained when $N_s = 12$ and NORF = 35. Since only twelve sub-bands are used in feature computation, there are 66 features available. Out of them, best 35 features provided ACC = 99%. The sub-bands used to compute these best features are shown in Table 6.3. In the Table 6.3, Cm is the feature having rank m and (a,b) denotes sub-band a and sub-band b which are used to compute feature Cm. The obtained SEN when obtained ACC = 99%, are $SEN_1 = 98.5\%$, $SEN_2 = 98\%$, and $SEN_3 = 100\%$. Similarly, the value of specificities $SPE_1 = 99.33\%$, $SPE_2 = 99.5\%$, and $SPE_3 = 99.67\%$.

It can be noted from Table 6.2 that, for other segment length also, the obtained ACC is at least 98%. However the number of features used for classification increases as the segment length decreases.

It can also be observed from Table 6.2 that the decrease in segment length decreases the ACC and increases the complexity of the system. Table 6.4 shows the comparison of the performance of ACC of proposed method with other existing methods using the same database (Andrzejak et al, 2001).

From this table, it can be observed that the proposed method obtained the better ACC as compared with other existing methods. The statistical analysis of computed features in (Bhattacharyya et al, 2017b; Peker et al, 2016; Tiwari et al, 2017; Tzallas et al, 2007), and proposed method are shown in Fig. 6.5 to Fig. 6.9. The figures shows the mean and standard deviation (SD) of features for various methods. The

Table 6.4: Summary of automated detection of seizure, seizure-free, and normal EEG signals using the same database.

Authors	Features	Classifier	Training and testing data selection	ACC (%)
(Tzallas et al, 2007)	Smoothed pseudo Wigner-Ville distribution based features	artificial neural network	50 % training and 50 % testing	97.72
(Acharya et al, 2011c)	recurrence quantification analysis features	SVM	3-fold cross-validation	95.6
(Acharya et al, 2012)	Approximate entropy, sample entropy, and Phase entropy	Fuzzy	3-fold cross-validation	98.1
(Peker et al, 2016)	Statistical features	Complex valued neural networks	10-fold cross-validation	98.28
(Tiwari et al, 2017)	Histogram of local binary pattern	SVM	10-fold cross-validation	98.8
(Bhattacharyya et al, 2017b)	TQWT-based multi-scale K-NN entropy	SVM	10-fold cross-validation	98.6
Proposed method	CIP from TQWT-FB	RF	10-fold cross-validation	99

mid point of the bar is the mean of the feature and half of the length of the bar is SD of feature when range of feature is shown in linear scale.

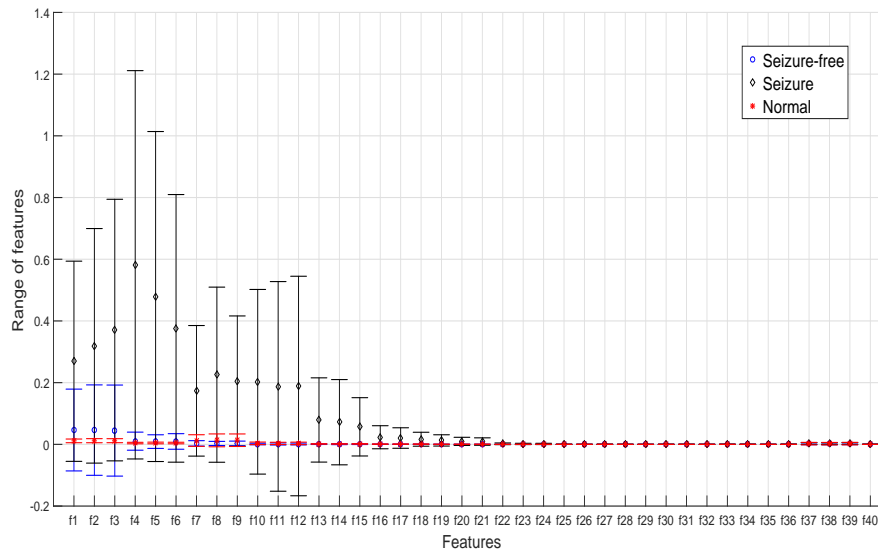


Figure 6.5: Statistical analysis (mean and SD) of features computed in (Tzallas et al, 2007).

6.6 Discussion

This work presents a novel technique based on TQWT-FB for the classification of epileptic EEG signals. The EEG signals are decomposed into narrow *BW* sub-band signals by TQWT-FB and features are computed by applying CIP on every

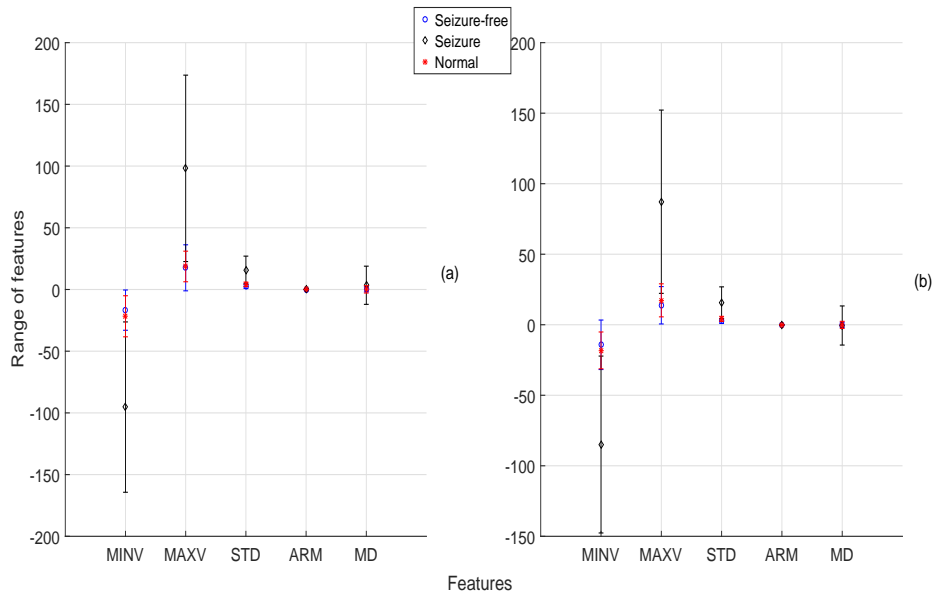


Figure 6.6: Statistical analysis (mean and SD) of (a) real part of features and (b) imaginary part of features computed in (Peker et al, 2016).

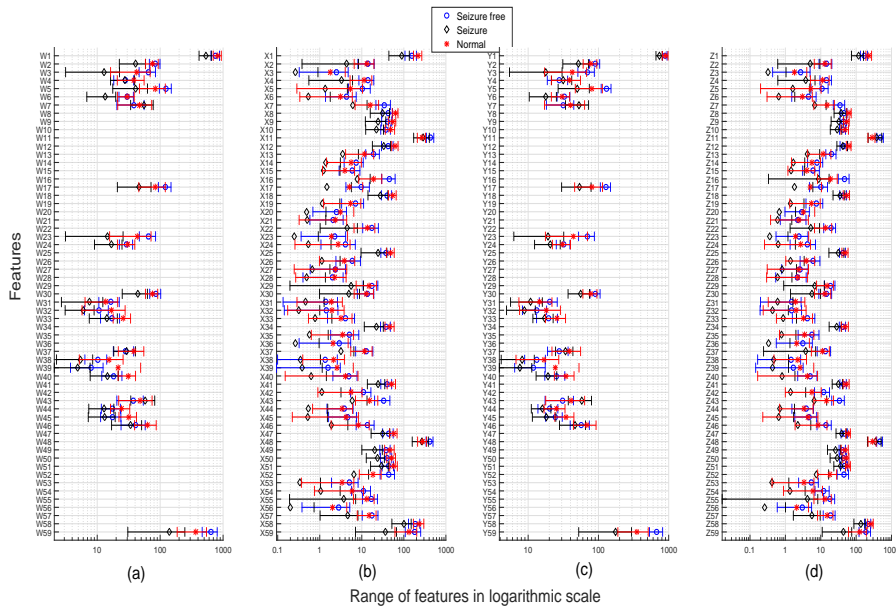


Figure 6.7: Statistical analysis (mean and SD) of computed (a) W features, (b) X features, (c) Y features, and (d) Z features, in (Tiwari et al, 2017).

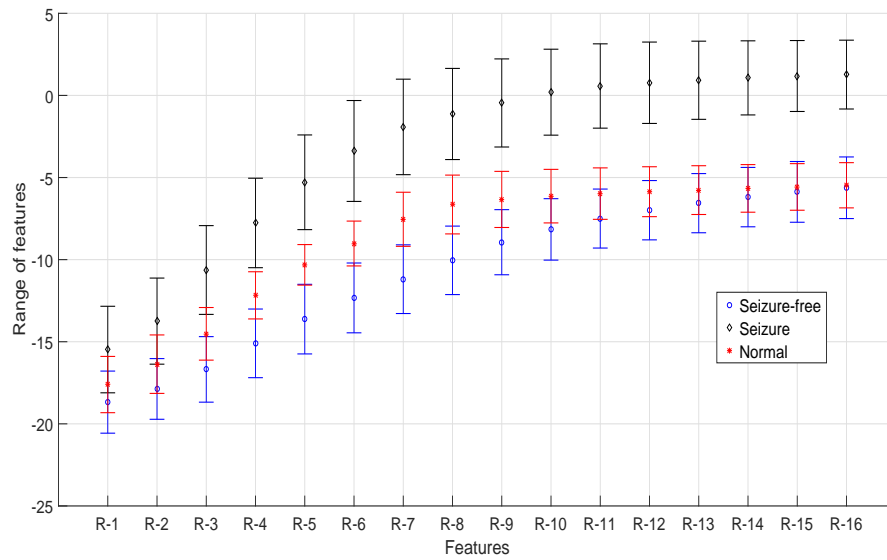


Figure 6.8: Statistical analysis (mean and SD) of features computed in (Bhattacharyya et al, 2017b).

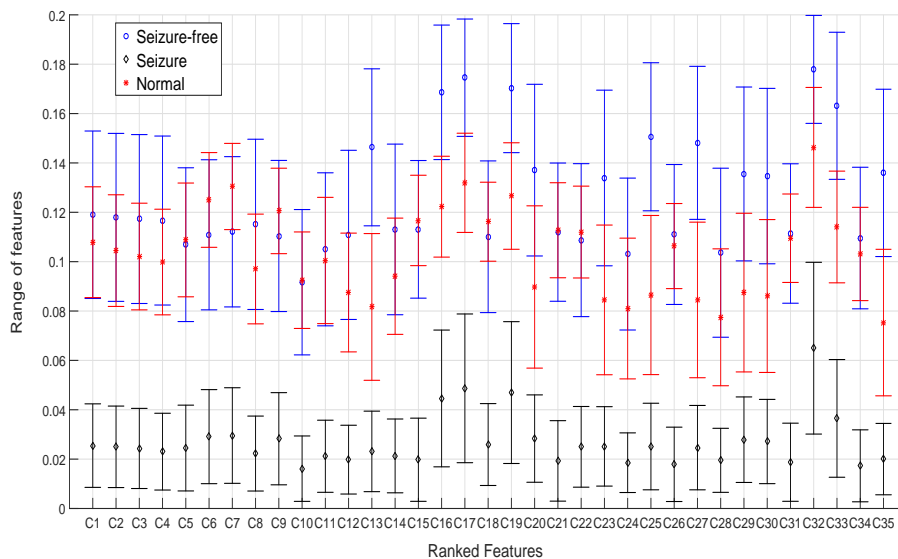


Figure 6.9: Statistical analysis (mean and SD) of features computed in our proposed method.

pair of sub-band signals. The CIP captures the similarity between two sub-band signals. To reduce the complexity of the proposed system, we have evaluated the optimal number of sub-band signals for computation of features instead of using all sub-band signals generated by TQWT-FB. These features are then ranked using RELIEFF algorithm in order to obtain significant features. We found that $N_s = 12$, $NORF = 35$ with RF classifier yielded the maximum $ACC = 99\%$.

The performance of proposed method in terms of obtained ACC is better than other existing methods as shown in Table 6.4. The features of EEG signals are analyzed using smoothed pseudo Wigner-Ville distribution (Tzallas et al, 2007). The smoothed pseudo WVD is partitioned into different T-F planes. For partitioning, three time windows and thirteen frequency sub-bands are chosen (Tzallas et al, 2007). The time windows TW1, TW2, and TW3 are from 0 to 7.86 seconds, 7.86 to 15.73 seconds, and 15.73 to 23.6 seconds respectively (Tzallas et al, 2007). Similarly, the frequency windows FW1, FW2, FW3, FW4, FW5, FW6, FW7, FW8, FW9, FW10, FW11, FW12, and FW13 are from 0 to 2 Hz, 2 to 4 Hz, 4 to 6 Hz, 6 to 8 Hz, 8 to 10 Hz, 10 to 12 Hz, 12 to 16 Hz, 16 to 20 Hz, 20 to 24 Hz, 24 to 28 Hz, 28 to 32 Hz, 32 to 36 Hz, and 36 to 40 Hz respectively. The T-F plane TdFe is obtained by applying time window TWd and FWe where $1 \leq d \leq 3$ and $1 \leq e \leq 13$. The features f1, f2, f3, f4, f5, f6, f7, f8, f9, f10, f11, f12, f13, f14, f15, f16, f17, f18, f19, f20, f21, f22, f23, f24, f25, f26, f27, f28, f29, f30, f31, f32, f33, f34, f35, f36, f37, f38, and f39 are computed from T1F1, T2F1, T3F1, T1F2, T2F2, T3F2, T1F3, T2F3, T3F3, T1F4, T2F4, T3F4, T1F5, T2F5, T3F5, T1F6, T2F6, T3F6, T1F7, T2F7, T3F7, T1F8, T2F8, T3F8, T1F9, T2F9, T3F9, T1F10, T2F10, T3F10, T1F11, T2F11, T3F11, T1F12, T2F12, T3F12, T1F13, T2F13, and T3F13 respectively. They are shown in Fig. 6.5. The last feature f40 is the energy of EEG signal. Then energy features f1 to f39 are computed from their respective T-F plane (Tzallas et al, 2007). We implemented the proposed method in (Tzallas et al, 2007) by using T-F toolbox available at (Auger et al, 1996). The statistical analysis of obtained features are shown in Fig. 6.5. It can be observed that mean of seizure EEG signal is notably

far from mean of seizure-free and normal EEG signals for few features. The p -value of each feature is less than 0.05.

In (Acharya et al, 2011c), recurrence quantification analysis method is employed. The features such as recurrence rate (feature 1), determinism (feature 2), mean diagonal line length (feature 3), longest diagonal line (feature 4), entropy (feature 5), laminarity (feature 6), trapping time (feature 7), longest vertical line (feature 8), and recurrence times (T1 and T2) are used to classify the EEG signals. The mean \pm SD of feature 1, 2, 3, 4, 5, 6, 7, 8, T1, and T2 for normal EEG signals are 0.0575808 ± 0.004212 , 0.26333 ± 0.04178 , 2.3101 ± 0.112 , 7.685 ± 1.5 , 0.70126 ± 0.156 , 0.35446 ± 0.05464 , 2.402 ± 0.126 , 7.195 ± 1.62 , 16.383 ± 1.21 , and 20.762 ± 1.32 respectively (Acharya et al, 2011c). Similarly for seizure-free class, the mean \pm SD of feature 1, 2, 3, 4, 5, 6, 7, 8, T1, and T2 are 0.0617364 ± 0.01391 , 0.48499 ± 0.127 , 2.6712 ± 0.668 , 17.425 ± 26.6 , 1.0463 ± 0.317 , 0.61359 ± 0.124 , 2.9401 ± 0.964 , 12.47 ± 8.97 , 15.159 ± 2.15 , and 26.371 ± 4.57 , respectively (Acharya et al, 2011c). For seizure EEG signals, the statistical analysis of feature 1, 2, 3, 4, 5, 6, 7, 8, T1, and T2 are 0.0671869 ± 0.008863 , 0.47018 ± 0.109 , 3.0637 ± 0.417 , 30.33 ± 16.1 , 1.373 ± 0.238 , 0.57155 ± 0.134 , 3.2156 ± 0.535 , 15.97 ± 7 , 14.294 ± 1.78 , and 24.509 ± 4.31 respectively (Acharya et al, 2011c). The p – values < 0.0001 for all features (Acharya et al, 2011c). The method proposed in (Acharya et al, 2012) used phase entropies (S1 and S2), approximate entropy, and sample entropy for classification. The mean \pm SD of approximate entropy, sample entropy, S1, and S2 for normal EEG signals are 2.2735 ± 0.0332 , 1.313 ± 0.12 , 0.57012 ± 0.0712 , and 0.76827 ± 0.03125 respectively (Acharya et al, 2012). In the same way, the mean \pm SD of approximate entropy, sample entropy, S1, and S2 for seizure-free EEG signals are 1.865 ± 0.331 , 0.99332 ± 0.189 , 0.47208 ± 0.06149 , and 0.68072 ± 0.0379 , respectively (Acharya et al, 2012). For seizure EEG signals, the mean \pm SD of approximate entropy, sample entropy, S1, and S2 are 1.9325 ± 0.215 , 0.92628 ± 0.139 , 0.48325 ± 0.155 , and 0.73184 ± 0.04555 respectively (Acharya et al, 2012). For all features in each class, the p -value is less than 0.0001 (Acharya et al, 2012).

The authors (Peker et al, 2016) used DTCWT to decompose input EEG signals. The decomposition by DTCWT generates complex wavelet coefficients. The computed features are minimum value (MINV), maximum value (MAXV), SD, arithmetic mean (ARM), and median (MD). The Fig. 6.6(a) and Fig. 6.6(b) shows the statistical analysis of real and imaginary parts of the features respectively. We have implemented the method proposed in (Peker et al, 2016) using matlab codes available at <http://eeweb.poly.edu/iselesni/WaveletSoftware/> to implement DTCWT. The obtained p -values are less than 0.0001 for most of the features.

The statistical analysis of features computed using the method proposed in (Tiwari et al, 2017) is shown in Fig. 6.7. In this method, the EEG signals are filtered by set of Gaussian filters having different SDs. Then the filtered EEG signals are subtracted to obtain pyramid of difference of Gaussian filtered signals (Tiwari et al, 2017). From difference of Gaussian signals, the local binary pattern at key points are obtained according to the method proposed in (Tiwari et al, 2017). Finally, the histograms of local binary pattern are taken as features and classified. In (Tiwari et al, 2017), the set of key points K2 and K3 are computed from second and third signals of difference of Gaussian pyramid respectively. In Fig. 6.7(a) features W1 to W59 are computed from second signal of difference of Gaussian pyramid at K2. Similarly, features X1 to X59 as shown in Fig. 6.7(b), are computed from the original EEG signal at K2. In Fig. 6.7(c) and (d), features Y1 to Y59 are computed from third signal of difference of Gaussian pyramid at K3 and features Z1 to Z59 are computed from original EEG signal at K3. There are few features whose mean and SD are zero for all classes. Therefore, in Fig. 6.7, the mean and SD of such features are not present as the range of features are shown in logarithmic scale. In this method, though the obtained ACC is high, the number of features used for classification is high. Most of the features of this method have p -values less than 0.0001.

The authors (Bhattacharyya et al, 2017b) have proposed a multi-scale entropy based on Q -factor computed by decomposing EEG signal into sub-bands by TQWT.

Then, from sub-bands, entropies based on K-NN, were estimated to classify epileptic EEG signals. The feature R_g is the K-NN entropy of reconstructed signal R (Bhattacharyya et al, 2017b). The reconstructed signal R is the summation of g sub-band signals obtained from sub-bands of TQWT (Bhattacharyya et al, 2017b). The statistical analysis of its features is shown in Fig. 6.8. Most of the features of seizure EEG signals are differentiable (distinct mean and SD values) from seizure-free and normal classes (p - value < 0.0001). The Fig. 6.9 shows the statistical analysis of features computed from proposed method. The proposed method obtained best ACC from 35 ranked features only when $N_s = 12$. The Fig. 6.9 shows the statistical analysis of these 35 ranked features. The mean and SD values of seizure EEG features is clearly separable from mean and SD of seizure-free and normal features. The mean and SD of few seizure-free and normal features are also clearly differentiable. The p -values of all 35 features are less than 0.0001 which shows the statistical significance of features. This also implies that, the confidence interval is more than 95%.

6.7 Summary

The proposed work addresses the classification of seizure, seizure-free, and normal EEG signals which vary in their energy level. The proposed technique explores this property in classifying EEG signals. The novelty of proposed method is the use of TQWT-FB and CIP. The TQWT-FB decomposes EEG signals into various sub-band signals which have different energy levels. Then CIP captures the similarity from optimum number of sub-band signals and classifies in to seizure, seizure-free, and normal EEG signals. The obtained CIP values are different for various EEG signals. It has been observed that the mean of features for seizure, seizure-free, and normal EEG signals are differentiable in most of the cases. Thus, the obtained CIP values from proposed method influence the classification performance. The proposed method computed the features from N_s selected sub-bands. The highest

ACC of 99% is achieved by our proposed method. Also the computed features are statistically significant as p -value of all features is less than 0.0001.

Chapter 7

Focal EEG signal detection based on TQWT-FB

7.1 Introduction

Epilepsy is a type of neurological disorder, which is characterized by unpredictable dysfunction of brain and can be identified by epileptic seizures. An epileptic seizure is a sudden occurrence of synchronous neurons activity in the brain (Fisher et al, 2005; Pachori, 2008).

According to world health organization, around 50 million people are affected with epilepsy globally (World Health Organization, 2018). In the world population, nearly 20% epileptic patients have generalized epilepsy that influences the whole brain, whereas, more than 60% epileptic patients have focal epilepsy, where the parts of brain are affected and these parts are mainly responsible for localized epileptic discharge (Gloor and Fariello, 1988; Pati and Alexopoulos, 2010). Focal epilepsy has inadequate control of seizures with drug and it is significant to remove these focal epileptic zones with the help of surgery (Kwan and Brodie, 2000; Kwan et al, 2010). A most common tool for the investigation of epilepsy is visual analysis of EEG signals recorded from the brain (Acharya et al, 2013a). The EEG signal records the electrical activity of the brain (Pachori and Sircar, 2008a; Penfield and Erickson,

1941). These EEG signals can be recorded from the scalp as well as intracranially (within the skull) from the brain. The localization of focal epileptic zones of the brain is possible by intracranial EEG recording because scalp EEG may fail to show ictal transitions in seizures originating from a small and deeply situated focal epileptic areas (Pati and Alexopoulos, 2010).

However, the visual analysis of EEG signals for identifying focal epileptic zones is a very time consuming and tedious task for the neurologists. Therefore, a computer based automated system is required to overcome the difficulties for the identification of focal EEG signals.

In the literature, the various signal processing based automated systems were proposed to identify focal epilepsy EEG signals (Acharya et al, 2019; Bhattacharyya et al, 2018, 2017a; Dalal et al, 2019; Das and Bhuiyan, 2016; Sharma and Pachori, 2018a; Sharma et al, 2014, 2015a,b; Singh and Pachori, 2017).

The method based on EMD with average variance and entropy features extracted from intrinsic mode functions IMFs together with LS-SVM classifier with radial basis function (RBF) kernel is used in (Sharma et al, 2014). The achieved classification ACC for this method is 85%. In another work, the EMD and LS-SVM have been also utilized with various entropies features and this work achieved a classification ACC of 87% for the classification of focal EEG signals (Sharma et al, 2015b). An automated classification system based on discrete WT, entropies features, and different classifiers has been proposed in (Sharma et al, 2015a). The classification ACC achieved for this method was 84% along with integrated index for focal and non-focal EEG signals. The EMD and discrete WT have been jointly used in a work for the classification of focal and non-focal EEG signals with an achieved classification ACC of 89.4% (Das and Bhuiyan, 2016). The rhythms based work using empirical WT with area using central tendency measure obtained from the reconstructed phase space plot has been also explored to classify focal class of EEG signals (Bhattacharyya et al, 2018). The obtained classification ACC was 90% for the classification of focal and non-focal EEG signals. The TQWT with multivari-

ate sub-band fuzzy entropy has been explored in (Bhattacharyya et al, 2017a), for the classification of focal EEG signals. The achieved maximum classification ACC in this work was 84.67%. The bivariate EMD based methodology has been also explored for the identification of focal EEG signals (Sharma and Pachori, 2018a). The obtained maximum classification ACC in this method is 84.01%. The rhythms of EEG signal based on Fourier method have been utilized for the classification of focal EEG signals (Singh and Pachori, 2017). The classification ACC achieved in this method is 89.70%. The entropy based features along with EMD have been also explored for the identification of focal epileptic zones. The classification ACC obtained in this method was 83.18%. In a recent review study, the classification based on 23 features has been proposed with an achieved classification ACC of 87.93% (Acharya et al, 2019).

In this present work, we have designed a novel methodology based on TQWT-FBs and mixture correntropy (MCE) to classify focal EEG signals. In this methodology, the first step is to decompose focal and non-focal EEG signals with TQWT-FBs into sub-band signals. These sub-band signals are considered for feature extraction. The MCE based features are computed from the sub-band signals. These extracted features are used in LS-SVM classifier with RBF kernel and 10-fold cross-validation technique. The classification task is first performed for 50 focal and 50 non-focal EEG signals for selecting the appropriate values of MCE parameters corresponding to maximum classification ACC. Later, the selected values of MCE parameters are used to classifying 3750 focal and 3750 non-focal EEG signals. The classification performance is also evaluated with different feature ranking methods in order to reduce the feature space. The proposed methodology can assist the clinicians during diagnosis and surgery of focal epileptic brain areas.

The remaining parts of the chapter are explained as follows: Section 7.2 contains description about the dataset. Section 7.3 explains brief description of methodology which includes the TQWT method with the description of TQWT-FBs, feature extraction, feature ranking, and LS-SVM classifier. Results and discussions parts

are included in Section 7.4. Finally, Section 7.5 summarizes this chapter.

7.2 Database

The EEG signals are collected from Bern-Barcelona EEG database (Andrzejak et al, 2001) which is publicly available. The intracranial EEG signals are recorded from five patients suffering with focal epilepsy. The database consists 7500 pairs of EEG signals which has 3750 focal pairs and 3750 non-focal pairs. The F_s of these EEG signals is 512 Hz with total time duration of 20 sec corresponding to 10,240 samples. The plot of "x" and "y" pairs of focal and non-focal EEG signals are depicted in Figs. 7.1 and 7.2, respectively (Andrzejak et al, 2012).

7.3 Proposed method

The block diagram of proposed method for classification of focal and non-focal EEG signals is shown in Fig. 7.3. It consist of three stages namely TQWT-FB, features computation and their ranking, and finally classifications. These stages are explained in following sub-sections.

7.3.1 TQWT-FB design

In this stage, the FB 1 and FB 2 as designed in sub-section 5.3.2 are used to decompose EEG signals. The EEG signals from channel "x" and "y" are fed to TQWT-FB separately and decomposed sub-band signals corresponding to channel "x" EEG signal and channel "y" EEG signal are used in feature computation.

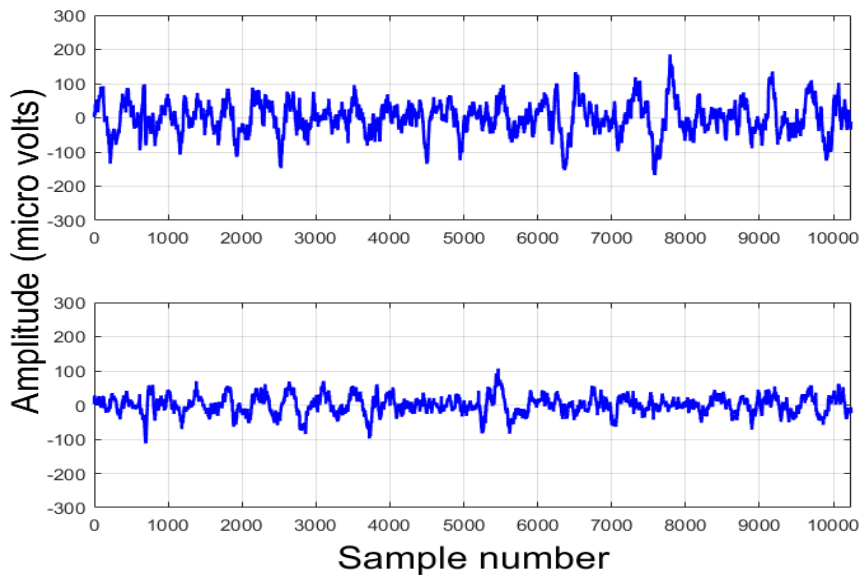


Figure 7.1: Plot of "x" and "y" pair of focal EEG signals

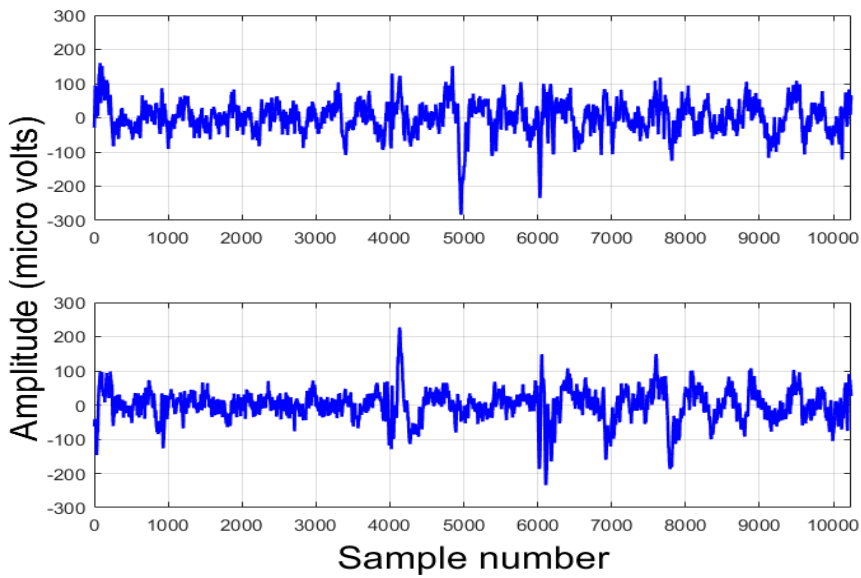


Figure 7.2: Plot of "x" and "y" pair of non-focal EEG signals

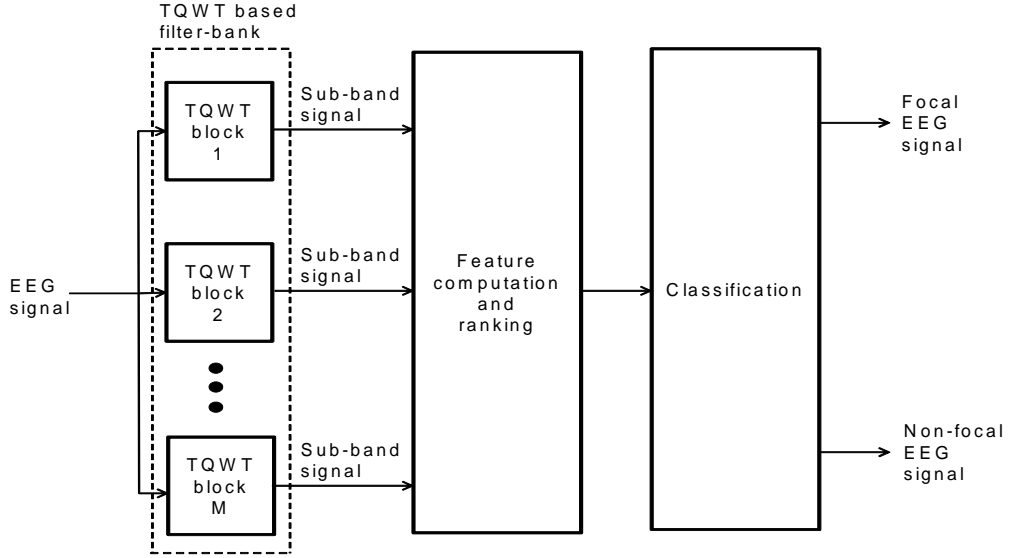


Figure 7.3: Block diagram for the detection of focal EEG signals.

7.3.2 Feature extraction

Feature extraction is an important step which is used to extract discriminative information from the signals and a MCE feature is used for the same purpose. A MCE is defined as a mixture of two Gaussian kernel functions which are used to measure nonlinear similarity between two random variables (Chen et al, 2018). Let, U and V be the two random variables then the MCE can be mathematically expressed as (Chen et al, 2018):

$$MC(U, V) = E[\beta\kappa_{\sigma_1}(U, V) + (1 - \beta)\kappa_{\sigma_2}(U, V)] \quad (7.1)$$

where MC denotes the MCE, $\kappa_{\sigma}(U, V) = e^{-\frac{(U-V)^2}{2\sigma^2}}$ is a Gaussian kernel, and β is the mixture coefficient with condition, $0 \leq \beta \leq 1$. The σ_1 and σ_2 represent kernel bandwidths of the Gaussian kernel functions $\kappa_{\sigma_1}(U, V)$ and $\kappa_{\sigma_2}(U, V)$, respectively. E denotes expectation operator.

In this work, a MCE feature is used to extract information from the sub-band signals obtained with bivariate "x" and "y" pairs of focal and non-focal EEG signals. The range of parameters σ_1 and σ_2 is selected between 0.1 and 2 with a step size of

0.1.

7.3.3 Feature ranking

Feature ranking is a test which is used to discard the less relevant features from the available features space. This test is basically used to select higher ranked features and the features with lower rank can be omitted in this test. Therefore, a highest classification ACC can be obtained with the less number of features using feature ranking test.

In this present work, Bhattacharyya space algorithm, entropy, receiver operating characteristic (Kerekes, 2008; Theodoridis and Koutroumbas, 2009), Students t-test (DeWayne et al, 2010), and Wilcoxon (Kruskal, 1957) feature ranking methods are used for ranking the features (Gupta et al, 2017; Liu and Motoda, 1998; Sharma et al, 2015a). The feature ranking methods are successfully found importance in (Sharma et al, 2015a, 2017a) for the classification of non-focal and focal EEG signals.

7.3.4 Classification

The SVM is a machine learning approach which is efficiently used to identify the patterns (Suykens and Vandewalle, 1999). In this method, the data is mapped into a higher dimensional input space and construct a optimal hyperplane (Suykens and Vandewalle, 1999). The discrimination function for this classifier can be written as follows(Suykens and Vandewalle, 1999):

$$v(x) = \text{sign}[w^T u(x) + b] \quad (7.2)$$

where w , b and $u(x)$ represent the d -dimensional weight vector, bias and mapping function, respectively.

To optimize the hyperplane in SVM algorithm, the distance from any one of the

classes to the hyperplane is maximized. This is an optimization issue and can be designed as the quadratic programming problem subject to inequality constraints (Suykens and Vandewalle, 1999). In case of LS-SVM only equality constraints are involved for the classification of two classes with a least square formulation. The formulation of the two-class classification problem in LS-SVM is given as follows (Suykens and Vandewalle, 1999):

$$\text{Minimize } \mathbb{J}(w, b, \xi) = \frac{1}{2}w^T w + \frac{\gamma}{2} \sum_{j=1}^N \xi_j^2 \quad (7.3)$$

$$z_j[w^T u(x_j) + b] = 1 - \xi_j \quad j = 1, 2, 3, 4, \dots, N. \quad (7.4)$$

where $\xi = (\xi_1, \xi_2, \xi_3, \xi_4, \dots, \xi_N)^T$.

The risk can be minimize by using (7.3) in Lagrangian equation which is defined as (Suykens and Vandewalle, 1999):

$$\mathbb{L}(w, b, \xi; \alpha) = \mathbb{J}(w, b, \xi) - \sum_{j=1}^N \alpha_j \{z_j[w^T u(x_j) + b] - 1 + \xi_j\} \quad (7.5)$$

where, α_j are Lagrange multipliers.

On solving (7.5), LS-SVM classifier can be denoted as (Suykens and Vandewalle, 1999):

$$v(x) = \text{sign} \left[\sum_{j=1}^N \alpha_j z_j F(x, x_j) + b \right] \quad (7.6)$$

where α_j are positive real constants, z_j is the j^{th} output pattern, x_j is the j^{th} input pattern, and $F(x, x_j)$ is a kernel function. In the present method, RBF kernel is utilized with classifier. The RBF kernel is defined as (Khandoker et al, 2007):

$$F(x, x_j) = e^{-\frac{\|x-x_j\|^2}{2\rho^2}} \quad (7.7)$$

The kernel parameter ρ is selected from the range between 0.5 and 2.5 with a step size of 0.1.

The LS-SVM is used in classification stage in this work. The LS-SVM classifier

is applied to distinguish the seizure and non-seizure EEG signals in (Bajaj and Pachori, 2012), to classify the epileptic seizure and seizure-free EEG signals (Sharma and Pachori, 2015, 2018b), to classify the focal and non focal EEG signals in (Gupta et al, 2018; Sharma et al, 2015b) and for the detection of normal and epileptic seizure EEG signals in (Pachori et al, 2015; Siuly et al, 2009). In (Patidar and Pachori, 2014; Patidar et al, 2015b), LS-SVM is also used to classify the heart sound signals.

In this present method, the classification is validated with 10-fold cross-validation technique (Kohavi, 1995) and in order to estimate the efficacy of the classifier, six distinct parameters are involved, which are ACC, SPE, SEN, Positive predictive value (PPV), Negative predictive value (NPV), and Matthews correlation coefficient (MCC). The ACC, SPE, and SEN are explained in Section 5.4. The PPV, NPV, and MCC are defined and expressed as follows:

1. Positive predictive value (PPV): It is calculated as the ratio of the accurately identified true positive samples to the total number of identified positive samples using following mathematical expression (Azar and El-Said, 2014):

$$PPV = \frac{TP}{TP + FP} \times 100(\%) \quad (7.8)$$

2. Negative predictive value (NPV): It is expressed as the ratio of the accurately identified true negative samples to the total number of identified negative samples as follows (Azar and El-Said, 2014):

$$NPV = \frac{TN}{TN + FN} \times 100(\%) \quad (7.9)$$

3. Matthews correlation coefficient (MCC): It is an additional argument to estimate the classification performance and can be expressed as follows (Azar and

Table 7.1: Classification performance measure parameters based on the maximum ACC obtained with 50 focal and 50 non-focal EEG signals on selected values from the range of RBF kernel and MCE parameters.

TQWT-FB	ACC (%)	SEN (%)	SPE (%)	PPV (%)	NPV (%)	MCC	Kernel parameter	MCE parameters		
							ρ	σ_1	σ_2	β
FB 1	83	72	94	93.18	77.16	0.68	2.3	0.1	0.3	0.8
	83	76	90	88.53	78.88	0.67	1.3	0.8	2	0.6
FB 2	83	80	86	86.67	81.67	0.67	2.1	1	1.5	0.3
	83	84	82	86.06	86.12	0.69	1.6	1.5	1.5	0.1
	83	82	84	86.29	84.62	0.68	1.7	1.8	1.6	0.2
	83	82	84	85.88	81.83	0.67	1.5	1.8	2	0.2
	83	78	88	88.33	82.08	0.68	2	1.8	2	0.8
	83	82	84	84.64	85.48	0.68	1.8	1.9	1.2	0.5
	83	82	84	85.31	84	0.68	1.6	2	1.9	0.7

Table 7.2: Classification performance measure parameters based on the maximum ACC obtained with 3750 focal and 3750 non-focal EEG signals on selected parameters of MCE.

TQWT-FB	ACC (%)	SEN (%)	SPE (%)	PPV (%)	NPV (%)	MCC	Kernel parameter	MCE parameters		
							ρ	σ_1	σ_2	β
FB 1	87.80	86.27	89.33	89.01	86.70	0.76	0.7	0.1	0.3	0.8
FB 2	87.28	87.23	87.33	87.32	87.25	0.75	1	1.5	1.5	0.1

El-Said, 2014):

$$MCC = \frac{TP \times TN - FN \times FP}{\sqrt{(TP + FN)(TP + FP)(TN + FN)(TN + FP)}} \quad (7.10)$$

7.4 Results and discussion

In order to detect focal epileptic zones from the EEG signals, a variety of computer-aided methods have been developed. These developed methods involve several features and various signal processing techniques. However, our proposed method has used a single MCE based features with TQWT-FB which performs well as compared to existing methodologies. The use of MCE provides a non-linear similarity

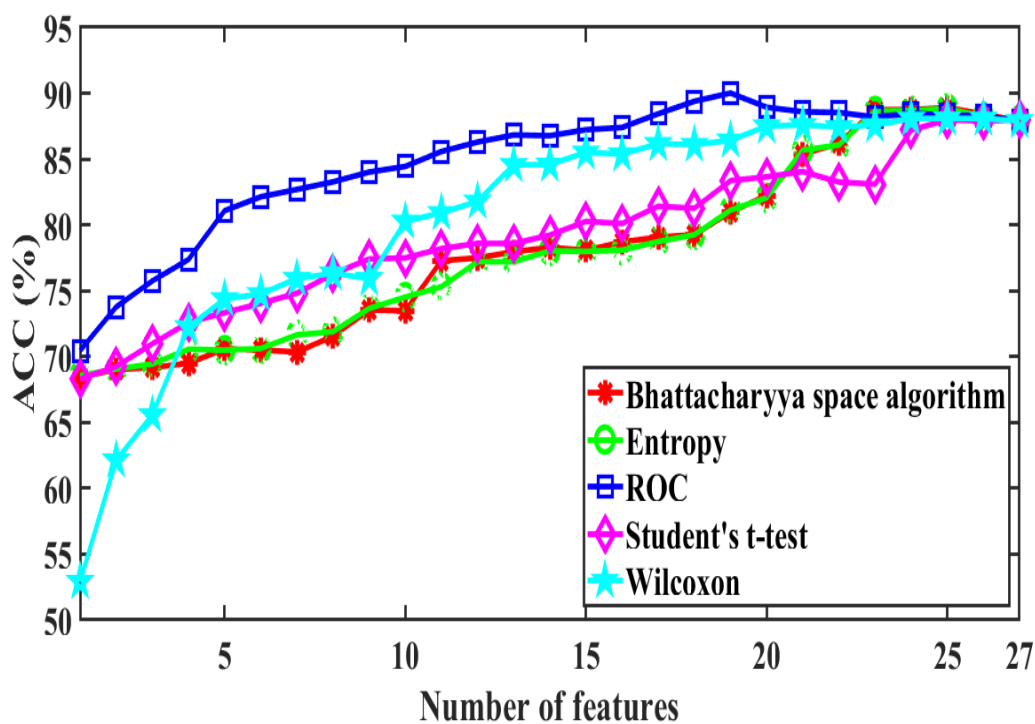


Figure 7.4: Variation of ACC with respect to number of features for different feature ranking methods obtained with FB 1.

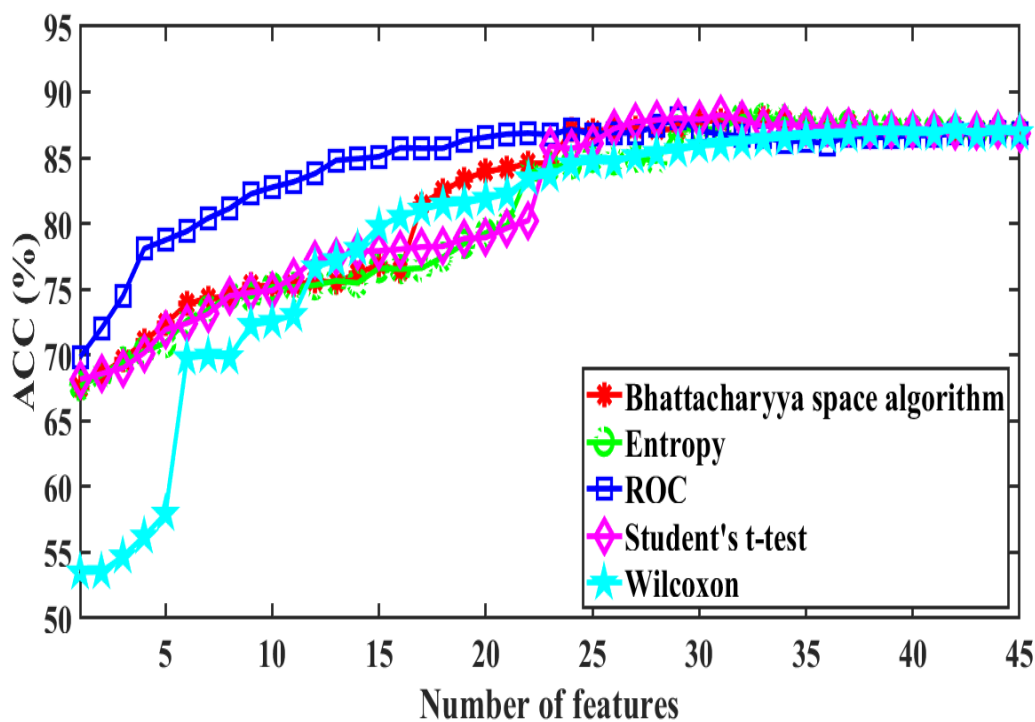


Figure 7.5: Variation of ACC with respect to number of features for different feature ranking methods obtained with FB 2.

Table 7.3: Classification performance measure parameters based on the maximum ACC obtained with feature ranking methods for 3750 focal and 3750 non-focal EEG signals.

TQWT-FB	Ranking method	Rank order	ACC (%)	SEN (%)	SPE (%)	PPV (%)	NPV (%)	MCC	Kernel parameter
									ρ
FB 1	Receiver operating characteristic	(1,10,9,11,4,8,12,5,7,13,2,16,14,6,3,15,17,18,19)	90.01	88.35	91.68	91.40	88.74	0.80	0.5
FB 2	Student's t-test	(17,18,16,19,15,20,21,14,22,23,13,8,24,9,12,11,10,25,27,28,29,7,2,26,30,1,3,31,6,4,5)	88.27	88.08	88.45	88.41	88.16	0.77	0.8

measure between bivariate focal and non-focal EEG signals. The developed method is first tested on 50 focal and 50 non-focal EEG signals for selecting the MCE parameters corresponding to maximum ACC then it is proceeded for 3750 focal and 3750 non-focal EEG signals. The Table 7.1 shows the maximum ACC obtained for FB 1 and FB 2 on selected values of RBF kernel and MCE parameters with 50 focal and 50 non-focal EEG signals. In Table 7.1, one can observe that classification performance parameters (SEN, SPE, PPV, NPV, and MCC) are changed corresponding to obtained maximum ACC of 83% for both the FBs. Therefore, we have chosen MCE parameters corresponding to maximum values of MCC parameter for the classification of 3750 focal and 3750 non-focal EEG signals because MCC is an additional parameter for the performance assessment of classification. The maximum classification accuracies for the classification of 3750 focal and 3750 non-focal EEG signals with FB 1 and FB 2 on selected values of MCE parameters corresponding to maximum MCC can be seen from Table 7.2. In order to optimize the developed methodology, we have also used four different feature ranking methods which will reduce the feature subspace and computational complexity without affecting the classification performance. Figs. 7.4 and 7.5 show the variation of ACC with number of features for different feature ranking methods obtained with FB 1 and FB 2, respectively. The maximum ACC obtained after feature ranking methods with rank order can also be seen in Table 7.3. From Table 7.3, it is clear that the achieved maximum ACC for FB 1 and FB 2 are 90.01% and 88.27% for the classification of 3750 focal and 3750 non-focal EEG signals, respectively. The obtained ACC is also compared with the existing methodologies and it can be observed from

Table 7.4: Comparison of the classification performance parameters for the proposed methodology with the existing methodologies.

Authors	ACC	SEN	SPE	PPV	NPV	MCC
(Zhu et al, 2013)	84%	-	-	-	-	-
(Sharma et al, 2015a)	84%	84%	84%	-	-	-
(Sharma et al, 2014)	85%	-	-	-	-	-
(Sharma et al, 2015b)	87%	90%	84%	87.29%	90.50%	0.76
(Das and Bhuiyan, 2016)	89.4%	90.7%	88.1%	-	-	-
(Bhattacharyya et al, 2018)	90%	88%	92%	-	-	-
(Bhattacharyya et al, 2017a)	84.67%	83.86%	85.46%	-	-	-
(Sharma and Pachori, 2018a)	84.01%	83.47%	84.56%	84.40%	83.68%	0.68
(Singh and Pachori, 2017)	89.70%	-	-	-	-	-
(Gupta and Pachori, 2019)	83.18%	85.78%	80.45%	-	-	-
(Acharya et al, 2019)	87.93%	89.97%	85.89%	-	-	-
Proposed work	90.01%	88.35%	91.68%	91.40%	88.74%	0.80

Table 7.4 that the achieved ACC shown with bold entry is higher in comparison to methodologies which have been selected for comparison.

Also the methodology of compared methods mentioned in Table 7.4 are presented in Table 7.5. In this table, decomposition method, used features, number of features used to produce best result, classifier used for classification by each method is mentioned. Also the number of EEG signals considered in each class and cross-validation technique used in classifier is mentioned in Table 7.5.

7.5 Summary

Large population of the world is affected from epilepsy. Undetected epilepsy may lead to long term complications, causing severe disorder problems. In the present work, focal epilepsy is considered to identify EEG signals corresponding to the focal epileptogenic zones. The TQWT-FBs are used to decompose the focal and non-focal EEG signals in to sub-band signals. From these sub-band signals, MCE based fea-

Table 7.5: Comparison of the methodology of compared methods and proposed method for focal EEG signal detection.

Authors	Method	Number of features used	Classification method	Number of EEG signals	Classification validation technique
(Zhu et al, 2013)	Delay permutation entropy	1	SVM	50 focal and 50 non-focal	-
(Sharma et al, 2015a)	Discrete WT, entropy measures	3	LS-SVM	50 focal and 50 non-focal	10-fold
(Sharma et al, 2014)	EMD, ASE, AVIF	5	LS-SVM	50 focal and 50 non-focal	10-fold
(Sharma et al, 2015b)	EMD, entropy measures	13	LS-SVM	50 focal and 50 non-focal	10-fold
(Das and Bhuiyan, 2016)	EMD-discrete WT, log-energy entropy	7	KNN	3750 focal and 3750 non-focal	-
(Bhattacharyya et al, 2018)	Empirical WT, reconstructed phase space, central tendency measure	4	LS-SVM	50 focal and 50 non-focal	10-fold
(Bhattacharyya et al, 2017a)	TQWT, multivariate sub-band fuzzy entropy	-	LS-SVM	3750 focal and 3750 non-focal	10-fold
(Sharma and Pachori, 2018a)	Bivariate EMD, bandwidth features	-	LS-SVM	3750 focal and 3750 non-focal	10-fold
(Singh and Pachori, 2017)	Fourier-based rhythms, bandwidth features	20	LS-SVM	50 focal and 50 non-focal	10-fold
(Gupta and Pachori, 2019)	EMD, Sharma Mittal entropy	9	LS-SVM	3750 focal and 3750 non-focal	10-fold
(Acharya et al, 2019)	23 different features	23	LS-SVM	3750 focal and 3750 non-focal	10-fold
Proposed work	TQWT-FB and MCE	19	LS-SVM	3750 focal and 3750 non-focal	10-fold

tures are computed. Ranked features are used as an input to the LS-SVM classifier for the diagnosis of focal epileptic zones from EEG signals. A 10-fold cross validation technique is involved to confirm the validation of the ACC. The highest ACC of 90.01% is achieved using RBF kernel function.

Chapter 8

Automated classification of hand movements using TQWT-FB with surface EMG signals

8.1 Introduction

A person with hand amputee can perform basic hand movement tasks with the help of an EPH. However, controlling the EPH in order to perform hand movement precisely is still a research problem (Sapsanis et al, 2013b). The controlling action can be performed using EEG signals or EMG signals. The EEG signals are generated due to the electrical activity of brain (Caton, 1875) and EMG represents the electrical activity of muscles (Sapsanis et al, 2013a). The use of EEG signals requires the proper positioning of electrodes on the scalp, which is uncomfortable (Kiguchi and Hayashi, 2012). On the other hand, using EMG signals require a glove containing EMG electrodes (Kiguchi and Hayashi, 2012). The characteristics of EMG signals vary with different muscles movement (Sapsanis et al, 2013a,b). The variations are more when EMG signals are recorded from hand instead of forearm (Finneran and O'Sullivan, 2013; Kurita et al, 2002). Hence, the EMG signals are usually recorded from forearm muscles as these muscles are in the resting position when different

hand movements are performed (Finneran and O’Sullivan, 2013; Kurita et al, 2002; Liu and Zhou, 2013).

The accurate classification of EMG signals can design an effective controller for EPH (Andrianesis and Tzes, 2008). This can be accomplished using advanced biosignal processing, biosensors, and pattern recognition techniques (Carroll and Alwarappan, 2012; Kaniusas, 2012). In literature, many methods are proposed for hand movement identification using EMG signals with good classification ACC (Oskoei and Hu, 2007). However, these methods are based on acquiring EMG signals from many electrodes (Oskoei and Hu, 2007). In many cases, the number of electrodes used are more than four (Oskoei and Hu, 2007). This would increase the cost of EPH design and also will be uncomfortable to use (Sapsanis et al, 2013b). Therefore, the designed EPH should be easy to use and the amputee person can perform different hand movements by executing corresponding action with EPH (Sapsanis et al, 2013b).

In literature, different studies are presented to classify different hand movements using EMG signals. In (Ouyang et al, 2014), the classification of four hand movements has been presented using the adaptive neuro-fuzzy interference system and in (Ju and Liu, 2014), the fuzzy Gaussian mixture models is proposed which used Willison amplitude and determinism to classify 10 hand movements. The classification of not only hand movements, but also movements of wrist and fingers has been performed in (Nazemi and Maleki, 2014). The authors performed classification of 52 classes using windowing method and MLP. In (Sapsanis et al, 2013a,b), the EMD is used to decompose the EMG signals into IMFs. Then features such as integrated EMG, zero-crossing, variance, slope sign changes, waveform length, Willison amplitude, kurtosis, skewness are extracted from them and original EMG signals are classified to six hand movements (Sapsanis et al, 2013b). In (Sapsanis et al, 2013a), apart from using features mentioned in (Sapsanis et al, 2013b), the authors also used SD, median, and kurtosis of instantaneous frequencies of IMFs. The authors in (Kakoty and Hazarika, 2011), used SVM and classified six hand movements. The

authors in (Khezri and Jahed, 2008) used wavelet TH method to classify three hand movements.

In (Akben, 2017), classification of six classes of hand movement is presented. The authors used correlation between energy histogram of each channel of data as feature, then cascaded structured classifier is used. The authors in (Ruangpaisarn and Jaiy, 2015) used singular value decomposition to extract features from sEMG signals. Then classifiers namely decision tree, k -NN, RBF, naive Bayes, and SMO classifiers are used to classify six different hand movements. The authors obtained best results using SMO classifier. The method proposed in (Iqbal et al, 2017) classified hand movements from sEMG signals. It is based on singular value decomposition and principal component analysis. The singular value decomposition is applied on the sEMG to obtain singular values and principal components. The statistical parameters of few principal components are used as features (Iqbal et al, 2017). Then, authors used hierarchical k -NN classifier for classification.

This chapter presents a novel methodology to classify six basic hand movements. The classification of the hand movement is done using sEMG signals obtained from two electrodes only. In this way, proposed method can be used for designing of comfortable and cost effective EPH. In the proposed method, the cross-covariance of sEMG signals is computed and termed as csEMG signal. Then, the csEMG signal is decomposed into the number of sub-band signals by a designed TQWT-FB. This FB consists of constant and narrow BW sub-bands which are generated from distinct value of Q -factor. Different Q -factor values in TQWT-FB are suitable to analyse different oscillatory csEMG signals obtained from non-stationary sEMG signals (Selesnick, 2011c). After decomposing csEMG signal, the features are computed using KRE from available sub-band signals. Finally classification of hand movements is performed using a k -NN classifier. The novelty of proposed method is the application of TQWT-FB and KRE in TQWT frame work to classify the hand movements.

In the remaining part of the chapter, the database used in this work in briefly

described in Sections 8.2. Then proposed methodology, performance measure, simulation results, and discussion are presented in Section 8.3, 8.4, 8.5, and 8.6 respectively. Finally the chapter is summarized in Section 8.7.

8.2 Database

The data used in this work is obtained from basic hand movements database (Sapsanis et al, 2013b). It can be downloaded from <https://archive.ics.uci.edu/ml/datasets/sEMG+for+Basic+Hand+movements#>. The data in the form of sEMG signal is collected from five subjects (three females and two males). The age of these subjects is in between 20 and 22 years. Each subject has performed six hand movements which are cylindrical (CY), hook (HO), lateral (LA), palmar (PA), spherical (SP), and tip (TI). In CY, LA, SP, and TI hand movements, subject holds CY, flat, SP, and small objects respectively. In PA hand movement, subject grasps an object with palm and in HO hand movement, subject supports a heavy load. More details regarding these hand movements can be found in (Sapsanis et al, 2013b). The sketch patterns of these hand movements from (Sapsanis et al, 2013b) are shown in Fig. 8.1.

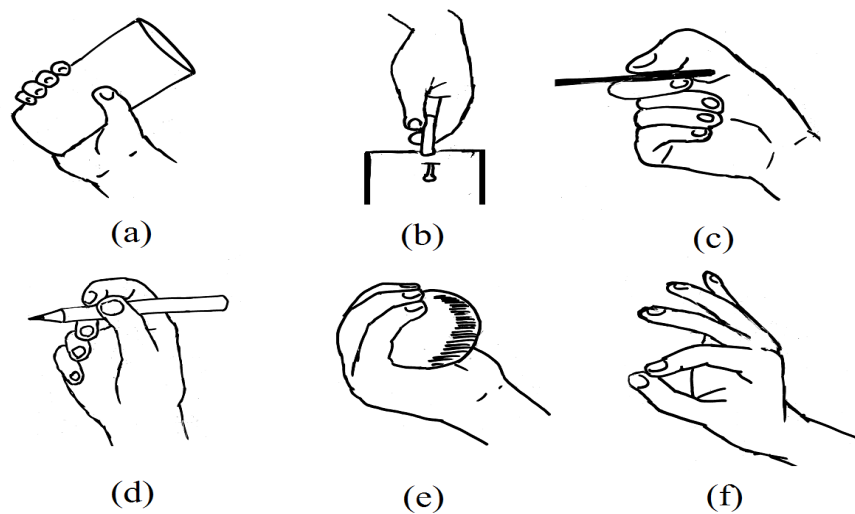


Figure 8.1: Basic hand movements. (a) cylindrical (CY), (b) hook (HO), (c) lateral (LA), (d) palmar (PA), (e) spherical (SP), and (f) tip (TI)

Each hand movement is repeated thirty times by each subject. Therefore, total number of hand movement tasks performed by each subject is 180. The duration of each hand movement task is six seconds. The force and speed to perform different hand movement tasks are left on subject's own choice.

For each hand movement task, the sEMG signals are recorded from two forearm sEMG electrodes (Sapsanis et al, 2013b). Hence the obtained data is sEMG signals from two channels. The F_s to collect the data is 500 Hz. The sample sEMG signals are shown in Fig. 8.2.

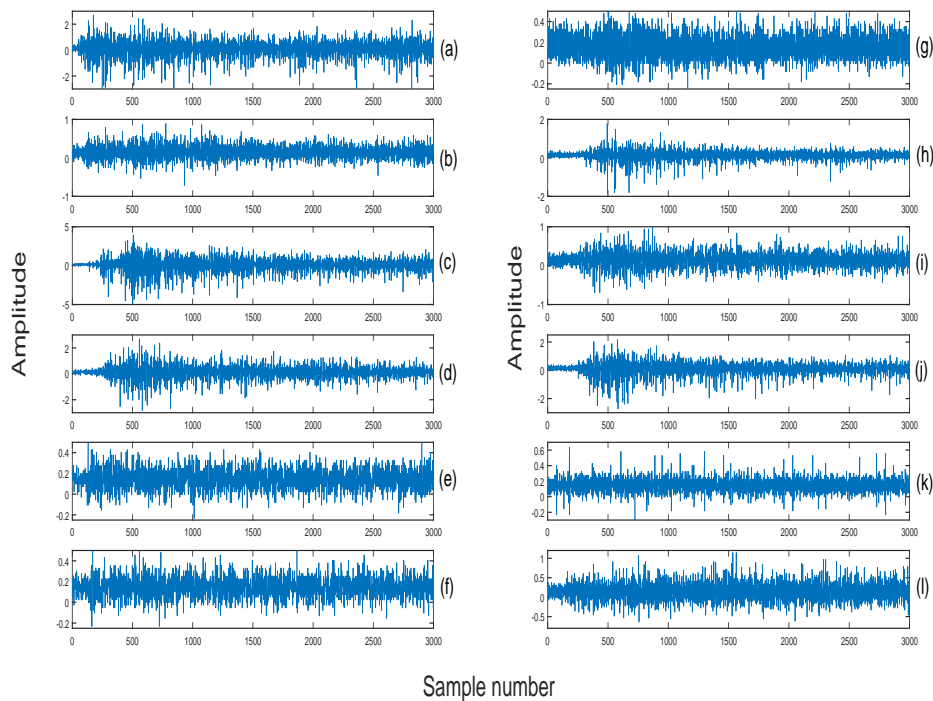


Figure 8.2: The sEMG signal corresponding to (a) CY acquired from electrode 1, (b) CY acquired from electrode 2, (c) HO acquired from electrode 1, (d) HO acquired from electrode 2, (e) LA acquired from electrode 1, (f) LA acquired from electrode 2, (g) PA acquired from electrode 1, (h) PA acquired from electrode 2, (i) SP acquired from electrode 1, (j) SP acquired from electrode 2, (k) TI acquired from electrode 1, and (l) TI acquired from electrode 2.

8.3 Proposed method

The proposed method for the classification of basic hand movements using sEMG signals consist of four stages. In the first stage, the csEMG signal is computed. Then in next stage, the csEMG signal is decomposed by a designed TQWT-FB. Then in third stage, the features are computed and ranked from decomposed csEMG signals. Finally, in the last stage, the classification using computed features is performed. The block diagram of proposed method is shown in Fig. 8.3.

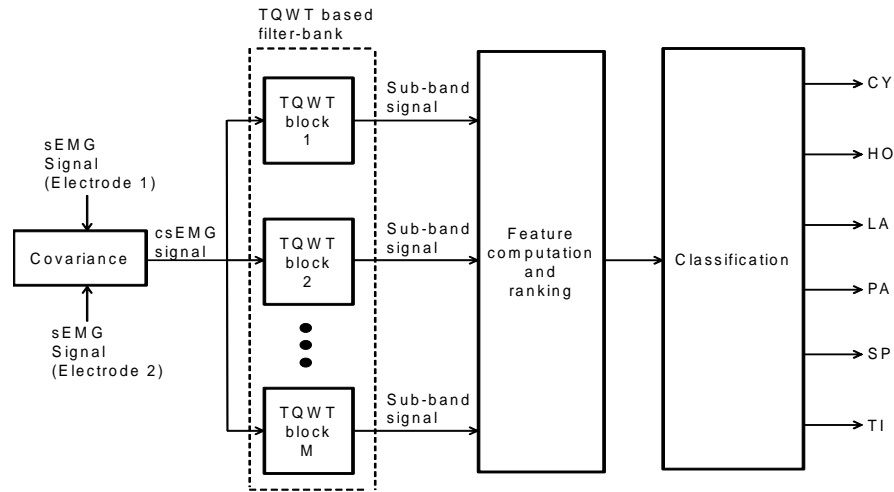


Figure 8.3: Block diagram of proposed method for basic hand movements classification.

8.3.1 Cross-covariance of sEMG signals

For each hand movement, the sEMG signals are available from two channels. In this stage, the csEMG signal is computed from sEMG signals. The cross-covariance estimates the covariance of one process with respect to other. The covariance of two sEMG signals represents their joint variability (Rice, 2007). After cross-covariance operation, the produced signal csEMG is fed to next stage.

8.3.2 Design of TQWT-FB

The Method II, as described in Section 2.2 is used to design TQWT-FB for classification problem addressed in this chapter. The BW of each sub-band is very narrow and equals to 0.01 (normalized frequency). The number of sub-bands in TQWT-FB are 161, which implies that 161 TQWT blocks are used in the designing of TQWT-FB. The $R = 9$ is allocated to each TQWT block. The assigned Q -factor and D values are shown in Fig. 8.4 and Fig. 8.5 respectively.

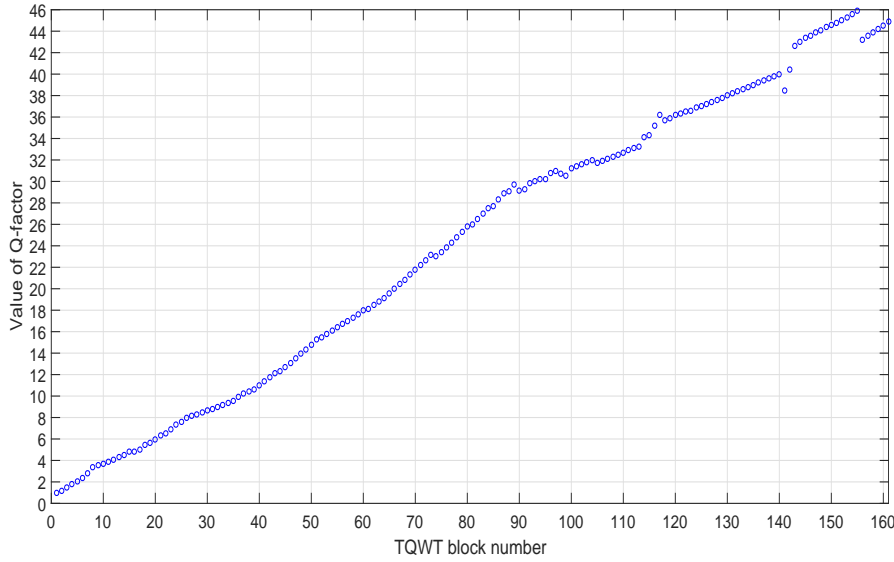


Figure 8.4: Assigned Q -factor values for different TQWT blocks.

The Fig. 8.6 shows the designed TQWT-FB.

8.3.3 Features computation and ranking

The features are collected by computing KRE from sub-band signals. The KRE determines the differential statistical entropy of the sub-band signal with the help of k -NNs sample. For a J -dimensional random variable $U (u_1, u_2, u_3, \dots, u_n)$, it is expressed mathematically as (Kraskov et al, 2004; Veselkov et al, 2010):

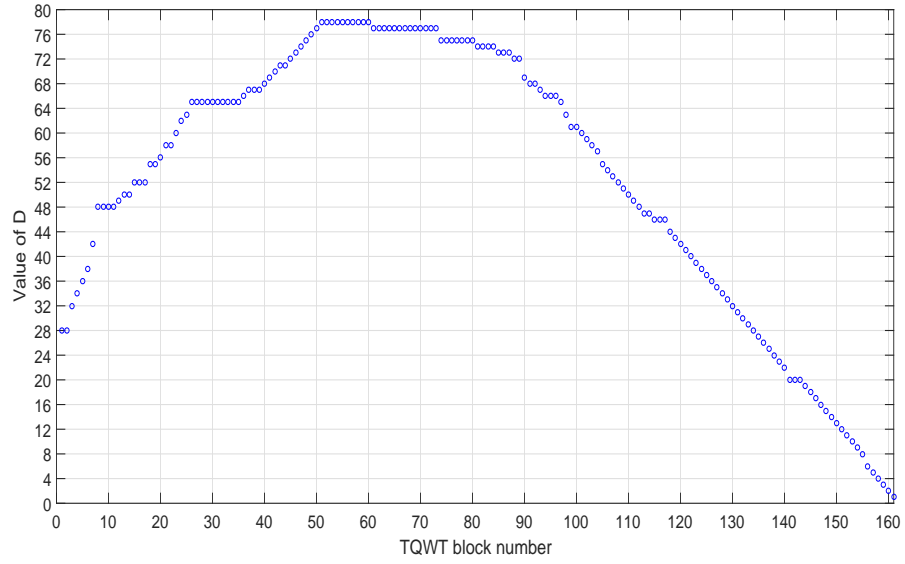


Figure 8.5: Assigned D values for different TQWT blocks.

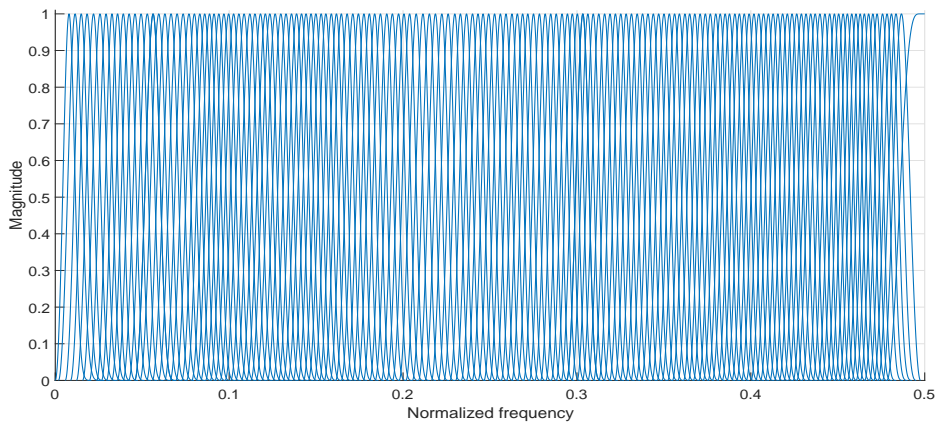


Figure 8.6: The designed TQWT-FB used in our proposed method.

$$\text{KRE}(u) = \alpha(n) - \alpha(k) + \log(V_J) + \frac{J}{n} \sum_{i=1}^n \log(d_i^k) \quad (8.1)$$

where $\alpha(\cdot)$ is the digamma function and for a variable z , it is expressed as (Kraskov et al, 2004):

$$\alpha(z) = \frac{1}{\Gamma(z)} \frac{d\Gamma(z)}{dz} \quad (8.2)$$

Here $\Gamma(\cdot)$ is the gamma function. The V_J in (8.1) indicates the volume of ball of J -dimension, which rely on sample space. It is defined for Euclidean form as (Veselkov et al, 2010):

$$V_J = \frac{\pi^{\frac{J}{2}}}{\Gamma(1 + \frac{J}{2})} \quad (8.3)$$

The d_i^k in (8.1) represents the distance between u_i and its k_f nearest neighbour samples. Here, u_i is the i^{th} random sample. The chosen value of k_f in proposed method is indicated in simulation results section. In (Kumar et al, 2016), the KRE is used to detect coronary artery disease.

After computing the features, they are ranked based on the level of significance. We have used three types of feature ranking methods. They are briefly described as follows:

1. Local learning-based clustering feature selection (LLCFS): This method is proposed in (Zeng and Cheung, 2011). In this method, a weight is assigned to each feature and then they are included in regularization of local learning-based clustering (LLC) to determine the relevance of each feature for clustering (Zeng and Cheung, 2011). The weights are computed in several iterations of clustering process. The weights of insignificant features decreases to zero (Zeng and Cheung, 2011).
2. Multi-cluster feature selection (MCFS): The MCFS method (Cai et al, 2010) selects features in such a way that the multi-cluster arrangement of data does

not alters. The method then solves optimization problem which involves L1-regularization least square and sparse eigen problem (Cai et al, 2010). From this, the method computes the MCFS score of each feature in order to rank them.

3. RELIEFF: The third type of ranking method used for feature ranking is RELIEFF algorithm (Kononenko et al, 1997; Robnik-Sikonja and Kononenko, 2003). In this algorithm, significance of a feature is identified as per its ability to differentiate nearby instances (Kononenko et al, 1997; Robnik-Sikonja and Kononenko, 2003). The algorithm after selecting a random instance, looks for its k -NNs which are from similar class and its k -NNs are from other classes (Kononenko et al, 1997; Robnik-Sikonja and Kononenko, 2003). Then, a quality variable is determined which is the function of selected instance, k -NNs from same class and k -NNs from other class. This variable indicates the significance of the feature. The variable k used in k -NN is termed as k_r in this work.

The ranking of features is implemented using feature selection library (Roffo et al, 2015, 2017).

8.3.4 Classification

We have tested three classifiers of different category, in this work. They are briefly explained below:

1. C4.5 classifier: It belongs to the category of tree based classifier. In classifier C4.5, a decision tree is constructed using top-down method. The construction of tree begins with training set (Ruggieri, 2002). The training set consists of attributes and class value. An attribute is specified to each decision node of tree to examine its capability to classify the training sample (Farid et al, 2014). In the beginning, the entire training set is associated with the root node,

and for each case, the assigned weight value is equal to one. The decision tree is then constructed by C4.5 algorithm which uses divide and conquer method (Farid et al, 2014; Quinlan, 1986). The attribute whose information gain is highest is chosen for test on a node. In the next step, child node is generated for every possible outcome of class. These steps are rerun for every attribute associated with each node in order to choose the finest attribute for the node. The C4.5 classifier has been used in (Sharma et al, 2017b) for classification of sleep stages using EEG signals.

2. SMO classifier: The SMO algorithm (Platt, 1998) is proposed to reduce the computational complexity in SVM classifier. The SMO algorithm decomposes the quadratic programming of SVM into sub-problems. Then SMO solves the smallest optimization problem at each stage using two Lagrange multipliers. The classifier SMO is used for the classification of vowel phonemes in (Boujelbene et al, 2008).
3. k -NN classifier: The classification model of k -NN classifier depends on nearest neighbour algorithm (Aha et al, 1991). The classification of the test data is performed by computing the distance from close training data. The variable k in k -NN and the distance are the two variables which can affect the classification performance. The variable k in k -NN classifier is termed as k_c . The value of k_c and distance used in classifier are mentioned in the simulation results section. The k -NN classifier is fast in computation and it does not presume the statistics of training samples. The k -NN classifier has been used in (Gupta et al, 2017) and (Das and Bhuiyan, 2016) for analysis of focal and non-focal EEG signals.

In this work, we have used WEKA software (Hall et al, 2009) to implement C4.5 and SMO classifiers. The k -NN classifier is implemented using `knnclassify` function from bioinformatics toolbox available in MATLAB.

8.4 Performance measure

The proposed method is tested on the data of five subjects. Therefore, the average of ACC obtained from each subject is considered as performance measure in this chapter. The definition of ACC can be found in Section 5.4.

8.5 Simulation results

In the proposed method, three types of ranking methods and classifiers are used. Hence, there are nine cases which are tested during the simulation. These cases are as follows:

1. Case-A: LLCFS is used for feature ranking and C4.5 is used for classification.
2. Case-B: LLCFS is used for feature ranking and SMO is used for classification.
3. Case-C: LLCFS is used for feature ranking and k -NN is used for classification.
4. Case-D: MCFS is used for feature ranking and C4.5 is used for classification.
5. Case-E: MCFS is used for feature ranking and SMO is used for classification.
6. Case-F: MCFS is used for feature ranking and k -NN is used for classification.
7. Case-G: RELIEFF is used for feature ranking and C4.5 is used for classification.
8. Case-H: RELIEFF is used for feature ranking and SMO is used for classification.
9. Case-I: RELIEFF is used for feature ranking and k -NN is used for classification.

In the proposed model, the KREs are computed as features from sub-band signals. The features are computed for different cases. In each case, the value of k_f is different for feature computation. The value of k_f is varied from 1 to 4. Then for each case of feature computation, the features are ranked. During RELIEFF ranking, different values of k_r are chosen. The chosen values of k_r are 1, 2, 3, and 4. Hence there are four cases of feature computation and four cases of RELIEFF feature ranking used in proposed model. Therefore, in Case-G, Case-H, and Case-I, there are sixteen cases of ranked features are available for classification.

In the classification stage, first the best rank feature is given to the classifier. The NORF is increased from 1 by appending the next highly significant feature in the descending order. For each NORF, the k_c is varied from 1 to 10 when k -NN classifier is used. For every NORF and k_c value, the classification ACC is noted. Among all ACCs, the maximum ACC is considered as the best classification result. The distance used in k -NN classifier is Euclidean distance.

When SMO and C4.5 classifiers are used in classification, the NORF is again varied from 1 to total number of features in the descending order by appending the features one by one. In SMO classifier, the polynomial kernel is used as kernel function. The classification is performed using leave one out cross-validation approach (Kohavi, 1995). The performance of proposed method is measured in terms of ACC. The obtained ACCs in (%) for different k_f values and cases (Case-A, Case-B, Case-C, Case-D, Case-E, and Case-F) are shown in Table 8.1. Similarly, Table 8.2, Table 8.3, and Table 8.4 show the obtained ACCs(%) for different cases (Case-G, Case-H, and Case-I) and various values of k_f and k_r . All these tables show obtained ACCs(%) for five subjects (S1, S2, S3, S4, and S5).

From Table 8.1 to Table 8.4, in each case, if we have considered the maximum ACC for each subject and computed their average ACC. The average ACC for Case-A, Case-B, Case-C, Case-D, Case-E, Case-F, Case-G, Case-H, and Case-I are 89.88%, 97.21%, 97.1%, 92.44%, 97.21%, 97.55%, 91.66%, 97.22%, and 98.55% respectively. It can be noted that Case-I is the best case among all. In this case,

Table 8.1: ACC(%) obtained for Case-A to Case-F with change in k_f .

Subject		Case-A	Case-B	Case-C	Case-D	Case-E	Case-F
		ACC(%)	ACC(%)	ACC(%)	ACC(%)	ACC(%)	ACC(%)
S1	$k_f = 1$	83.88	96.66	95.55	90	96.66	97.22
	$k_f = 2$	82.22	96.66	95.55	85.55	97.22	96.11
	$k_f = 3$	81.11	96.66	95.55	87.22	96.66	96.11
	$k_f = 4$	81.66	96.66	95.55	83.88	96.66	96.66
S2	$k_f = 1$	91.11	95	94.44	87.77	94.44	93.88
	$k_f = 2$	87.22	95	93.88	86.66	94.44	94.44
	$k_f = 3$	90.55	95	93.88	91.66	94.44	95
	$k_f = 4$	89.44	95	94.44	89.44	94.44	95
S3	$k_f = 1$	90	97.77	97.77	92.22	97.77	98.33
	$k_f = 2$	91.66	97.77	98.33	91.11	97.77	97.77
	$k_f = 3$	93.33	97.77	98.33	93.33	97.77	97.77
	$k_f = 4$	90	97.77	96.66	93.33	97.77	97.77
S4	$k_f = 1$	88.88	97.77	98.33	95	97.22	98.33
	$k_f = 2$	87.22	97.77	98.33	93.88	97.77	98.33
	$k_f = 3$	86.11	97.77	98.88	90.55	97.77	98.88
	$k_f = 4$	87.22	97.77	98.33	90.55	97.77	98.33
S5	$k_f = 1$	91.66	98.88	98.33	90.55	98.88	97.77
	$k_f = 2$	91.66	98.88	98.33	92.22	98.88	97.77
	$k_f = 3$	92.22	98.88	98.33	92.22	98.88	98.33
	$k_f = 4$	91.66	98.88	97.77	90.55	98.88	98.33

Table 8.2: ACC(%) obtained for Case-G with change in k_r and k_f .

Subject		$k_r = 1$	$k_r = 2$	$k_r = 3$	$k_r = 4$
		ACC(%)	ACC(%)	ACC(%)	ACC(%)
S1	$k_f = 1$	88.44	86.11	91.11	90
	$k_f = 2$	88.33	91.11	88.88	90
	$k_f = 3$	88.88	91.11	88.33	88.88
	$k_f = 4$	87.77	87.77	86.66	86.66
S2	$k_f = 1$	82.77	85.55	85.55	86.11
	$k_f = 2$	81.66	83.88	82.77	83.33
	$k_f = 3$	89.44	88.88	89.44	89.44
	$k_f = 4$	87.77	88.88	88.88	89.44
S3	$k_f = 1$	91.11	91.66	91.11	91.11
	$k_f = 2$	91.66	90.55	90.55	91.66
	$k_f = 3$	91.11	92.22	92.22	92.22
	$k_f = 4$	90.55	91.11	91.11	91.66
S4	$k_f = 1$	91.66	91.11	88.33	91.11
	$k_f = 2$	90.55	89.44	88.33	91.11
	$k_f = 3$	88.33	90.55	88.33	90.55
	$k_f = 4$	89.44	91.66	90	91.11
S5	$k_f = 1$	91.11	92.22	92.77	90.55
	$k_f = 2$	91.66	93.33	93.88	91.66
	$k_f = 3$	91.11	92.77	93.33	91.11
	$k_f = 4$	91.66	92.22	92.77	91.66

Table 8.3: ACC(%) obtained for Case-H with change in k_r and k_f .

Subject		$k_r = 1$	$k_r = 2$	$k_r = 3$	$k_r = 4$
		ACC(%)	ACC(%)	ACC(%)	ACC(%)
S1	$k_f = 1$	97.22	96.66	97.22	97.22
	$k_f = 2$	97.77	97.22	97.22	97.22
	$k_f = 3$	97.77	97.22	97.22	97.22
	$k_f = 4$	97.77	97.22	97.22	97.22
S2	$k_f = 1$	94.44	95	95	95
	$k_f = 2$	94.44	95	95	95
	$k_f = 3$	95	95	95	95
	$k_f = 4$	95	95	94.44	94.44
S3	$k_f = 1$	97.77	98.33	98.88	98.88
	$k_f = 2$	97.77	98.33	98.88	98.88
	$k_f = 3$	97.77	98.33	98.88	98.88
	$k_f = 4$	97.77	98.33	98.33	98.33
S4	$k_f = 1$	98.33	97.77	97.77	97.77
	$k_f = 2$	98.33	97.77	97.77	97.77
	$k_f = 3$	97.77	97.77	97.77	97.77
	$k_f = 4$	97.77	97.77	97.77	97.77
S5	$k_f = 1$	98.88	98.88	98.88	98.88
	$k_f = 2$	98.88	98.88	98.88	98.88
	$k_f = 3$	98.88	98.88	98.88	98.88
	$k_f = 4$	98.88	98.88	98.88	98.88

Table 8.4: ACC(%) obtained for Case-I with change in k_r and k_f .

Subject		$k_r = 1$	$k_r = 2$	$k_r = 3$	$k_r = 4$
		ACC(%)	ACC(%)	ACC(%)	ACC(%)
S1	$k_f = 1$	97.77	97.22	98.33	98.33
	$k_f = 2$	97.22	97.77	98.33	98.33
	$k_f = 3$	97.77	97.77	98.33	98.33
	$k_f = 4$	97.77	98.33	98.33	98.33
S2	$k_f = 1$	95	97.22	97.77	97.77
	$k_f = 2$	95	96.66	97.22	97.77
	$k_f = 3$	95	96.66	97.22	97.77
	$k_f = 4$	95.55	96.66	97.22	97.77
S3	$k_f = 1$	99.44	98.33	98.33	98.33
	$k_f = 2$	98.88	98.33	98.33	98.88
	$k_f = 3$	99.44	98.33	98.88	98.33
	$k_f = 4$	99.44	99.44	98.33	98.88
S4	$k_f = 1$	98.33	98.33	98.88	98.33
	$k_f = 2$	98.33	98.83	98.33	98.88
	$k_f = 3$	98.33	98.33	98.33	98.88
	$k_f = 4$	98.33	98.33	98.33	98.88
S5	$k_f = 1$	97.77	98.33	98.33	98.33
	$k_f = 2$	97.77	98.33	98.33	98.33
	$k_f = 3$	97.77	98.33	98.33	98.33
	$k_f = 4$	97.77	98.33	98.33	98.33

Table 8.5: Results of highest ACC obtained for each subject for different values of k_c and NORF.

Subject	ACC(%)	k_c	NORF	k_f	k_r
S1	98.33	3	34	1	3
S2	97.77	1	24	1	3
S3	99.44	1	28	1	1
S4	98.88	1	121	1	3
S5	98.33	4	79	1	2

the maximum ACC achieved for S1, S2, S3, S4, and S5 is 98.33%, 97.78%, 99.44%, 98.89%, and 98.33% respectively. The Table 8.5 shows the values of k_c and NORF for which maximum ACC is achieved using minimum values of k_f and k_r for each subject in Case-I.

The statistical analysis of computed ranked features corresponding to maximum ACC presented in Table 8.5, are shown in Fig. 8.7 to Fig. 8.11. In these figures, mean and SD of features are shown bar chart. The center of the bar indicates the mean and 0.5 times the length of the bar is SD of the feature. The x axis in these figures shows the ranked features (F_i) where i is the rank of feature F .

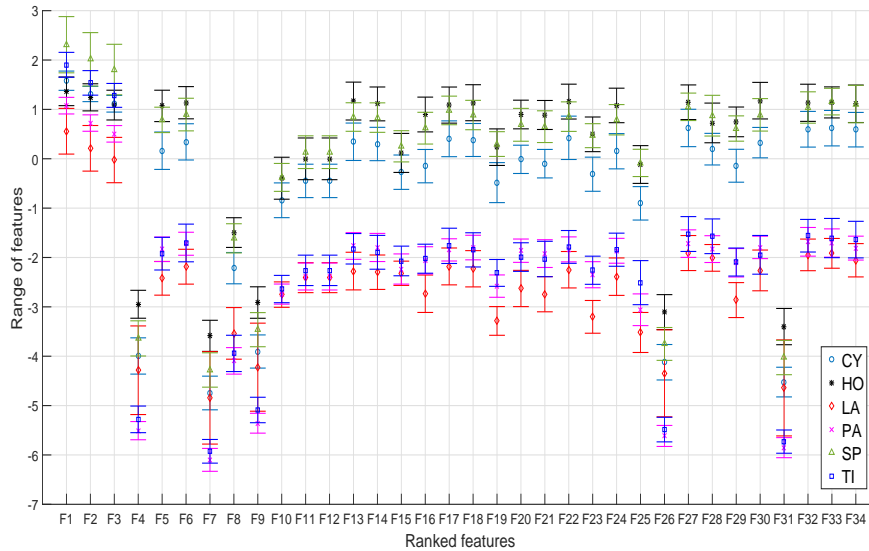


Figure 8.7: Statistical analysis (mean and SD) of features for S1 data.

The p -value of features shown in Fig. 8.7 to Fig. 8.11 are mentioned in Table 8.6 to Table 8.10 respectively.

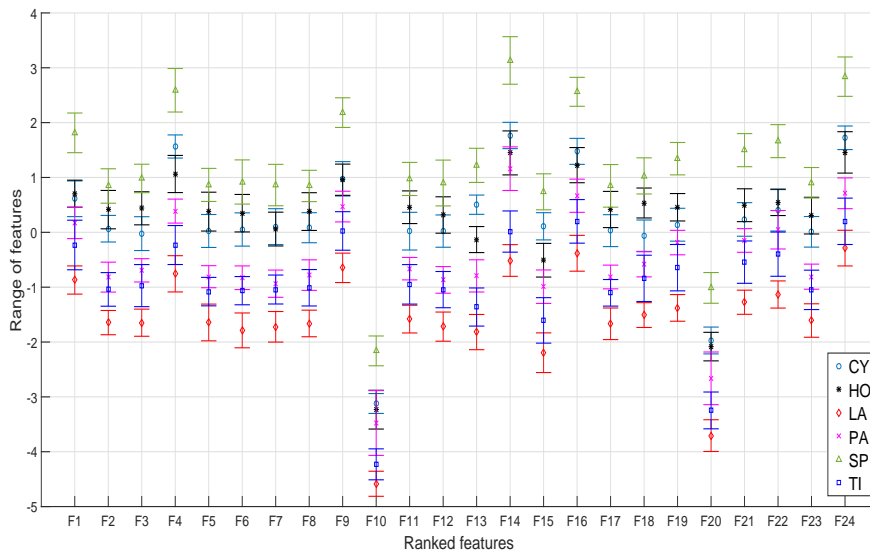


Figure 8.8: Statistical analysis (mean and SD) of features for S2 data.

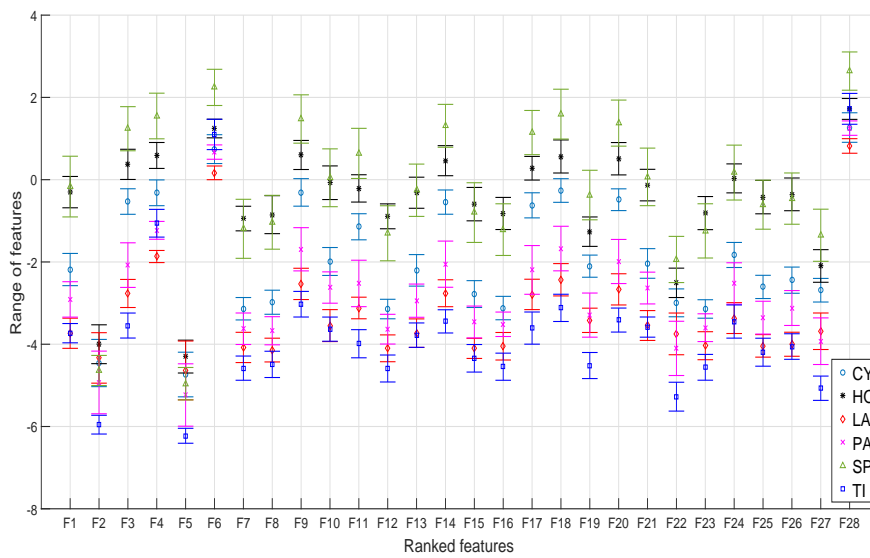
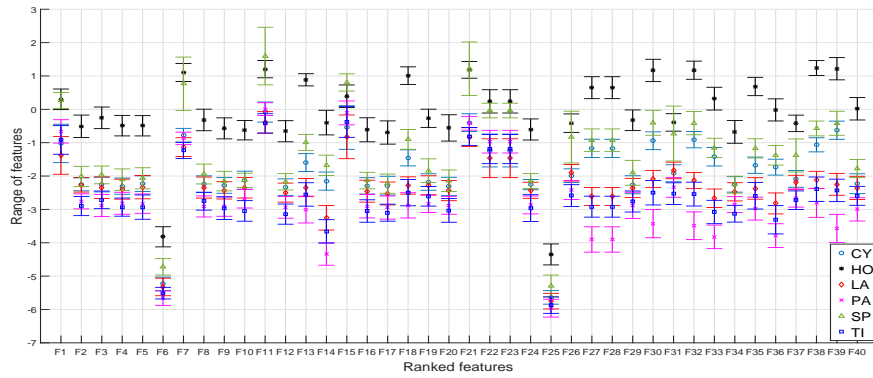
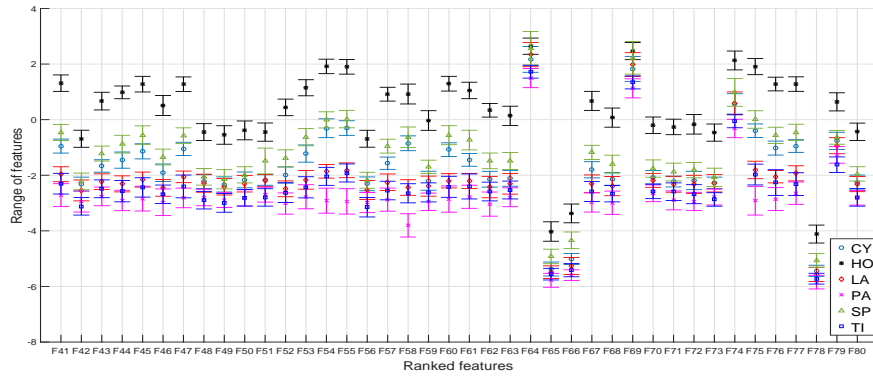


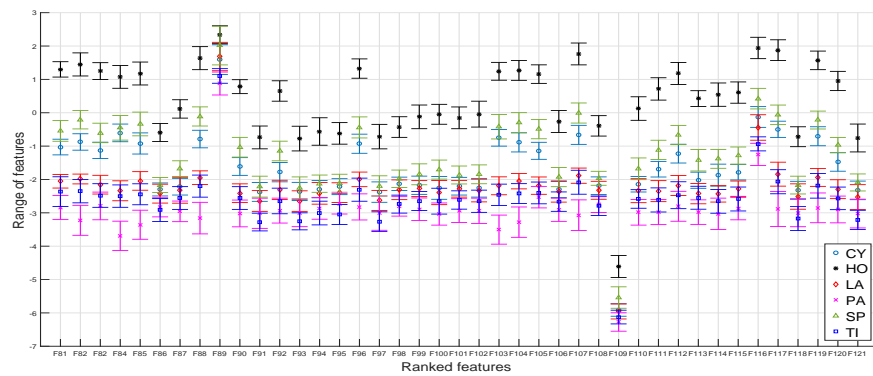
Figure 8.9: Statistical analysis (mean and SD) of features for S3 data.



(a)

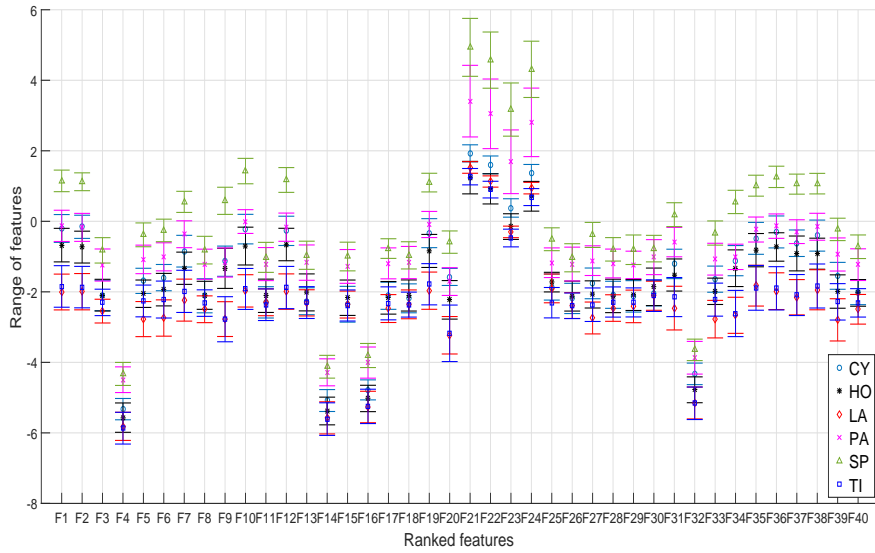


(b)

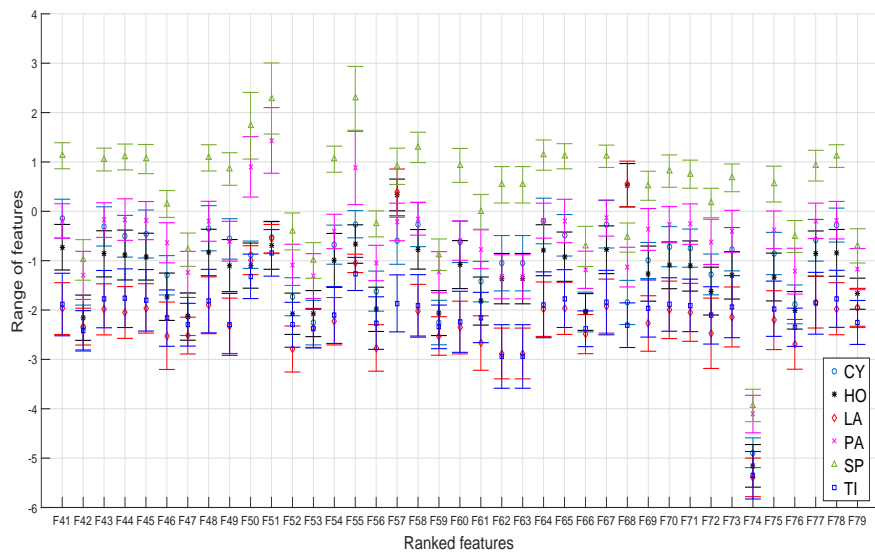


(c)

Figure 8.10: Statistical analysis (mean and SD) of features: (a) F1 to F40, (b) F41 to F80, and (c) F81 to 121, for S4 data.



(a)



(b)

Figure 8.11: Statistical analysis (mean and SD) of features: (a) F1 to F40 and (b) F41 to F79, for S5 data.

Table 8.6: The p -values of all features extracted from S1 data.

Feature	p -value						
F1	1.38×10^{-28}	F10	1.28×10^{-28}	F19	6.64×10^{-33}	F28	2.21×10^{-30}
F2	1.54×10^{-28}	F11	5.43×10^{-29}	F20	4.28×10^{-33}	F29	7.06×10^{-33}
F3	2.64×10^{-28}	F12	5.43×10^{-29}	F21	5.44×10^{-33}	F30	4.51×10^{-31}
F4	1.54×10^{-27}	F13	4.32×10^{-31}	F22	8.91×10^{-31}	F31	1.42×10^{-26}
F5	3.99×10^{-32}	F14	3.49×10^{-31}	F23	4.47×10^{-33}	F32	1.95×10^{-29}
F6	4.21×10^{-31}	F15	2.67×10^{-29}	F24	5.31×10^{-32}	F33	1.15×10^{-29}
F7	3.79×10^{-27}	F16	1.25×10^{-32}	F25	1.98×10^{-32}	F34	8.84×10^{-30}
F8	9.44×10^{-31}	F17	2.56×10^{-30}	F26	1.56×10^{-27}		
F9	2.93×10^{-27}	F18	7.81×10^{-31}	F27	2.60×10^{-29}		

Table 8.7: The p -values of all features extracted from S2 data.

Feature	p -value						
F1	4.98×10^{-31}	F7	9.51×10^{-33}	F13	2.25×10^{-34}	F19	2.66×10^{-32}
F2	8.01×10^{-33}	F8	1.06×10^{-32}	F14	2.10×10^{-32}	F20	8.59×10^{-32}
F3	2.41×10^{-33}	F9	7.44×10^{-32}	F15	1.37×10^{-33}	F21	3.42×10^{-32}
F4	2.77×10^{-34}	F10	8.31×10^{-30}	F16	1.09×10^{-32}	F22	6.83×10^{-31}
F5	8.43×10^{-33}	F11	6.33×10^{-33}	F17	4.80×10^{-33}	F23	9.70×10^{-33}
F6	3.52×10^{-33}	F12	1.02×10^{-32}	F18	7.25×10^{-33}	F24	3.39×10^{-33}

The confusion matrix obtained for highest ACC as mentioned in Table 8.5 for each subject is shown in Table 8.11 to Table 8.15.

The performance of proposed method is compared with the other existing methods using the basic hand movements database (Sapsanis et al, 2013b), is shown in Table 8.16. From Table 8.16, it can be noted that the obtained average ACC(%) is better than the average ACC(%) reported by other existing methods. Also, the obtained ACC(%) for each subject is better than most of the other existing methods.

Table 8.8: The p -values of all features extracted from S3 data.

Feature	p -value						
F1	9.84×10^{-33}	F8	6.96×10^{-33}	F15	8.19×10^{-33}	F22	2.20×10^{-31}
F2	5.14×10^{-18}	F9	2.88×10^{-34}	F16	6.80×10^{-33}	F23	1.04×10^{-32}
F3	1.75×10^{-34}	F10	5.86×10^{-33}	F17	2.54×10^{-34}	F24	2.83×10^{-32}
F4	3.75×10^{-34}	F11	1.80×10^{-34}	F18	3.10×10^{-34}	F25	1.14×10^{-32}
F5	1.86×10^{-18}	F12	8.40×10^{-33}	F19	7.35×10^{-34}	F26	5.46×10^{-33}
F6	3.59×10^{-29}	F13	9.49×10^{-33}	F20	1.42×10^{-34}	F27	4.82×10^{-33}
F7	2.03×10^{-32}	F14	1.23×10^{-34}	F21	4.47×10^{-33}	F28	5.73×10^{-28}

Table 8.9: The p -values of all features extracted from S4 data.

Feature	p -value						
F1	2.71×10^{-25}	F32	1.86×10^{-34}	F63	3.82×10^{-29}	F94	2.33×10^{-27}
F2	3.34×10^{-29}	F33	3.97×10^{-34}	F64	3.61×10^{-19}	F95	5.22×10^{-28}
F3	1.07×10^{-27}	F34	3.05×10^{-29}	F65	5.70×10^{-27}	F96	1.39×10^{-33}
F4	4.92×10^{-27}	F35	2.07×10^{-32}	F66	2.90×10^{-30}	F97	2.84×10^{-27}
F5	7.00×10^{-27}	F36	1.58×10^{-33}	F67	2.52×10^{-32}	F98	1.54×10^{-28}
F6	9.94×10^{-29}	F37	3.39×10^{-30}	F68	3.24×10^{-30}	F99	6.39×10^{-29}
F7	1.08×10^{-28}	F38	3.95×10^{-33}	F69	4.38×10^{-21}	F100	2.10×10^{-28}
F8	3.60×10^{-28}	F39	1.05×10^{-33}	F70	7.68×10^{-28}	F101	9.23×10^{-29}
F9	8.65×10^{-28}	F40	8.84×10^{-29}	F71	2.70×10^{-27}	F102	3.07×10^{-27}
F10	2.31×10^{-28}	F41	2.92×10^{-33}	F72	4.50×10^{-28}	F103	5.17×10^{-34}
F11	2.30×10^{-27}	F42	6.38×10^{-27}	F73	1.00×10^{-27}	F104	1.16×10^{-34}
F12	3.33×10^{-29}	F43	3.22×10^{-32}	F74	4.98×10^{-29}	F105	3.33×10^{-32}
F13	6.31×10^{-33}	F44	1.24×10^{-32}	F75	1.57×10^{-33}	F106	7.84×10^{-27}
F14	4.50×10^{-34}	F45	5.61×10^{-33}	F76	1.74×10^{-33}	F107	2.38×10^{-34}
F15	1.53×10^{-22}	F46	5.63×10^{-31}	F77	3.81×10^{-33}	F108	2.34×10^{-28}
F16	1.19×10^{-27}	F47	2.10×10^{-33}	F78	1.08×10^{-27}	F109	3.17×10^{-25}
F17	3.07×10^{-27}	F48	4.11×10^{-27}	F79	2.57×10^{-28}	F110	2.29×10^{-29}
F18	9.81×10^{-33}	F49	5.99×10^{-27}	F80	2.92×10^{-28}	F111	1.49×10^{-32}
F19	1.05×10^{-27}	F50	2.34×10^{-27}	F81	1.96×10^{-33}	F112	1.47×10^{-32}
F20	3.18×10^{-27}	F51	5.73×10^{-30}	F82	1.13×10^{-34}	F113	6.69×10^{-31}
F21	6.00×10^{-29}	F52	2.38×10^{-31}	F83	7.34×10^{-33}	F114	1.71×10^{-31}
F22	5.15×10^{-25}	F53	2.02×10^{-32}	F84	1.28×10^{-33}	F115	1.53×10^{-32}
F23	5.15×10^{-25}	F54	1.47×10^{-33}	F85	1.67×10^{-34}	F116	6.59×10^{-32}
F24	3.99×10^{-28}	F55	1.38×10^{-33}	F86	1.24×10^{-26}	F117	2.02×10^{-33}
F25	3.39×10^{-24}	F56	5.10×10^{-28}	F87	4.24×10^{-29}	F118	1.28×10^{-27}
F26	2.75×10^{-28}	F57	6.18×10^{-33}	F88	1.66×10^{-34}	F119	1.35×10^{-33}
F27	5.82×10^{-34}	F58	9.93×10^{-34}	F89	2.07×10^{-22}	F120	1.54×10^{-32}
F28	5.82×10^{-34}	F59	9.96×10^{-29}	F90	8.56×10^{-33}	F121	2.27×10^{-28}
F29	4.83×10^{-27}	F60	1.58×10^{-32}	F91	7.89×10^{-28}		
F30	1.95×10^{-34}	F61	2.13×10^{-32}	F92	4.71×10^{-32}		
F31	1.11×10^{-27}	F62	1.06×10^{-29}	F93	1.15×10^{-27}		

Table 8.10: The p -values of all features extracted from S5 data.

Feature	p -value						
F1	2.68×10^{-30}	F21	6.02×10^{-30}	F41	2.58×10^{-30}	F61	1.19×10^{-28}
F2	1.21×10^{-30}	F22	4.31×10^{-30}	F42	1.83×10^{-21}	F62	2.18×10^{-29}
F3	1.64×10^{-23}	F23	1.90×10^{-30}	F43	1.79×10^{-30}	F63	2.18×10^{-29}
F4	3.39×10^{-25}	F24	5.38×10^{-30}	F44	1.27×10^{-29}	F64	8.07×10^{-30}
F5	2.24×10^{-28}	F25	3.78×10^{-24}	F45	1.15×10^{-29}	F65	1.43×10^{-29}
F6	2.63×10^{-28}	F26	4.93×10^{-22}	F46	2.09×10^{-28}	F66	2.02×10^{-25}
F7	2.15×10^{-29}	F27	8.58×10^{-28}	F47	9.68×10^{-24}	F67	1.19×10^{-29}
F8	3.12×10^{-23}	F28	2.06×10^{-23}	F48	2.30×10^{-29}	F68	2.73×10^{-32}
F9	4.10×10^{-29}	F29	2.36×10^{-22}	F49	1.45×10^{-29}	F69	5.33×10^{-29}
F10	8.33×10^{-31}	F30	1.36×10^{-20}	F50	3.22×10^{-26}	F70	2.92×10^{-29}
F11	9.30×10^{-21}	F31	5.79×10^{-29}	F51	1.89×10^{-25}	F71	2.13×10^{-29}
F12	3.47×10^{-30}	F32	1.97×10^{-25}	F52	2.48×10^{-28}	F72	1.55×10^{-27}
F13	7.55×10^{-21}	F33	5.01×10^{-28}	F53	1.22×10^{-21}	F73	2.30×10^{-28}
F14	1.28×10^{-24}	F34	6.85×10^{-29}	F54	6.41×10^{-30}	F74	1.77×10^{-24}
F15	1.65×10^{-20}	F35	7.62×10^{-29}	F55	1.27×10^{-31}	F75	1.85×10^{-29}
F16	2.25×10^{-24}	F36	2.19×10^{-30}	F56	2.24×10^{-28}	F76	9.15×10^{-27}
F17	2.20×10^{-23}	F37	1.50×10^{-30}	F57	6.82×10^{-28}	F77	5.22×10^{-29}
F18	2.96×10^{-22}	F38	8.46×10^{-30}	F58	2.05×10^{-30}	F78	2.92×10^{-30}
F19	1.49×10^{-30}	F39	3.42×10^{-28}	F59	1.77×10^{-23}	F79	6.17×10^{-23}
F20	4.43×10^{-28}	F40	1.25×10^{-24}	F60	1.11×10^{-29}		

Table 8.11: Confusion matrix obtained for the proposed method using S1 data.

		Predicted					
		CY	HO	LA	PA	SP	TI
Actual	CY	29	1	0	0	0	0
	HO	0	30	0	0	0	0
	LA	0	0	29	1	0	0
	PA	0	0	1	29	0	0
	SP	0	0	0	0	30	0
	TI	0	0	0	0	0	30

Table 8.12: Confusion matrix obtained for the proposed method using S2 data.

		Predicted					
		CY	HO	LA	PA	SP	TI
Actual	CY	30	0	0	0	0	0
	HO	0	30	0	0	0	0
	LA	0	0	29	0	0	1
	PA	0	0	0	30	0	0
	SP	0	0	0	0	30	0
	TI	0	0	1	2	0	27

Table 8.13: Confusion matrix obtained for the proposed method using S3 data.

		Predicted					
		CY	HO	LA	PA	SP	TI
Actual	CY	30	0	0	0	0	0
	HO	0	30	0	0	0	0
	LA	0	0	29	1	0	0
	PA	0	0	0	30	0	0
	SP	0	0	0	0	30	0
	TI	0	0	0	0	0	30

Table 8.14: Confusion matrix obtained for the proposed method using S4 data.

		Predicted					
		CY	HO	LA	PA	SP	TI
Actual	CY	30	0	0	0	0	0
	HO	0	30	0	0	0	0
	LA	0	0	30	0	0	0
	PA	0	0	1	29	0	0
	SP	0	0	0	0	30	0
	TI	0	0	1	0	0	29

Table 8.15: Confusion matrix obtained for the proposed method using S5 data.

		Predicted					
		CY	HO	LA	PA	SP	TI
Actual	CY	30	0	0	0	0	0
	HO	0	30	0	0	0	0
	LA	0	1	29	0	0	0
	PA	0	0	0	30	0	0
	SP	0	0	0	0	30	0
	TI	0	0	0	2	0	28

Table 8.16: Comparison of proposed method based on ACC(%) with other existing methods using the basic hand movements database (Sapsanis et al, 2013b).

	(Sapsanis et al, 2013b)	(Ruangpaisarn and Jaiy, 2015)	(Akben, 2017)	(Iqbal et al, 2017)	Proposed method
Subject	ACC(%)	ACC(%)	ACC(%)	ACC(%)	ACC(%)
S1	87.25	96.67	93.04	82.78	98.33
S2	88.05	98.89	86.66	87.67	97.78
S3	85.53	96.67	97	83.11	99.44
S4	90.42	98.89	99.23	90	98.89
S5	94.80	100	97.66	90	98.33
Average ACC(%)	89.21	98.22	94.72	86.71	98.55

8.6 Discussion

The proposed method shows the application of TQWT-FB for the classification of basic hand movements using sEMG signals. The TQWT-FB decomposes csEMG signals into number of constant BW sub-band signals and then KREs features are computed from these sub-band signals. Then features are ranked and finally classifier classifies the basic hand movements. Here, three types of feature ranking (LLCFS, MCFS, and RELIEEFF) methods and three types of classifiers (C4.5, SMO, and k -NN) are used. Through simulations, we conclude that the RELIEEFF algorithm and k -NN classifier performs the best. The proposed method has been tested using sEMG data acquired from five subjects. The ACC is used to evaluate the performance of the proposed method. The ACC is computed for each subject individually and then average ACC of 98.55% is achieved by our proposed method.

During the recording of sEMG signals from subjects, the applied force and speed to perform hand movement tasks are left on the subject’s own will. Therefore, the obtained optimum value of k_f , k_r , and k_c to obtain maximum ACC, are different

for each subject. Also there is difference in NORF, statistical parameters (mean and SD) in each case. In the case of S1, the minimum value of k_f and k_r to achieve maximum ACC is 1 and 3 respectively. From the Fig. 8.7, it can be observed that the features of CY, HO, and SP hand movements are mostly separable from the features of LA, PA, and TI hand movements. The Table 8.11 shows the confusion matrix generated during the classification of hand movements for S1 data. The actual hand movements are shown in the second left column and predicted hand movements by the classifier are mentioned in the second row. It can be observed that all HO, SP, and TI hand movements are predicted correctly by our proposed method. On the other hand, one CY is misclassified as HO, one LA is misclassified as PA, and one PA is misclassified as LA by the classifier. Hence, obtained ACC = 98.33% in this case.

When the data from S2 is considered in the proposed method, the minimum value of k_f and k_r required to get maximum ACC is 1 and 3 respectively. The Fig. 8.8 shows the statistical analysis of proposed method when S2 data is considered. It can be observed from this figure that the features are not well separated in this case. However, generally the features corresponding to SP hand movements have highest values and features corresponding to LA hand movements have lowest value as compared to other features. From Table 8.12, it can be noted that the TI hand movement is classified with least ACC. Once it is classified as LA and twice it is classified as PA. Also the LA has been misclassified as TI once. The number of misclassification is more in this case as there is less separation between the features. Hence, the obtained ACC = 97.77% for S2 data.

We have obtained the best performance for S3 data. The proposed method achieved ACC = 99.44% with minimum value of k_f and k_r set to one. The statistical analysis of computed ranked features is shown in Fig. 8.9. In few cases, features corresponding to CY, HO, SP, and TI are clearly separable. Also from Table 8.13, it can be observed that only LA is misclassified as PA once. Therefore, the obtained ACC is more than 99% in this case. Using data of S4 subject, we have achieved

ACC = 98.89% for minimum k_f and k_r equal to one and three respectively. The features corresponding to HO, are clearly separable from other features for most of the cases as shown in Fig. 8.10. The range of values of other features are mostly overlapping. In this case, both PA and TI are misclassified as LA once. Hence, the obtained ACC is close to 99%.

The statistical analysis of ranked features obtained for S5 data is shown in Fig. 8.11. These features are obtained using $k_f = 1$ and ranked using $k_r = 2$. Generally, the features corresponding to SP hand movement are clearly separable from other features. The LA is misclassified as HO once and TI is misclassified as PA twice as shown in Table 8.15. The obtained ACC = 98.33% in this case. The Kruskal-Wallis test (McKight and Najab, 2010) has been used to compute p -value of ranked features as shown in Fig. 8.7 to Fig. 8.11. The Kruskal-Wallis test has also been used in (Bhati et al, 2017b; Pachori, 2008; Sharma and Pachori, 2015) to quantify the features. The p -values are less than 0.0001 for all features of all subjects which shows the statistical significance of features. This can be observed in Table 8.6 to Table 8.10.

It can be noted from Table 8.1 to Table 8.4 that the variation in the values of k_f and k_r affects the ACC. It can be observed from Table 8.4, that the maximum ACC can be achieved as the value of k_f increases. Except for S3 data, high value of k_r also produces the best ACC. The performance of the proposed method in terms of ACC is compared with other existing methods and is shown in Table 8.16. The abbreviation used to represent subjects are different in methods compared in Table 8.16. In methods (Sapsanis et al, 2013b), (Iqbal et al, 2017), and proposed method, the S1, S2, S3, S4, and S5 in Table 8.16, represent subjects female 1, female 2, female 3, male 1, and male 2 respectively, from database (Sapsanis et al, 2013b). In case of method proposed by (Ruangpaisarn and Jaiy, 2015), the subjects of database in (Sapsanis et al, 2013b) are represented by abbreviations S1, S2, S3, S4, and S5. Whereas in case of methodology proposed by (Akben, 2017), the S1, S2, S3, S4, and S5 in Table 8.16, represents Subject 1, Subject 2, Subject 3, Subject 4, and Subject

5 respectively. The obtained ACC by proposed method is above 97.5% in each case and in the case of (Ruangpaisarn and Jaiy, 2015), the minimum obtained ACC is 96.67% for S1 and S2. The method proposed in (Sapsanis et al, 2013b) and (Iqbal et al, 2017) did not obtain the ACC more than 95% in any case. However, the obtained average ACC by the proposed method is 98.55% which is better than the other existing methods.

The proposed model can be implemented using IOT technique to improve the quality of life of the hand amputee subjects. As shown in Fig. 8.12, the developed trained model is kept in the cloud. The same trained model is also kept in the hardware connected to EPH. When amputee subject wants to perform a hand movement task, the sEMG signals from the pair of electrodes are sent to the hardware and web server simultaneously. The trained model in the hardware will diagnose the class of sEMG signals and accordingly EPH would perform hand movement task instantly. The sEMG signals are also sent to the server in the cloud. The class of this incoming test sEMG data will be determined by trained model in the cloud and then it will be stored in the cloud. This stored sEMG data in the cloud can be used to train the model and as a result the performance of the model is continuously improved. The proposed model yields best result with k -NN classifier which suits the model implemented in IOT technique. The k -NN classifier classifies the class of a sample based on its k -NNs. Practically, In a long time span, a hand amputee person would perform a particular hand movement with almost same force and speed. Therefore the location of samples corresponding to a particular hand movement will be close to each other in the space. Similarly, location of samples corresponding to the other hand movement will be close to each other at some other location. Hence, when a new hand movement is performed by the amputee person, then its corresponding sample is most likely to be located near to the other samples of same hand movement. This can be observed from Fig. 8.7 to Fig. 8.11, where the SD of features is usually low. Thus it suggest that the feature of a particular hand movement is concentrated about their mean. Then most likely, the k -NN classifier can easily

identify the correct class of this new test sample. The k -NN classifier is simple and easy to implement.

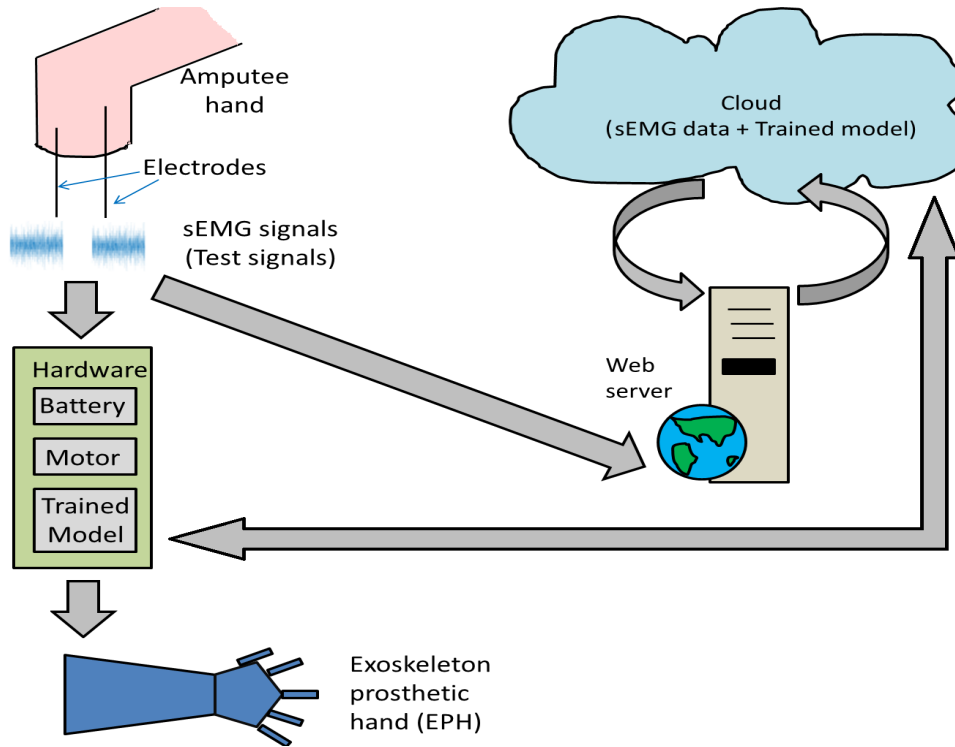


Figure 8.12: Illustration of web-based application of the proposed model using IOT.

8.7 Summary

A novel method to classify the basic hand movements using TQWT-FB with sEMG signals is presented in this chapter. The TQWT-FB decomposes csEMG signals into the set of sub-band signals and then KRE features are extracted. The proposed method obtained the average ACC of 98.55% when tested using five subjects. The proposed method used sEMG signals recorded from two electrodes. Hence the proposed method is suitable to design low cost EPH and comfortable to use. The obtained maximum ACC for each subject depends on k_f , k_r , k_c , and NORF. For large value of k_f and k_r , maximum ACC can be achieved. The computed p -value of all features in each case is less than 0.0001.

Chapter 9

Conclusion and future work

9.1 Conclusion

The analysis of non-stationary signals can be performed using TQWT-FB. The TQWT-FB consist of narrow BW sub-bands which can be spanned over entire frequency range of signal. The sub-bands of TQWT-FB are generated corresponding to different value of Q -factors which results in generation of different mother wavelets for the analysis of signal. Unlike TQWT, there is no requirement of tuning the Q -factor according to oscillatory nature of signal. The TQWT-FB can analyse signals with different oscillatory behaviours.

The TQWT-FB is applied for the reduction of cross-terms in the WVD. The cross-terms appears in the WVD due to its quadratic nature. To reduce cross-terms, the multi-component or non-linear FM non-stationary signal is decomposed into sub-band signals by TQWT-FB. Then components existing at different time interval in a sub-band signal are separated by TDS section. Then the WVD of the segmented component are computed in order to obtain cross-terms free WVD. The normalized Renyi entropy as performance measure proves the efficacy of proposed method.

Since TQWT-FB is able to decompose signal into narrow and constant BW sub-band signals, its usefulness is shown in the estimation of IFF of speech signals.

The TQWT-FB decomposes speech signal into several sub-band signal due to which FFC of speech signal also decomposes into sub-band signal. After components segmentation by TDS section, the SFFC extraction unit generates FFC with scaled amplitude. The Hilbert transform is applied on SFFC in order to obtain IFF of speech signal. Low value of GE(%) in clean as well as noisy conditions shows that the proposed method is good in estimating IFF.

The application of TQWT-FB is also shown in developing the computer-aided automatic diagnosis system. Such system is helpful to doctors or experts who spend lot of time in analysing the physiological signals to detect the disease. One such application is shown in screening of sleep apnea. The two-class classification problem is address in which apneic and non-apneic events in ECG signals are classified. In the proposed method, the segment of ECG signal is decomposed by TQWT-FB. Then the CCE features are computed from decomposed sub-band signal and ranked using students t-test. Then in final stage RF classifier produces the most accurate result.

Similarly TQWT-FB is applied in the classification of epileptic EEG signals for diagnosis. The classification of seizure, seizure-free, and normal EEG signals (three-class classification) is performed by decomposition EEG signals by TQWT-FB. The sub-band signals produced are then used in the computation of CIP features. The computed features are then ranked using RELIEFF algorithm and RF classifier classifies the EEG signals. The ACC obtained by proposed method is higher than other existing methods.

Another problem related to focal epilepsy is addressed in which classification of focal and non-focal EEG signals (two-class classification) is performed. The sub-band signals obtained by TQWT-FB after decomposing EEG signals are used in computation of MCE features. Then, various ranking methods are applied and ranked features are fed to LS-SVM classifier. The obtained ACC is this problem is better than compared methods.

The TQWT-FB is applied in the designing of controller of EPH. The EPH is

used by hand amputee person for performing basic hand movements. The proposed method classifies six basic hand movements. First the csEMG signal is obtained by computing cross-covariance of sEMG signals obtained from two electrodes. Then the designed TQWT-FB decomposed csEMG signal into very narrow BW sub-band signals. In the next stage, the KRE features are computed from these sub-band signals. The KRE features are then ranked and classified by various method. Through simulation, it is found that the RELIEFF method and k -NN classifier produces the best result in classification when proposed method is tested on the data of five subjects.

9.2 Future work

The proposed TQWT-FB has been applied for the analysis of non-stationary signals. There are two methods proposed for the designing of TQWT-FB as mentioned in Section 2.2. However, proper comparison of TQWT-FBs designed by different methods can be done in future. This includes the effect of sub-band selection, number of TQWT blocks used in constructing TQWT-FB, etc. Also the comparison of proposed TQWT-FB with TQWT can be done in future.

In the cross-terms reduction in WVD using TQWT-FB, the chosen components are either separated in frequency-domain or in T-F domain. In future, the proposed methodology can be modified for the WVD based T-F representation of multicomponent non-stationary signals, whose components are overlapped in T-F domain. The modification is needed as the proposed method is not effective when more than one component lies in a sub-band. Also proposed method is tested only when signals are corrupted by AWGN at different SNRs. Therefore, in future, we intended to test our proposed method in coloured noise and also in negative SNRs. Also, we intend to do comparison of proposed method in terms of Rényi with ideal T-F representation and WVD of signal in future. The proposed TDS section is energy based segmentation method. In future, it can be made noise robust by adding entropy

information.

The TQWT-FB used for cross-terms reduction in WVD is developed by method I as suggested in Section 2.2. The aim here is to reduce cross-terms from WVD and therefore the BW of sub-bands must be such that more than one component of multi-component non-stationary signal must not lie in same sub-band at a particular time instant. Therefore, the BW of sub-bands in TQWT-FB designed using method I is kept narrow. Here, the choice of sub-bands in designing TQWT-FB is random. In future, the effect of different number of sub-bands on proposed method can be tested along with the robustness of proposed method to such changes. In addition to this, the future work also include the testing of proposed method when TQWT-FB designed using method II as presented in Section 2.2 is applied.

The TQWT-FB is also applied for estimating the IFF of speech signals. The proposed method is tested on speech signals of two male and female speakers available from CMU Arctic database. In future, the proposed method can be tested on more speech signals and other databases. Also, the optimal value of TH and F_{TH} can be determine from various speech signals in order to implement proposed method and test its efficacy. The analysis is performed under AWGN. Therefore, some other noise such as babble can be used to evaluate the performance of proposed method. In future, the sparse coefficients obtained from proposed TQWT-FB can be compared with sparse coefficients when speech is decomposed by TQWT.

The developed TQWT-FB is also employed in classification of physiological signals for constructing computer-aided diagnosis system. The structure of proposed methods for classification problems involve signal decomposition by TQWT-FB, feature computation and ranking, and classifier. The features in classification problems are different since there is no direct relationship between choice of feature and classification problem is given in literature. Therefore, the deep learning techniques can be applied in future for such classification problems. The deep learning is an emerging technique which automatically learns the good features from the input data. Also, the real world data do not have class labeled on it, hence deep learning

is useful in such applications where features could learn in an unsupervised way. In addition, the proposed method can be tested on huge database for validation. The proposed method has been applied for the screening of sleep apnea from single lead ECG signals. In future, the apnea-hypopnea index can also be taken into account for screening of apnea syndrome. Also, the proposed TQWT-FB can also be applied for the diagnosis of other disease such as Alzheimer, insomnia, narcolepsy, sleep walking, and hypersomnia etc.

Bibliography

- Accardo A, Affinito M, Carrozzi M, Bouquet F (1997) Use of the fractal dimension for the analysis of electroencephalographic time series. *Biological Cybernetics* 77:339–350
- Acharya UR, Molinari F, Sree SV, Chattopadhyay S, Ng KH, Suri JS (2012) Automated diagnosis of epileptic EEG using entropies. *Biomedical Signal Processing and Control* 7:401–408
- Acharya UR, Sree SV, Swapna G, Martis RJ, Suri JS (2013a) Automated EEG analysis of epilepsy: A review. *Knowledge-Based Systems* 45:147 – 165
- Acharya UR, Yanti R, Zheng JW, Krishnan MMR, Tan JH, Martis RJ, Lim CM (2013b) Automated diagnosis of epilepsy using CWT, HOS and texture parameters. *International Journal of Neural Systems* 23:1350009
- Acharya UR, Hagiwara Y, Deshpande SN, Suren S, Koh JEW, Oh SL, Arunkumar N, Ciaccio EJ, Lim CM (2019) Characterization of focal EEG signals: A review. *Future Generation Computer Systems* 91:290–299
- Acharya UR, Chua CK, Lim TC, Dorothy, Suri JS (2009) Automatic identification of epileptic EEG signals using nonlinear parameters. *Journal of Mechanics in Medicine and Biology* 9:539–553
- Acharya UR, Chua EC, Faust O, Lim TC, Lim LFB (2011a) Automated detection of sleep apnea from electrocardiogram signals using nonlinear parameters. *Physiological Measurement* 32:287–303

- Acharya UR, Dua S, Du X, Sree SV, Chua CK (2011b) Automated diagnosis of glaucoma using texture and higher order spectra features. *IEEE Transactions on Information Technology in Biomedicine* 15:449–455
- Acharya UR, Sree SV, Chattopadhyay S, Yu W, Ang PCA (2011c) Application of recurrence quantification analysis for the automated identification of epileptic EEG signals. *International Journal of Neural Systems* 21:199–211
- Acharya UR, Sree SV, Suri JS (2011d) Automatic detection of epileptic EEG signals using higher order cumulant features. *International Journal of Neural Systems* 21:403–414
- Acharya UR, Ng EYK, Eugene LWJ, Noronha KP, Min LC, Nayak KP, Bhandary SV (2015a) Decision support system for the glaucoma using Gabor transformation. *Biomedical Signal Processing and Control* 15:18–26
- Acharya UR, Vidya KS, Ghista DN, Lim WJE, Molinari F, Sankaranarayanan M (2015b) Computer aided diagnosis of diabetic subjects by heart rate variability signals using discrete wavelet transform method. *Knowledge-Based Systems* 81:56–64
- Adeli H, Zhou Z, Dadmehr N (2003) Analysis of EEG records in an epileptic patient using wavelet transform. *Journal of Neuroscience Methods* 123:69–87
- Adeli H, Ghosh-Dastidar S, Dadmehr N (2007) A wavelet-chaos methodology for analysis of EEGs and EEG subbands to detect seizure and epilepsy. *IEEE Transactions on Biomedical Engineering* 54:205–211
- Afkhami RG, Azarnia G, Tinati MA (2016) Cardiac arrhythmia classification using statistical and mixture modeling features of ECG signals. *Pattern Recognition Letters* 70:45–51
- Aha DW, Kibler D, Albert MK (1991) Instance-based learning algorithms. *Machine Learning* 6:37–66

- Akben SB (2017) Low-cost and easy-to-use grasp classification, using a simple 2-channel surface electromyography (sEMG). *Biomedical Research* 28:577–582
- American Academy of Sleep Medicine Task Force (1999) Sleep-related breathing disorders in adults: Recommendations for syndrome definition and measurement techniques in clinical research. *Sleep* 22:667–689
- Amirmazlaghani M, Amindavar H (2013) Statistical modeling and denoising Wigner-Ville distribution. *Digital Signal Processing* 23:506–513
- Andrianesis K, Tzes A (2008) Design of an anthropomorphic prosthetic hand driven by shape memory alloy actuators. In: *Proceedings of 2nd IEEE RAS and EMBS International Conference on Biomedical Robotics and Biomechatronics*, pp 517–522
- Andrzejak RG, Schindler K, Rummel C (2012) Nonrandomness, nonlinear dependence, and nonstationarity of electroencephalographic recordings from epilepsy patients. *Physical Review E* 86:046206
- Andrzejak RG, Lehnertz K, Mormann F, Rieke C, David P, Elger CE (2001) Indications of nonlinear deterministic and finite-dimensional structures in time series of brain electrical activity: dependence on recording region and brain state. *Physical Review* 64:061907
- Arce GR, Hasan SR (2000) Elimination of interference terms of the discrete Wigner distribution using nonlinear filtering. *IEEE Transactions on Signal Processing* 48:2321–2331
- Arqub OA (2017) Adaptation of reproducing kernel algorithm for solving fuzzy Fredholm-Volterra integrodifferential equations. *Neural Computing and Applications* 28:1591–1610
- Arqub OA, Abo-Hammour Z (2014) Numerical solution of systems of second-order boundary value problems using continuous genetic algorithm. *Information Sciences* 279:396–415

- Auger F, Flandrin P, Goncalves P, Lemoine O (1996) Time-frequency toolbox. CNRS-Rice University
- Azar AT, El-Said SA (2014) Performance analysis of support vector machines classifiers in breast cancer mammography recognition. *Neural Computing and Applications* 24:1163–1177
- Azarbarzin A, Moussavi Z (2013) Snoring sounds variability as a signature of obstructive sleep apnea. *Medical Engineering & Physics* 35:479–485
- Bajaj V, Pachori RB (2012) Classification of seizure and nonseizure EEG signals using empirical mode decomposition. *IEEE Transactions on Information Technology in Biomedicine* 16:1135–1142
- Baraniuk R (2009) Bat echolocation chirp. <http://dsp.rice.edu/software/TFA/RGK/BAT/batsig.bin.Z/>
- Baraniuk RG, Jones DL (1993) A signal-dependent time-frequency representation: Optimal kernel design. *IEEE Transactions on Signal Processing* 41:1589–1602
- Barkat B (2001) Instantaneous frequency estimation of nonlinear frequency-modulated signals in the presence of multiplicative and additive noise. *IEEE Transactions on Signal Processing* 49:2214–2222
- Bayram I (2013) An analytic wavelet transform with a flexible time-frequency covering. *IEEE Transactions on Signal Processing* 61:1131–1142
- Berger H (1929) Uber das elektroencephalogramm des menschen. *Arch Psychiatr Nervenkr* 87:527–570
- Bhati D, Pachori RB, Gadre VM (2017a) A novel approach for time-frequency localization of scaling functions and design of three-band biorthogonal linear phase wavelet filter banks. *Digital Signal Processing* 69:309–322
- Bhati D, Sharma M, Pachori RB, Gadre VM (2017b) Time-frequency localized three-band biorthogonal wavelet filter bank using semidefinite relaxation and nonlinear

least squares with epileptic seizure EEG signal classification. *Digital Signal Processing* 62:259–273

Bhattacharyya A, Sharma M, Pachori RB, Sircar P, Acharya UR (2018) A novel approach for automated detection of focal EEG signals using empirical wavelet transform. *Neural Computing and Applications* 29:47–57

Bhattacharyya A, Pachori RB, Acharya UR (2017a) Tunable-Q wavelet transform based multivariate sub-band fuzzy entropy with application to focal EEG signal analysis. *Entropy* 19:99

Bhattacharyya A, Pachori RB, Upadhyay A, Acharya UR (2017b) Tunable-Q wavelet transform based multiscale entropy measure for automated classification of epileptic EEG signals. *Applied Sciences* 7:385

Boashash B (2003) *Time-Frequency Signal Analysis and Processing: A Comprehensive Reference*. Elsevier

Boashash B, Mesbah M, Colditz P (2003) *Time–frequency detection of EEG abnormalities*. Elsevier

Boersma P (1993) Accurate short-term analysis of the fundamental frequency and the harmonics-to-noise ratio of a sampled sound. In: *Proceedings of The Institute of Phonetic Sciences*, pp 97–110

Boersma P, Weenink D (2013) Praat: Doing phonetics by computer [computer program]. <http://www.praat.org/>

Boujelbene SZ, Mezghani DBA, Ellouze N (2008) Vowel phoneme classification using SMO algorithm for training support vector machines. In: *Proceedings of 3rd International Conference on Information and Communication Technologies: From Theory to Applications*, pp 1–5

Box JF (1987) Guinness, Gosset, Fisher, and small samples. *Statistical Science* 2:45–52

- Breiman L (1996) Bagging predictors. *Machine Learning* 24:123–140
- Breiman L (2001) Random Forests. *Machine Learning* 45:5–32
- Broek EL, Spitters M (2013) Physiological signals: The next generation authentication and identification methods!? In: *Proceeding of European Intelligence and Security Informatics Conference (EISIC)*, pp 159–162
- Cai D, Zhang C, He X (2010) Unsupervised feature selection for multi-cluster data. In: *Proceedings of the 16th ACM SIGKDD international conference on Knowledge discovery and data mining*, pp 333–342
- Carroll D, Alwarappan S (2012) Recent Advances in Biosensors and Biosensing Protocols. *Journal of Biosensors and Bioelectronics*
- Caton R (1875) The electric currents of brain. *British Medical Journal* 2:278
- Chen B, Wang X, Lu N, Wang S, Cao J, Qin J (2018) Mixture correntropy for robust learning. *Pattern Recognition* 79:318 – 327
- Chen G (2014) Automatic EEG seizure detection using dual-tree complex wavelet-Fourier features. *Expert Systems with Applications* 41:2391–2394
- Chen L, Zhang X, Song C (2015a) An automatic screening approach for obstructive sleep apnea diagnosis based on single-lead electrocardiogram. *IEEE Transactions on Automation Science and Engineering* 12:106–115
- Chen L, Zhang X, Wang H (2015b) An obstructive sleep apnea detection approach using kernel density classification based on single-lead electrocardiogram. *Journal of Medical Systems* 39:47
- Choi HI, Williams WJ (1989) Improved time-frequency representation of multicomponent signals using exponential kernels. *IEEE Transactions on Acoustics, Speech and Signal Processing* 37:862–871

- Claassen TACM, Mecklenbrauker WFG (1980) The Wigner distribution-A tool for time-frequency signal analysis. Part I: Continuous-time signals. *Philips Journal of Research* 35:217–250
- Cohen I, Raz S, Malah D (1999) Adaptive suppression of Wigner interference-terms using shift-invariant wavelet packet decompositions. *Signal Processing* 73:203–223
- Cohen L (1966) Generalized phase-space distribution functions. *Journal of Mathematical Physics* 7:781–786
- Cohen L (1995) *Time-frequency analysis*. Ed Englewood Cliffs, NJ: Prentice Hall
- Dalal M, Tanveer M, Pachori RB (2019) Automated identification system for focal EEG signals using fractal dimension of FAWT-based sub-bands signals. In: *Proceedings of Machine Intelligence and Signal Analysis*, pp 583–596
- Das AB, Bhuiyan MIH (2016) Discrimination and classification of focal and non-focal EEG signals using entropy-based features in the EMD-DWT domain. *Biomedical Signal Processing and Control* 29:11–21
- Daubechies I (1992) *Ten Lectures on Wavelets*. Society for Industrial and Applied Mathematics
- Daubechies I, Lu J, Wu HT (2011) Synchrosqueezed wavelet transforms: an empirical mode decomposition-like tool. *Applied and Computational Harmonic Analysis* 30:243–261
- Deller JR, Hansen JHL, Proakis JG (2011) *Discrete-Time Processing of Speech Signals*. Wiley-India
- DeWayne RD, Sue BS, Conover WJ (2010) Teaching rank-based tests by emphasizing structural similarities to corresponding parametric tests. *Journal of Statistics Education* 18
- Dragomiretskiy K, Zosso D (2014) Variational mode decomposition. *IEEE Transactions on Signal Processing* 62:531–544

- Farid DM, Zhang L, Rahman CM, Hossain MA, Strachan R (2014) Hybrid decision tree and naive Bayes classifiers for multi-class classification tasks. *Expert Systems with Applications* 41:1937–1946
- Faust O, Acharya UR, Ng EYK, Fujita H (2016) A review of ECG-Based diagnosis support systems for obstructive sleep apnea. *Journal of Mechanics in Medicine and Biology* 16:1640004
- Finneran A, O’Sullivan L (2013) Effects of grip type and wrist posture on forearm EMG activity, endurance time and movement accuracy. *International Journal of Industrial Ergonomics* 43:91–99
- Fisher RS, Boas WVE, Blume W, Elger C, Genton P, Lee P, Engel J (2005) Epileptic seizures and epilepsy: definitions proposed by the international league against epilepsy (ILAE) and the international bureau for epilepsy (IBE). *Epilepsia* 46:470–472
- Flandrin P, Borgnat P (2010) Time-frequency energy distributions meet compressed sensing. *IEEE Transactions on Signal Processing* 58:2974–2982
- Flandrin P, Baraniuk RG, Michel O (1994) Time-frequency complexity and information. In: *Proceedings of ICASSP ’94. IEEE International Conference on Acoustics, Speech and Signal Processing*, pp III–329
- Fraïwan L, Lweesy K, Khasawneh N, Wenz H, Dickhaus H (2012) Automated sleep stage identification system based on timefrequency analysis of a single EEG channel and random forest classifier. *Computer Methods and Programs in Biomedicine* 108:10–19
- Gaunaurd GC, Strifors HC (1996) Signal analysis by means of time-frequency (Wigner-type) distributions-applications to sonar and radar echoes. *Proceedings of the IEEE* 84:1231–1248
- Genuera R, Poggi JM, Malot CT, Villa-Vialaneix N (2017) Random forests for big data. *Big Data Research* 9:28–46

- Ghosh PK, Ortega A, Narayanan S (2007) Pitch period estimation using multipulse model and wavelet transform. In: Proceedings of Interspeech, pp 2761–2764
- Ghosh-Dastidar S, Adeli H, Dadmehr N (2007) Mixed-band wavelet-chaos-neural network methodology for epilepsy and epileptic seizure detection. *IEEE Transactions on Biomedical Engineering* 54:1545–1551
- Gloor P, Fariello RG (1988) Generalized epilepsy: some of its cellular mechanisms differ from those of focal epilepsy. *Trends in Neurosciences* 11:63–68
- Goldberg R, Riek L (2000) A practical handbook of speech coders. CRC press
- Goldberger AL, Amaral LAN, Glass L, Hausdorff JM, Ivanov PC, Mark RG, Mietus JE, Moody GB, Peng CK, Stanley HE (2000) Physiobank, physiotoolkit, and physionet components of a new research resource for complex physiologic signals. *Circulation* 101:e215e220
- Gomez S, Naranjo V, Miralles R (2011) Removing interference components in time-frequency representations using morphological operators. *Journal of Visual Communication and Image Representation* 22:401–410
- Grochenig K (2001) Foundations of Time-Frequency Analysis. Birkhauser
- Guler NF, Ubeyli ED, Guler I (2005) Recurrent neural networks employing Lyapunov exponents for EEG signals classification. *Expert Systems with Applications* 29:506–514
- Guo L, Rivero D, Pazos A (2010) Epileptic seizure detection using multiwavelet transform based approximate entropy and artificial neural networks. *Journal of Neuroscience Methods* 193:156–163
- Gupta S, Krishna KH, Pachori RB, Tanveer M (2018) Fourier-Bessel series expansion based technique for automated classification of focal and non-focal EEG signals. In: International Joint Conferences on Neural Network (IJCNN), pp 1–6

- Gupta V, Pachori RB (2019) A new method for classification of focal and non-focal eeg signals. In: Machine Intelligence and Signal Analysis, pp 235–246
- Gupta V, Bhattacharyya A, Pachori RB (2017) Classification of seizure and non-seizure EEG signals based on EMD-TQWT method. In: 22nd International Conference on Digital Signal Processing (DSP), pp 1–5
- Gupta V, Priya T, Yadav AK, Pachori RB, Acharya UR (2017) Automated detection of focal EEG signals using features extracted from flexible analytic wavelet transform. Pattern Recognition Letters 94:180–188
- Hajinoroozi M, Mao Z, Huang Y (2015) Prediction of drivers drowsy and alert states from EEG signals with deep learning. In: Proceedings of IEEE 6th International Workshop on Computational Advances in Multi-Sensor Adaptive Processing, pp 493–496
- Hall M, Frank E, Holmes G, Pfahringer B, Reutemann P, Witten IH (2009) The WEKA data mining software: an update. SIGKDD Explorations 11:10–18
- Hassan AR (2015a) A comparative study of various classifiers for automated sleep apnea screening based on single-lead electrocardiogram. In: Proceedings of International Conference on Electrical Electronic Engineering, pp 45–48
- Hassan AR (2015b) Automatic screening of obstructive sleep apnea from single-lead electrocardiogram. In: Proceedings of International Conference on Electrical Engineering and Information Communication Technology, pp 1–6
- Hassan AR (2016) Computer-aided obstructive sleep apnea detection using normal inverse Gaussian parameters and adaptive boosting. Biomedical Signal Processing and Control 29:22–30
- Hassan AR, Haque MA (2016) Computer-aided obstructive sleep apnea screening from single-lead electrocardiogram using statistical and spectral features and bootstrap aggregating. Biocybernetics and Biomedical Engineering 36:256–266

- Hassan AR, Haque MA (2017) An expert system for automated identification of obstructive sleep apnea from single-lead ECG using random under sampling boosting. *Neurocomputing* 235:122–130
- Hassan AR, Siuly S, Zhang Y (2016) Epileptic seizure detection in EEG signals using tunable-Q factor wavelet transform and bootstrap aggregating. *Computer Methods and Programs in Biomedicine* 137:247–259
- Hess W (1983) *Pitch Determination of Speech Signals: Algorithms and Devices*. Springer-Verlag
- Hlawatsch F, Manickam TG, Urbanke RL, Jones W (1995) Smoothed pseudo Wigner distribution, Choi-Williams distribution, and cone-kernel representation: Ambiguity-domain analysis and experimental comparison. *Signal Processing* 43:149–168
- Huang H, Pan J (2006) Speech pitch determination based on Hilbert-Huang transform. *Signal Processing* 86:792 – 803
- Huang NE, Shen Z, Long SR, Wu MC, Shih HH, Zheng Q, Yen NC, Tung CC, Liu HH (1998) The empirical mode decomposition and the Hilbert spectrum for nonlinear and non-stationary time series analysis. In: *Proceedings of the Royal Society of London A: Mathematical, Physical and Engineering Sciences*, vol 454, pp 903–995
- Huang NE, Shen Z, Long SR (1999) A new view of nonlinear water waves: the Hilbert spectrum. *Annual Review of Fluid Mechanics* 31:417–457
- Huijse P, Estevez PA, Protopapas P, Zegers P, Principe JC (2012) An information theoretic algorithm for finding periodicities in stellar light curves. *IEEE Transactions on Signal Processing* 60:5135–5145
- Iqbal O, Fattah SA, Zahin S (2017) Hand movement recognition based on singular value decomposition of surface EMG signal. In: *Proceedings of IEEE Region 10 Humanitarian Technology Conference*, pp 837–842

- Jain P, Pachori RB (2013) Marginal energy density over the low frequency range as a feature for voiced/non-voiced detection in noisy speech signals. *Journal of the Franklin Institute* 350:698–716
- Jain P, Pachori RB (2014) Event-based method for instantaneous fundamental frequency estimation from voiced speech based on eigenvalue decomposition of the Hankel matrix. *IEEE/ACM Transactions on Audio, Speech, and Language Processing* 22:1467–1482
- Jain P, Pachori RB (2015) An iterative approach for decomposition of multi-component non-stationary signals based on eigenvalue decomposition of the Hankel matrix. *Journal of the Franklin Institute* 352:4017–4044
- Janbakhshi P, Shamsollahi MB (2018) Sleep apnea detection from single-lead ECG using features based on ECG-derived respiration (EDR) signals. *IRBM* pp 206–218
- Javaheri S, Dempsey JA (2013) Central sleep apnea. *Comprehensive Physiology* 3:141–163
- Joshi D, Tripathi A, Sharma R, Pachori RB (2017) Computer aided detection of abnormal EMG signals based on tunable-Q wavelet transform. In: *Proceedings of 4th International Conference on Signal Processing and Integrated Networks*, pp 544–549
- Ju Z, Liu H (2014) Human hand motion analysis with multisensory information. *IEEE/ASME Transactions on Mechatronics* 19:456–466
- Kadambe S, Boudreaux-Bartels GF (1992a) A comparison of the existence of ‘cross terms’ in the Wigner distribution and the squared magnitude of the wavelet transform and the short-time Fourier transform. *IEEE Transactions on Signal Processing* 40:2498–2517

- Kadambe S, Boudreaux-Bartels GF (1992b) Application of the wavelet transform for pitch detection of speech signals. *IEEE Transactions on Information Theory* 38:917–924
- Kakoty NM, Hazarika SM (2011) Recognition of grasp types through principal components of DWT based EMG features. In: *Proceedings of IEEE International Conference on Rehabilitation Robotics*, pp 1–6
- Kaniusas E (2012) *Fundamentals of Biosignals*. Springer
- Kerekes J (2008) Receiver operating characteristic curve confidence intervals and regions. *IEEE Geoscience and Remote Sensing Letters* 5:251–255
- Kesper K, Canisius S, Penzel T, Ploch T, Cassel W (2012) ECG signal analysis for the assessment of sleep-disordered breathing and sleep pattern. *Medical & Biological Engineering & Computing* 50:135–144
- Khan NA, Taj IA, Jaffri MN, Ijaz S (2011) Cross-term elimination in Wigner distribution based on 2D signal processing techniques. *Signal Processing* 91:590–599
- Khan YU, Gotman J (2003) Wavelet based automatic seizure detection in intracerebral electroencephalogram. *Clinical Neurophysiology* 114:898–908
- Khandoker AH, Lai DTH, Begg RK, Palaniswami M (2007) Wavelet-based feature extraction for support vector machines for screening balance impairments in the elderly. *IEEE Transactions on Neural Systems and Rehabilitation Engineering* 15:587–597
- Khandoker AH, Karmakar CK, Palaniswami M (2009) Automated recognition of patients with obstructive sleep apnoea using wavelet-based features of electrocardiogram recordings. *Computers in Biology and Medicine* 39:88–96
- Khezri M, Jahed M (2008) Surface electromyogram signal estimation based on wavelet thresholding technique. In: *Proceedings of 30th Annual International*

- Conference of the IEEE Engineering in Medicine and Biology Society, pp 4752–4755
- Kiguchi K, Hayashi Y (2012) A study of EMG and EEG during perception-assist with an upper-limb power-assist robot. In: Proceedings of IEEE International Conference on Robotics and Automation, pp 2711–2716
- Kohavi R (1995) A study of cross-validation and bootstrap for accuracy estimation and model selection. In: Proceedings of the 14th International Joint Conference on Artificial Intelligence, pp 1137–1143
- Kominek J, Black A (2004a) The CMU ARCTIC databases for speech synthesis. http://www.festvox.org/cmu_arctic
- Kominek J, Black A (2004b) The CMU Arctic speech databases. In: Proceedings of Fifth ISCA Workshop on Speech Synthesis, pp 223–224
- Kononenko I, Simec E, Robnik-Sikonja M (1997) Overcoming the myopia of inductive learning algorithms with RELIEFF. *Applied Intelligence* 7:39–55
- Kraskov A, Stoegbauer H, Grassberger P (2004) Estimating Mutual Information. *Physical Review* 69:066138
- Kruskal WH (1957) Historical notes on the Wilcoxon unpaired two-sample test. *Journal of the American Statistical Association* 52:356–360
- Kumar M, Pachori RB, Acharya UR (2017) Characterization of coronary artery disease using flexible analytic wavelet transform applied on ECG signals. *Biomedical Signal Processing and Control* 31:301–308
- Kumar M, Pachori RB, Acharya UR (2016) An efficient automated technique for CAD diagnosis using flexible analytic wavelet transform and entropy features extracted from HRV signals. *Expert Systems With Applications* 63:165–172

- Kumar TS, Kanhangad V (2018) Gabor filter-based one-dimensional local phase descriptors for obstructive sleep apnea detection using single-lead ECG. *IEEE Sensors Letters* 2:1–4
- Kurita Y, Tada M, Matsumoto Y, Ogasawara T (2002) Simultaneous measurement of the grip/load force and the finger EMG: Effects of the grasping condition. In: *Proceedings of 11th IEEE International Workshop on Robot and Human Interactive Communication*, pp 217–222
- Kwan P, Brodie MJ (2000) Early identification of refractory epilepsy. *New England Journal of Medicine* 342:314–319
- Kwan P, Arzimanoglou A, Berg AT, Brodie MJ, Allen HW, Mathern G, Moshe SL, Perucca E, Wiebe S, French J (2010) Definition of drug resistant epilepsy: consensus proposal by the ad hoc task force of the ILAE commission on therapeutic strategies. *Epilepsia* 51:1069–1077
- Lee SH, Lim JS, Kim JK, Yang J, Lee Y (2014) Classification of normal and epileptic seizure EEG signals using wavelet transform, phase-space reconstruction, and Euclidean distance. *Computer Methods and Programs in Biomedicine* 116:10–25
- Lehnertz K, Elger CE (1995) Spatio-temporal dynamics of the primary epileptogenic area in temporal lobe epilepsy characterized by neuronal complexity loss. *Electroencephalography and Clinical Neurophysiology* 95:108–117
- Lerga J, Sucic V (2009) Nonlinear IF estimation based on the pseudo WVD adapted using the improved sliding pairwise ICI rule. *IEEE Signal Processing Letters* 16:953–956
- Li Y, Xue B, Hong H, Zhu X (2014) Instantaneous pitch estimation based on empirical wavelet transform. In: *Proceedings of Nineteenth International Conference on Digital Signal Processing*, pp 250–253

- Li Y, Luo ML, Li K (2016) A multiwavelet-based time-varying model identification approach for time-frequency analysis of EEG signals. *Neurocomputing* 193:106–114
- Liang SF, Wang HC, Chang WL (2010) Combination of EEG complexity and spectral analysis for epilepsy diagnosis and seizure detection. *EURASIP Journal on Advances in Signal Processing* 2010:853434
- Lippmann R (1987) An introduction to computing with neural nets. *IEEE ASSP Magazine* 4:4–22
- Liu H, Motoda H (1998) Feature selection for knowledge discovery and data mining. Springer Science & Business Media
- Liu J, Zhou P (2013) A novel myoelectric pattern recognition strategy for hand function restoration after incomplete cervical spinal cord injury. *IEEE Transactions on Neural Systems and Rehabilitation Engineering* 21:96–103
- Liu WY (2013) Auto term window method and its parameter selection. *Measurement* 46:3113–3118
- Liu WY, Han JG, Jiang JL (2013) A novel ball bearing fault diagnosis approach based on auto term window method. *Measurement* 46:4032–4037
- Madyastha RK, Aazhang B (1994) An algorithm for training multilayer perceptrons for data classification and function interpolation. *IEEE Transactions on Circuits and Systems I: Fundamental Theory and Applications* 41:866–875
- Mallat S (1999) *A Wavelet Tour of Signal Process*. Academic Press
- Mallat S (2009) *A Wavelet Tour of Signal Processing: The Sparse Way*. Elsevier
- Mallat S, Zhang Z (1993) Matching pursuits with time-frequency dictionaries. *IEEE Transactions on Signal Processing* 41:3397–3415

- McKight PE, Najab J (2010) Kruskal-Wallis Test. The Corsini Encyclopedia of Psychology
- Mendez MO, Bianchi AM, Matteucci M, Cerutti S, Penzel T (2009) Sleep apnea screening by autoregressive models from a single ECG lead. *IEEE Transactions on Biomedical Engineering* 56:2838–2850
- Mertins A (1999) *Signal Analysis: Wavelets, Filter Banks, Time-Frequency Transforms and Applications*. John Wiley
- Moulines E, Charpentier F (1990) Pitch-synchronous waveform processing techniques for text-to-speech synthesis using diphones. *Speech Communication* 9:453–467
- Narasimhan SV, Haripriya AR, Kumar BKS (2008) Improved Wigner-Ville distribution performance based on DCT/DFT harmonic wavelet transform and modified magnitude group delay. *Signal Processing* 88:1–18
- Nazemi A, Maleki A (2014) Artificial neural network classifier in comparison with LDA and LS-SVM classifiers to recognize 52 hand postures and movements. In: *Proceedings of 4th International Conference on Computer and Knowledge Engineering*, pp 18–22
- Nguyen HD, Wilkins BA, Cheng Q, Benjamin BA (2014) An online sleep apnea detection method based on recurrence quantification analysis. *IEEE Journal of Biomedical and Health Informatics* 18:1285–1293
- Noll AM (1964) Short-time spectrum and cepstrum techniques for vocal-pitch detection. *The Journal of the Acoustical Society of America* 36:296–302
- Ocak H (2009) Automatic detection of epileptic seizures in EEG using discrete wavelet transform and approximate entropy. *Expert Systems with Applications* 36:2027–2036

- Orhan U, Hekim M, Ozer M (2011) EEG signals classification using the K-means clustering and a multilayer perceptron neural network model. *Expert Systems with Applications* 38:13475–13481
- Oshaughnessy D (2000) *Speech Communication: Human and Machine*. Wiley-IEEE Press
- Oskoei MA, Hu H (2007) Myoelectric control systems-A survey. *Biomedical Signal Processing and Control* 2:275–294
- Ouyang G, Zhu X, Ju Z (2014) Dynamical characteristics of surface EMG signals of hand grasps via recurrence plot. *IEEE Journal of Biomedical and Health Informatics* 18:257–265
- Oweis RJ, Abdulhay EW (2011) Seizure classification in EEG signals utilizing Hilbert-Huang transform. *BioMedical Engineering OnLine* 10:38
- Pachori RB (2008) Discrimination between ictal and seizure-free EEG signals using empirical mode decomposition. *Research Letters in Signal Processing* 2008:1–5
- Pachori RB, Bajaj V (2011) Analysis of normal and epileptic seizure EEG signals using empirical mode decomposition. *Computer Methods and Programs in Biomedicine* 104:373–381
- Pachori RB, Patidar S (2014) Epileptic seizure classification in EEG signals using second-order difference plot of intrinsic mode functions. *Computer Methods and Programs in Biomedicine* 113:494–502
- Pachori RB, Sircar P (2006) Analysis of multicomponent nonstationary signals using Fourier-Bessel transform and Wigner distribution. In: *Proceedings 14th European Signal Processing Conference*, pp 1–5
- Pachori RB, Sircar P (2007) A new technique to reduce cross terms in the Wigner distribution. *Digital Signal Processing* 17:466–474

- Pachori RB, Sircar P (2008a) EEG signal analysis using FB expansion and second-order linear TVAR process. *Signal Processing* 88:415–420
- Pachori RB, Sircar P (2008b) Time-frequency analysis using time-order representation and Wigner distribution. In: *Proceedings of IEEE Tencon Conference*, pp 1–6
- Pachori RB, Sircar P (2010) Analysis of multicomponent AM-FM signals using FB-DESA method. *Digital Signal Processing* 20:42–62
- Pachori RB, Sharma R, Patidar S (2015) Classification of normal and epileptic seizure EEG signals based on empirical mode decomposition. Springer
- Pati S, Alexopoulos AV (2010) Pharmaco-resistant epilepsy: From pathogenesis to current and emerging therapies. *Cleveland Clinic Journal of Medicine* 77:457–467
- Patidar S, Pachori RB (2014) Classification of cardiac sound signals using constrained tunable-Q wavelet transform. *Expert Systems with Applications* 41:7161–7170
- Patidar S, Panigrahi T (2017) Detection of epileptic seizure using Kraskov entropy applied on tunable-Q wavelet transform of EEG signals. *Biomedical Signal Processing and Control* 34:74–80
- Patidar S, Pachori RB, Acharya UR (2015a) Automated diagnosis of coronary artery disease using tunable-Q wavelet transform applied on heart rate signals. *Knowledge-Based Systems* 82:1–10
- Patidar S, Pachori RB, Garg N (2015b) Automatic diagnosis of septal defects based on tunable-Q wavelet transform of cardiac sound signals. *Expert Systems with Applications* 42:3315–3326
- Patidar S, Pachori RB, Upadhyay A, Acharya UR (2017) An integrated alcoholic index using tunable-Q wavelet transform based features extracted from EEG signals for diagnosis of alcoholism. *Applied Soft Computing* 50:71–78

- Peker M (2016) An efficient sleep scoring system based on EEG signal using complex-valued machine learning algorithms. *Neurocomputing* 207:165–177
- Peker M, Sen B, Delen D (2016) A novel method for automated diagnosis of epilepsy using complex-valued classifiers. *IEEE Journal of Biomedical and Health Informatics* 20:108–118
- Penfield W, Erickson TC (1941) *Epilepsy and cerebral localization*, Charles C. Thomas
- Penzel T, Moody GB, Mark RG, Goldberges AL, Peter JH (2000) The Apnea-ECG Database. *Computers in Cardiology* 27:255–258
- Penzel T, McNames J, Chazal P, Raymond B, Murray A, Moody G (2002) Systematic comparison of different algorithms for apnoea detection based on electrocardiogram recordings. *Medical and Biological Engineering and Computing* 40:402–407
- Pikula S, Benes P (2014) A new method for interference reduction in the smoothed pseudo Wigner-Ville distribution. In: *Proceedings of 8th International Conference on Sensing Technology*, pp 599–603
- Platt J (1998) Fast training of support vector machines using sequential minimal optimization. In: *Advances in Kernel Methods - Support Vector Learning*, MIT Press
- Polat K, Gunes S (2007) Classification of epileptiform EEG using a hybrid system based on decision tree classifier and fast Fourier transform. *Applied Mathematics and Computation* 187:1017–1026
- Quinlan JR (1986) Induction of decision trees. *Machine Learning* 1:81–106
- Rabiner L (1977) On the use of autocorrelation analysis for pitch detection. *IEEE Transactions on Acoustics, Speech, and Signal Processing* 25:24–33

- Rankine L, Mesbah M, Boashash B (2007) IF estimation for multicomponent signals using image processing techniques in the time-frequency domain. *Signal Processing* 87:1234–1250
- Rao M, Seth S, Xu J, Chen Y, Tagare H, Principe JC (2011) A test of independence based on a generalized correlation function. *Signal Processing* 91:15–27
- Rathore PS, Pachori RB (2013) Instantaneous fundamental frequency estimation of speech signals using DESA in low-frequency region. In: *Proceedings of International Conference on Signal Processing and Communication*, pp 470–473
- Reddy GRS, Rao R (2017) Automated identification system for seizure EEG signals using tunable-Q wavelet transform. *Engineering Science and Technology, an International Journal* 20:1486–1493
- Rehman N, Mandic DP (2010) Multivariate empirical mode decomposition. In: *Proceedings of The Royal Society of London A: Mathematical, Physical and Engineering Sciences*, pp 1291–1302
- Reilly RB, Lee TC (2010) Electrograms (ECG, EEG, EMG, EOG). *Technology and Health Care* 18:443–458
- Rice J (2007) *Mathematical Statistics and Data Analysis*. Cengage Learning
- Rioul O, Vetterli M (1991) Wavelets and signal processing. *IEEE signal processing magazine* 8:14–38
- Robnik-Sikonja M, Kononenko I (2003) Theoretical and empirical analysis of ReliefF and RReliefF. *Machine Learning* 53:23–69
- Roffo G, Melzi S, Cristani M (2015) Infinite Feature Selection. In: *Proceedings of IEEE International Conference on Computer Vision*, pp 4202–4210
- Roffo G, Melzi S, Castellani U, Vinciarelli A (2017) Infinite Latent Feature Selection: A Probabilistic Latent Graph-Based Ranking Approach. In: *Proceedings of IEEE International Conference on Computer Vision*, pp 1398–1406

- Ross M, Shaffer H, Cohen A, Freudberg R, Manley H (1974) Average magnitude difference function pitch extractor. *IEEE Transactions on Acoustics, Speech and Signal Processing* 22:353–362
- Ruangpaisarn Y, Jaiy S (2015) sEMG signal classification using SMO algorithm and singular value decomposition. In: *Proceedings of 7th International Conference on Information Technology and Electrical Engineering*, pp 46–50
- Ruggieri S (2002) Efficient C4.5 [classification algorithm]. *IEEE Transactions on Knowledge and Data Engineering* 14:438–444
- Samiee K, Kovacs P, Gabbouj M (2015) Epileptic seizure classification of EEG time-series using rational discrete short-time Fourier transform. *IEEE Transactions on Biomedical Engineering* 62:541–552
- Sang TH, Williams WJ (1995) Renyi information and signal-dependent optimal kernel design. In: *Proceedings of International Conference on Acoustics, Speech, and Signal Processing*, pp 997–1000
- Santamaria I, Pokharel PP, Principe JC (2006) Generalized correlation function: definition, properties, and application to blind equalization. *IEEE Transactions on Signal Processing* 54:2187–2197
- Sapsanis C, Georgoulas G, Tzes A (2013a) EMG based classification of basic hand movements based on time-frequency features. In: *Proceedings of 21st Mediterranean Conference on Control and Automation*, pp 716–722
- Sapsanis C, Georgoulas G, Tzes A, Lymberopoulos D (2013b) Improving EMG based classification of basic hand movements using EMD. In: *Proceedings of 35th Annual International Conference of the IEEE EMBS*, pp 5754–5757
- Sattar F, Salomonsson G (1999) The use of a filter bank and the Wigner-Ville distribution for time-frequency representation. *IEEE Transactions on Signal Processing* 47:1776–1783

- Schlotthauer G, Torres ME, Rufiner HL (2009) A new algorithm for instantaneous F0 speech extraction based on ensemble empirical mode decomposition. In: Proceedings of Seventeenth European Signal Processing Conference, pp 2347–2351
- Schlotthauer G, Persia LED, Larrateguy LD, Milone DH (2014) Screening of obstructive sleep apnea with empirical mode decomposition of pulse oximetry. *Medical Engineering & Physics* 36:1074–1080
- Sejdi E, Djurovi I, Jiang J (2009) Time-frequency feature representation using energy concentration: An overview of recent advances. *Digital Signal Processing* 19:153–183
- Selesnick IW (2011a) Resonance-based signal decomposition: A new sparsity-enabled signal analysis method. *Signal Processing* 91:2793–2809
- Selesnick IW (2011b) TQWT toolbox guide. Electrical and Computer Engineering Polytechnic Institute of New York University
- Selesnick IW (2011c) Wavelet transform with tunable Q-factor. *IEEE Transactions on Signal Processing* 59:3560–3575
- Seshadri G, Yegnanarayana B (2011) Performance of an event-based instantaneous fundamental frequency estimator for distant speech signals. *IEEE Transactions on Audio, Speech, and Language Processing* 19:1853–1864
- Sharma M, Pachori RB (2017a) A novel approach to detect epileptic seizures using a combination of tunable-Q wavelet transform and fractal dimension. *Journal of Mechanics in Medicine and Biology* 17:1740003
- Sharma R, Pachori RB (2015) Classification of epileptic seizures in EEG signals based on phase space representation of intrinsic mode functions. *Expert Systems with Applications* 42:1106–1117
- Sharma R, Pachori RB (2018a) Automated classification of focal and non-focal EEG

- signals based on bivariate empirical mode decomposition. In: *Biomedical Signal and Image Processing in Patient Care*, IGI Global
- Sharma R, Pachori RB, Gautam S (2014) Empirical mode decomposition based classification of focal and non-focal EEG signals. In: *Proceedings of International Conference on Medical Biometrics*, pp 135–140
- Sharma R, Pachori RB, Acharya UR (2015a) An integrated index for the identification of focal electroencephalogram signals using discrete wavelet transform and entropy measures. *Entropy* 17:5218–5240
- Sharma R, Pachori RB, Acharya UR (2015b) Application of entropy measures on intrinsic mode functions for the automated identification of focal electroencephalogram signals. *Entropy* 17:669–691
- Sharma R, Kumar M, Pachori RB, Acharya UR (2017a) Decision support system for focal EEG signals using tunable-Q wavelet transform. *Journal of Computational Science* 20:52–60
- Sharma R, Pachori RB, Upadhyay A (2017b) Automatic sleep stages classification based on iterative filtering of electroencephalogram signals. *Neural Computing and Applications* 28:2959–2978
- Sharma RR, Pachori RB (2017b) A new method for non-stationary signal analysis using eigenvalue decomposition of the Hankel matrix and Hilbert transform. In: *Proceedings of 4th International Conference on Signal Processing and Integrated Networks (SPIN)*, pp 484–488
- Sharma RR, Pachori RB (2018b) Time-frequency representation using IEVDHM-HT with application to classification of epileptic EEG signals. *IET Science, Measurement & Technology* 12:72–82
- Shriberg E, Ferrer L, Kajarekar S, Venkataraman A, Stolcke A (2005) Modeling prosodic feature sequences for speaker recognition. *Speech Communication* 46:455–472

- Singh P, Pachori RB (2017) Classification of focal and nonfocal EEG signals using features derived from Fourier-based rhythms. *Journal of Mechanics in Medicine and Biology* 17:1740002
- Singh P, Joshi SD, Patney RK, Saha K (2017) The Fourier decomposition method for nonlinear and non-stationary time series analysis. *Proceedings of the Royal Society A: Mathematical, Physical and Engineering Sciences* 473:20160871
- Siuly, Li Y, Wen P (2009) Classification of EEG signals using sampling techniques and least square support vector machines. In: *International Conference on Rough Sets and Knowledge Technology*, Springer Berlin Heidelberg, pp 375–382
- Song C, Liu K, Zhang X, Chen L, Xian X (2016) An obstructive sleep apnea detection approach using a discriminative hidden Markov model from ECG signals. *IEEE Transactions on Biomedical Engineering* 63:1532–1542
- Srinivasan V, Eswaran C, Sriraam N (2005) Artificial neural network based epileptic detection using time-domain and frequency-domain features. *Journal of Medical Systems* 29:647–660
- Stankovic L (1994) An analysis of some time-frequency and time-scale distributions. *Annals of Telecommunications* 49:505
- Stankovic L (2001) A measure of some time-frequency distributions concentration. *Signal Processing* 81:621 – 631
- Subasi A (2007) EEG signal classification using wavelet feature extraction and a mixture of expert model. *Expert Systems with Applications* 32:1084–1093
- Subasi A, Gursoy MI (2010) EEG signal classification using PCA, ICA, LDA and support vector machines. *Expert Systems with Applications* 37:8659–8666
- Suykens JAK, Vandewalle J (1999) Least squares support vector machine classifiers. *Neural Processing Letters* 9:293–300

- Tan LN, Alwan A (2013) Multi-band summary correlogram-based pitch detection for noisy speech. *Speech Communication* 55:841–856
- Taori R, Sluijter RJ, Kathmann E (1995) Speech compression using pitch synchronous interpolation. In: *Proceedings of International Conference on Acoustics, Speech, and Signal Processing*, pp 512–515
- Theodoridis S, Koutroumbas K (2009) Feature selection. In: *Pattern Recognition (Fourth Edition)*, Academic Press, pp 261 – 322
- Thomas M, Jacob R, Lethakumary B (2012a) Comparison of WVD based time-frequency distributions. In: *Proceedings of International Conference on Power, Signals, Controls and Computation*, pp 1–8
- Thomas M, Lethakumary B, Jacob R (2012b) Performance comparison of multi-component signals using WVD and Cohen’s class variants. In: *Proceedings of IEEE International Conference on Computing, Electronics and Electrical Technologies*, pp 717–722
- Tiwari AK, Pachori RB, Kanhangad V, Panigrahi BK (2017) Automated diagnosis of epilepsy using key-point-based local binary pattern of EEG Signals. *IEEE Journal of Biomedical and Health Informatics* 21:888–896
- Tripathy RK (2018) Application of intrinsic band function technique for automated detection of sleep apnea using HRV and EDR signals. *Biocybernetics and Biomedical Engineering* 38:136–144
- Tzallas AT, Tsipouras MG, Fotiadis DI (2009) Epileptic seizure detection in EEGs using time-frequency analysis. *IEEE Transactions on Information Technology in Biomedicine* 13:703–710
- Tzallas AT, Tsipouras MG, Fotiadis DI (2007) Automatic seizure detection based on time-frequency analysis and artificial neural networks. *Computational Intelligence and Neuroscience* 2007

- Ubeyli ED (2010) Lyapunov exponents/probabilistic neural networks for analysis of EEG signals. *Expert Systems with Applications* 37:985–992
- Upadhyay A, Pachori RB (2015a) A new method for determination of instantaneous pitch frequency from speech signals. In: *Proceedings of Signal Processing and Signal Processing Education Workshop*, pp 325 – 330
- Upadhyay A, Pachori RB (2015b) Instantaneous voiced/non-voiced detection in speech signals based on variational mode decomposition. *Journal of the Franklin Institute* 352:2679–2707
- Upadhyay A, Sharma M, Pachori RB (2017) Determination of instantaneous fundamental frequency of speech signals using variational mode decomposition. *Computers & Electrical Engineering* 62:630–647
- Varon C, Caicedo A, Testelmans D, Buyse B, Huffel SV (2015) A novel algorithm for the automatic detection of sleep apnea from single-lead ECG. *IEEE Transactions on Biomedical Engineering* 62:2269–2278
- Veprek P, Scordilis MS (2002) Analysis, enhancement and evaluation of five pitch determination techniques. *Speech Communication* 37:249 – 270
- Veselkov KA, Pahomov VI, Lindon JC, Volynkin VS, Crockford D, Osipenko GS, Davies DB, Barton RH, Bang JW, Holmes E, Nicholson JK (2010) A metabolic entropy approach for measurements of systemic metabolic disruptions in pathophysiological States. *Journal of Proteome Research* 9:3537–3544
- Wang Y, Jiang YC (2010) New time-frequency distribution based on the polynomial Wigner-Ville distribution and L class of Wigner-Ville distribution. *IET Signal Processing* 4:130–136
- White DP (2006) Sleep apnea. *Proceedings of the American Thoracic Society* 3:124–128

- Williams WJ, Brown ML, Hero AO (1991) Uncertainty, information, and time-frequency distributions. In: *Advanced Signal Processing Algorithms, Architectures, and Implementations II*, pp 144–157
- Witte H, Iasemidis LD, Litt B (2003) Special issue on epileptic seizure prediction. *IEEE Transactions on Biomedical Engineering* 50:537–539
- World Health Organization (2018) Epilepsy. URL <http://www.who.int/news-room/fact-sheets/detail/epilepsy>
- Wu Z, Huang NE (2009) Ensemble empirical mode decomposition: a noise-assisted data analysis method. *Advances in adaptive data analysis* 1:1–41
- Xianglong L, Jinghuai G (2009) Instantaneous frequency estimation using WVD and local SVD. In: *2nd International Congress on Image and Signal Processing*, pp 1–4
- Xie B, Minn H (2012) Real-time sleep apnea detection by classifier combination. *IEEE Transactions on Information Technology in Biomedicine* 16:469–477
- Xu D, Erdogmus D (2010) *Renyi’s entropy, divergence and their nonparametric estimators*, Springer New York, pp 47–102
- Xu JW, Paiva ARC, Park IL, Principe JC (2008) A reproducing kernel Hilbert space framework for information-theoretic learning. *IEEE Transactions on Signal Processing* 56:5891–5902
- Yegnanarayana B, Murty KSR (2009) Event-based instantaneous fundamental frequency estimation from speech signals. *IEEE Transactions on Audio, Speech, and Language Processing* 17:614–624
- Young T, Peprad P, Palta M, Hla KM, Finn L, Morgan B, Skatrud J (1997) Population-based study of sleep-disordered breathing as a risk factor for hypertension. *Archives of Internal Medicine* 157:1746–1752

Zeng H, Cheung Y (2011) Feature selection and kernel learning for local learning-based clustering. *IEEE Transactions on Pattern Analysis and Machine Intelligence* 33:1532–1547

Zhu G, Li Y, Wen PP, Wang S, Xi M (2013) Epileptogenic focus detection in intracranial EEG based on delay permutation entropy. In: *AIP Conference Proceedings*, American Institute of Physics, vol 1559, pp 31–36

List of publications

Publications from thesis

Journal papers:

1. R.B. Pachori and A. Nishad, Cross-terms reduction in the WignerVille distribution using tunable-Q wavelet transform. *Signal Processing*, 120 (2016) 288–304.
2. A. Nishad, R.B. Pachori, and U.R. Acharya, Application of TQWT based filter-bank for sleep apnea screening using ECG signals, *Journal of Ambient Intelligence and Humanized Computing*, In press, 2018.
3. A. Nishad, A. Upadhyay, R.B. Pachori, and U.R. Acharya, Automated classification of hand movements using tunable-Q wavelet transform based filter-bank with surface electromyogram signals, *Future Generation Computer Systems*, 93 (2019), 96–110.
4. A. Nishad and R.B. Pachori, Classification of epileptic electroencephalogram signals using tunable-Q wavelet transform based filter-bank, *Journal of Ambient Intelligence and Humanized Computing*, third revision submitted.

Conference papers:

1. A. Nishad and R.B. Pachori, Instantaneous fundamental frequency estimation of speech signals using tunable-Q wavelet transform, *International Conference on Signal Processing and Communications (SPCOM)*, pp. 157–161, 2018, India.
2. V. Gupta, A. Nishad, and R.B. Pachori, Focal EEG signal detection based on constant-bandwidth TQWT filter-banks, *IEEE International Conference on Bioinformatics and Biomedicine*, 2018, Spain.